

**The Geology of Sulphide-Facies Iron-Formations  
and Associated Rocks in the  
Lower Steel River - Little Steel Lake  
Area, Terrace Bay, Ontario**

by

**Bernard Rolf Schnieders**



**A Thesis Submitted in Partial  
Fulfillment of the Requirements  
for the Degree of Master of Science**

**Lakehead University, Thunder Bay, Ontario**

**November, 1987**

ProQuest Number: 10611759

All rights reserved

INFORMATION TO ALL USERS

The quality of this reproduction is dependent upon the quality of the copy submitted.

In the unlikely event that the author did not send a complete manuscript and there are missing pages, these will be noted. Also, if material had to be removed, a note will indicate the deletion.



ProQuest 10611759

Published by ProQuest LLC (2017). Copyright of the Dissertation is held by the Author.

All rights reserved.

This work is protected against unauthorized copying under Title 17, United States Code  
Microform Edition © ProQuest LLC.

ProQuest LLC.  
789 East Eisenhower Parkway  
P.O. Box 1346  
Ann Arbor, MI 48106 - 1346

Permission has been granted to the National Library of Canada to microfilm this thesis and to lend or sell copies of the film.

The author (copyright owner) has reserved other publication rights, and neither the thesis nor extensive extracts from it may be printed or otherwise reproduced without his/her written permission.

L'autorisation a été accordée à la Bibliothèque nationale du Canada de microfilmer cette thèse et de prêter ou de vendre des exemplaires du film.

L'auteur (titulaire du droit d'auteur) se réserve les autres droits de publication; ni la thèse ni de longs extraits de celle-ci ne doivent être imprimés ou autrement reproduits sans son autorisation écrite.

ISBN 0-315-44805-9

**FRONTISPIECE**

VIEW OF BEDROCK EXPOSURE (KINGDOM PROPERTY)  
LOOKING NORTH TO SANTOY BAY, LAKE SUPERIOR.

(ii)



ABSTRACT

The Lower Steel River - Little Steel Lake area is located about 25 km east of Terrace Bay, Ontario. Seventeen iron-formations were investigated within this metamorphosed Archean volcanic and sedimentary terrain, which represents a portion of the Abitibi - Wawa Subprovince of the Superior Structural Province.

Sulphide-facies iron-formations are the dominant chemical sedimentary rocks in the Schreiber - Terrace Bay area, and represent deposition during quiescent periods in clastic accumulation and in volcanic activity. The iron-formations commonly mark contacts between the volcanic and sedimentary rocks. They are interbedded with carbonaceous slates at the base of sedimentary successions and overlain by DE turbidites. This suggests chemical sedimentation on a subaqueous basinal plain slightly distal to an outer fan.

Sulphide-facies iron-formations consist of a mixture of chemical and clastic components, and while highly variable, the iron-formations in the study area contain three commonly recognizable units: 1) pyritic-carbonaceous slate; 2) disseminated, massive, laminated and nodular pyrite; and 3) chert or siliceous sedimentary rock. Sedimentary textures and structures combined with trace element abundances and geochemical evidence support the mixing of clastic and chemical components, and a hydrothermal source for the iron. Exhalative discharge probably occurred episodically as moderate- to low-temperature solutions percolated through near-surface pillowed volcanics and, once vented, deposited a blanket of chemical sediment. Vent-proximal deposits include massive and layered pyrite; the domal and colloform varieties support the existence of organic mats. The presence of carbon is interpreted as a relic of the organic activity. Pyritic-carbonaceous slates consisting of alternating chemical and clastic components represent vent-distal deposits. Radial structures within pyrite nodules provide evidence of diagenetic transformation and tectonic deformation.

Structural evidence suggests that the study area was affected by a complex folding event related to one deformational episode, probably preceded by syn-sedimentary slumping in some areas. The competency differences between sedimentary and volcanic rocks, combined with the fine-grained nature of the sedimentary rocks (DE turbidites and iron-formation) at major volcanic-sedimentary contacts, focussed deformation and dike emplacement in the contact areas.

### ACKNOWLEDGEMENTS

I would like to thank the Mines and Minerals Division, Ministry of Northern Development and Mines, and especially Mr. Ken Fenwick, for supporting this study and allowing me the opportunity to work in the Schreiber - Terrace Bay area between March 1983 and March 1987.

Special thanks and appreciation are due to Dr. Phil Fralick, whose help, suggestions and enthusiasm in the field and during laboratory work and writing, were indispensable. I also thank Dr. Fred Kehlenbeck for his assistance and suggestions regarding the structural geology, and for his constructive editing of the written text, Dr. Graham Borradaile who reviewed the structural data, and Dr. Roger Mitchell, Dr. Garth Platt and Dr. Steve Kissin for their suggestions and editorial comments.

The assistance of Dr. Tom Griffith, Allan MacKenzie, Keith Pringnitz, Ain Raitsakas, Ross Chuchman and Eleanor Jensen, with the geochemical analyses and X-ray diffraction studies, and the staff at the Geoscience Laboratories, Toronto, is much appreciated.

I thank Dr. Tim Barrett (IREM-MERI, McGill University) for some initial ideas as well as suggestions and advice throughout various phases of the study, and for review and editing of the thesis.

My associates at the Ministry of Northern Development and Mines, namely Alan Speed, who assisted in various phases of the study, George Patterson, John Scott, John Mason, Al McTavish, Mickey Gamble, Patrica Perry, Susan Koski and Annabelle Downton provided valuable advice and support. Discussions with Mark Smyk (Carleton University) are also appreciated.

Last, but definitely not least, I would like to thank my family; my wife Joni and daughter Whitney, who had the patience to tolerate my efforts in completing a part-time thesis in conjunction with a full-time job.

TABLE OF CONTENTS

	<u>PAGE</u>
FRONTISPIECE.....	ii
ABSTRACT.....	iii
ACKNOWLEDGEMENTS.....	iv
TABLE OF CONTENTS.....	v
LIST OF FIGURES.....	viii
LIST OF TABLES.....	xi
LIST OF PHOTOGRAPHS.....	xii
<u>CHAPTER 1: INTRODUCTION.....</u>	<u>1</u>
Location of the Study Area.....	1
General Geology.....	1
Purpose of the Study.....	6
Methods of Investigation.....	6
Exploration History.....	7
Classification and Studies of Other Iron-Formations.....	8
Classifications.....	8
Facies Associations: Depositional Environments.....	11
Sources of Iron: Genetic Models.....	13
<u>CHAPTER 2: STRUCTURAL GEOLOGY.....</u>	<u>15</u>
Introduction.....	15
Structural Elements.....	15
Folds.....	20
Dominant Folds.....	24
Detailed Structural Elements of the Lower Steel	
River-Little Steel Lake Area.....	25
1) Kingdom Area.....	25
Area 1.....	25
Area 2.....	33
Area 3.....	33
Area 4.....	35
Area 5.....	36
Area 6.....	40
2) Lawson Island.....	40
3) Steel River Highway Area.....	43
4) Black Fox Lake Area.....	43
Overall Distribution of Structural Features.....	43
Faulting.....	49
Discussion.....	49
<u>CHAPTER 3: ROCKS ASSOCIATED WITH IRON-FORMATION.....</u>	<u>56</u>
Introduction.....	56
Volcanic Rocks.....	58
Sedimentary Rocks.....	64
Intrusive Rocks.....	79
Mafic Intrusions.....	83
Effect of Intrusions on Sediments.....	84
Felsic Intrusions.....	85



	<u>PAGE</u>
<u>CHAPTER 4: IRON-FORMATION AND RELATED CHEMICAL AND CLASTIC COMPONENTS</u> .....	90
General.....	90
Composition of the Iron-Formations.....	90
Clastic Components.....	90
a) Pyritic-Carbonaceous Slate.....	90
b) Tuffaceous Component.....	90
Chemical or Biochemical Components.....	101
a) Pyrite.....	102
1) Fine-grained, Disseminated Pyrite.....	105
2) Massive Pyrite.....	108
3) Nodular Pyrite.....	113
4) Recrystallized Pyrite.....	121
5) Brecciated Pyrite.....	126
6) Other Sulphides.....	126
b) Chert.....	127
c) Carbonates.....	134
d) Oxides.....	134
e) Carbonaceous Component.....	135
<u>CHAPTER 5: DEPOSITIONAL ENVIRONMENTS</u> .....	137
Sedimentology; Clastic Units.....	137
Sedimentology; Iron-Formation.....	141
Geochemical Constraints.....	148
a) Co/Ni Ratios.....	148
1) Pyrite in Chert.....	148
2) Massive Pyrite.....	152
3) Radial Nodules.....	152
4) Colloform Nodules.....	152
5) Pyritic-Carbonaceous Slate.....	152
b) Hydrogenous versus Hydrothermal Input.....	154
c) Clastic - Chemical Mixing.....	154
<u>CHAPTER 6: POSSIBLE MODERN AND ANCIENT ANALOGUES</u> .....	161
a) Modern Polymetallic Deposits.....	161
b) Ancient Polymetallic Deposits.....	166
Cyprus Type.....	166
Besshi Type.....	167
Kuroko Type.....	167
Archean Volcanogenic Deposits.....	168
c) Implications for the Study Area.....	168
<u>CHAPTER 7: CONCLUSIONS</u> .....	171
<u>REFERENCES</u> .....	174

	<u>PAGE</u>
<u>APPENDICES</u> .....	184
<u>APPENDIX A</u> .....	185
Mineralogical Summary.....	185
<u>APPENDIX B</u> .....	186
X-ray Fluorescence Spectrography.....	186
Trace Elements.....	187
Accuracy and Precision.....	187
Discussion.....	188
X-ray Diffraction.....	189
<u>APPENDIX C</u> .....	190
Representative Duplicate Chemical Analyses for Two Samples.....	190
<u>APPENDIX D</u> .....	195
Exploration History.....	195
Map 1: Geology of the Lower Steel River- Little Steel Lake Area.....	Back Pocket

LIST OF FIGURES

<u>FIGURE NUMBER</u>	<u>TITLE</u>	<u>PAGE</u>
FIGURE 1:1	LOCATION MAP SHOWING THE SCHREIBER-TERRACE BAY STUDY AREA.	2
FIGURE 1:2	CHEMICAL SEDIMENTARY ROCKS AND IRON FORMATION IN THE SCHREIBER-TERRACE BAY AREA.	4
FIGURE 1:3	THESIS AREA LOCATION MAP: LOWER STEEL RIVER-LITTLE STEEL LAKE AREA.	5
FIGURE 2:1	DETAILED STRUCTURE AREAS.	17
FIGURE 2:2	AXIAL PLANAR CLEAVAGE AND FOLD TERMINOLOGY.	21
FIGURE 2:3	STRUCTURAL FACING.	23
FIGURE 2:4	KINGDOM AREA STRUCTURE.	26
2:4 (A,B)	KINGDOM STRUCTURAL DETAILS.	27
2:4 (C,D,E)	KINGDOM STRUCTURAL DETAILS.	28
2:4 (F,G)	KINGDOM STRUCTURAL DETAILS.	29
2:4 (H)	KINGDOM STRUCTURAL DETAILS.	30
2:4 (I,J,K,L)	KINGDOM STRUCTURAL DETAILS.	31
FIGURE 2:5	KINGDOM SECTION: STRUCTURAL FACING OF FOLDS.	32
FIGURE 2:6	STRUCTURAL FACING VARIATION IN PANELS.	34
FIGURE 2:7	VARIATIONS IN STRUCTURAL FACING OF FOLDS.	34
FIGURE 2:8	REFOLDED FOLD: BLACK FOX LAKE OCCURRENCE.	46
FIGURE 2:9	FOLD AXES MAXIMA.	46
FIGURE 2:10	STRUCTURAL DATA.	47
FIGURE 2:11 (A)	HYPOTHETICAL SECTION - WALKER (1967).	52
2:11 (B)	HYPOTHETICAL SECTION: KINGDOM AREA.	52
FIGURE 2:12 (A)	HYPOTHETICAL SECTION - PRESENT STUDY.	53
2:12 (B)	DETAILED HYPOTHETICAL SECTION: KINGDOM AREA.	53
FIGURE 3:1	DETAILED GEOLOGY OF THE KINGDOM OCCURRENCE.	57

<u>FIGURE NUMBER</u>	<u>TITLE</u>	<u>PAGE</u>
FIGURE 3:2	ALTERATION OF PILLOW RIMS (KINGDOM PROPERTY).	65
FIGURE 3:3	AFM PLOT OF METAVOLCANIC AND MAFIC INTRUSIVE ROCKS.	66
FIGURE 3:4	DETAILED GEOLOGY OF THE LITTLE STEEL HIGHWAY OCCURRENCE.	67
FIGURE 3:5	DETAILED GEOLOGY OF THE LITTLE STEEL RAILWAY OCCURRENCE.	68
FIGURE 3:6	STRATIGRAPHICAL COLUMN: STEEL RIVER AREA - SECTION 1.	72
FIGURE 3:7	STRATIGRAPHICAL COLUMN: STEEL RIVER AREA - SECTION 2.	73
FIGURE 3:8	DETAILED GEOLOGY OF THE BLACK FOX OCCURRENCE.	80
FIGURE 3:9	DETAILED GEOLOGY OF THE SIMARD-SWETZ OCCURRENCE.	86
FIGURE 4:1	TYPE SECTION: KINGDOM OCCURRENCE.	92
FIGURE 4:2	TYPE SECTION: SIMARD-SWETZ AND BLACK FOX LAKE OCCURRENCES.	96
FIGURE 5:1	VERTICAL SEQUENCE GRAPH: BED NUMBER VERSUS THICKNESS, SECTIONS 1 AND 2, STEEL RIVER AREA.	138
FIGURE 5:2	SUBMARINE FAN MODEL (WALKER, 1976).	140
FIGURE 5:3	THEORETICAL PALEOTOPOGRAPHIC RECONSTRUCTION OF AN ARCHEAN TERRAIN (SHEGELSKI, 1976).	144
FIGURE 5:4	HYPOTHETICAL DEPOSITIONAL SETTINGS OF IRON-FORMATIONS IN THE SCHREIBER-TERRACE BAY AREA.	145
FIGURE 5:5	GEOLOGICAL SECTION OF THE KINGDOM OCCURRENCE.	146

<u>FIGURE NUMBER</u>	<u>TITLE</u>	<u>PAGE</u>
FIGURE 5:6	PLOT OF Co VERSUS Ni.	153
FIGURE 5:7	TERNARY DIAGRAM FOR Fe/Mn/(Ni+ Cu+Co) x 10 IN CHERT AND PYRITE- CARBONACEOUS SLATE.	155
FIGURE 5:8	PLOT OF Ti VERSUS Al.	156
FIGURE 5:9	PLOT OF Fe/Ti VERSUS Al/(Al+Fe+Mn).	158
FIGURE 5:10	Fe/Al/(Si/5) RATIOS IN CHEMICAL AND CLASTIC SEDIMENTARY ROCKS.	159
FIGURE 6:1	GENETIC MODELS FOR MODERN METALLIFEROUS SEDIMENTS AND POLYMETALLIC DEPOSITS.	162

LIST OF TABLES

<u>TABLE NUMBER</u>	<u>TITLE</u>	<u>PAGE</u>
TABLE 1:1	CHEMICAL SEDIMENTARY ROCKS AND IRON FORMATIONS IN THE SCHREIBER-TERRACE BAY AREA.	3
TABLE 1:2	CLASSIFICATION OF ALGOMAN IRON-FORMATIONS.	10
TABLE 3:1	COMPOSITION OF METAVOLCANIC ROCKS ASSOCIATED WITH IRON- FORMATION.	63
TABLE 3:2	COMPOSITION OF METASEDIMENTARY ROCKS ASSOCIATED WITH IRON- FORMATION.	78
TABLE 3:3	COMPOSITION OF MAFIC INTRUSIVE ROCKS ASSOCIATED WITH IRON-FORMATION.	82
TABLE 3:4	COMPOSITION OF FELSIC INTRUSIVE ROCKS ASSOCIATED WITH IRON- FORMATION.	89
TABLE 4:1	COMPOSITION OF PYRITIC- CARBONACEOUS SHALE/SLATE IN THE IRON-FORMATION.	100
TABLE 4:2	COMPARISON OF LIGHT AND DARK CHERT LAYERS, MORLEY PROPERTY.	131
TABLE 4:3	COMPOSITIONS OF NON-SULPHIDE CHEMICAL RICH SEDIMENTS ASSOCIATED WITH IRON-FORMATION.	133
TABLE 5:1	COMPOSITION OF SULPHIDE MINERALIZATION CONCENTRATES FROM IRON-FORMATION.	150
TABLE 5:2	COBALT/NICKEL RATIOS: PYRITE CONCENTRATES.	151

LIST OF PHOTOGRAPHS

<u>PHOTOGRAPH</u>	<u>TITLE</u>	<u>PAGE</u>
FRONTISPIECE	VIEW OF BEDROCK EXPOSURE (KINGDOM PROPERTY) LOOKING NORTH TO SANTOY BAY, LAKE SUPERIOR.	ii
2:1	BEDDING - CLEAVAGE INTERSECTION LINEATION, KINGDOM SECTION.	19
2:2	DISRUPTED BEDDING ORIENTED ALONG CLEAVAGE AND THE DEVELOPMENT OF MICROLITHONS, KINGDOM SECTION.	19
2:3	FOLDING IN SEDIMENTARY ROCKS, WITH AXIAL PLANAR CLEAVAGE DEVELOPED, KINGDOM SECTION.	38
2:4	MINOR FOLDS IN PYRITIC-CARBONACEOUS SLATE (IRON-FORMATION), KINGDOM PROPERTY.	38
2:5	ALTERED PILLOW SELVAGES AND SELVAGE THICKENING ORIENTED ALONG CLEAVAGE, KINGDOM PROPERTY.	42
2:6	ERODED PILLOW OUTLINE: KINGDOM PROPERTY.	42
2:7	REFOLDED FOLD IN PYRITIC-CARBONACEOUS SLATE, BLACK FOX PROPERTY.	45
3:1	VARIOLITIC LAVA LEVEL DISPLAYING QUARTZ FILLED DRAIN AWAY LEVELS, JACKFISH PILLOW LAVA EXPOSURE.	61
3:2 (A)	SEDIMENTARY TEXTURES AND STRUCTURES: STEEL RIVER AREA.	61
3:2 (B)	RIP-UP CLASTS; STEEL RIVER AREA.	71
3:2 (C)	CROSS STRATIFICATION IN SILTSTONE LAYER, STEEL RIVER AREA.	71
3:3	PHOTOMICROGRAPH OF CHLORITE SCHIST WITH ZIRCON CRYSTALS, LITTLE STEEL HIGHWAY OCCURRENCE.	76
3:4	DURCHBEWEGUNG TEXTURE IN PYRRHOTITE, LITTLE STEEL HIGHWAY OCCURRENCE.	76
4:1 (A)	FOLDED TURBIDITE (SILTSTONE-SLATE) DISPLAYING AXIAL PLANAR CLEAVAGE AND PYRITE NODULE, BLACK FOX OCCURRENCE.	95

<u>PHOTOGRAPH</u>	<u>TITLE</u>	<u>PAGE</u>
4:1 (B)	PHOTOMICROGRAPH OF FOLDED TURBIDITE DISPLAYING GRAIN SIZE GRADATION AND AXIAL PLANAR CLEAVAGE, BLACK FOX OCCURRENCE.	95
4:2	PRESSURE SHADOW QUARTZ (BOEHM LAMELLAE) FORMING WEDGE OR LENS- SHAPED STRUCTURES, IN CONTACT WITH PYRITE NODULE, BLACK FOX OCCURRENCE.	104
4:3	TUFFACEOUS COMPONENT, INCLUDING VOLCANIC SHARDS AND FRAGMENTS WITHIN SILICEOUS SEDIMENTARY ROCK, LITTLE STEEL RAILWAY OCCURRENCE.	104
4:4	PHOTOMICROGRAPH OF ALTERNATING LAMINATIONS OF PYRITE, SILICEOUS SEDIMENT AND CLASTIC MATERIAL, SIMARD-SWETZ OCCURRENCE.	107
4:5	MASSIVE AND LAMINATED PYRITE, KINGDOM PROPERTY.	107
4:6	FINELY LAMINATED PYRITE, AS INTERPILLOW SEDIMENTARY ROCK, KINGDOM PROPERTY.	110
4:7	PHOTOMICROGRAPH OF LAMINATED PYRITE, DISPLAYING CHEMICAL AND CLASTIC RICH LAMINATIONS, KINGDOM PROPERTY.	110
4:8	FINELY LAMINATED PYRITE, DISPLAYING SLUMP STRUCTURES, BRECCIATION AND SHALE INTERCALATIONS, MORLEY PROPERTY.	112
4:9	MASSIVE PYRITE DISPLAYING LOAD CAST STRUCTURES, MORLEY PROPERTY.	112
4:10	PHOTOMICROGRAPH OF "BOX WORK"-LIKE TEXTURE OF PYRITE LAMINATION IN CONTACT WITH OXIDE-SILICATE-RICH LAMINATION, KINGDOM PROPERTY.	115
4:11 (A)	COLLOFORM OR CONCENTRIC NODULE IN PYRITIC-CARBONACEOUS SLATE, FINLAYSON LAKE AREA.	115
4:11 (B)	COLLOFORM NODULE DISPLAYING ALTERNATING CONCENTRICALLY BANDED PYRITE AND CLASTIC-RICH BANDS, MORLEY PROPERTY.	118



<u>PHOTOGRAPH</u>	<u>TITLE</u>	<u>PAGE</u>
4:11 (C)	PHOTOMICROGRAPH OF COLLOFORM NODULE, DISPLAYING PYRITE-RICH LAMINATIONS AND CLASTIC-RICH LAMINATIONS, MORLEY PROPERTY.	118
4:12 (A)	RADIAL NODULE, MORLEY PROPERTY.	120
4:12 (B)	DEFORMED NODULAR PYRITE LAYER, BLACK FOX LAKE OCCURRENCE.	120
4:12 (C)	NODULAR PYRITE WITH QUARTZ PRESSURE SHADOWS, BLACK FOX LAKE OCCURRENCE.	123
4:12 (D)	REVERSE SIDE OF 4:12 (C) DISPLAYING REDUCTION IN SIZE OF PYRITIC AREA (CORRODED NODULE), AND AN INCREASE IN SIZE OF SILICEOUS AREA, BLACK FOX LAKE AREA.	123
4:13	INCREASED DEFORMATION OF PYRITE NODULE LAYER, BLACK FOX LAKE OCCURRENCE.	125
4:14 (A)	ALTERNATING DARK AND LIGHT LAMINATIONS IN CHERT, MORLEY PROPERTY.	125
4:14 (B)	PHOTOMICROGRAPH OF DARK AND LIGHT COLORED CHERT LAMINATIONS, MORLEY PROPERTY (UNCROSSED NICOLS).	129
4:14 (C)	PHOTOMICROGRAPH OF DARK AND LIGHT COLORED CHERT LAMINATIONS, MORLEY PROPERTY (CROSSED NICOLS).	129

## 1) INTRODUCTION

### LOCATION OF THE STUDY AREA (LOWER STEEL RIVER - LITTLE STEEL LAKE AREA)

The Lower Steel River - Little Steel Lake area is located about 250 km by road east of Thunder Bay, Ontario, and 25 km east of the community of Terrace Bay (Figures 1:1, 1:2). This 10 km<sup>2</sup> area lies northeast of Santoy Bay, Lake Superior, and forms part of the Abitibi-Wawa Subprovince of the Superior Structural Province. (Figure 1:3). The area contains several good exposures of Algoman-Type banded iron-formation within a relatively complex geological setting. Excellent outcrop exposure along Highway 17, the C.P.R. line and the shore of Lake Superior is accessible by road, rail and water. The area has been previously mapped at a scale of 1 : 31,680 by Walker (1967).

Seventeen occurrences of iron-formation within a 30 km radius of the Lower Steel River were investigated in order to facilitate a more complete understanding of iron-rich rocks in the district (Figure 1:2, Table 1:1).

### GENERAL GEOLOGY

The Schreiber-Terrace Bay area is underlain by Early to Late Precambrian rocks (Map 1, in pocket). The Archean rocks consist of a metavolcanic-metasedimentary sequence which has been intruded by granitic-syenitic plutons and metagabbroic dikes and sills. The metavolcanic rocks include mafic massive and pillowed flows, mafic tuff, and felsic pyroclastic rocks. The metasedimentary rocks consist predominantly of graded turbiditic sequences (poorly sorted sandstone and argillite), minor conglomerate and iron-formation.

# LOCATION MAP SHOWING THE SCHREIBER-TERRACE BAY STUDY AREA

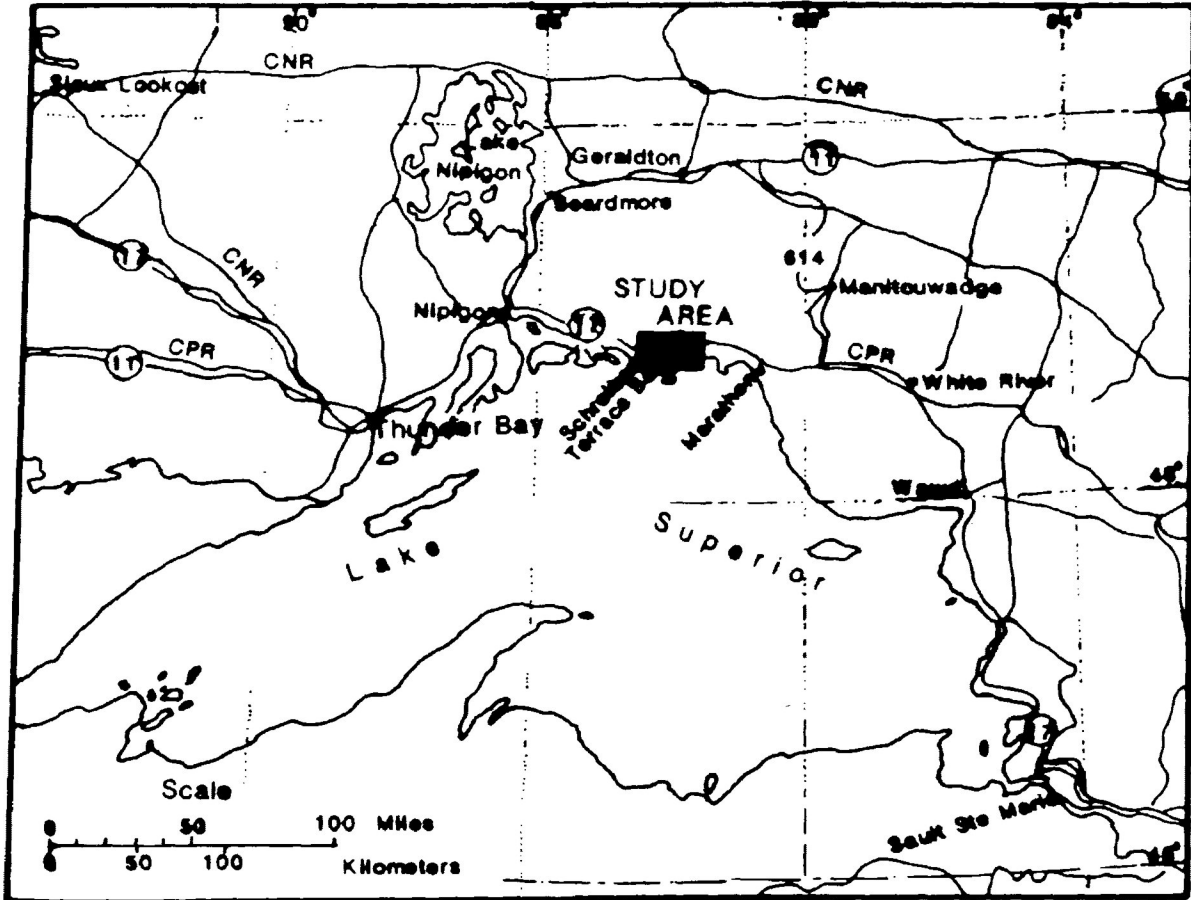


FIGURE 1:1

**CHEMICAL SEDIMENTARY ROCKS AND IRON FORMATIONS  
IN THE SCHREIBER-TERRACE BAY AREA**

**TABLE 1:1**

<b>OCCURRENCE</b>	<b>WORK PERFORMED</b>
1. Black Fox	Detailed
2. Bozena Lake	-
3. Cumberland	-
4. Downey East	Reconnaissance
5. Downey West	Reconnaissance
6. Elwood	-
7. Empress	-
8. Goldbar Lake	Reconnaissance
9. Harkness-Hays	Detailed
10. Kingdom	Detailed
11. Lamont Lake	-
12. Little Bruin	Reconnaissance
13. Little Santoy	-
14. Little Steel Highway	Detailed
15. Little Steel Railway	Detailed
16. Morley Pyrite	Detailed
17. Morley Road	Reconnaissance
18. Otisse	-
19. Otisse Sulphur	-
20. Schreiber Beach	Reconnaissance
21. Schreiber Pyramid	-
22. Schreiber Rail	Reconnaissance
23. Schreiber Road	Reconnaissance
24. Silver Sceptre	Reconnaissance
25. Simard-Swetz	Detailed
26. Victoria Lake	-
27. Von Lake	-
28. Wildrose	Reconnaissance

**FIGURE 1:2**

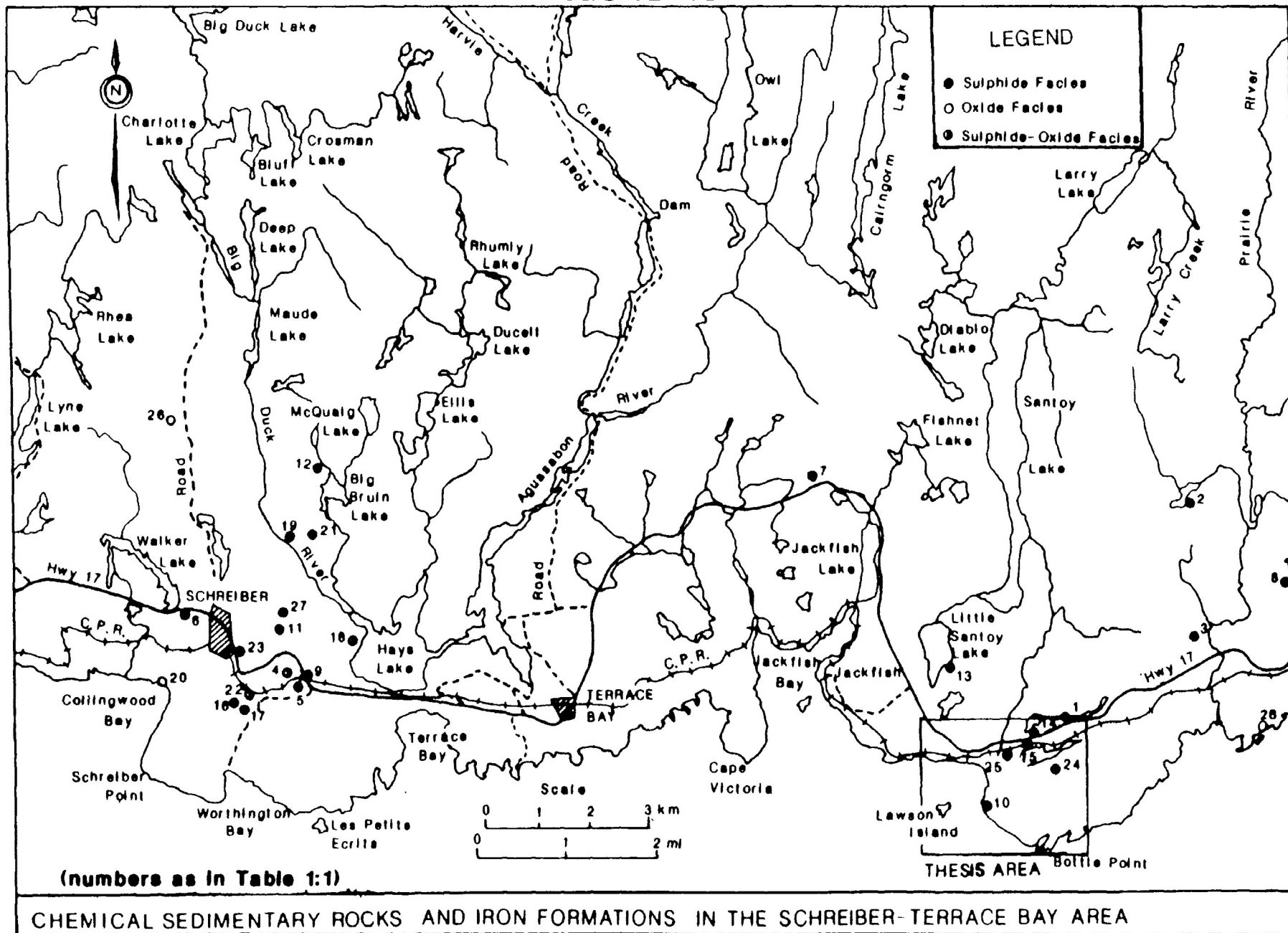
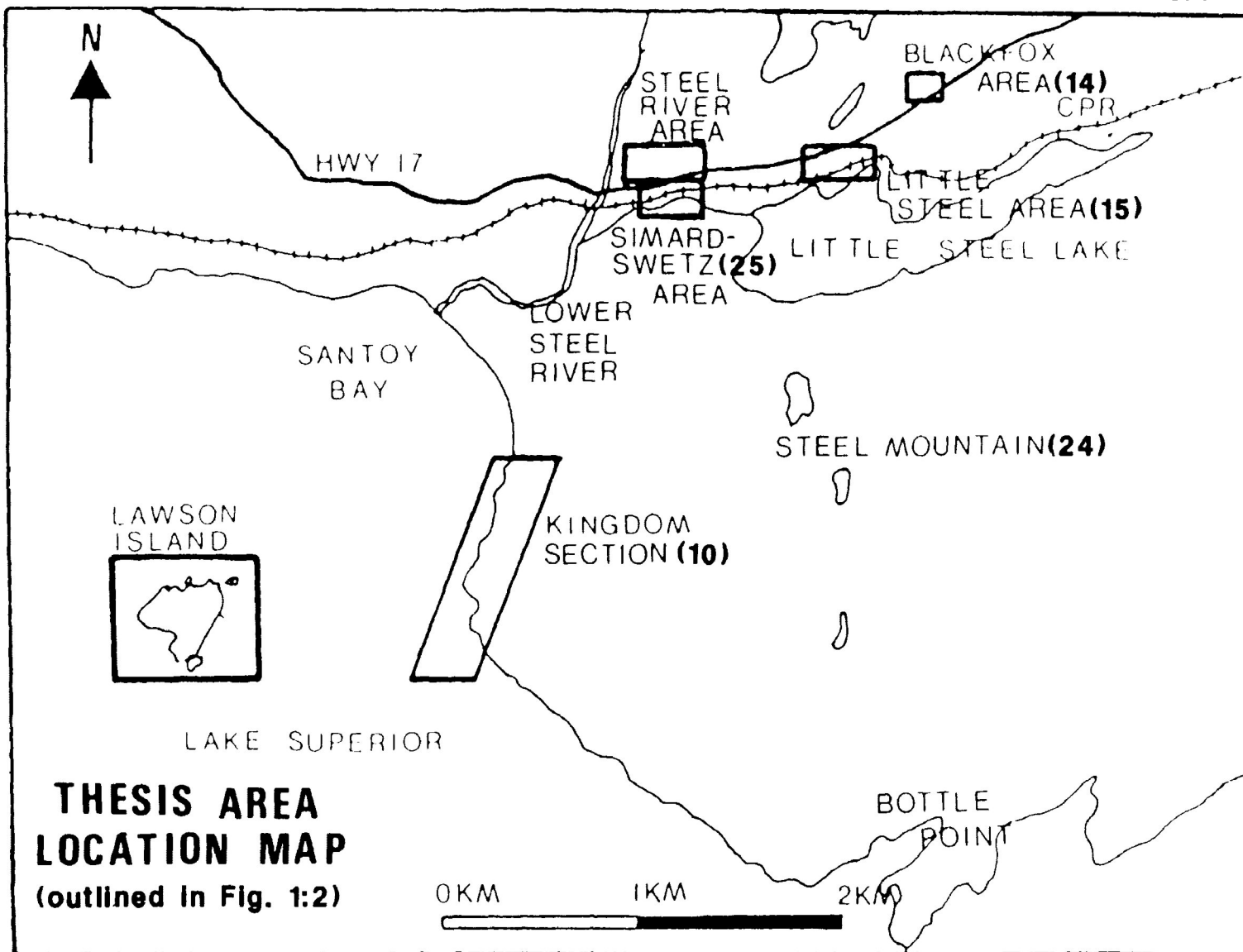


**Figure 1:3**

**LOWER STEEL RIVER - LITTLE STEEL LAKE AREA**



**THESIS AREA  
LOCATION MAP**  
(outlined in Fig. 1:2)

Mafic intrusive rocks include metagabbroic, metadioritic and local ultramafic sills, dikes and tabular stocks. Whether these rocks represent late intrusions, low level feeders to the mafic metavolcanic rocks, or coarse-grained portions of mafic metavolcanic flows, is generally unknown (Walker, 1967).

Felsic bodies such as the Terrace Bay Batholith intrude the metavolcanic and metasedimentary rocks. This 25 km long by 8 km wide batholith consists predominantly of medium-grained granodiorite, and minor dioritic to granitic rocks (Marmont, 1984).

Middle Precambrian rocks unconformably overlie the Early Precambrian succession. The Animikie Group, which includes the Gunflint and Rove Formations, consists of conglomerate, greywacke, algal chert, ferruginous and dolomitic chert-carbonates (Superior-Type Iron-Formation), black pyritic shale, argillite, tuff and minor basalt.

Late Precambrian sedimentary rocks disconformably overlie Early and Middle Precambrian units. The Sibley Group, which includes the Pass Lake, RosSPORT and Kama Hill Formations, consists of conglomerate, sandstone, dolomite, chert and mudstone. Keweenawan rocks are represented by Logan diabase, gabbro, peridotite and the Osler Group. The Osler Group is composed of tholeiitic basalts, minor rhyolite, and conglomeratic interflow sediments.

Late Precambrian intrusive rocks consist of alkalic and carbonatite complexes such as the Port Coldwell Alkalic Complex and the Prairie Lake Carbonatite, as well as mafic to felsic dikes.

## PURPOSE OF THE STUDY

The purpose of this study was to use a combination of stratigraphic, sedimentological and geochemical methods to document and interpret the various depositional environments of iron-formations in the Lower Steel River - Little Steel Lake area.

The study additionally supplements the database on banded iron-formations, providing information on: a) geological settings, b) stratigraphy, c) geometry and structure, d) sedimentology, e) genesis, and f) depositional environments.

## METHODS OF INVESTIGATION

Field and laboratory methods in the present study include analysis of assessment data, reconnaissance and detailed mapping, detailed logging, sampling, petrologic and mineralogic studies, and major and trace element geochemistry. Geochemical analyses were performed at Lakehead University and at the Geoscience Laboratories, Ontario Geological Survey, Toronto.

Mapping was conducted at scales of 1:31,680 and 1:1,200 during the field seasons of 1983, 1984 and 1985. Detailed mapping and logging of outcrops, trenches and stratigraphic sections was performed at a scale of 1:100. Some 200 rock samples were collected from the study area of which 100 were slabbed or cut with a diamond saw, and 50 were polished or spray-coated. The importance of slabbed sections when studying iron-formations cannot be overly emphasized. Few primary structures are observable in unslabbed or uncut field samples. In addition,



approximately 50 thin sections and 40 polished thin sections were studied.

## EXPLORATION HISTORY

To aid with the study of the Lower Steel River - Little Steel Lake area, an assessment search was carried out. This provided data on the exploration history and previous work, as well as information on the locations of iron-formations. Appendix C summarizes the data from the Resident Geologist's Files, Ontario Ministry of Northern Development and Mines, Thunder Bay.

## CLASSIFICATIONS AND STUDIES OF OTHER IRON-FORMATIONS

### Classifications

During the past 30 years, numerous classifications have been proposed for iron-formations. Two major types of Precambrian banded iron-formations were suggested by Gross (1965);

1) Algoman-Type: iron-rich rocks generally greater than 2.5 - 2.6 billion years in age, deposited in a tectonically active geosynclinal environment.

2) Superior-Type: iron-rich rocks ranging in age from 1.8 to 2.5 billion years, deposited in a tectonically stable basin, and usually containing sedimentary structures similar to carbonate rocks.

Gross (1965) further classified iron-formations based on the following parameters; 1) geometry, 2) internal structure, and 3) present mineralogy.

Shegelski (1978) modified Gross's (1965) classification on the basis of the iron-formations he studied in the Sturgeon Lake -

Savant Lake area, and created a fourth parameter for Archean iron-formations, that of the host or associated rocks.

Shegelski's modified version of Gross's classification of Archean iron-formations is displayed in Table 1:2.

Shegelski (1971) noted that in lacustrine environments hydrated iron oxides were precipitated at the water-sediment interface, but upon burial were converted into metastable sulphides and eventually into pyrite. Thus iron sulphides can be formed within a sediment which initially accumulated in oxidizing waters. Dimroth (1975) suggested that depositional environments and diagenetic processes are the major factors controlling the mineralogy of iron-formations.

Gross (1965) and Shegelski (1978) defined three types of Algoman iron-formation associations, as shown in Table 1:2 (see also Gross, 1980): 1) mafic to felsic volcanic association; 2) felsic volcanic association; and 3) graded greywacke-siltstone association.

Dimroth (1975) classified iron-formations on the basis of: i) sedimentary structures, ii) associated rocks, and iii) internal structures of the iron-formation. Dimroth (1977a) further defined a two-fold facies classification system based on: i) sedimentary structures and textures, and ii) mineralogy. Other classifications have been based on: i) chemical characteristics (Beukes, 1973), ii) physical characteristics (Wolf, 1980); and iii) facies associations (James, 1954; Eichler, 1976; Dimroth, 1977a)

TABLE 1:2

Classification of Algoman Iron Formations

(Shegelski, 1978; modified after Gross, 1965)

<u>Parameter for Classification</u>	<u>(i) Mafic to Felsic Volcanic Association</u>	<u>(ii) Felsic Volcanic Association</u>	<u>(iii) Graded Greywacke-Siltstone Association</u>
(a) Host Rock	pillowed basalt, andesite felsic flows or pyroclastics	felsic flows or pyroclastics, volcaniclastics, minor greywackes	graded greywackes, siltstones and pelites
(b) Geometry*	thickness: length approx. 1: 100 thickness: 30 m - 300 m  en echelon lenses between host rocks	thickness: length approx. 1: 100 thickness: 15 m  interlayered sequences with host rocks and with Algoman type (i)	thickness: length approx. 1: 1000 to 10,000 thickness: 15 cm  thin laminated beds inter-layered with host rocks
(c) Internal Structure (primary)	banded (beds 1 cm) and minor laminations	banded or laminated; also nodules and disseminations	laminated (down to .03 mm); rarely banded
(d) Present Mineralogy (major)	oxides, silicates carbonates and sulphides of iron interbanded with chert	graphite, iron sulphides, minor chert, magnetite plus clastic component	iron oxides (magnetite predom.), chert, minor pyrite plus chlorite
Chemical and/or Clastic Facies Component	chemical: mixed, major clastic: minor	chemical: sulphide, major organic carbon, minor clastic: tuff-shale, major	chemical: oxide, major chemical or clastic: silicates, minor

\* Dimensions are only rough approximations as there is great variability in geometry among these three types of deposits

## Facies Associations : Depositional Environments

The facies concept was first applied to iron-formation by James (1954). It was used to classify iron-formation depending whether iron oxide, silicate, sulphide or carbonate minerals dominated.

Sequences of oxide - carbonate - silicate - sulphide-facies iron-formations have been interpreted to represent the progression from a shallow water, oxidizing environment of deposition to a deep water, reducing environment (Gross, 1965; James, 1966; Walker 1967). However, Shegelski (1978) suggested the sulphide-facies iron-formation could be associated with submarine volcanic calderas and their flanks, while oxide-facies were deposited in association with pelites and greywackes at greater depths in the basin.

Fralick (in press) has postulated that the differences in mineralogy, internal structure and thickness of the layering of iron-formations in the Beardmore-Geraldton area may be due in part to the distance of the depositional site from the exhaling hydrothermal solutions. Clearly, care must be taken when using chemical facies of iron-formations in attempting to determine the depositional environment.

The sulphide-facies has been the most controversial classification of iron-formation over the past two decades. James (1966) used the term "sulphide-bearing graphitic slate" to refer to pyritic-carbonaceous shales, whereas Dimroth (1977a) employed the term "iron-rich shales". Shegelski (1978) noted that while many pyritic-carbonaceous shales contain more than 15 percent iron, they were dominated by a clastic component and should be

termed "iron-rich shales" rather than iron-formation. Pyritic-carbonaceous shales or sulphide facies iron-formation can occur in two of the three main lithological associations (Table 1:2) suggested by Shegelski (1978);

1) Algoman Mafic to Felsic Association (Mixed Facies). The iron-formation is generally well banded (layers greater than 1 cm thick) but poorly laminated (less than 1 cm thick). The mineralogy is diverse, consisting of iron oxides, sulphides, silicates and carbonates; chert and carbonaceous shale are also associated. These iron-formations, which are associated with volcanic successions, are considered to be a mixed facies. Thick accumulations of chemical sediment indicate that abundant iron and silica were supplied. Volcanic hydrothermal exhalations are favoured for the source of the iron.

2) Algoman Felsic Volcanic Association (Sulphide Facies). Pyritic-carbonaceous shales less than 15 m thick are commonly associated with felsic pyroclastic piles. The shales are massive or laminated, highly carbonaceous, and contain accumulations of iron sulphides as disseminations, layers and nodules. Minor sulphides also occur within turbiditic sedimentary rocks and mafic volcanic rocks. They generally appear to be spatially associated with the proximal flanks of felsic volcanoes (Shegelski, 1978).

## Sources of Iron : Genetic Models

The source of the iron and chemical components in iron-formations have been a controversial topic. The two main theories proposed are:

1) Volcanic association - exhalative hydrothermal source. Iron is introduced during volcanic activity by fumaroles or hot springs; it is derived from leaching of the underlying volcanic rocks, (Goodwin, 1962; Gross, 1965; Cloud, 1973; Sangster and Scott, 1976; Shegelski, 1978). Shegelski (1978) suggested that the main period of exhalative activity occurred late in the volcanic cycle, with most chemical sediment deposition during a quiescent period following the volcanic interval.

2) Biogenic association - leached sedimentary source. Iron is derived through erosion, leaching of the continents, and transported by drainage systems to a marine environment. The iron is eventually precipitated from seawater as a result of biogenic activity, possibly due to algal blooms (Beukes, 1973; Eugster and Ming, 1973; Drever, 1974).

Simonson (1985) worked on several Precambrian iron-formations in the Lake Superior area, and examined three genetic models: evaporative, biogenic and hydrothermal (volcanic-exhalative). He concluded that the only genetic hypothesis that appeared to be consistent with all of the sedimentological constraints is the hydrothermal model.

In a paper relevant to the sulphide-facies iron-formations of the present study, Williams et al. (1982) emphasized the important sulphide-producing process of dissimilatory sulfate

reduction, in which organic compounds (or H<sub>2</sub>S) are oxidized and sulphate is simultaneously reduced to hydrogen sulphide. These authors noted that the formation of pyrite is complex, involving several reactions between iron and sulphide, and producing iron monosulphide phases such as mackinawite and sulphur-rich phases such as greigite. Conditions for the formation of biogenic sulphide concentrations occur today in stratified, anoxic basins like the Black Sea.

Williams et al. (1982) also examined exhalative and biological processes which could produce highly pyritic, base metal-poor deposits. The interaction between seawater and hot metal-rich fluids, as in "smokers" at seafloor spreading ridges can favor establishment of local biological communities which may aid in the production of biogenic sulphides. The existence of biological matter around Precambrian seafloor vent sites may provide an explanation for the abundant carbonaceous matter associated with numerous stratiform sulphide deposits, including the pyritic-carbonaceous slate facies of the study area.

Pandalai et al. (1983) described a Precambrian bedded pyrite deposit hosted by black carbonaceous shales in India. Co/Ni ratios of the massive pyrite support a non-biogenic origin, and suggested that much of the iron probably was contributed by submarine exhalative activity.

## 2) STRUCTURAL GEOLOGY

### INTRODUCTION

In order to carry out any study on iron-formation in the region, it is a prerequisite to understand the structure. Such structural knowledge is necessary to determine the original stratigraphic relationships, and therefore to make an assessment of the depositional environments of the chemical and clastic metasedimentary rocks.

Walker (1967), on the basis of reconnaissance mapping in the Jackfish-Middleton Area, found that while the iron-formations reflect the general structure locally, they are neither laterally continuous nor sufficiently distinctive to serve as reliable marker horizons. Walker (1967, Map 2107) reported a northeast to east structural trend between Jackfish Bay and Middleton which swings into a northwesterly trend between Santoy Lake and the Aguasabon River. He recorded easterly trending isoclinal folds with subhorizontal-plunging fold axes. Based on local top indicators, Walker suggested that the metavolcanic rocks stratigraphically overlie the metasedimentary rocks in the Bottle Point and Kingdom Area (Map 1). He also interpreted the structure between Jackfish Bay and the lower Steel River (Figure 1:2) as an easterly plunging anticline. South of Jackfish Bay, upright folds occur, whereas east of Little Santoy Lake these structures are overturned 60 degrees to the south.

### STRUCTURAL ELEMENTS

A detailed structural analysis of the entire thesis area was not the object of this study. In any case, only localized areas



contain the required structural elements. These locations are the Kingdom, Lawson Island, Steel River and Blackfox Areas (Figure 2:1). Although structural interpretations and conclusions are based on data from these areas, they may be applicable to regional structural relationships.

The Kingdom Area represents an area of about  $0.25 \text{ km}^2$ , underlain by metavolcanic and metasedimentary rocks. Since all rocks in the area have been metamorphosed the prefix "meta" will be deleted. Sedimentary rocks consist of well-stratified greywackes, siltstones, shale, slate and iron-formation. Orientations of bedding planes (So) were readily determined and graded bedding provided younging directions in the sedimentary rocks. These strata are in contact with a sequence of volcanic rocks composed of mafic pillowed, amygdaloidal and massive flows. Younging directions were difficult to define in the pillowed metavolcanic rocks and impossible to determine in the more massive flows.

Cleavage (S1) is well developed in the fine-grained siltstones and slates. This cleavage is less obvious in outcrops of the coarser-grained sedimentary and volcanic rocks. Thin section examination indicates that only one dominant cleavage is present in all sedimentary rock types.

Bedding-cleavage intersection lineations (Photo 2:1) and orientations of minor fold axes were recorded wherever possible. Where direct measurements could not be made, the lineation was obtained stereographically from the intersection of cleavage and bedding. The constructed orientations are close to the observed values. Small-scale conjugate kinks, similar folds and ptygmatic folds occur in the finer-grained and finely laminated rocks.

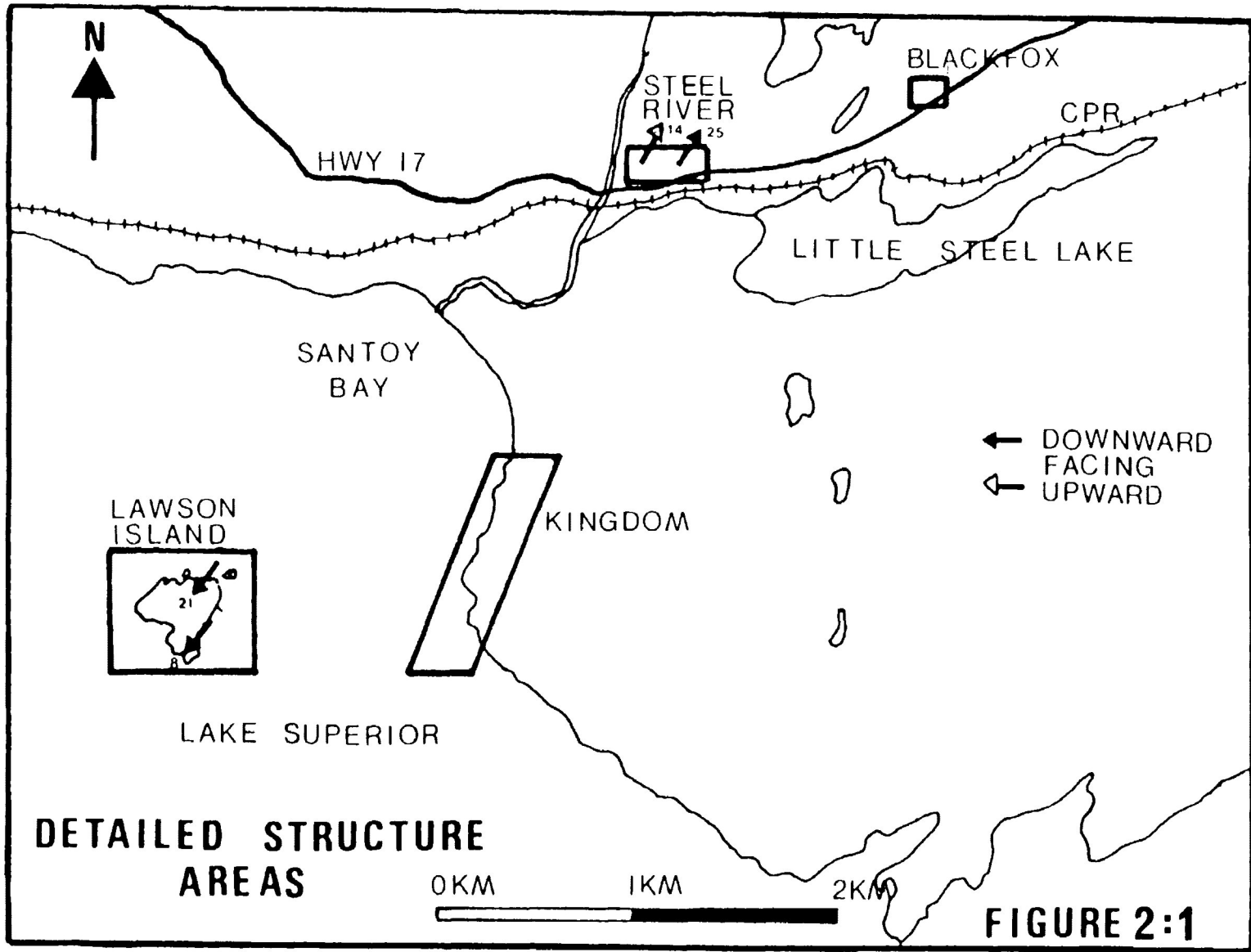
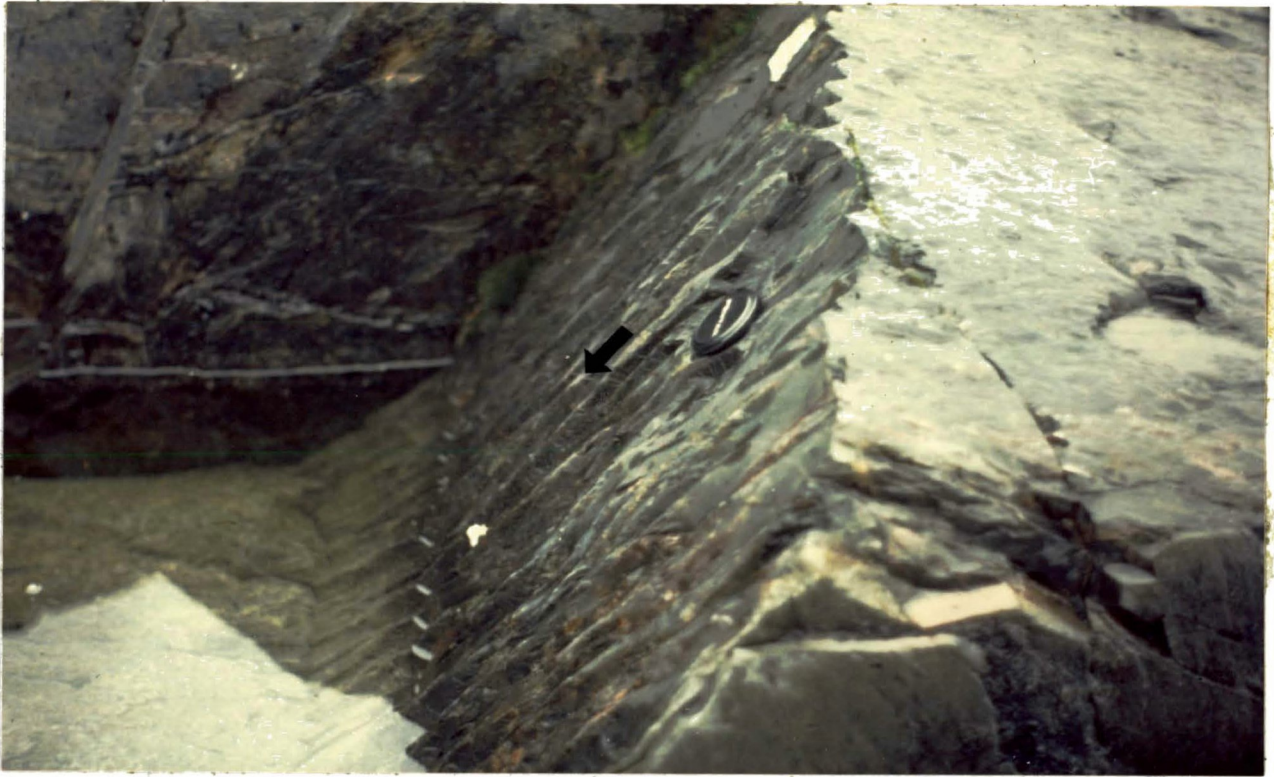


**PHOTO 2:1**      BEDDING - CLEAVAGE INTERSECTION  
LINEATION (ARROW,  $S_0/S_1$ ), KINGDOM  
SECTION.

**PHOTO 2:2**      DISRUPTED BEDDING (DB) ORIENTED ALONG  
CLEAVAGE AND THE DEVELOPMENT OF  
MICROLITHONS (M), KINGDOM SECTION.

COLOUR PHOTOGRAPHS SHOULD NOT BE USED. THEY WILL APPEAR AS GREY OR BLACK. WE RECOMMEND THAT THE COPY OF THE THESIS SUBMITTED FOR MICROFILMING INCLUDE BLACK AND WHITE PHOTOGRAPHS REPRINTED FROM THE COLOUR PHOTOGRAPHS BY A PHOTOGRAPHER IF NECESSARY.

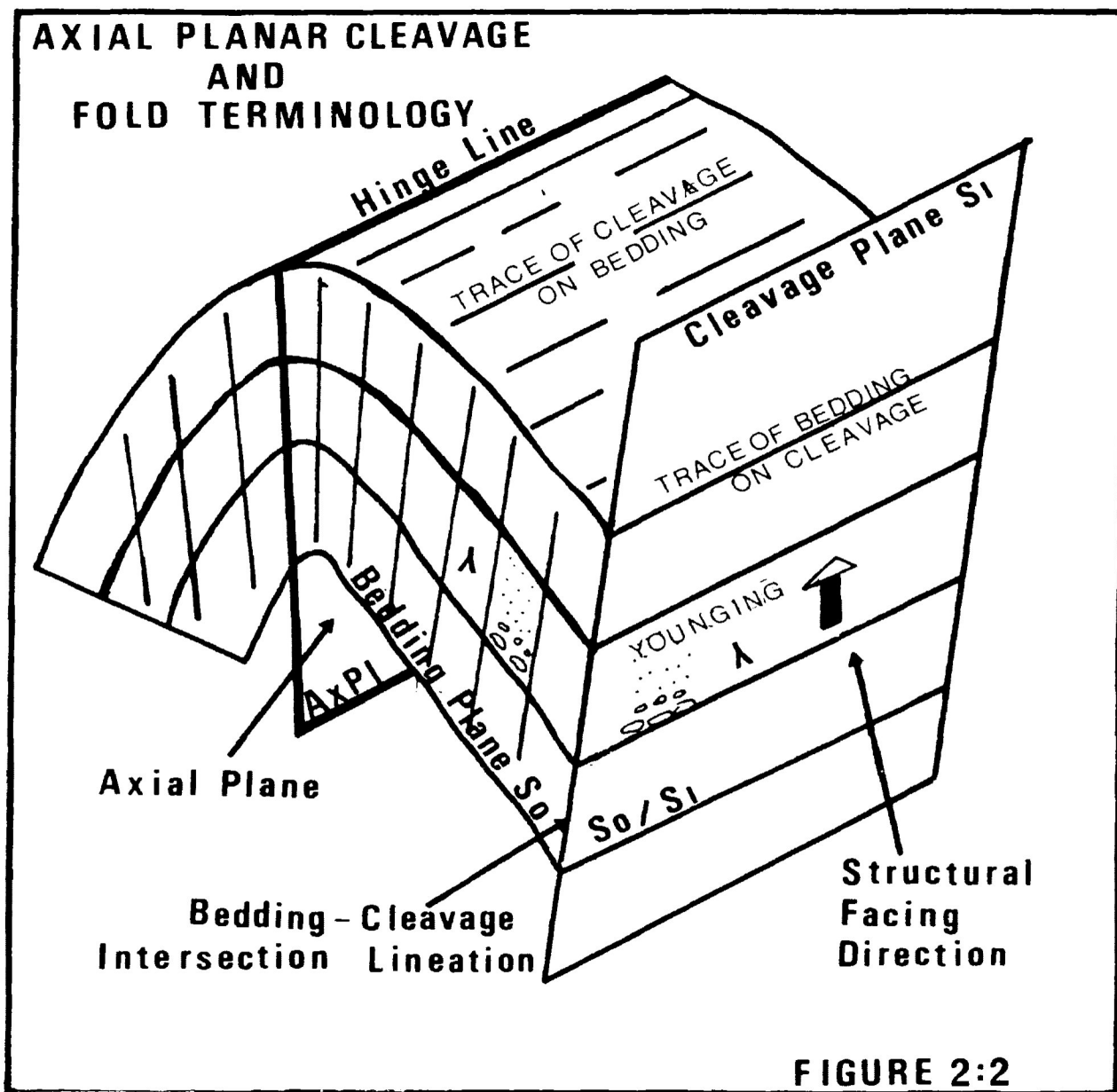
LORSQUE MICROFILMEES, LES PHOTOGRAPHIES EN COULEUR PARAISSENT GRISES OU NOIRES. NOUS RECOMMANDONS QUE L'EXEMPLAIRE DE LA THESE A MICROFILMER SOIT ACCOMPAGNE PLUTOT DE PHOTOGRAPHIES EN NOIR ET BLANC PRODUITES A PARTIR DES PHOTOGRAPHIES EN COULEURS PAR UN PHOTOGRAPHE, SI NECESSAIRE.



**FOLDS**

Structural mapping in rocks of the Kingdom Area utilized several techniques, including use of axial planar cleavage, the cleavage-bedding and intersection lineation rules and the concept of structural facing of folds (Borradaile, 1976, 1980). Figure 2:2 displays the axial planar cleavage model and fold terminology. Some structural concepts are outlined briefly below.

- i) Cleavage-Bedding Rule: When the cleavage-bedding angle and bedding orientation differ in two separate outcrops in a singly folded region, a fold must lie between the two.
  
- ii) Intersection Lineation Rule: A consequence of the axial planar cleavage model is that the cleavage and bedding intersect in a line which is parallel to the hinge-line of the folds of a single phase. Borradaile (1980) stated that this is only strictly true if the fold's profile is consistent in shape at various points along the hinge. The measurement of these lineations at different outcrops can therefore be used to indicate the trend of the hinge-line of the major folds in that area.
  
- iii) Structural Facing of Folds: Cummins and Shackleton (1955) first suggested and used the concept of structural facing in the Southwest Highlands of Scotland, and Shackleton (1958) expanded the idea and defined the younging direction for strata at the hinges of primary folds (Shackleton's Rule). Borradaile (1976) extended the application of structural facing by showing that the facing direction of primary folds can be obtained at any point on a folded surface by projecting the younging direction on that point onto an axial planar cleavage. If the cleavage is axial



planar, then the component of the younging direction when projected onto it, is always parallel to the facing direction of the folds. Figures 2:3A through D exhibit the concept of structural facing.

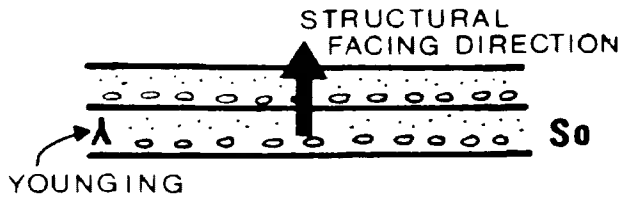
Borradaile (1976) also noted that, in the absence of pronounced plunge variations, the structural facing direction of the first deformation phase can reflect the direction in which the stratigraphy as a whole is getting younger (although local younging directions when measured around a folded sequence will vary considerably). Kehlenbeck (1986) described examples of this in the Beardmore-Geraldton Area, where local younging directions vary widely in orientation. Kehlenbeck (1984) advised caution in using localized data to infer stratigraphic younging direction over a large area. This is an important factor to consider in Walker's (1967) stratigraphic and structural interpretations of the study area, and will be discussed in a later section.

Borradaile (1976) suggested that reversals in the structural facing of folds of a given generation make it possible to identify areas where stratigraphy was previously affected by deformational episodes, such as slumping or even recumbent folding. Such reversals could also be attributed to sheath folds (Cobbold and Quinquis, 1980) and examples of reversals have been illustrated by Borradaile (1982) in the Flanders Area.



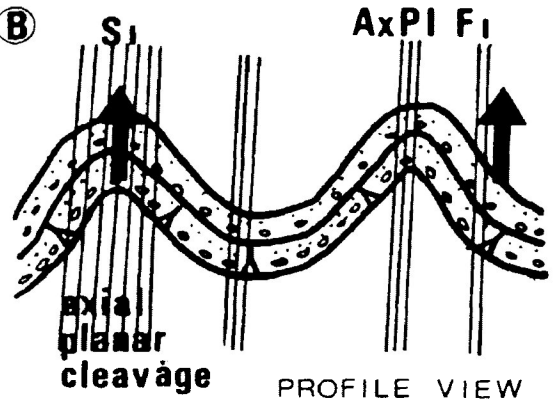
**STRATIGRAPHIC SEQUENCE**

**FIGURE 2:3 (A)**



**FOLDED SEQUENCE**

**(B)**



**GRADED BEDS**

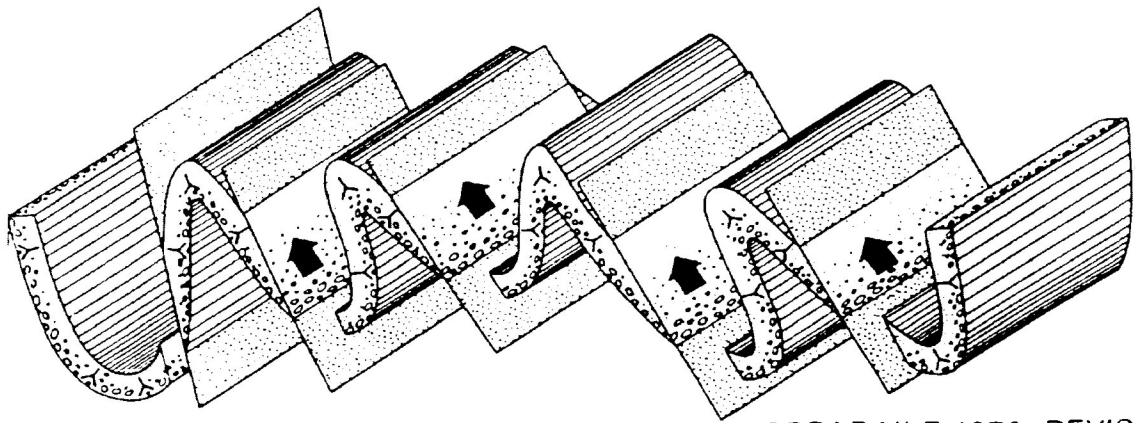
**STRUCTURAL FACING IN A SET OF FOLDS**

**(C)**

Way-up or younging  
 local top direction  
 of individual beds
 

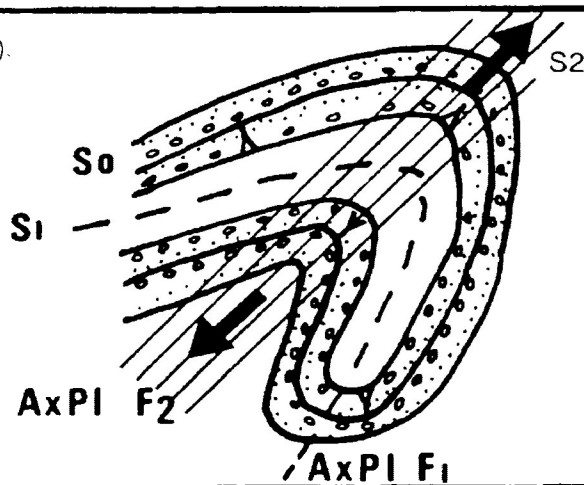

 Structural facing  
 way-up of the  
 stratigraphic sequence
 


 Cleavage / schistosity  
 surface parallel to  
 axial plane of folds



BORRADAILE 1976, REVISED

**(D)**



**REFOLDED FOLD**

**Note the Reversal in the Structural Facing Direction**

## DOMINANT FOLDS

In the Kingdom Area, folds up to several metres in amplitude and wavelength are evident in the sedimentary rocks. Hinge lines generally trend E-NE or W-SW and vary in plunge from 35 degrees to vertical. Minor folds commonly trend NE and have shallow plunges up to 30 degrees. Folds range from sideways-closing or neutral folds (Ramsay, 1967) to antiformal and synformal structures.

A pervasive, well developed cleavage (S1) is present in the Kingdom Area. At fold hinges, the S1 cleavage is coplanar, or almost so, with the axial plane of the folds. Borradaile (1978) has shown that where non-axial planar cleavage exists, as in transected folds, the intersection lineations vary systematically in orientation. Bedding-cleavage intersection lineations in the opposite limbs of single folds from the Kingdom Area are essentially coaxial (Figure 2:4H). Thus the S1 cleavage represents an axial planar cleavage to a dominant set of folds.

Structural facing of dominant folds in the Kingdom Area was obtained from exposures where bedding, cleavage and local younging could be recorded. In several outcrops, fold hinges are exposed and permit direct measurements of the structural facing. Elsewhere, the cleavage forms near-vertical surfaces which display the trace of the bedding and the local younging direction (Photo 2:1). Structural facing directions were also obtained stereographically and from tectonic profiles.

## DETAILED STRUCTURAL ELEMENTS OF THE LOWER STEEL RIVER-LITTLE STEEL LAKE AREA

Four separate localities containing important structural elements were identified at Kingdom Areas 1 through 6, Lawson Island, Steel River and Blackfox Lake (Figure 2:1). The Kingdom locality contained some of the best exposures and therefore was subjected to the most detailed study. Most of the structural elements described above are shown in Figures 2:4 and 2:5.

### 1) KINGDOM AREA

Area 1: Average bedding and cleavage attitudes are shown in Figure 2:4 (i). Minor fold axes of symmetric M and W folds in the northern section of Area 1 commonly trend 65 to 70 degrees and plunge 30 to 40 degrees. Figure 2:4 (A) (see Figure 2:4 for location) shows an outcrop sketch of this area, together with a lower hemisphere equal area projection, a tectonic profile and the structural facing direction; these figures also illustrate the bedding-cleavage relationship. Structural facing directions are down to the southwest, varying in plunge from 40 to 58 degrees (Figure 2:5). This suggests that the folds are either antiformal synclines or synformal anticlines. The downward plunge of the structural facing direction appears perpendicular to the hinges of minor folds.

The northern and southern sections of Area 1 are separated by a northeast-striking, subvertical shear zone about 1 metre wide, which is developed in the fine-grained slates.

In the southern section of Area 1 axes of minor folds vary in trend and plunge (Figure 2:4B). Structural facing directions are

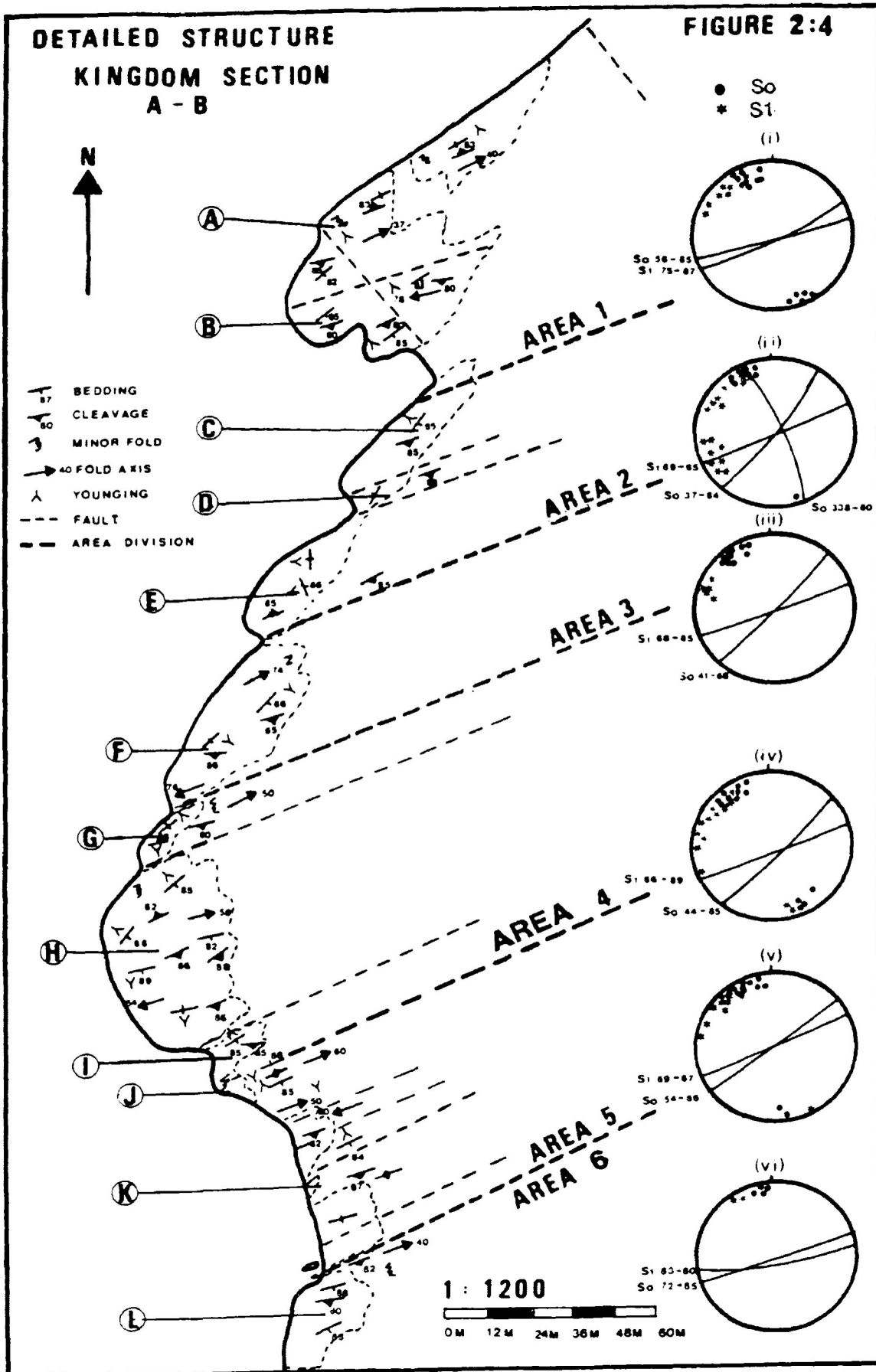


FIGURE 2:4 (A)

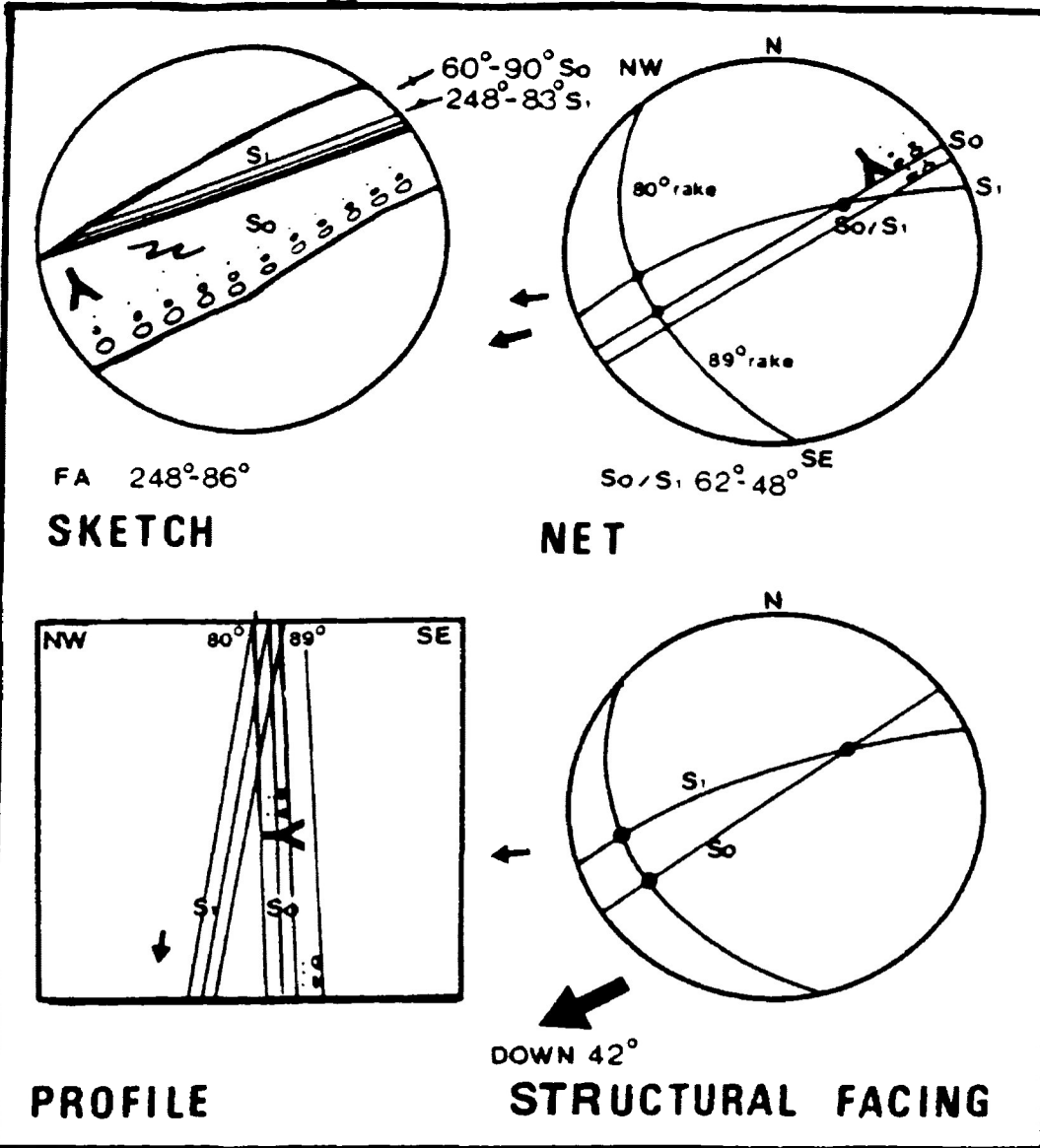


FIGURE 2:4 (B)

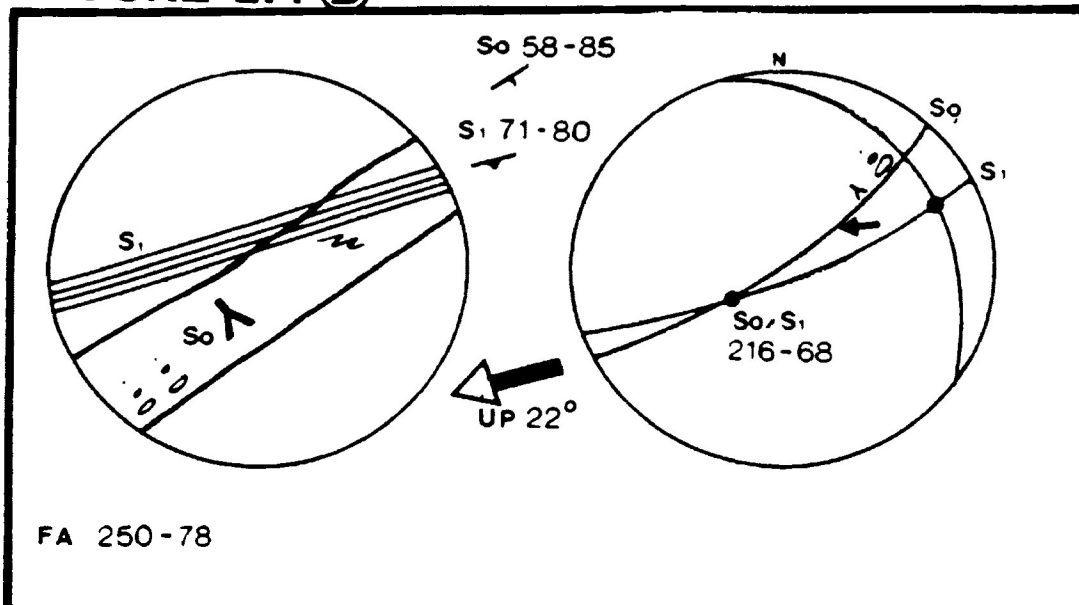
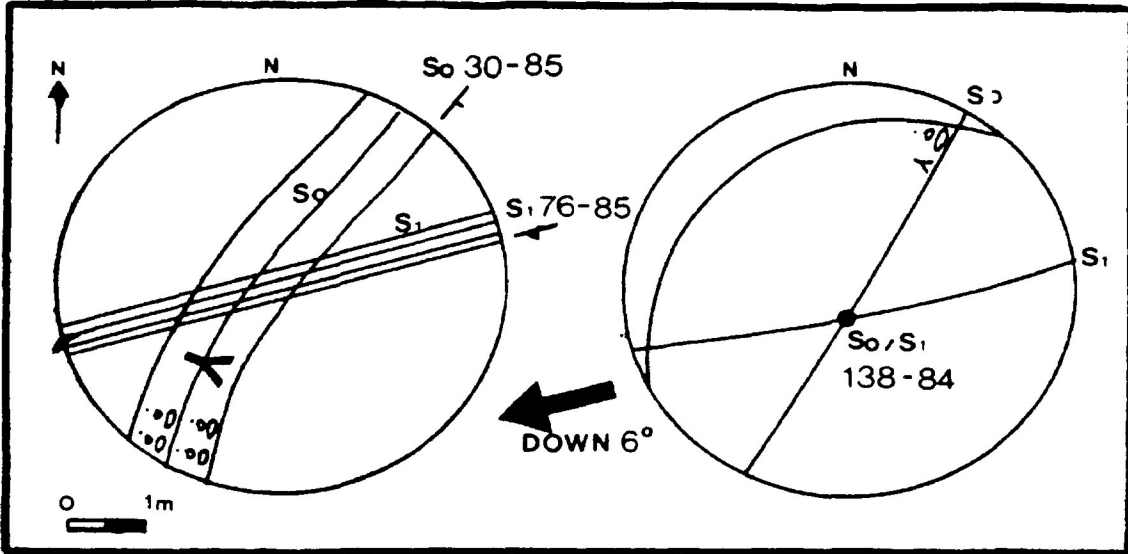
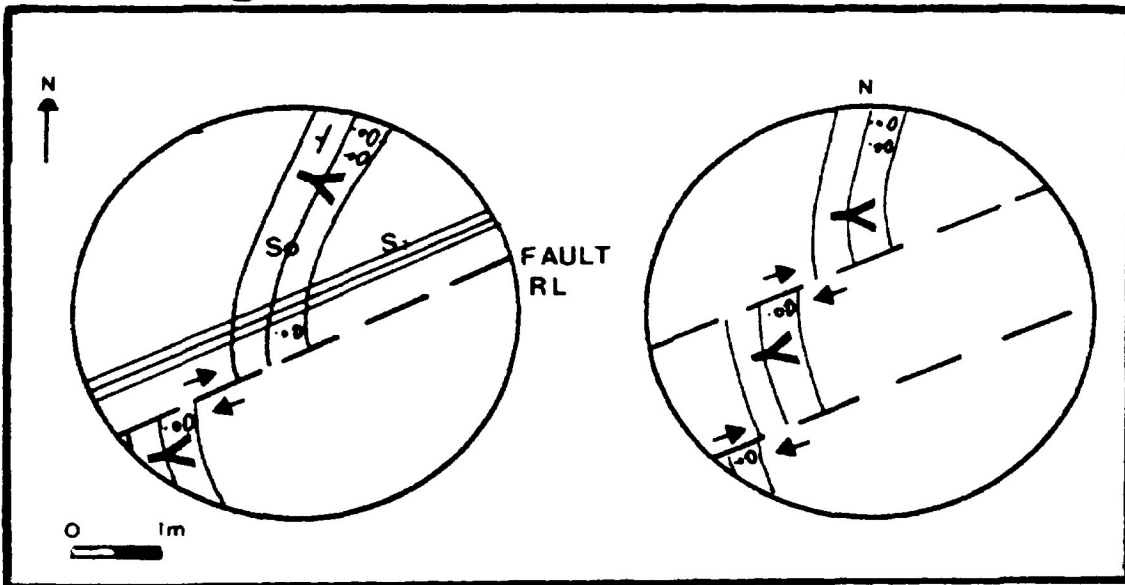


FIGURE 2 : 4 (C)



(D)



(E)

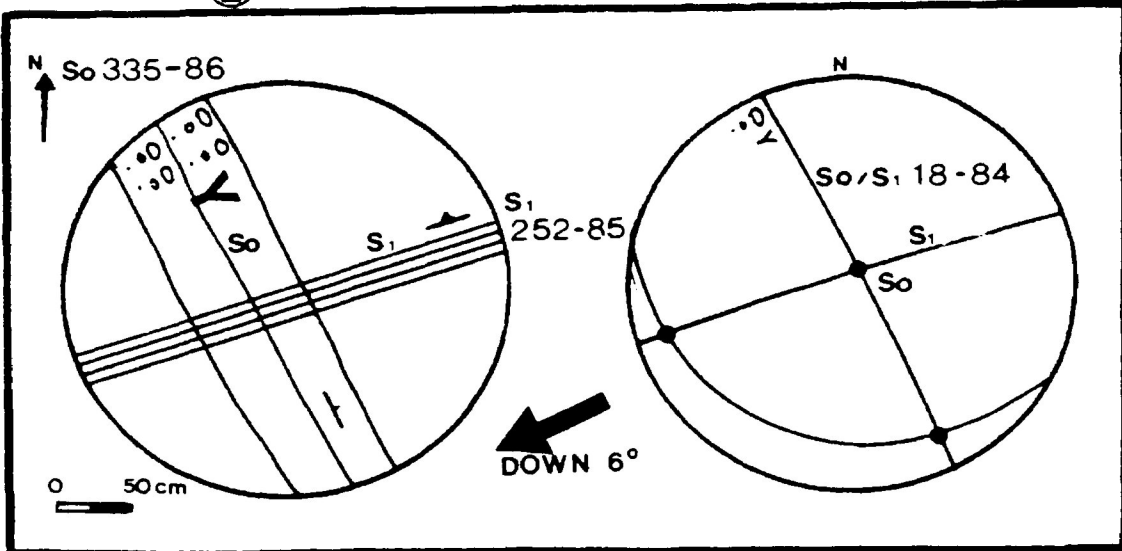
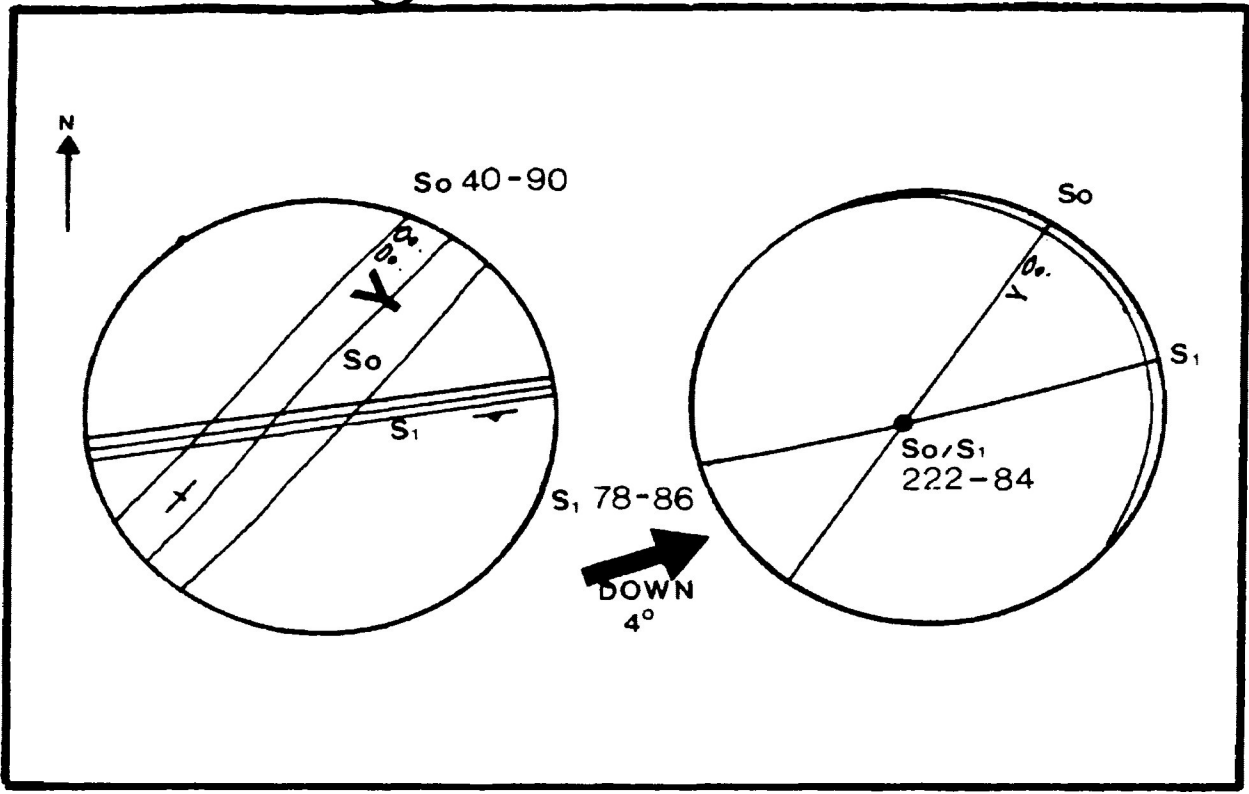


FIGURE 2 : 4 (F)



(G)

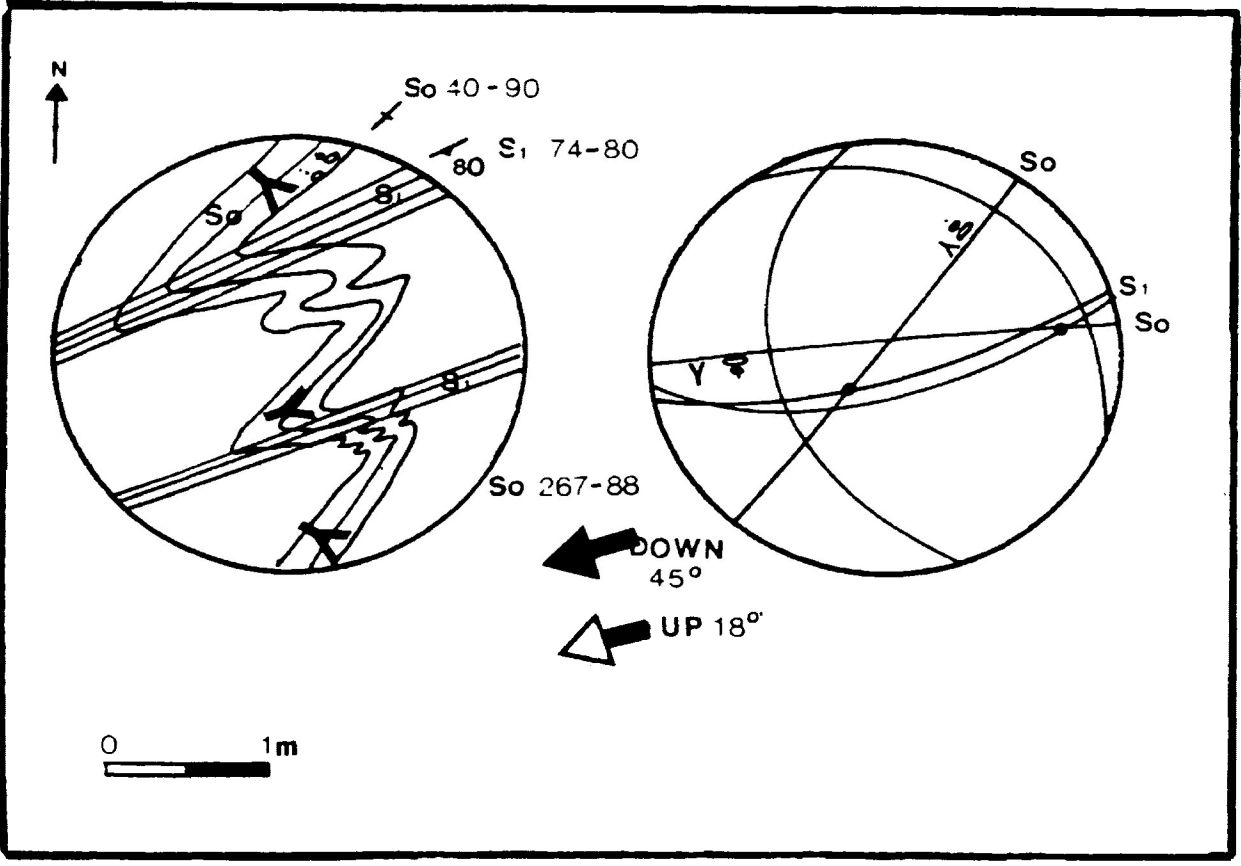
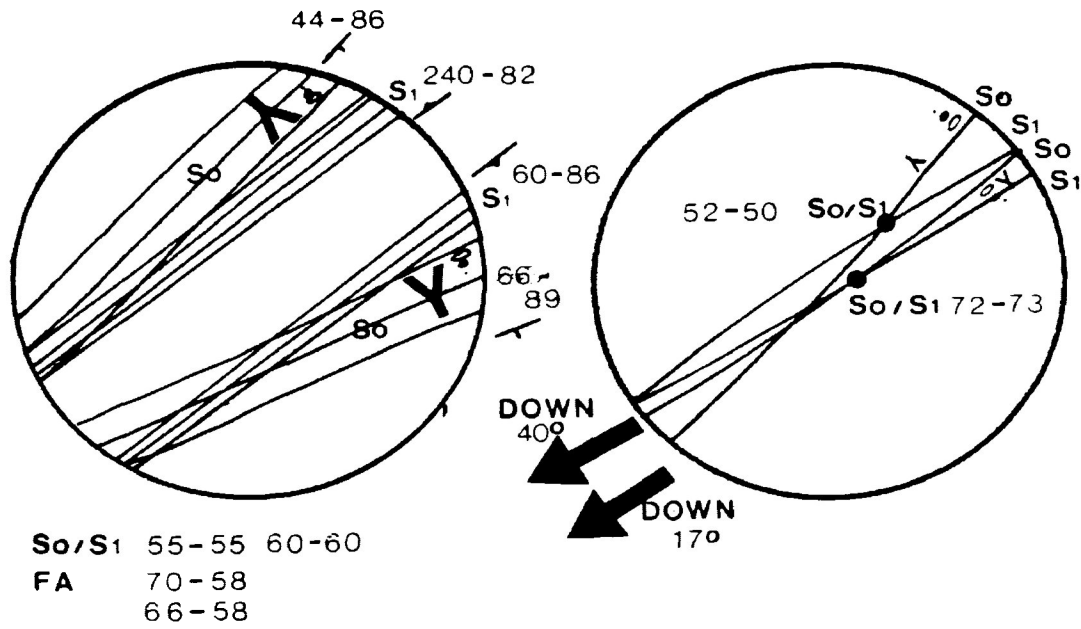
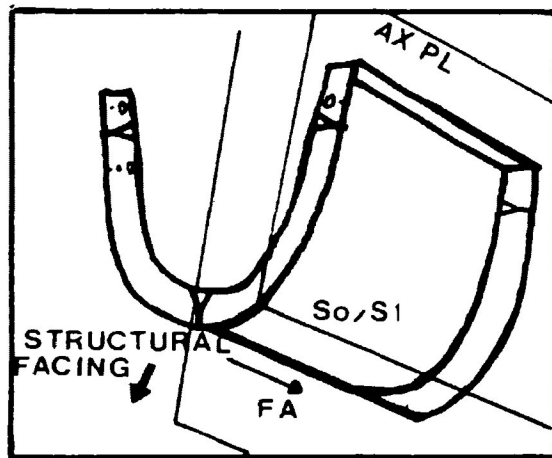


FIGURE 2 : 4 (H)



**F2 FOLD**

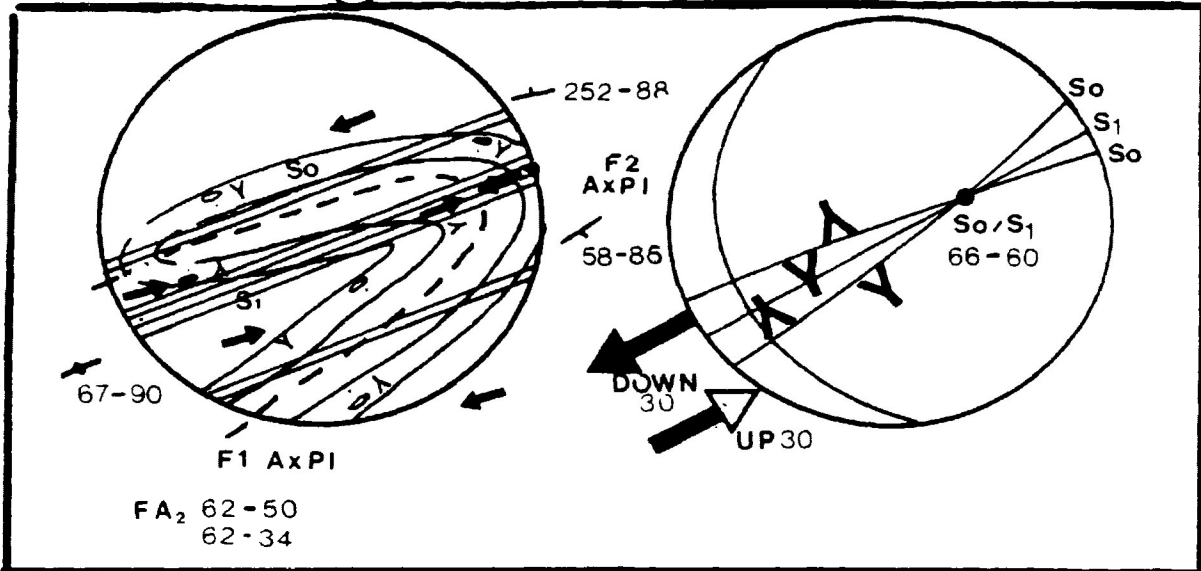


**SKETCH**

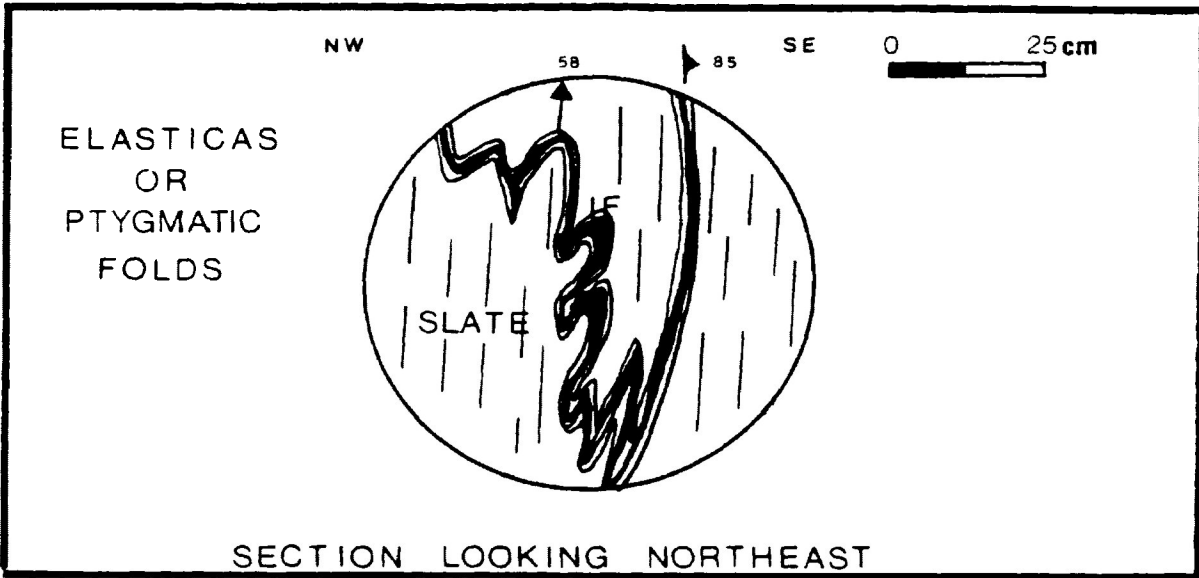
SYNFORMAL ANTICLINE -  
 SIDWAYS CLOSING



FIGURE 2 : 4 (I)

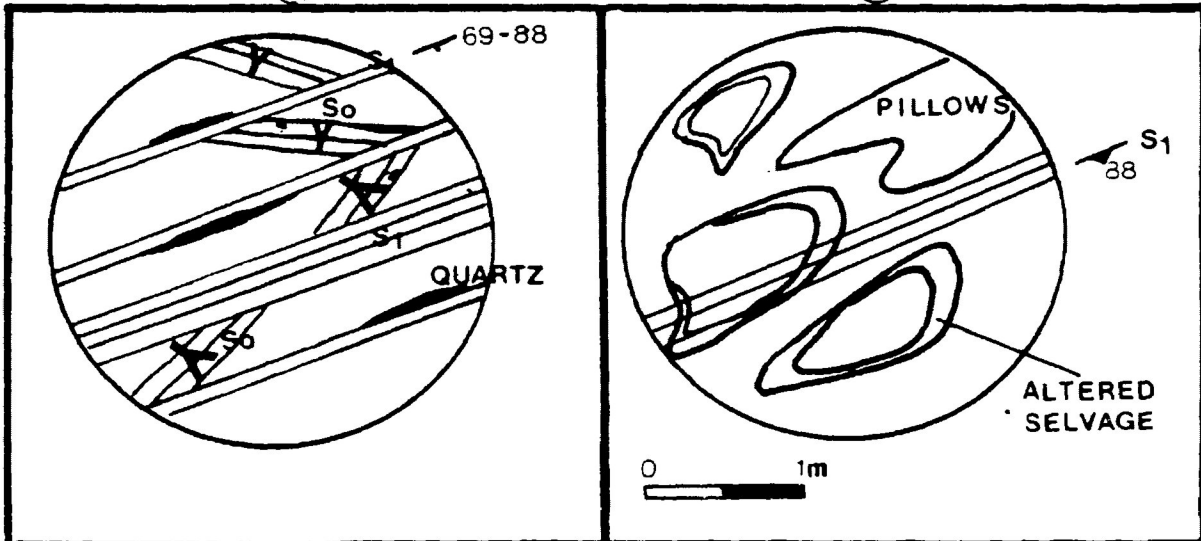


(J)



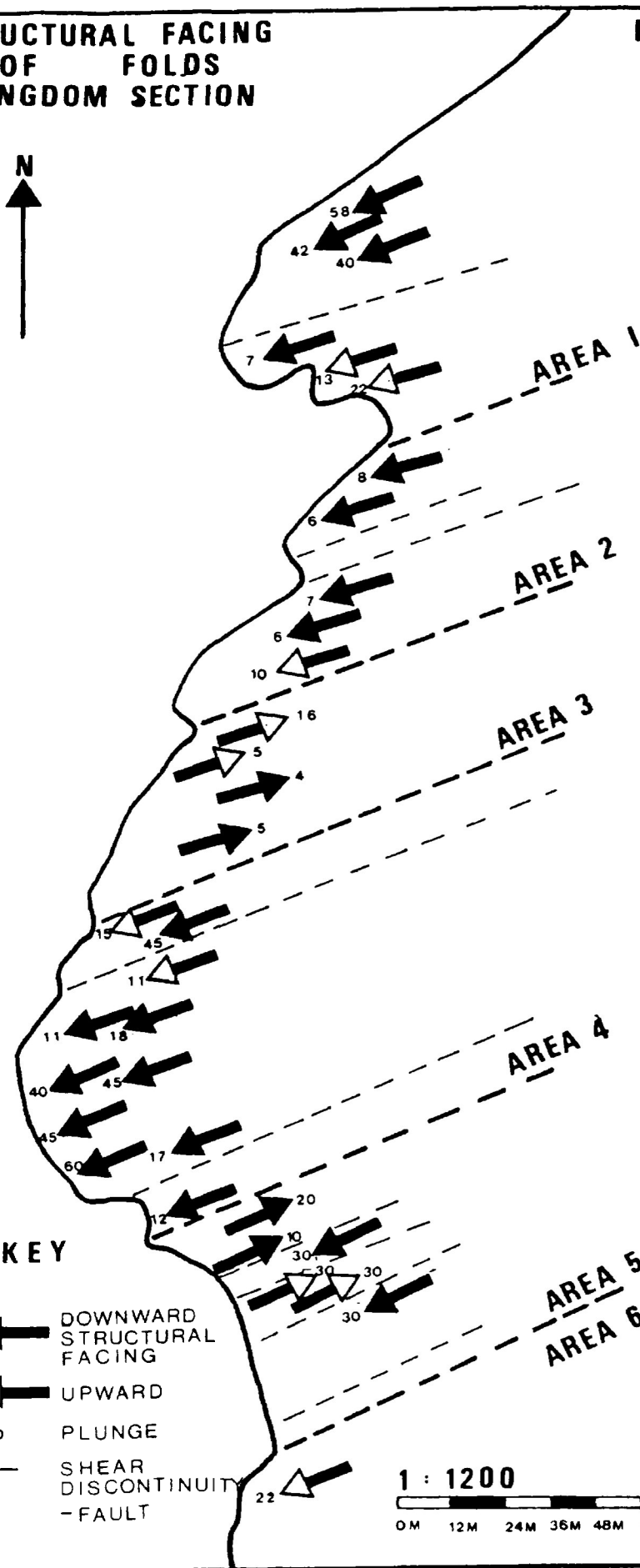
(K)

(L)





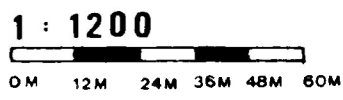
# STRUCTURAL FACING OF FOLDS KINGDOM SECTION

FIGURE 2:5



### KEY

-  DOWNWARD STRUCTURAL FACING
-  UPWARD
- 10 PLUNGE
- - - SHEAR DISCONTINUITY - FAULT



to the southwest, but they vary in plunge from down 7 degrees in the northwest, to up 22 degrees in the southeast (Figure 2:5). Variation in the structural facing direction of hypothetical panels and folds is shown in Figures 2:6 and 2:7. Borradaile (1982) arbitrarily designated folds with plunges of more than 60 degrees (structural facing plunges < 30 degrees) as "sideways-facing" (Figure 2:6). On this basis, folds in the southern section could be designated as sideways-facing.

Area 2: Areas 1 and 2 are separated by a 1 to 1.5 metre shear zone in the fine-grained slates. Field evidence (Figure 2:4 (ii)) indicates that there are two main bedding attitudes, reflecting the orientations of fold limbs. Figures 2:4 (C) and (E) display the local bedding, cleavage and younging directions. The structural facing direction indicates southwest-facing folds, with the facing direction varying in plunge from 8 degrees down, to 10 degrees up. Thus the folds are again sideways-facing. This Area probably represents a dominant fold hinge or closure.

Figure 2:4 (D) displays small scale strike-slip faults developed along narrow shear zones. The sense of motion is right-lateral or dextral; the maximum offset of the disrupted beds was 75 cm (Photo 2:2). These features are similar to the microlithons or "gleitbretter" (gliding boards) structures described by Ramsay (1967). They are formed by the buckling and rupturing of competent layers. Limbs of the folds may become stretched, thinned and even ruptured, with displacement or transposition producing parallel slabs (Ramsay, 1967).

Area 3: Figure 2:4 (iii) shows the trends of minor fold axes, and the attitudes of cleavage and varying bedding plane orientations.

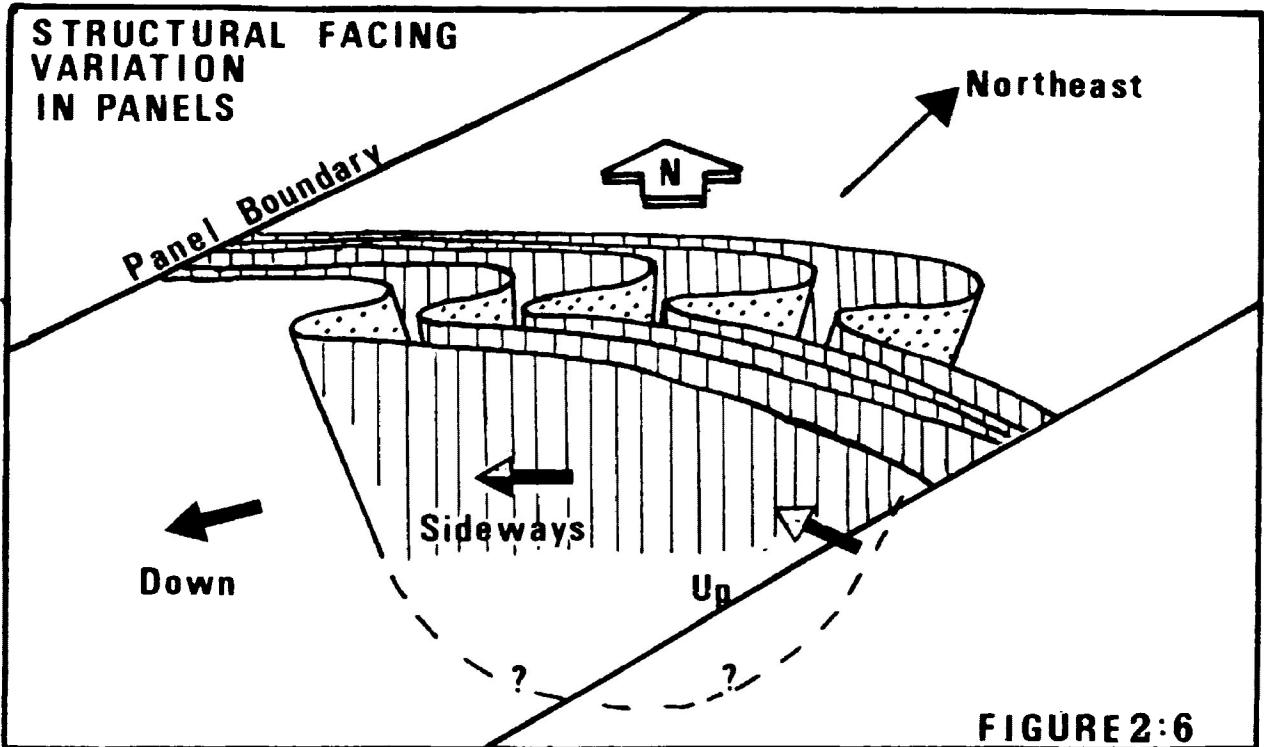


FIGURE 2:6

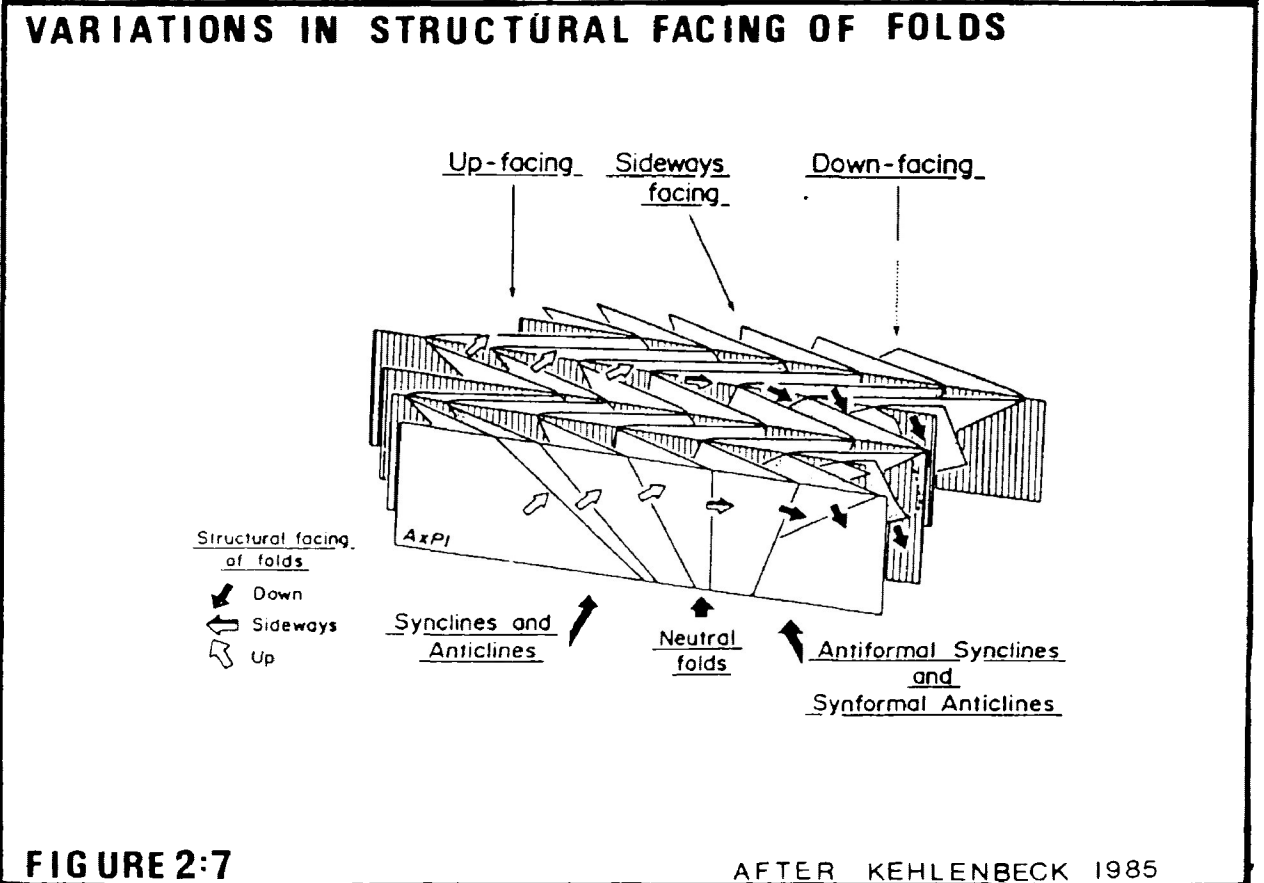


FIGURE 2:7

AFTER KEHLENBECK 1985

Local younging directions, bedding, cleavage and structural facing directions are given in 2:4 (F). An important feature is the reversed, northeast direction of structural facing. The plunge of the structural facing varies from 16 degrees up in the northern section, to 5 degrees down in the southern section. Again, these folds are sideways-facing; the younging of the stratigraphy as a whole is to the northeast.

Figure 2.4 (G) displays a section of small-scale, minor M folds, with axial planar cleavage and a southwest structural facing direction opposite to that of Area 3. The plunge of the facing direction varies greatly from 45 degrees down, to 18 degrees up. This suggests a curvilinear fold hinge, comparable to the Flanders model of Borradaile (1982). However, due to microlithon structures, structural facing measurements in this area should be viewed with caution.

Area 3 is separated from Area 4 by a 15 metre-wide panel of metasedimentary rocks, bounded by shear zones.

Area 4: Bedding and cleavage attitudes of Area 4 show significant variations (Figure 2:4 (iv)). Figure 2:4 (H) displays data for a fold closure. The equal area projections summarize the bedding and cleavage attitudes, the bedding-cleavage (So/S1) intersection lineations and the structural facing direction. The fold is a synform; from the downward plunge of the structural facing direction a synformal anticline is inferred. Bedding-cleavage lineations trend from 52 to 66 degrees northeast; plunges vary from 50 to 73 degrees (Photo 2:1). Axes of major folds (FA) trend from 246 to 260 degrees southwest and plunge 64 to 72 degrees.

The plunge of the folds in Area 4 varies from 79 degrees in the northern section to 30 degrees in the southern section, resulting in respective sideways-facing to downward-facing structures. The stratigraphy in the southern section has therefore been inverted, and the structural facing direction is consistently to the southwest (Figure 2:5).

Area 5: Bedding and cleavage orientations in Area 5 are shown in Figure 2:4 (v). The near vertical dips and similar strike directions of these planar elements result in steep to subvertical intersection lineations. Fold axis orientations plunge steeply to the northeast or southwest.

In one location, younging and cleavage relationships suggest the presence of a possible refolded fold (Photo 2:3) although the exact closure cannot be identified. The fold is about 1 metre in wavelength and the interlimb angle is nearly zero, indicating that the fold is tight to isoclinal (Ramsay, 1967). Figure 2:4 (I) shows the structure and possible axial planar traces produced during hypothetical F1 and F2 folding events. The inferred F2 fold axis (FA2) trends northeast and plunges steeply. However, a second cleavage was not observed in the exposure, suggesting the possibility of a complex, single deformational folding event. The fold represents a sideways-facing to antiformal fold, because the fold plunges steeply to the northeast and is upward-facing.

A reversal in the structural facing direction of the dominant folds is observed in this section of Area 5. Facing is to the southwest and northeast, indicating that stratigraphy as a whole youngs in these directions. The plunges of the folds indicate sideways-facing folds; however downward-facing structures are

**PHOTO 2:3** FOLDING IN SEDIMENTARY ROCKS, WITH  
AXIAL PLANER CLEAVAGE DEVELOPED,  
KINGDOM SECTION.

**PHOTO 2:4** MINOR FOLDS IN PYRITIC-CARBONACEOUS  
SLATE (IRON-FORMATION), KINGDOM  
PROPERTY.





present and imply inverted stratigraphy. Figure 2:3 displays the possible development of such a refolded fold (see also the Black Fox Occurrence).

Field evidence suggests that both the average thickness and average grain size of the sedimentary rocks decrease from Area 1 to Area 5; some of the finest-grained slates or mudstones occur in the latter. In the southern section of Area 5, numerous shear zones, disrupted bedding, and microlithons are also evident. Ramsay (1967) noted that the width of microlithons is controlled by the thickness of the competent layers; thus microlithons developed in thick layers (sandstone-slate beds) will be wider than microlithons developed in thin layers (siltstone-slate beds). This feature is observed in the Kingdom Area, especially in Area 5.

In the southern section of Area 5, bedding is disrupted to the point where it is impossible to follow individual beds laterally. Only the actual shear and discontinuity planes which developed parallel to the cleavage are evident. Numerous quartz veins are orientated subparallel to the shear planes (Figure 2:4 K).

A ptygmatic structure is developed in a thin lens of folded iron-formation consisting of about 3 cm of chert, magnetite, pyrite and slate (Figure 2:4 (J)). This structure has been modified and disrupted by shearing and the production of microlithons. Ptygmatic folds are produced by horizontal shortening within a competent layer leading to buckling (Ramsay, 1967). In this case, the competent layer was probably iron-formation, with mudstone-slate acting less competently. The attitude of the ptygmatic folds resembles the dominant folds in the area (Figure 2:4 J).

Area 6: A ten metre thick diabase dikes cuts schistosity at a low angle and forms the boundary between Areas 5 and 6 (Map 1). Area 6 lithologies include iron-formation, slate, felsic porphyry, a diabase dike and mafic metavolcanics. A strongly developed cleavage or schistosity is observed within the slates and iron-formation. The structural facing direction is down to the southwest at 22 degrees indicating that the folds are sideways facing. Centimetre-scale, buckled M and W folds occur within the iron-formation (Photo 2:4).

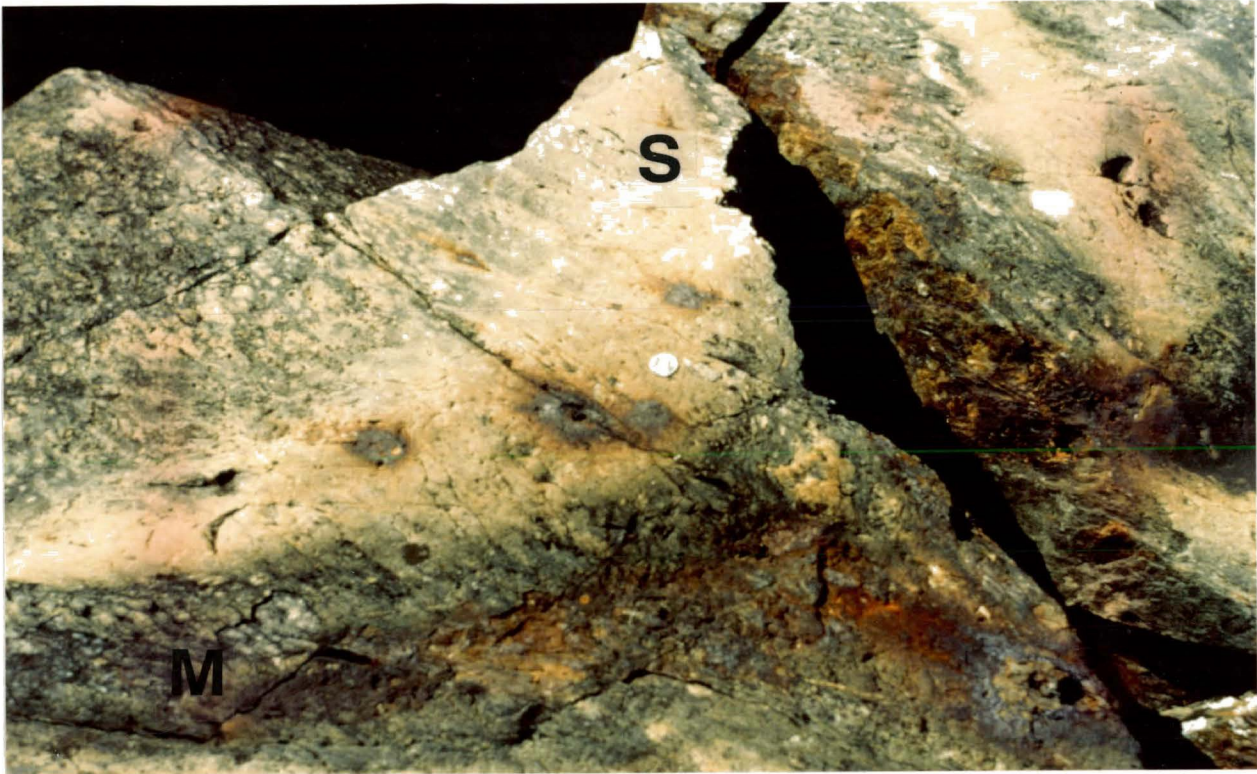
Younging directions were determined from the pillowed volcanic rocks. Although pillows are deformed they have pear-like terminations and well-defined but thickened selvages (Figure 2:4 (L), Photo 2:5). Using the method of Borradaile and Poulsen (1981), strain ratios for the Kingdom pillows vary from 1.75 to 2.50. The strain is in a direction parallel to the schistosity or axial planar cleavage. Pillow cusps indicate that the younging direction for the volcanics is towards the north. This suggests that the iron-formation, which is less than 10 m away to the north, structurally if not stratigraphically, overlies the pillow lavas.

## 2) LAWSON ISLAND

Bedrock on Lawson Island consists predominantly of sedimentary rocks; structurally the area is very similar to the Kingdom Area. Bedding attitudes range from 80 to 90 degrees, and cleavage from 60 to 85 degrees. Structural facing directions are to the southwest and vary in plunge from 8 to 22 degrees downward, indicating sideways-facing folds (Figure 2:1).

**PHOTO 2:5**      ALTERED PILLOW SELVAGES (S) AND  
SELVAGE THICKENING ORIENTED ALONG  
CLEAVAGE, KINGDOM PROPERTY. NOTE:  
PEAR-LIKE TERMINATIONS AND IRON-  
RICH MATRIX (M) SURROUNDING PILLOWS.

**PHOTO 2:6**      ERODED PILLOW OUTLINE: KINGDOM  
PROPERTY. NOTE: HAMMER HEAD  
INDICATES TOP DIRECTION TOWARDS  
THE IRON-FORMATION.



### 3) STEEL RIVER HIGHWAY AREA

Sedimentary rocks to the east of the Steel River bridge on Highway 17 are slightly overturned. Average bedding and cleavage surfaces are, respectively, 235 - 82 degrees northwest, and 70 - 88 degrees south. Structural facing directions to the northeast, plunging from 14 degrees up to 25 degrees down, indicate sideways-facing folds. As in the Kingdom Area, microlithons or slices of metasediments are separated, respectively, by cleavage discontinuities and shear zones.

### 4) BLACKFOX LAKE AREA

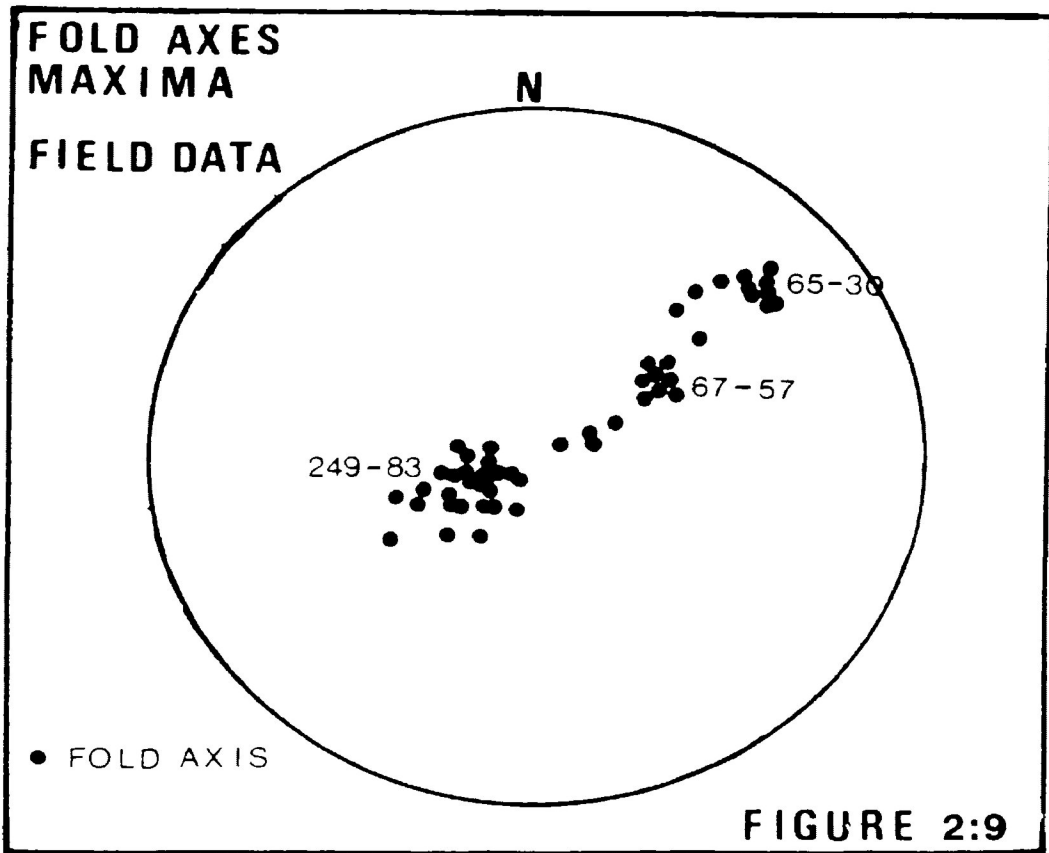
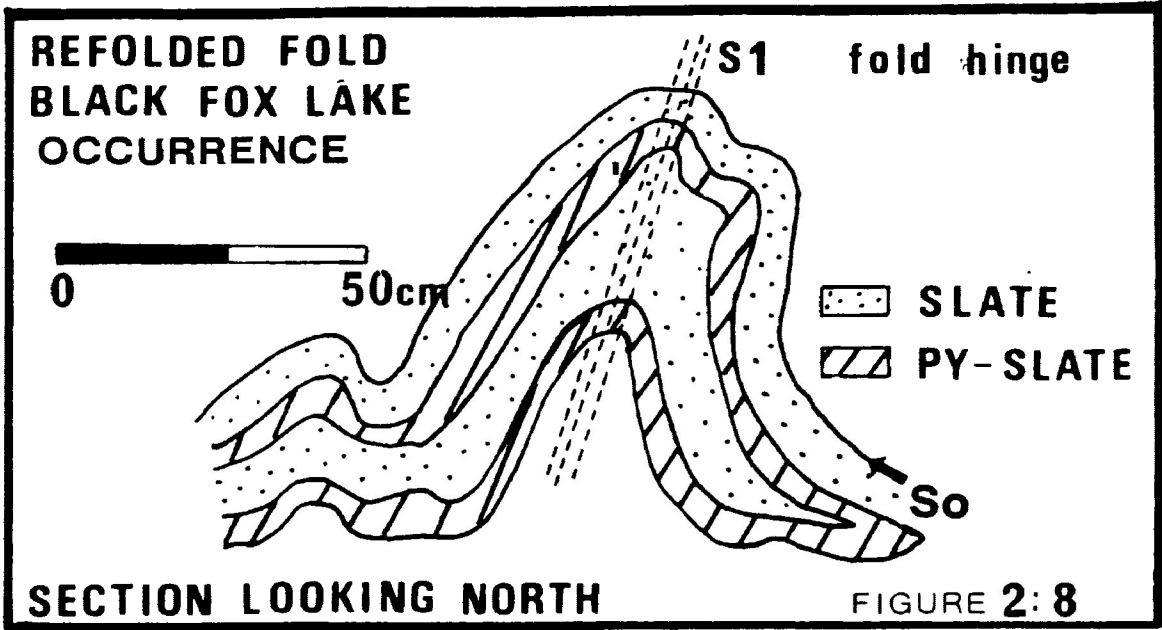
An outcrop of slate and iron-formation in this area features a refolded fold, although only one cleavage is dominant (Photo 2:7 and Figure 2:8). The trend and plunge of the fold axes is 68 - 40 degrees. Minor M folds are present in the slate and iron-formation; they trend northeast and plunge 30 to 40 degrees.

## OVERALL DISTRIBUTION OF STRUCTURAL FEATURES

Figures 2:9 and 2:10 display all bedding-cleavage intersection lineations from the study area. These lineations appear to lie along a great circle girdle. The pole of the lineations corresponds closely to the maximum of the poles to the axial planar cleavage. Kehlenbeck (1984) reported a similar distribution in the Hazelwood Lake Area. This distribution suggests three possibilities: that the S1 cleavage was developed in rocks which were previously folded or had curvilinear surfaces, that S1 is developed along S0 surfaces which are curvilinear, or that S1 was developed in the rocks and has been

**PHOTO 2:7**      REFOLDED FOLD IN PYRITIC-  
CARBONACEOUS SLATE, BLACK  
FOX PROPERTY.

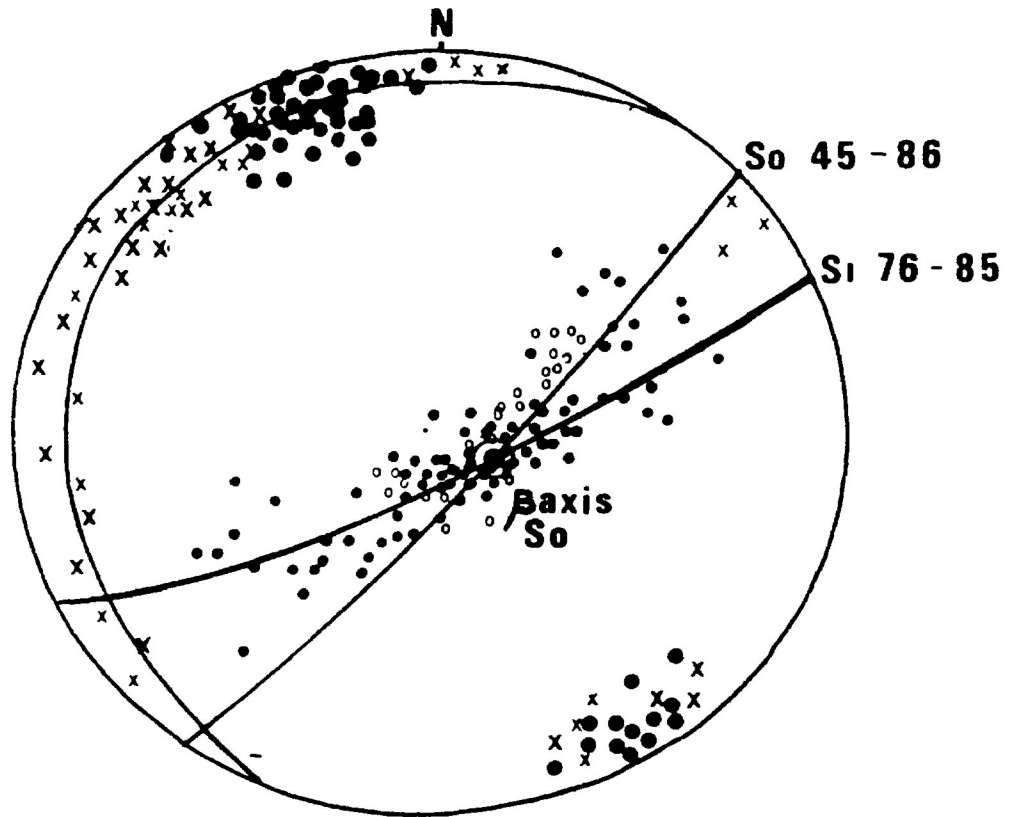






## STRUCTURAL DATA

FIGURE 2:10



- x poles to bedding (So)
- poles to cleavage (Si)
- intersection lineation So / Si (net)(calculated)
- intersection lineation (field)(observed)

folded subsequently. As shown in Figure 2:10, the axial planar cleavage has a fairly constant orientation, suggesting that the lattermost of the three possibilities has not occurred.

The So/S1 intersection lineation varies greatly with respect to the orientations of the surface that is being folded (ie So). In several of the dominant folds in the Kingdom Area, it appears that the surface undergoing folding varied little in attitude (Figure 2:4 H). In other areas where dominant folds are not evident, bedding attitudes are variable, leading to a wide range in So/S1 intersection lineations.

Although the structural facing direction in the Kingdom Area varies from upward to sideways to downward (Figures 2:4, 2:6, 2:7), most of the folds are sideways-facing. Fold axes vary in attitude (Figure 2:9); as in the case of the bedding-cleavage intersection lineation, they appear to conform to the same great circle girdle. However, a large maximum is observed at 249 - 83 degrees, and smaller maxima are present at 65 - 30 degrees and 67 - 57 degrees.

Variations in the So/S1 and hinge line trends of the dominant folds may be attributed to imprinting of the S1 cleavage on a curvilinear surface. If the dominant folds observed were generated on such a surface, then a high degree of variation in hinge line trends would result. The curvilinear nature of So in some cases may have resulted from an earlier deformation which could have included folding. However, the fold maxima data (Figure 2:10) do not reflect earlier fold axes.

## FAULTING

The only field evidence of faulting in this area is represented by numerous examples of shear zones and shear cleavage. Displacement along shear surfaces is evident on a local scale (Figure 2:4 D). A dextral sense of motion with up to 1 metre of displacement was observed on several of the shear zones.

## DISCUSSION

Field evidence suggests two possible structural histories for the rocks of the thesis area: 1) two separate folding events, or 2) a complex folding event during one deformational period.

Although two exposures in the thesis area provide evidence of refolded folds, such folds are developed in fine-grained iron-formation and slate, and therefore may reflect soft sediment deformation effects such as slumping. Fold axes and hinge data lie along a great circle girdle, suggest curvilinear fold axes or hinges. Reversals in the structural facing direction are also present, although such evidence can suggest several folding events and deformational periods, only one dominant cleavage is present. Since this is axial planar to the dominant folds, it is assumed to be related to the dominant folding event.

Turner and Weiss (1963) describe complex folds which result from very heterogeneous deformational paths during one period of deformation. This can produce non-planar, non-cylindrical folds with curvilinear hinges and curvilinear axial surfaces. Non-cylindrical folds have been described as sheathlike or as "sheath folds" (Dalziel & Bailey, 1968; Carreras et al., 1977; Rhodes & Gayer, 1977). Lacassin and Mattauer (1985) attributed

their formation to progressive deformation involving "deflections" in the folded layers, which produces curvilinear folds. These authors have reinterpreted several areas previously thought to have been affected by two major folding events, as the result of deformation during one period of progressive shearing (sheath folding). Borradaile (1986, personal communication) suggested that in the present study area, a complex folding event related to one deformational period is more likely than polyphase deformation, due to only one observed cleavage.

Sideways-facing dominant folds in the thesis area have steeply plunging fold axes. Where downward-facing structures occur, true synformal anticlines and antiformal synclines can be inferred. Kehlenbeck (1984) suggested that this may indicate geometric properties of the earlier structure of the rocks, or previous folding episodes. Folds appear to be flattened parallel folds (Class 1B of Ramsay, 1967), which have been modified by displacements parallel to the S1 cleavage and the development of shear surfaces. Such displacements have disrupted the fold structures and bedding, and produced subparallel panels, slices, and microlithons.

At Kingdom, where the stratigraphy as a whole becomes younger to the northeast in those panels with a structural facing direction to the northeast. In the panels where the structural facing direction is southwest, the converse is true (Figure 2:5). Between Jackfish and the lower Steel River, volcanic rocks have been folded into an easterly plunging anticline (Walker, 1967). To the south of Jackfish, the fold is upright, but east of Little Santoy Lake it is overturned. Walker (1967) suggested that in the Bottle Point Area, the strata are greatly compressed into a tight

syncline. On the basis of top determinations, he suggested that the volcanic rocks stratigraphically overlies the sedimentary rocks to the north. Evidence from Walker's map (2107) indicates that the top indicators used were from the Kingdom Area, specifically Areas 3, 4 and 5. Field evidence shown in Figures 2:4 and 2:5 now indicates that these areas contain reversals in both the younging and the structural facing of the stratigraphy. Within the sedimentary rocks closest to the volcanics, the formation of microlithons becomes intense. Top indicators in Area 5 are variable and should not be used to determine younging. In Areas 4 and 5, downward structural facing directions are dominant (Figure 2:5), and synformal anticlines and antiformal synclines are present (Figure 2:4 H). This suggests that the folds are sideways-facing to inverted or overturned, and that the stratigraphy in this area is also inverted.

Figures 2:11 A and B displays Walker's (1967) model for the relationship between the sedimentary rocks and volcanic rocks in the Kingdom Area. Gently plunging anticlines and synclines are present, the sedimentary rocks are in contact with the volcanic rocks, and a fault trends parallel to the cleavage in the metavolcanics. According to Walker, younging in both the volcanic and sedimentary rocks is to the southeast. Based on Walker's data, the iron-formation is hosted by the sedimentary rocks and not at the sedimentary-volcanic contact.

Structural interpretations of the Kingdom Area are shown in Figure 2:12 A based on a model of complex to polyphase folding. Figure 2:12 B gives details, including downward- and sideways-facing structures in the sedimentary rocks, and the presence of microlithons. Sedimentary rocks become thinner-bedded and

### HYPOTHETICAL SECTION - WALKER (1967)

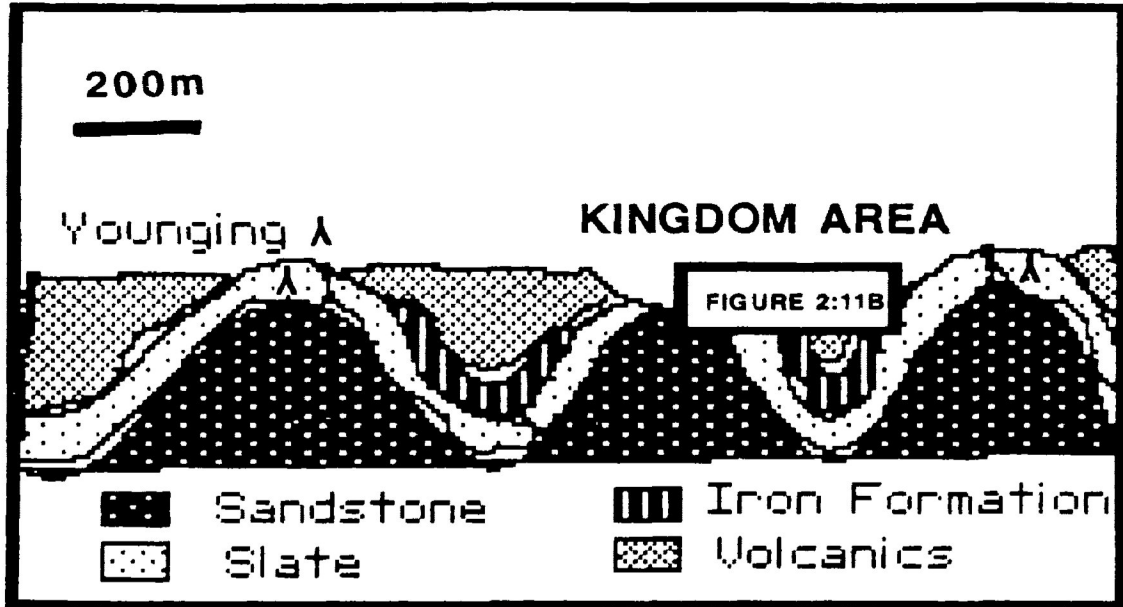


FIGURE 2:11A

### DETAILED HYPOTHETICAL SECTION : KINGDOM AREA

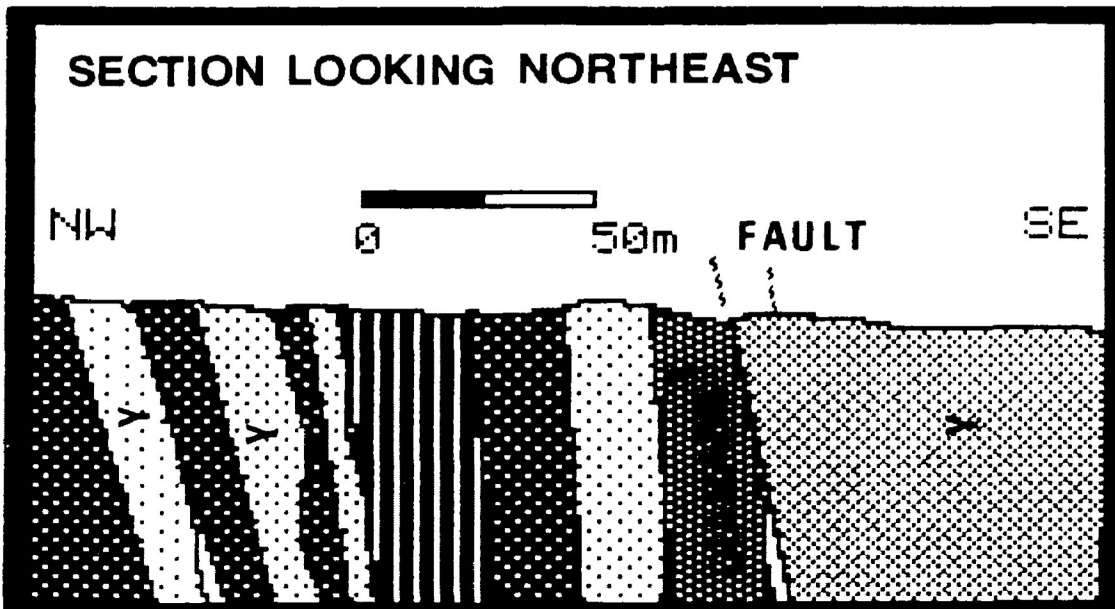


FIGURE 2:11B

## HYPOTHETICAL SECTION -PRESENT STUDY

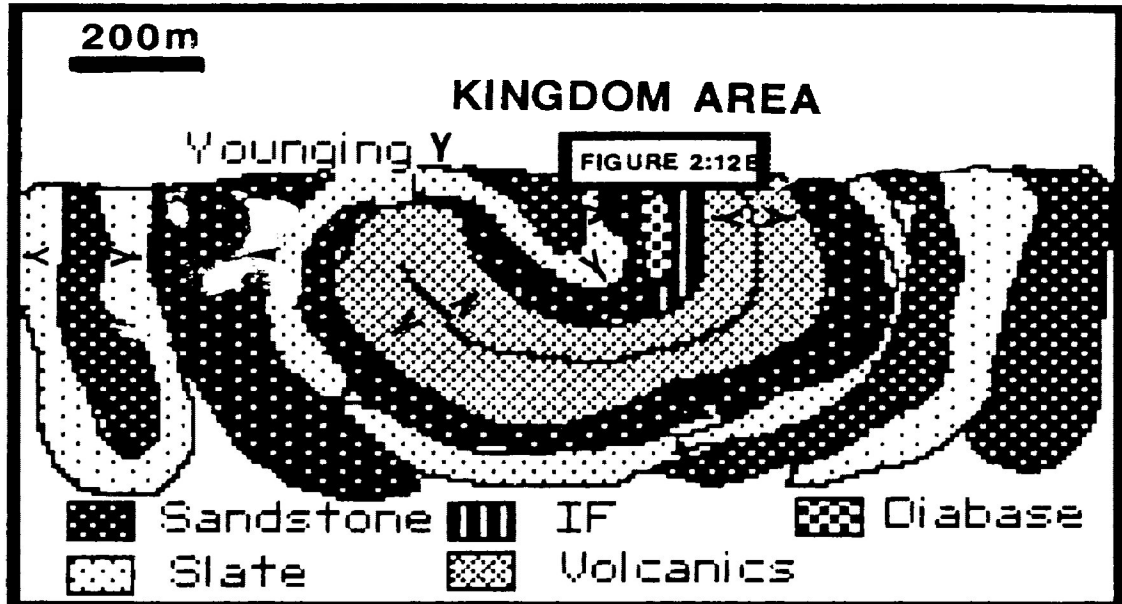


FIGURE 2:12A

## DETAILED HYPOTHETICAL SECTION : KINGDOM AREA

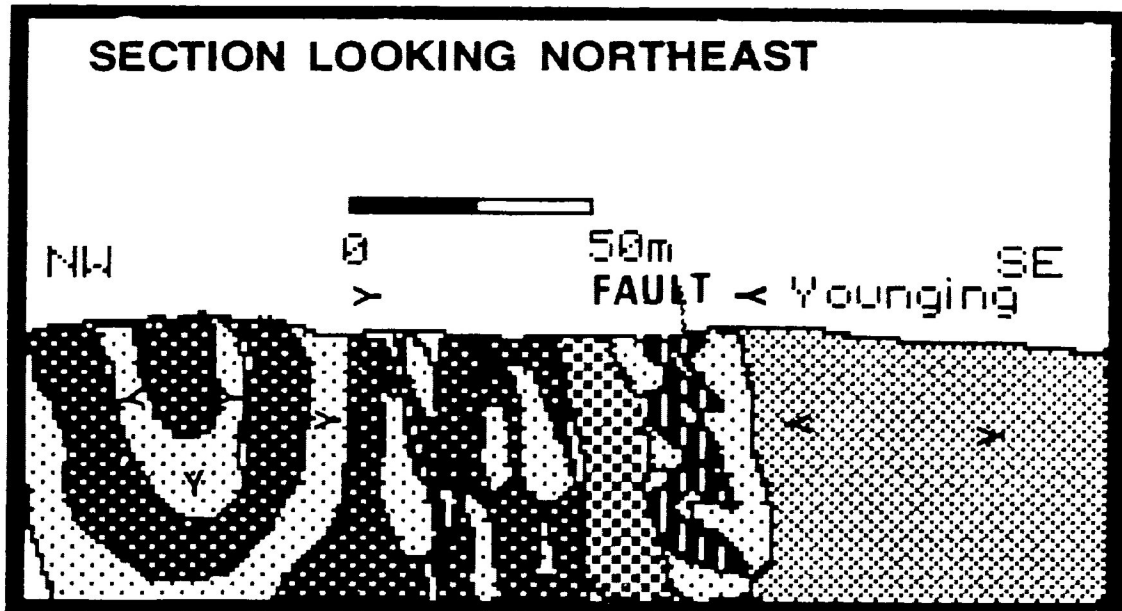


FIGURE 2:12B

finer-grained towards the sediment-volcanic contacts.

Iron-formation and a diabase dike are situated near the metasediment-metavolcanic contact. Felsic dikes intrude the iron-formation and other fine-grained sedimentary rocks. The location of the diabase dike, combined with the microlithon development and pronounced shear cleavage, are evidence for a fault at this level.

Top determinations from the pillowed volcanic rocks, vesicular rims and graded beds in interpillow sedimentary rocks indicate that the volcanic rocks young towards the iron-formation ( Figure 2:12 B and Photo 2:7). Assuming that the iron-formation is in stratigraphic contact with the volcanic rocks, it would therefore be younger. If so, the iron-formation marks the transition from a volcanic cycle through a quiescent period into active turbidite sedimentation.

Within the study area, contacts between fine-grained sedimentary rocks (including iron-formations) and volcanic rocks are areas of significant deformation, and commonly sites of dike emplacement. The competency difference together with the fine-grained nature of the sedimentary rocks, is apparently responsible for focusing the deformation. Deformation along cleavage planes within the fine-grained rocks leads to the common microlithons and transposed panels in these areas. The shear planes are subparallel to the axial planar cleavage, which is considered to be related to a single dominant folding event.

Although it has been suggested previously that the sedimentary rocks are older than the volcanics in the Kingdom Area, the presence of downward-facing structures, microlithon development, and observed younging indicators render this interpretation



questionable. Evidence collected in this study supports the opposite relationship.

### 3) ROCKS ASSOCIATED WITH IRON-FORMATION

#### INTRODUCTION

The sulphide-facies iron-formations are commonly associated with mafic to intermediate volcanic rocks and sedimentary rocks, and commonly intruded by dikes. Detailed work was carried out on seven iron-formations and associated chemical sedimentary rocks. The following paragraphs summarize the geological setting of each area.

**Kingdom** (Figures 1:3, 3:1): A northeast-striking iron-formation up to 40 m wide is situated between altered mafic to intermediate, pillowed to massive volcanic rocks, and turbiditic (DE) sedimentary rocks. A 10 m wide diabase dike intrudes along the contact between iron-formation and turbiditic rocks. Felsic porphyry dikes intrude the iron-formation parallel to the cleavage.

**Simard-Swetz** (Figures 1:3,): A three metre-wide northeast-striking iron-formation is situated between chlorite schist interpreted as deformed mafic rocks, and a wacke-siltstone sedimentary assemblage. A felsic porphyry intrudes along the contact between the iron-formation and turbiditic rocks.

**Little Steel Highway** (Figures 1:3, 3:4): Two northeast-striking, chert or siliceous schist units less than 50 cm thick are associated with mafic intrusive, pillow lavas and siltstone-slate beds. The chert occurs along a sedimentary-volcanic contact, where a mafic dike has also been emplaced.

# DETAILED GEOLOGY OF THE KINGDOM OCCURRENCE

- 1 PILLOWED METAVOLCANIC FLOWS, VARIOLITIC
- 1a MASSIVE, AMYGDALOIDAL FLOWS
- 3a CHERT
- 3b CARBONATE
- 3c PYRITIC-CARBONACEOUS SLATE, LAMINATED
- 3d BEDDED PYRITE
- 4 FELSIC PORPHYRY
- 5 DIABASE
- SHORELINE
- - - - - OUTCROP
- - - - - GEOLOGICAL BOUNDARY
- ~ ~ ~ FAULT
- oo° COBBLE BEACH
- BEDDING
- CLEAVAGE
- (Fig. 4:1)  
A — B DETAILED SECTION
- ③ SAMPLE NUMBER BRS-3
- FOLD AXIS

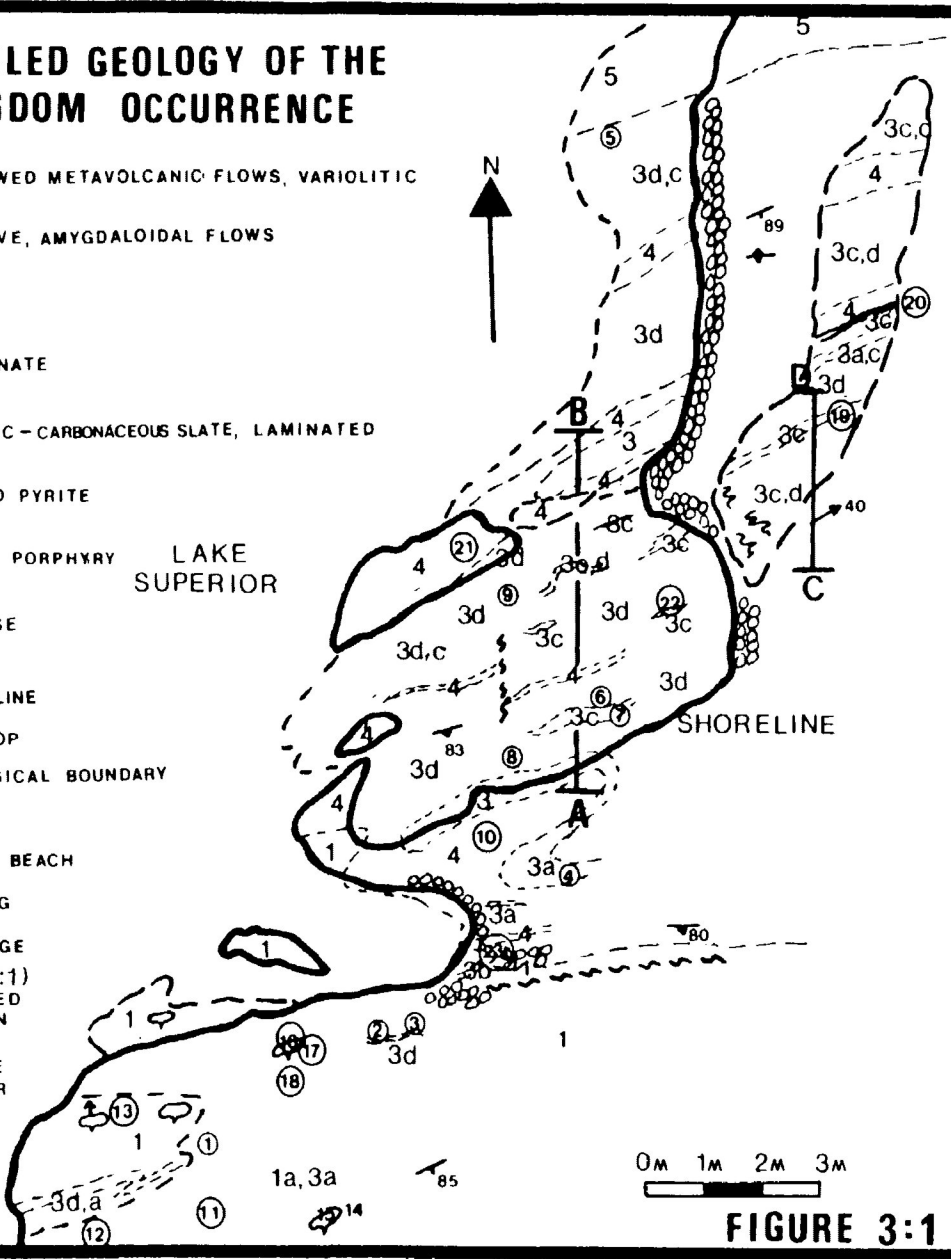


FIGURE 3:1

Little Steel Railway (Figures 1:3, 3:5): This is an extension of the Little Steel Highway occurrence; the geology is similar except that more brecciated chert and mafic dikes are present.

Black Fox Lake (Figures 1:3, 3:8): Sulphide-facies iron-formation is situated between mafic and felsic dike rocks and DE siltstone-slate turbiditic rocks.

Morley Pyrite (Figure 1:3): Sulphide-facies iron-formation, up to 5 m wide, strikes to the northwest and is situated between intermediate porphyritic to fragmental volcanic rocks and DE siltstone-slate turbiditic rocks. The turbidites are overlain by mafic pillow lavas.

Harkness-Hays (Figure 1:3,): A sulphide-facies iron-formation up to 6 m wide is situated between intermediate and mafic volcanic rocks.

## VOLCANIC ROCKS

The volcanic rocks associated with the iron-formations are predominantly mafic to intermediate flows, including pillowed, massive, porphyritic and amygdaloidal varieties. A tuffaceous component was noted in several of the chemical sedimentary rocks, as discussed in Chapter 4. Excellent exposures of pillowed flows are present 2 km west of the Steel River bridge, along the south side of Highway 17 (Map 1). The Jackfish lavas consist of moderately deformed, variolitic pillows with clearly defined selvages. Varioles are generally present within the 20 cm zone adjacent to the selvage. They display radiating or fibrous textures, and are commonly coalesced as clots and layers. The production of varioles and spherules has been attributed to the

devitrification of glass around scattered nuclei due to a rapid crystallization of a viscous magma or melt (Williams et al., 1954).

Within the pillows, lava levels and drain-away levels provide excellent bedding markers (Photo 3:1). At the Kingdom occurrence (Figure 3:1), individual pillows are up to 2 m in length, and display large altered varioles up to 2 cm in diameter. The pillow selvages unlike the Jackfish pillows, are gradational into the cores over about 15 cm; they appear to become more felsic outwards. Microscopic examination and XRD data indicate that the pillow rims are enriched in albite, quartz, carbonate and pyrite, whereas the cores consist of uralite, chlorite, muscovite, quartz, carbonate, albite, oligoclase and saussurite. Amygdules are filled with quartz, chlorite and carbonate; variolites consist of radiating, plumose quartz and feldspar.

Whole-rock analyses (Table 3:1) were conducted on pillows located at various distances from the iron-formation. One pair of samples, representing a pillow center (BRS-14) and rim (BRS-15), is located 30 meters from the iron-formation; another pair, samples BRS-16 and 17 (Photos 2:5, 2:6) are about 10 m from the iron-formation. Analyses indicate that the pillow centers contain between 61.1 and 63.8 % SiO<sub>2</sub>, while the pillow rims contain up to 69.9 % SiO<sub>2</sub>. The pillow rim closer to the iron-formation (Figure 3:2) is more enriched in SiO<sub>2</sub>. Pillow rims are depleted in total iron (as Fe<sub>2</sub>O<sub>3</sub>) and enriched in sulphur (as pyrite) relative to cores.

The pillow selvages are enriched in CaCO<sub>3</sub>, and in one case, K<sub>2</sub>O (data for the other sample pair are problematic : see Geochemical Methods : Discussion, Appendix B). Na<sub>2</sub>O contents are

**PHOTO 3:1** VARIOLITIC LAVA LEVEL DISPLAYING QUARTZ FILLED DRAIN AWAY LEVELS, JACKFISH PILLOW LAVA EXPOSURE, HIGHWAY 17.

**PHOTO 3:2(A)** SEDIMENTARY TEXTURES AND STRUCTURES: STEEL RIVER AREA. NOTE: NEAR CLASSICAL TURBIDITE, DISPLAYING PARALLEL LAMINATIONS, LOADED RIPPLES, CROSS-BEDDING AND GRAIN SIZE GRADATION.

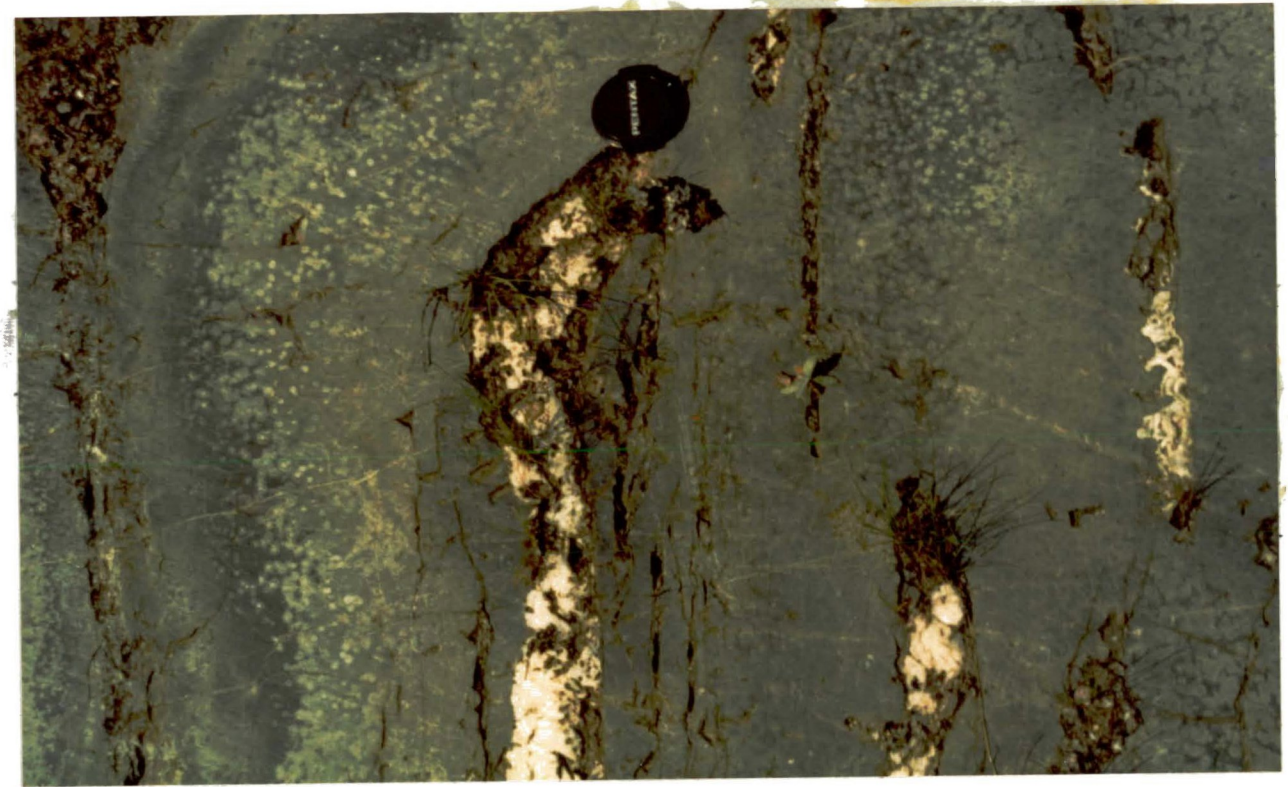


TABLE 3:1 - SAMPLE DESCRIPTIONSAMPLE NUMBER

BRS-14	Pillow Core, Kingdom Property. Sample collected 30 m from sulphide-facies iron-formation. Thin section displays amygdules filled with quartz and carbonate. Analysis performed at Lakehead University.
BRS-14 (D)	Duplicate sample of BRS-14. Analysis performed at Geoscience Laboratories, Toronto.
BRS-15	Pillow Rim of same pillow as BRS-14, Kingdom Property. Sample collected from 30 m away from IF. A thin section displays abundant plagioclase feldspar in matrix or groundmass. Analysis performed at Lakehead University.
BRS-15 (D)	Duplicate sample of BRS-15. Analysis performed at Geoscience Laboratories, Toronto.
BRS-16	Pillow Centre, Kingdom Property. Sample collected 10 m from iron-formation. Analysis performed at Lakehead University.
BRS-17	Pillow Rim of same pillow as BRS-16, Kingdom Property. Sample collected 10 m from iron-formation. Analysis performed at Lakehead University.
BRS-47	Pillow breccia fragments, Little Steel Highway occurrence. Sample is of felsic appearing, stretched fragments in a more mafic matrix. Thin section displays fragments with abundant plagioclase feldspar, carbonate and quartz hosted by a pennite-schist. Analysis performed at Lakehead University.
BRS-55B	Intermediate metavolcanic rock, Morley Property. Sample is of volcanic rock associated with Morely Iron-Formation. The rock displays a clotted appearance. Analysis performed at Geoscience Laboratories, Toronto.

NOTE : All analyses indicated on the following Tables refer to major element analysis unless otherwise stated



TABLE 3:1  
COMPOSITION OF METAVOLCANIC ROCKS  
ASSOCIATED WITH IRON-FORMATION

Sample No.	BRS-14	BRS-14(D)	BRS-15	BRS-15(D)	BRS-16	BRS-17	BRS-47	BRS-55B
	<u>CORE</u>		<u>RIM</u>		<u>CORE</u>	<u>RIM</u>		
Majors WT(%)								
SiO <sub>2</sub>	63.84	61.0	67.69	67.2	61.14	69.92	62.06	58.3
Al <sub>2</sub> O <sub>3</sub>	15.33	15.5	13.52	13.8	16.38	13.43	12.60	15.7
Fe <sub>2</sub> O <sub>3</sub> (T)	6.48	5.86	2.62	2.94	7.28	2.46	5.70	6.41
Fe <sub>2</sub> O <sub>3</sub>	2.2	---	1.47	---	---	---	---	---
FeO	3.80	4.29	1.02	1.75	---	---	---	---
Fe	---	---	---	---	---	---	---	---
MgO	1.06	1.84	0.79	0.86	1.29	0.81	1.18	3.44
CaO	3.58	3.70	2.25	2.54	1.42	2.66	5.99	5.82
Na <sub>2</sub> O	4.03	4.11	4.48	4.52	3.88	2.40	3.54	3.61
K <sub>2</sub> O	0.72	1.20	0.83	1.72	0.79	1.60	1.12	0.81
TiO <sub>2</sub>	0.53	0.53	0.72	0.46	0.55	0.46	1.90	0.64
P <sub>2</sub> O <sub>5</sub>	0.14	0.07	0.13	0.07	0.14	0.03	0.55	0.07
MnO	0.13	0.13	0.10	0.10	0.09	0.10	0.14	0.14
C	---	---	---	---	---	---	---	---
CO <sub>2</sub>	2.57	2.60	3.30	3.22	2.09	3.30	3.45	2.53
H <sub>2</sub> O	1.89	N/A	0.63	N/A	2.07	0.72	2.07	N/A
S	---	0.28	---	0.52	---	---	---	0.15
LOI	4.46	4.1	3.93	3.8	4.16	4.02	5.52	4.5
TOTAL	99.84	98.0	97.06	98.0	97.13	97.02	100.3	99.4
Traces								
Au (ppb)	---	---	---	---	---	21	---	---
Ag (ppm)	---	---	---	---	---	2	---	---
Co (ppm)	---	17	---	25	20	11	---	---
Cr (ppm)	---	11	---	10	Nil	Nil	---	---
Cu (ppm)	---	29	---	34	34	17	---	---
Ni (ppm)	---	31	---	19	33	15	---	---
Pb (ppm)	---	Nil	---	Nil	Nil	Nil	---	---
Zn (ppm)	---	68	---	46	74	25	---	---

(D) Represents Duplicate Analysis  
--- Not Analysed

04

similar in the core (BRS-14) and rim (BRS-15) of the pillow located 30 m from the iron-formation; however, in the sample 10 m from the iron-formation the rim is depleted (Figure 3:2). On an AFM ternary plot, the pillow rims display alkali enrichment relative to the cores (Figure 3:3). The pillow cores fall within the tholeiitic field, while the rims lie within the calc-alkaline field.

Chert, bedded or laminated pyrite, pyritic-carbonaceous slate and hyaloclastite commonly occur between the pillows (Photo 2:5). At Kingdom, intra-pillow hyaloclastites generally consists of altered pillow rim fragments within a chloritic, pyrite-rich matrix. Pillow breccia hyaloclastite (BRS-47) at the Little Steel Highway occurrence (Figure 1:3, 3:4) consist of elongated and altered sections of pillow rims within a clastic sedimentary matrix. The pillow fragments contain abundant feldspar, epidote, chlorite and calcite.

At Schreiber Beach, mafic pillowed volcanics and a massive mafic to intermediate flow are separated by one metre of oxide-facies iron-formation.

Footwall volcanic rocks at the Morley Pyrite deposit consist of intermediate massive and porphyritic rocks interbedded with minor amounts of fragmental and tuffaceous material. An analysis of this rock type is given in Table 3:1 (BRS-55B). Volcanic rocks in the hanging wall consists predominantly of mafic to intermediate pillowed and massive flows with up to 10 % pyrite.

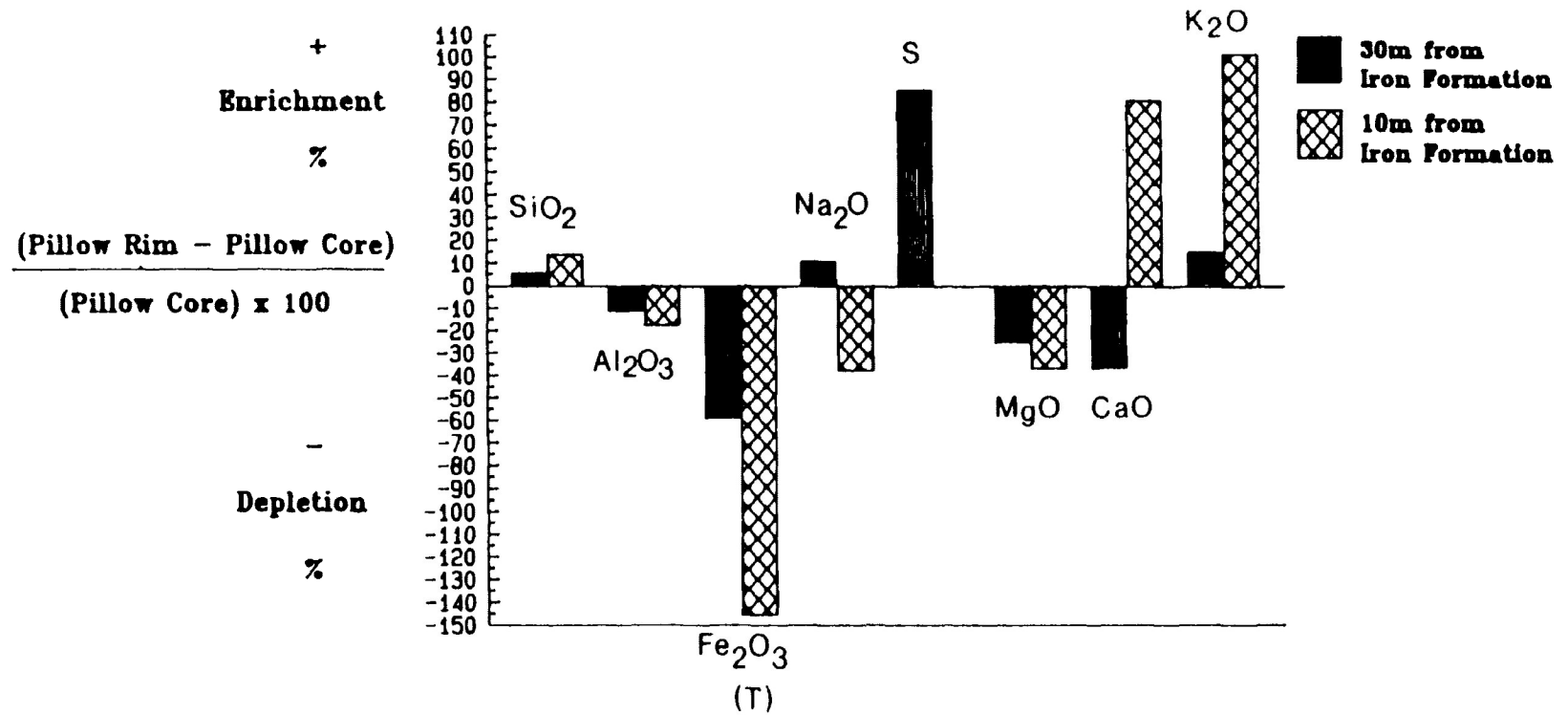
## SEDIMENTARY ROCKS

The clastic sedimentary rocks which commonly host the iron-formations consist of lithic wacke (greywacke), siltstone

# Alteration of Pillow Rims (Kingdom Property)

## Enrichment/Depletion of Major Element Concentrations

(Figure 3:2)



**AFM PLOT OF METAVOLCANIC  
AND MAFIC INTRUSIVE ROCKS**

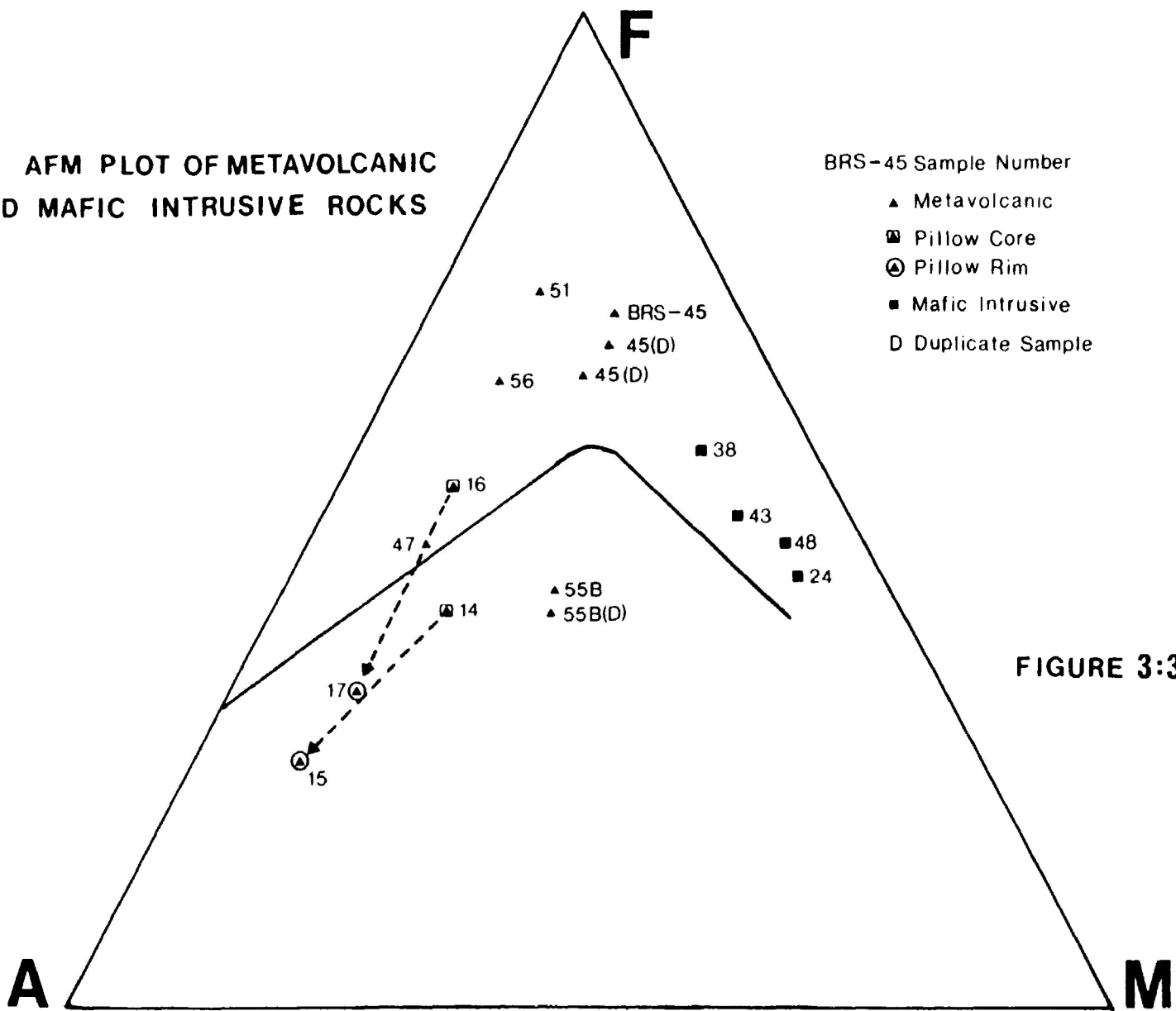


**FIGURE 3:3**

# DETAILED GEOLOGY OF THE LITTLE STEEL HIGHWAY OCCURRENCE

Section Looking  
South



0m

1m

2m

1c

4

3b

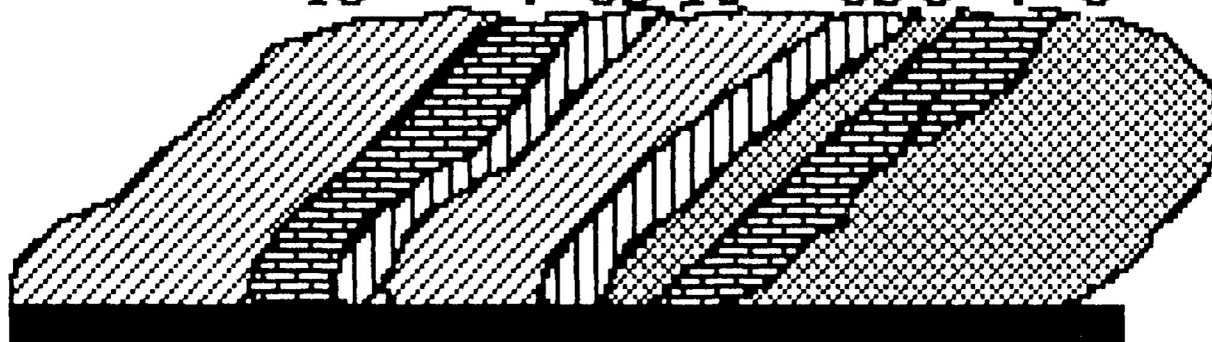
1c

3b

5

4

5



Highway 17





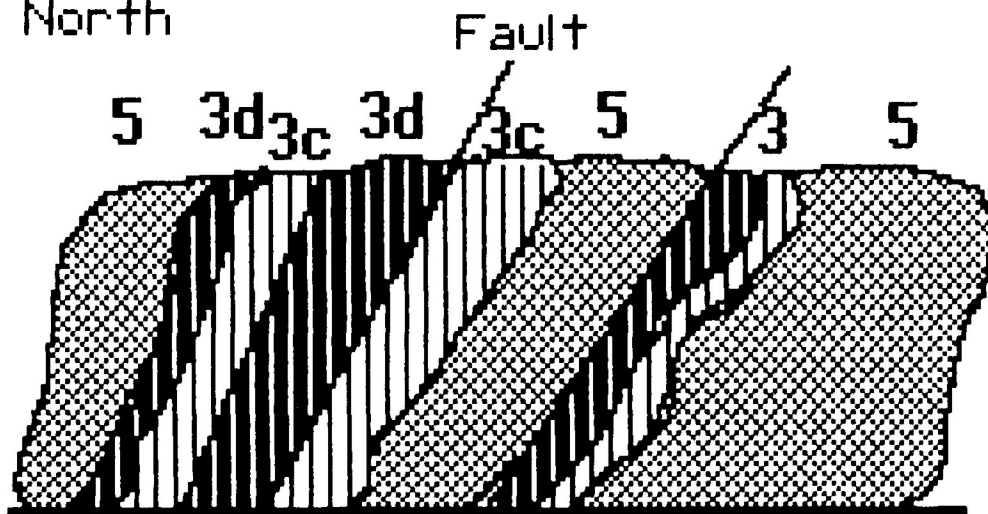
- |   |                                       |  |                 |
|---|---------------------------------------|--|-----------------|
|  <b>1c</b> | Pillowed Flows,<br>Pillow Breccia     |  <b>4</b> | Slate           |
|  <b>3b</b> | Chert, laminated<br>Clastic component |  <b>5</b> | Mafic Intrusive |

FIGURE 3:4

# DETAILED GEOLOGY OF THE LITTLE STEEL RAILWAY OCCURRENCE

Section Looking  
North



3c Laminated Chert
  5 Mafic Intrusive  
 3d Chert Breccia, Fault Gouge

0m 1m 2m

FIGURE 3:5

and slate. A variety of slate containing abundant pyrite and carbon is closely related to iron-formation deposition and will be discussed in the following chapter.

In the Lower Steel River - Little Steel Lake area, well-bedded, mostly graded lithic wacke, siltstone and slate are present. Detailed stratigraphic sections measured near the Steel River bridge (Figure 1:3) are shown in Figures 3:6 and 3:7. Interpretation of their depositional environments is presented in Chapter 5.

Examination of 76 beds over about 50 m of section (Figures 3:6 and 3:7) indicated no reversals in either the younging or structural facing directions. In the thesis area, the total thickness of the Steel River sedimentary succession is estimated to be 600 - 800 m. Primary textures include graded bedding, parallel lamination (Photo 3:2A), convolute lamination, cross-bedding (Photo 3:2C), load casts, erosional contacts, flame structures, ripples and loaded ripples (Photo 3:2A ), rip-up clasts (Photo 3:2B ) and scour structures.

The graded beds in both the Steel River Bridge and Kingdom areas represent turbidites. Bouma (1962) defined five divisions, A to E, in a complete turbidite. Division A represents a rapidly deposited graded interval. Division B results from traction in the upper flow regime and commonly displays parallel stratification, while division C results from traction in the lower flow regime and displays cross-lamination. Division D represents deposition of fines (silt and clay) and is commonly parallel-laminated, while division E, the pelitic portion, represents turbiditic fine-grained rainout followed by pelagic

**PHOTO 3:2(B)** RIP-UP CLASTS: STEEL RIVER AREA.  
NOTE: MUDSTONE CLASTS IN A  
SILTSTONE LAYER.

**PHOTO 3:2(C)** CROSS STRATIFICATION IN SILTSTONE  
LAYER, STEEL RIVER AREA.







# STRATIGRAPHIC COLUMN STEEL RIVER AREA - SECTION 2

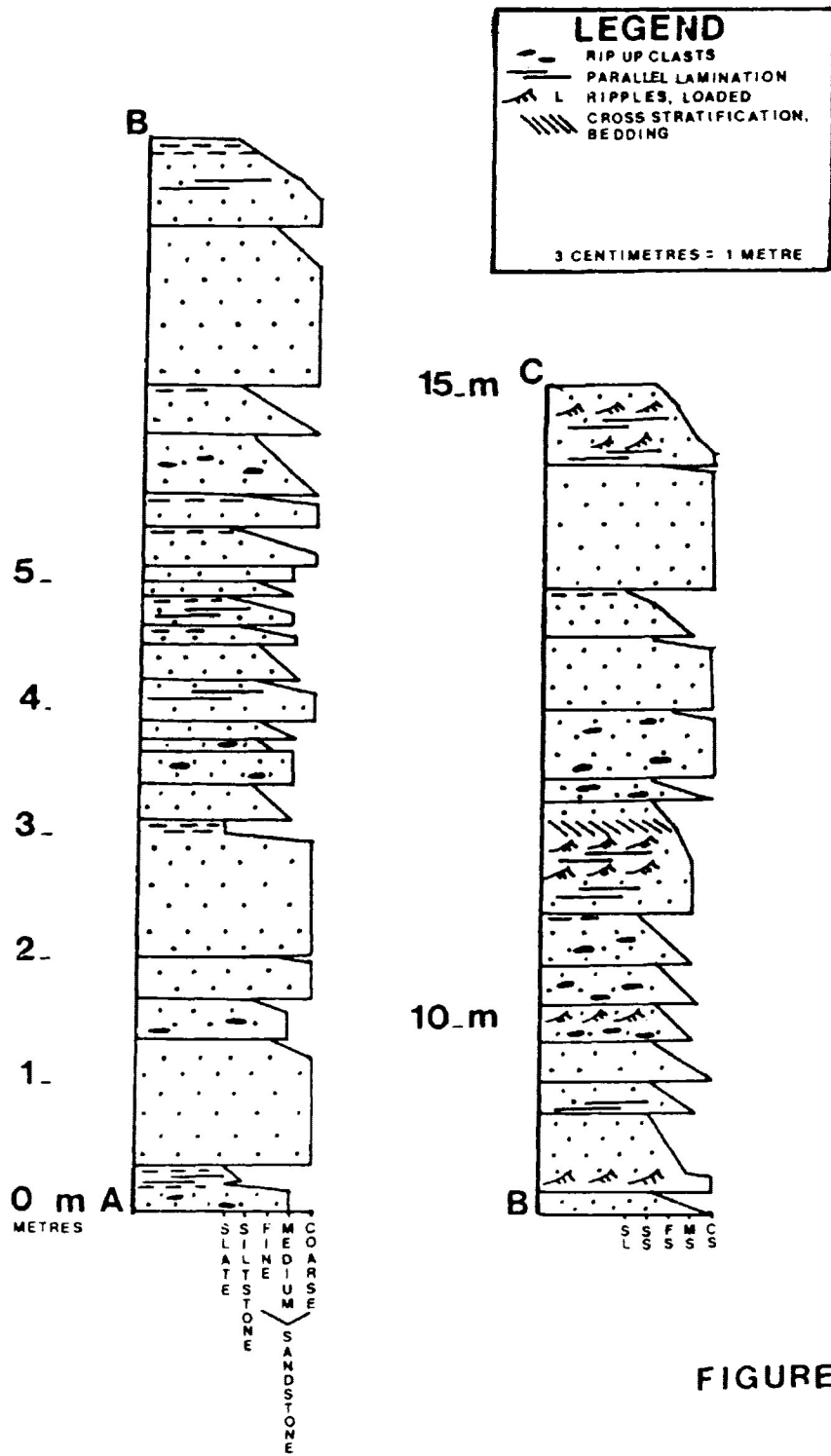


FIGURE 3:7

sedimentation. Classical ABCDE turbidites can vary in width from several centimetres to several metres.

Sequences in the Lower Steel River - Little Steel Lake area contain turbidites ranging from ABCBCD and ABCBCDE types (near-complete turbidite) to AE ("proximal"), CDE and BDE ("medial-distal"), and DE and E(t) ("distal-pelagic") types. AA and AE turbidites are considered to represent channel-proximal deposits, while the complete ABCDE turbidites are deposited more distally to the channel, possibly on a fan lobe (Walker, 1976). Lithic wacke-siltstone layers up to 3 m thick and ABCDE turbidites are commonly graded, and contain thinner turbiditic mudstone and pelagic rainout layers. The medial-distal turbidites consist of thin (up to 20 centimeters) lithic wacke-siltstone layers and thinner layers of rainout mudstone. The distal-pelagic turbidites consist of thinly bedded, fine-grained siltstone, turbiditic mudstone and pelagic layers; distal-pelagic successions can be up to several tens of metres in thickness.

Lithic wackes contain lithic fragments, quartz, and lesser albite and orthoclase feldspar. Possible volcanic shards were observed in several samples. Minor minerals include hornblende, chlorite, epidote, sericite, carbonate and biotite. The wackes appear to vary from quartz-rich near the Steel River Bridge area to more lithic (volcanic) in the Kingdom area. The quartz and feldspar grains are angular to subrounded.

Siltstones consist of quartz, albite, sericite, chlorite, carbonate and biotite. The carbonate, which is also present in veinlets, is considered to be authigenic.

Chemical analysis of sample BRS-41 (Table 3:2), a siltstone layer in a CDE/DE turbidite assemblage several hundred metres

**PHOTO 3:3**      PHOTOMICROGRAPH OF CHLORITE  
SCHIST WITH ZIRCON CRYSTALS,  
LITTLE STEEL HIGHWAY OCCURRENCE.  
SCALE BAR REPRESENTS 1 mm.

**PHOTO 3:4**      DURCHBEWEGUNG TEXTURE IN  
PYRRHOTITE, LITTLE STEEL  
HIGHWAY OCCURRENCE. ARROW  
POINTS TO PYRRHOTITE. SCALE  
BAR REPRESENTS 1 cm.

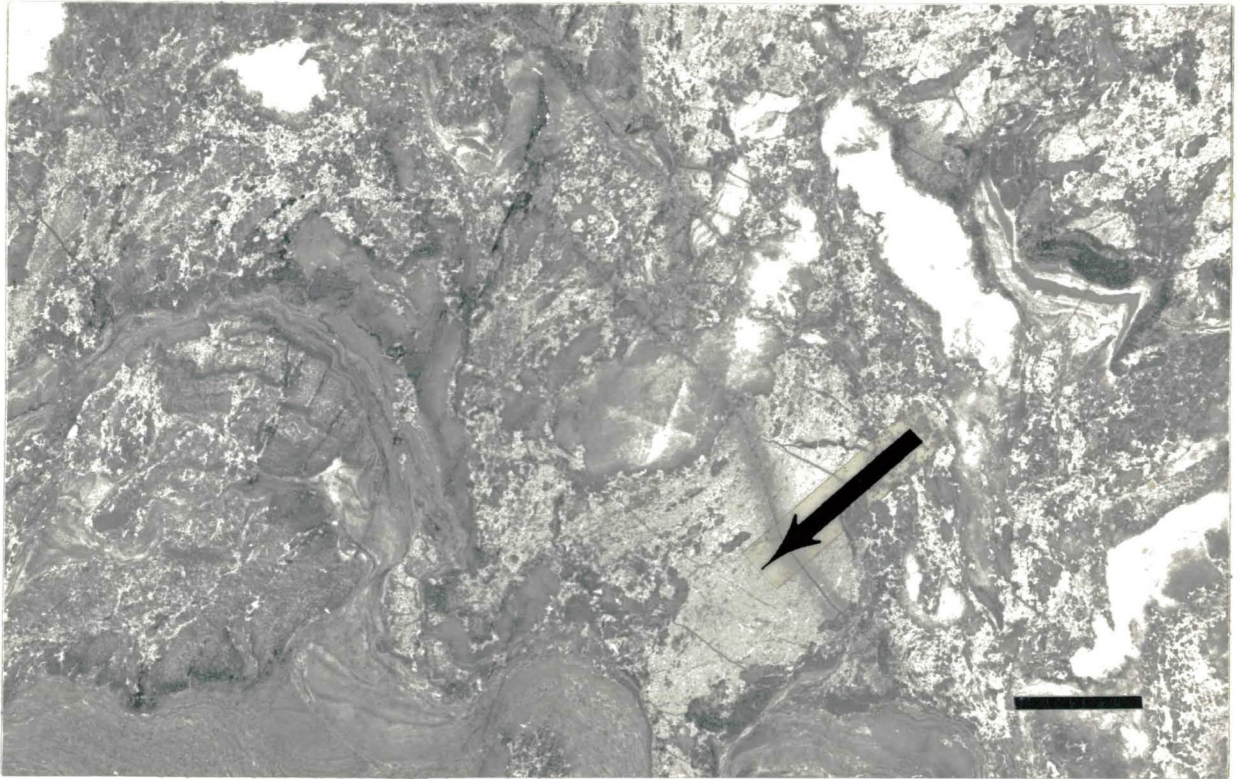
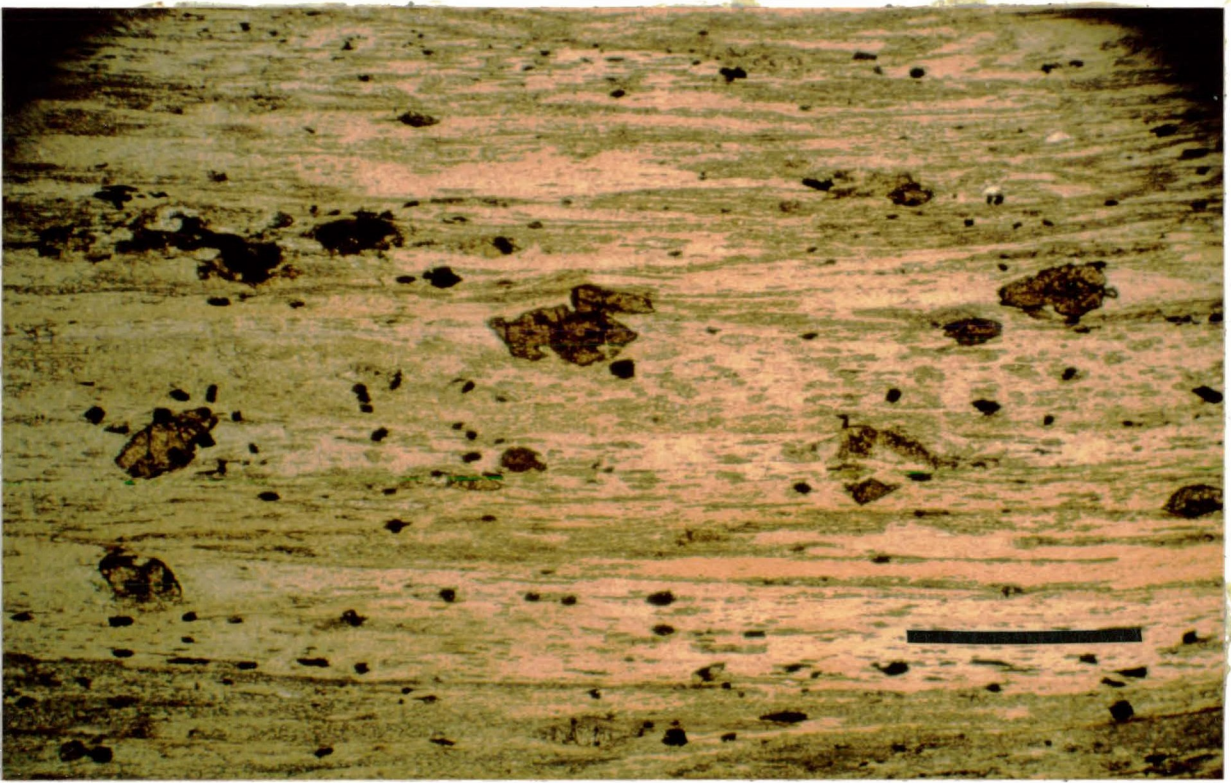


TABLE 3:2 - SAMPLE DESCRIPTIONS

<u>SAMPLE NUMBER</u>	
BRS-23	DE turbidite, shale or slate component, Kingdom Property. Sample collected several hundred metres from the iron-formation. Extremely fine-grained rock with an excellent cleavage. Analysis performed at Lakehead University.
BRS-23 (D)	Duplicate sample of BRS-23. Analysis performed at Geoscience Laboratories, Toronto.
BRS-33	Medium-grained greywacke from the Simard-Swetz Property. Thin section displays sub-rounded quartz grains in a sericite, feldspar matrix. The rock displays some fabric and deformation.
BRS-37	Fine-grained DE turbidite, slate component, displaying folding and axial planar cleavage. Pyrite present along axial planar cleavage. Photo 4:1B
BRS-41	Siltstone-Shale, Black Fox Property. Sample collected 500 m away from the sulphide-facies iron-formation. Analysis performed at the Geoscience Laboratories, Toronto.
BRS-46	Pillow Breccia Matrix, interpillow sediment, Little Steel Highway occurrence. Sample is of dark green matrix of pillow breccia. Altered fragments are represented by sample BRS-47 (Table 3:1). A strong schistosity is present. Analysis performed at Lakehead University.

TABLE 3:2  
COMPOSITION OF METASEDIMENTARY  
ROCKS ASSOCIATED WITH IRON-FORMATION

Sample No.	BRS-23	BRS-23(D)	BRS-33	BRS-37	BRS-41	BRS-46
SiO <sub>2</sub>	30.9	32.6	51.55	53.7	61.4	41.81
Al <sub>2</sub> O <sub>3</sub>	17.76	17.9	14.59	16.3	17.0	17.88
Fe <sub>2</sub> O <sub>3</sub> (T)	18.83	24.3	9.77	7.6	5.80	20.45
Fe <sub>2</sub> O <sub>3</sub>	0.1	---	---	---	---	1.99
FeO	17.18	---	---	---	---	16.66
Fe	14.0	---	---	4.80	3.39	N/A
MgO	6.27	7.02	1.59	1.6	1.91	9.37
CaO	4.59	5.81	10.69	1.8	1.25	2.89
Na <sub>2</sub> O	1.11	0.71	2.01	3.94	3.03	1.52
K <sub>2</sub> O	0.16	0.77	0.01	3.18	3.94	0.15
TiO <sub>2</sub>	2.21	2.79	0.48	0.28	0.78	2.98
P <sub>2</sub> O <sub>5</sub>	0.26	0.28	0.11	0.16	0.07	0.26
MnO	0.65	0.59	0.14	Nil	0.02	0.29
C	---	---	---	2.0	0.3	---
CO <sub>2</sub>	0.66	0.60	5.93	8.36	1.88	1.17
H <sub>2</sub> O	6.57	---	3.23	---	---	1.80
S	---	0.04	---	2.36	2.60	0.15
LOI	7.23	5.2	9.16	6.5	4.30	2.97
TOTAL	88.28	98.0	100.01	99.2	99.5	98.78
Co (ppm)	64	---	---	17	30	---
Cr (ppm)	233	---	---	14	24	---
Cu (ppm)	124	---	---	45	128	42
Mn (ppm)	4780	---	---	73	114	---
Ni (ppm)	16	---	---	49	26	---
Pb (ppm)	Nil	---	---	10	10	---
Zn (ppm)	270	---	---	36	119	62

(D) Represents Duplicate Analysis  
--- Not Analysed



away from the Black Fox occurrence, indicates 61.4% SiO<sub>2</sub>, 5.80% total iron (Fe<sub>2</sub>O<sub>3</sub>) and 0.3% carbon (amorphous carbon or graphite). The sample is considered to represent an average siltstone.

The mudstones contain coarser detrital quartz and plagioclase shards within a matrix of quartz, sericite, carbonate and chlorite. The shards suggest a possible tuffaceous component at certain localities such as the Kingdom occurrence. Laminations about 0.20 mm thick are formed by alternation of quartz-rich bands and opaque-rich bands of iron sulphides. Kingdom sample BRS-23 (Table 3:2) is from the rainout-mudstone part of a DE turbidite.

Sample BRS-46 (Table 3:2) represents fine-grained rainout sediment forming the matrix of a pillow breccia unit at the Little Steel Highway occurrence (Figure 3:4). It is a chlorite-muscovite schist (Photo 3:3) with accessory sphene, zircon, carbonate and pyrite.

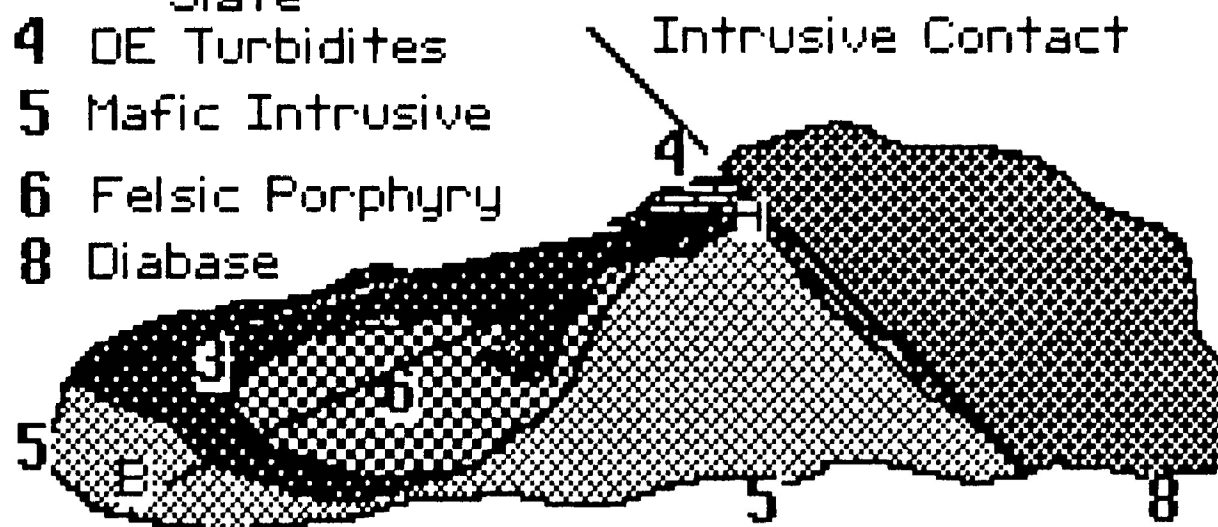
Carbonate-carbon analyses were performed on samples of mudstone and slate in order to determine the carbon component of total carbon. These samples, which occurred several hundred metres from the iron-formations, had values ranging from below the detection limit to 0.09%.

#### INTRUSIVE ROCKS

Mafic and felsic intrusives are commonly associated with the iron-formations in the Lower Steel River - Little Steel Lake area.

# DETAILED GEOLOGY OF THE BLACK FOX LAKE OCCURRENCE

- 3 Graphitic-Pyritic Slate
- 4 DE Turbidites
- 5 Mafic Intrusive
- 6 Felsic Porphyry
- 8 Diabase



Section looking North

0m 1m 2m 3m

FIGURE 3:8

TABLE 3:3 - SAMPLE DESCRIPTIONS

<u>SAMPLE NUMBER</u>	
BRS-24	Medium-grained, mafic intrusive cross-cutting meta-sedimentary rocks, Simard-Swetz occurrence. Thin section displays hornblende, biotite, plagioclase, epidote, chlorite and carbonate. Analysis performed at Lakehead University.
BRS-38	Mafic intrusive dike, Black Fox Lake occurrence. Dark green to black, medium-grained rock, cross-cutting metavolcanics. Thin section displays hornblende, quartz, plagioclase, chlorite, epidote and carbonate. Analysis performed at Lakehead University.
BRS-43	Mafic intrusive, Black Fox Lake occurrence. Coarse-grained and carbonatized mafic intrusive rock. Analysis performed at Lakehead University.
BRS-45	Deformed mafic intrusive rock or mafic metavolcanic rock, Little Steel Highway occurrence. Fine-grained rock with minor clots. Thin section indicates rock is a chlorite schist with abundant carbonate and sericite. Epidote and clinozoisite are also present. Analysis performed at Lakehead University.
BRS-45 (D) 1	Duplicate of BRS-45. Analysis performed at Lakehead University.
BRS-45 (D) 2	Duplicate of BRS-45. Analysis performed at Geoscience Laboratories, Toronto.
BRS-48	Mafic to ultramafic intrusive rock, Little Steel Railway occurrence. Medium-grained, highly carbonatized rock, with abundant quartz-carbonate veining. Thin section displays hornblende, plagioclase, sericite, epidote, chlorite, quartz and carbonate. Analysis performed at Lakehead University.

TABLE 3:3  
 COMPOSITION OF MAFIC INTRUSIVE  
 ROCKS ASSOCIATED WITH IRON-FORMATION

Sample No.	BRS-24	BRS-38	BRS-43	BRS-45	BRS-45(D) 1	BRS-45(D) 2	BRS-48
SiO <sub>2</sub>	46.69	50.80	48.00	50.09	50.31	50.0	44.77
Al <sub>2</sub> O <sub>3</sub>	10.31	14.21	10.63	16.47	16.12	15.0	10.43
Fe <sub>2</sub> O <sub>3</sub> (T)	10.10	13.08	10.84	11.90	12.25	11.8	13.37
Fe <sub>2</sub> O <sub>3</sub>	---	5.64	---	---	---	---	---
FeO	---	6.66	---	---	---	---	---
Fe	---	---	---	---	---	---	---
MgO	10.43	7.03	8.10	2.61	2.57	2.71	12.04
CaO	9.06	4.84	11.94	8.33	8.39	9.17	8.67
Na <sub>2</sub> O	1.58	1.62	1.89	1.71	---	2.26	1.96
K <sub>2</sub> O	0.11	0.61	0.09	0.01	Nil	0.46	0.01
TiO <sub>2</sub>	0.55	0.91	0.59	2.23	2.24	2.35	0.65
P <sub>2</sub> O <sub>5</sub>	0.03	0.11	0.19	0.47	0.40	0.25	0.16
MnO	0.21	0.17	0.19	0.29	0.27	0.25	0.26
C	---	---	---	---	---	---	---
CO <sub>2</sub>	4.99	3.52	4.38	3.89	---	3.44	3.62
H <sub>2</sub> O	3.04	2.61	3.51	2.78	---	---	3.78
S	---	0.03	---	---	---	0.19	---
LOI	8.03	6.13	7.89	6.67	---	5.8	7.40
TOTAL	97.10	99.09	100.35	100.78	---	100.00	99.74

(D) Represents Duplicate Analysis  
 --- Not Analysed

## MAFIC INTRUSIONS

Meta-gabbro and meta-diorite dikes, sills and tabular bodies in the thesis area are described by Walker (1967). He was uncertain as to whether these mafic intrusives represented feeders to volcanic flows, or coarse-grained portions of mafic volcanic flows, or had no relation to volcanism. Walker (1967) also noted that in the area northeast of the Steel River bridge, the mafic intrusives contain rotated blocks of greywacke and slate. In one outcrop near the Little Steel occurrence, two generations of mafic intrusives with crosscutting relationships were observed; both crosscutting the sedimentary rocks and one intruding the other.

Metagabbros are present at the Simard-Swetz, Little Steel Highway and Railway occurrences (Figure 3:4, 3:5), and at Black Fox (Figure 3:8). The intrusives are commonly parallel to the foliation or cleavage, which in many of the areas is parallel to the sediment layering. The intrusives vary in width from less than 1 metre up to several tens of metres; textures range from fine-grained near the chilled margins to coarse-grained in more central portions. The mafic intrusives also vary in the degree of deformation from well-preserved crystalline varieties to highly sheared, fine-grained schists. Carbonate alteration is common. At one exposure near Black Fox Lake (Figure 3:8), a carbonate-quartz vein system contains sulphides and a green muscovite.

Chemical analyses of 6 samples from basic intrusions in the Lower Steel River - Little Steel Lake area (Table 3:3), are consistent with variably altered gabbroic compositions. Samples

contain 44.8 to 50.8% SiO<sub>2</sub>, with several percent secondary carbonate.

Late mafic dikes crosscut all rock types of the thesis area. Walker (1967) recorded both lamprophyre and diabase dikes. A late diabase dike up to ten metres in width is present at the Kingdom Occurrence. Late mafic dikes generally strike to the northwest.

Sample BRS-45, from the Little Steel Highway area (Figure 3:5, Map 1), was interpreted in the field as a mafic intrusive. Microscopic examination indicates that it is a fine-grained, chlorite-sericite schist also containing epidote and clinozoisite, with carbonate replacing plagioclase. Primary textures of this rock have been destroyed by metamorphism and deformation, making its original nature uncertain. Triplicate analyses are given in Table 3:3.

Gabbros in the Simard-Swetz and Little Steel areas contain plagioclase, sericite, carbonate, saussurite, chlorite, epidote, quartz, hornblende and biotite. Calcite is common in the matrix and as late crosscutting carbonate veins. Gabbros varied from relatively fresh and coarse-grained to fine-grained, carbonatized and foliated schists.

#### EFFECT OF INTRUSIONS ON SEDIMENTS

At the Little Steel Railway and Highway occurrences a mafic intrusive is in contact with a chemical sedimentary unit consisting of chert, cherty tuff and ash (sample BRS-44 and 51, Table 3:2). The mafic rock displays variable degrees of carbonatization and chloritization. In areas of more extreme deformation such as the Little Steel Highway and Black Fox occurrences, brecciation and fracturing of sedimentary rocks

occurs close to the intrusives. As penetrative deformation intensifies, cataclasis, disorientation and fragmentation occur in both the sedimentary rocks and mafic intrusions.

A texture similar to "Durchbewegung" (Craig and Vaughan, 1981) was observed in pyrrhotite mineralization at the Little Steel Highway occurrence (Photo 3:4) where a mafic dike intrudes the sedimentary rocks. These deformed chemical sedimentary units contain abundant pyrrhotite and magnetite; less deformed sedimentary rocks further from the intrusives contain predominantly pyrite. Stanton (1972) stated that in regard to contact metamorphosed ores that pyrite is converted to magnetite with an increase in the proportion of pyrrhotite; the best documented examples involve the intrusion of dikes into large sulphide orebodies. This contact metamorphic process appears to have operated on iron-formations at the Little Steel Highway and Black Fox Occurrences.

#### FELSIC INTRUSIONS

Quartz-feldspar- and feldspar-porphyrific intrusions are associated with several of the iron-formations in the Lower Steel River-Little Steel Lake area. The porphyries occur as dikes up to several metres in width and commonly intrude the iron-formations. They are white to pinkish, and fine- to medium-grained. The carbonatized varieties weather to a reddish-brown color. At the Kingdom occurrence, the porphyry is more resistant to erosion than the fine-grained chemical and clastic sedimentary rocks, and produce erosional remnants or pillars on the Lake Superior shoreline. A felsic porphyry dike (BRS-42) up to 1 metre wide

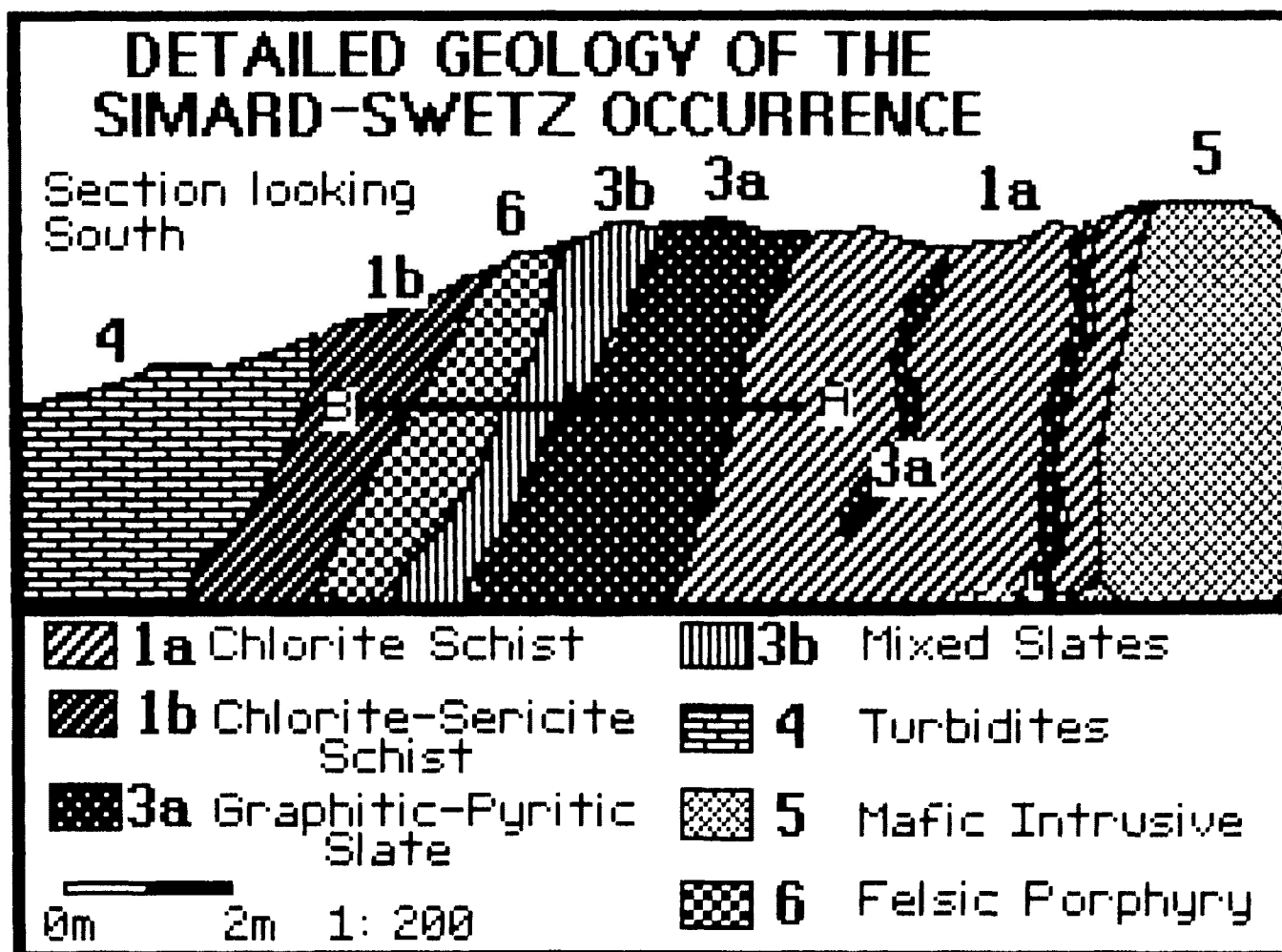


**FIGURE 3: 9**



intrudes schist and slate at the Simard-Swetz occurrence (Figure 3:9).

Three samples of felsic, porphyritic intrusive rock (BRS-10, 32 and 42) have closely comparable compositions consistent with a dacitic parent magma (Table 3:4). The felsic intrusives vary from weakly altered porphyries to highly altered and deformed schists. In the less deformed porphyries, phenocrysts of quartz and saussuritized and sericitized sodic plagioclase are present in a matrix of quartz, feldspar, sericite, carbonate and minor chlorite. Opaques and sulphides are less abundant in the weakly deformed varieties, while up to 15 % pyrite is present in more deformed intrusives. At the Kingdom occurrence the porphyry (BRS-10) is now represented by a quartz-sericite-carbonate schist, with accessory chlorite, pyrite and magnetite.

TABLE 3:4 - SAMPLE DESCRIPTIONSAMPLE NUMBER

- BRS-10 Felsic porphyritic intrusive rock, Kingdom occurrence. Rock has small quartz phenocrysts. Thin section indicates the rock is a quartz-sericite schist. Large idiomorphic pyrite crystals. Rock contains muscovite, sericite, quartz, and minor chlorite. Analysis performed at Lakehead University.
- BRS-10 (A) Highly mineralized, pyrite-rich sample of the porphyry unit. Analysed for trace elements at the Geoscience Laboratories, Toronto.
- BRS-10 (D) Duplicate of BRS-10. Trace element analysis performed at the Geoscience Laboratories, Toronto.
- BRS-32 Felsic dike rock, Simard-Swetz occurrence. Rock contains disseminated pyrite. White to pink coloured rock displays a faint banding. Thin section indicates the rock is a quartz-carbonate-sericite schist, with recrystallized pyrite. Analysis performed at Lakehead University.
- BRS-42 Folded felsic porphyry, Black Fox Lake occurrence. Rock contains disseminate pyrite. Thin section displays large feldspars (microcline?) partly or completely altered to sericite. Analysis performed at Lakehead University.

TABLE 3:4  
COMPOSITION OF FELSIC INTRUSIVE  
ROCKS ASSOCIATED WITH IRON-FORMATION

Sample No.	BRS-10	BRS-10(A)	BRS-10(D)	BRS-32	BRS-42
SiO <sub>2</sub>	66.07	---	---	64.32	67.66
Al <sub>2</sub> O <sub>3</sub>	14.84	---	---	14.73	14.5
Fe <sub>2</sub> O <sub>3</sub> (T)	3.49	---	---	4.63	2.47
FeO	---	---	---	---	---
Fe	---	---	---	---	---
MgO	1.62	---	---	0.71	0.21
CaO	3.13	---	---	3.18	3.39
Na <sub>2</sub> O	4.01	---	---	5.74	4.29
K <sub>2</sub> O	1.54	---	---	0.07	0.78
TiO <sub>2</sub>	0.51	---	---	0.58	0.40
P <sub>2</sub> O <sub>5</sub>	0.01	---	---	0.04	0.09
MnO	0.09	---	---	0.01	0.01
C	---	---	---	---	---
CO <sub>2</sub>	3.73	---	---	3.56	2.75
H <sub>2</sub> O	1.26	---	---	0.63	1.08
S	---	---	---	---	---
LOI	4.99	---	---	4.19	3.83
TOTAL	97.31	---	---	98.21	97.64
Au (ppb)	---	2120	---	---	---
Ag (ppm)	---	25	---	---	---
Co (ppm)	34	---	34	---	15
Cr (ppm)	10	---	10	---	18
Cu (ppm)	20	221	20	---	32
Ni (ppm)	35	---	35	---	7
Pb (ppm)	Nil	---	Nil	---	16
Zn (ppm)	82	227	82	---	110

(D) Represents Duplicate Analysis

--- Not Analysed

#### 4) IRON-FORMATION AND RELATED CHEMICAL AND CLASTIC COMPONENTS

##### GENERAL

Of the iron-formations studied in the Schreiber - Terrace Bay area, 80 % were sulphide-facies, 15 % were oxide-facies, and 5 % were represented by silicate- or carbonate-facies. The iron-formations are intimately associated with volcanic rocks and marine clastic sedimentary rocks, all of which have undergone regional metamorphism, commonly to the greenschist or lower amphibolite facies.

##### COMPOSITION OF THE IRON-FORMATIONS

If one uses the definition of iron-formation which includes any chemical sedimentary unit containing more than 15 % iron (James, 1966), it would be very difficult to subdivide or separate the iron-formations from the "related" chemical and clastic sedimentary components. The term "related" is used to include associated components such as chert and black carbonaceous slate. Due to the intricate interlayering and interlamination of chert, pyritic-carbonaceous slate and iron-rich chemical sedimentary rocks, those sequences which average 15% or more iron will be classified as sulphide-facies iron-formations. The various components of the iron-formations are discussed in the following sections.

##### CLASTIC COMPONENTS

###### a) Pyritic-Carbonaceous Slate

This lithology ranges in thickness from several centimetres to a maximum of 20 m (Kingdom occurrence). Folding appears to have

produced structural thickening in several locations. The slate units display well developed cleavage and locally a schistose fabric.

Easdon (1969) recognized 5 varieties of metamorphosed carbonaceous shales from the Rouyn-Val d'Or area: 1) massive, generally structureless slate, barren of sulphides, 2) a massive variety displaying variable amounts of massive, disseminated or nodular pyrite, 3) well layered, pyrite-poor slate, with cherty and graphitic laminae, 4) a well layered, graphitic variety; and 5) sulphide-rich, graphitic slate. Similar varieties of pyritic-carbonaceous slate were observed in the present study. However, because many of the categories are intimately intercalated with each other and with layers and laminations of chert and massive sulphides, a useful classification of iron-rich sedimentary rocks was not plausible.

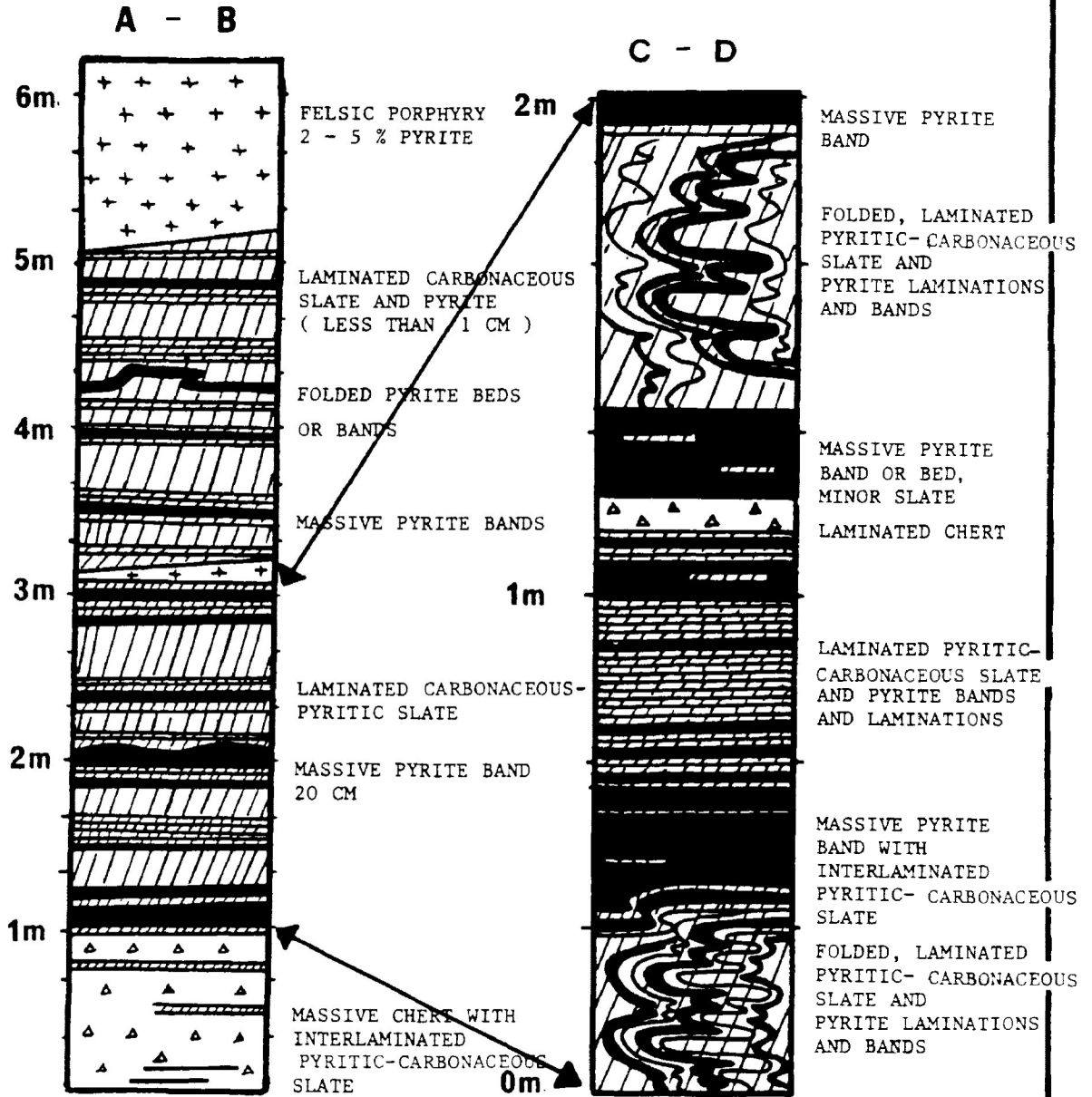
At the Kingdom occurrence (Figure 3:1, 4:1) pyritic-carbonaceous slates up to 20 m thick contain chert layers up to several meters thick, as well as massive pyrite beds and lenses up to 25 cm wide. Diamond drilling in 1986 intersected up to 67 m of iron-formation, which is interpreted as representing a true thickness of at least 40 m (Don Penner, Kingdom Resources, Vancouver, pers. comm., 1986). The slate is interlaminated with alternating siltstone, pyrite and chert. Massive sulphides and chert are described in the chemical component section.

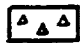


Alternating DE turbidites and slaty mudstones occur at the Morley Pyrite, Simard-Swetz and Black Fox occurrences (Photo 4:1 A&B). The DE turbidites are rich in iron within several metres of truly pyritic-carbonaceous slates. Fine-grained layers are opaque-rich (carbon, pyrite) whereas coarser-grained layers are



**DETAILED KINGDOM SECTIONS**

(From Figure 3:1)

**TYPE SECTIONS**



-  CHERT, MASSIVE, LAMINATED,
-  PYRITIC- CARBONACEOUS SLATE  
BEDDED, LAMINATED
-  FINE-GRAINED DISSEMINATED PYRITE

-  MASSIVE PYRITE, BEDDED,
-  FELSIC PORPHYRY

**FIGURE 4:1**

quartz-rich and opaque-poor. DE turbidites less than 5 mm thick at the Black Fox occurrence (Photo 4:1 A&B) appear to grade into pyritic-carbonaceous slate overlain by a near-massive and nodular pyrite bed (Photo 4:12B).

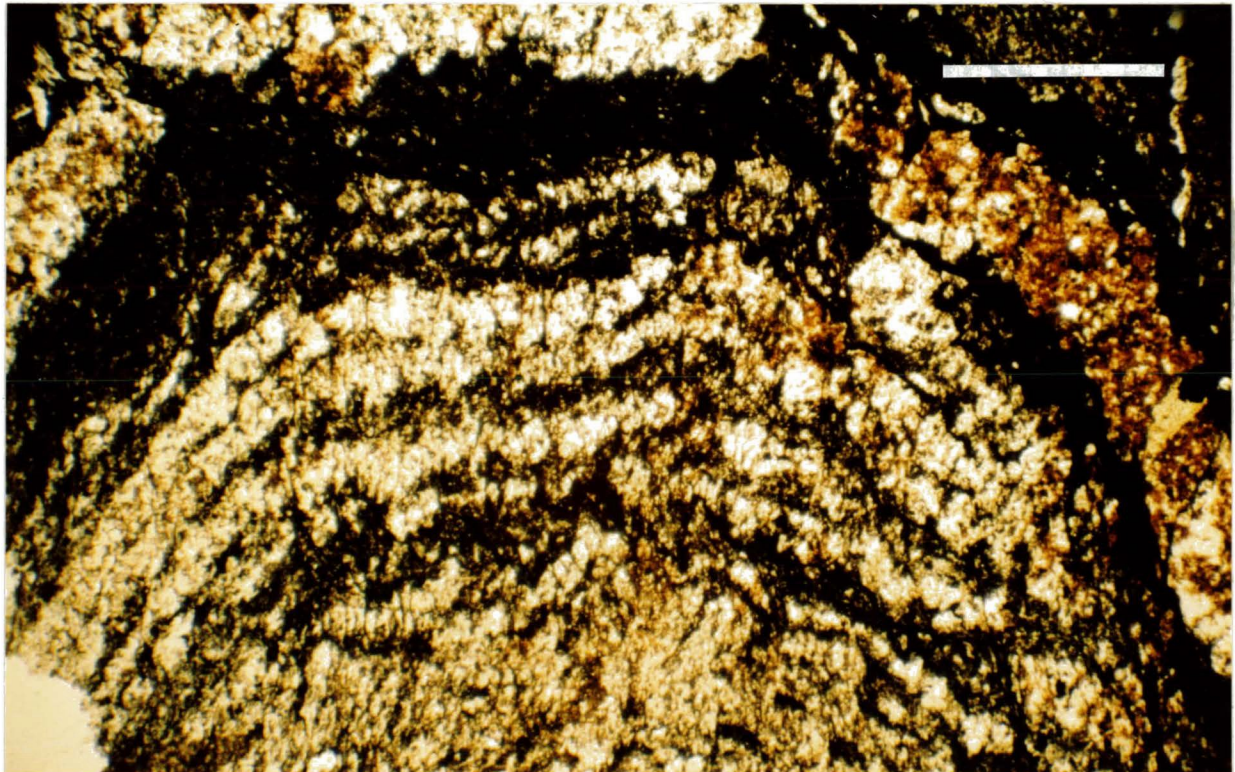
The Simard-Swetz occurrence (Figure 4:2) is characterized by mineralogical banding of sulphides, carbonaceous material and chert. The pyritic-carbonaceous slates consist of interlaminated siltstone, slate and chert, together with pyrite layers, lenses, disseminated grains and nodules. Occasionally pyrite occurs as individual grains aligned in a thin train. At the Kingdom, pyritic laminations are paper-thin ( $<0.01\text{mm}$ ), whereas at the Simard-Swetz and Morley properties, pyrite forms layers up to tens of centimetres thick. Thin slate laminations occur within the massive pyrite beds at the Morley property (Photo 4:8).

Microscopic examination reveals that the pyritic-carbonaceous slates contain detrital quartz and feldspar in a matrix of quartz, sericite, carbonate, chlorite, pyrite, and carbon. Angular fragments of quartz and feldspar in the Kingdom and Morley slates suggest a possible tuffaceous component. At the Kingdom occurrence (Figure 4:1), lamellar or feather (pressure shadow) quartz is present in lenses, commonly filling dilatant zones. Pressure shadow quartz or "Boehm" lamellae is interpreted as secondary or remobilized quartz; it is commonly associated with deformed pyrite beds at the Kingdom, Simard-Swetz and Black Fox occurrences. Easdon (1969) described lamellar quartz with undulatory extinction which formed "pressure shadows" surrounding pyrite nodules. The wedge-shaped quartz "shadows" produce an augen-like texture in hand specimen. Similar textures are present at the Black Fox occurrence (Photo 4:2). Localized deformation

**PHOTO 4:1(A)** FOLDED DE TURBIDITE (SILTSTONE-SLATE) DISPLAYING AXIAL PLANAR CLEAVAGE AND PYRITE NODULE, BLACK FOX OCCURRENCE. SCALE BAR REPRESENTS 1 cm. SAMPLE BRS-39.

**PHOTO 4:1(B)** PHOTOMICROGRAPH OF FOLDED DE TURBIDITE AND AXIAL PLANAR CLEAVAGE, BLACK FOX OCCURRENCE. SCALE BAR REPRESENTS 1 mm. SAMPLE BRS-37.





TYPE SECTIONS

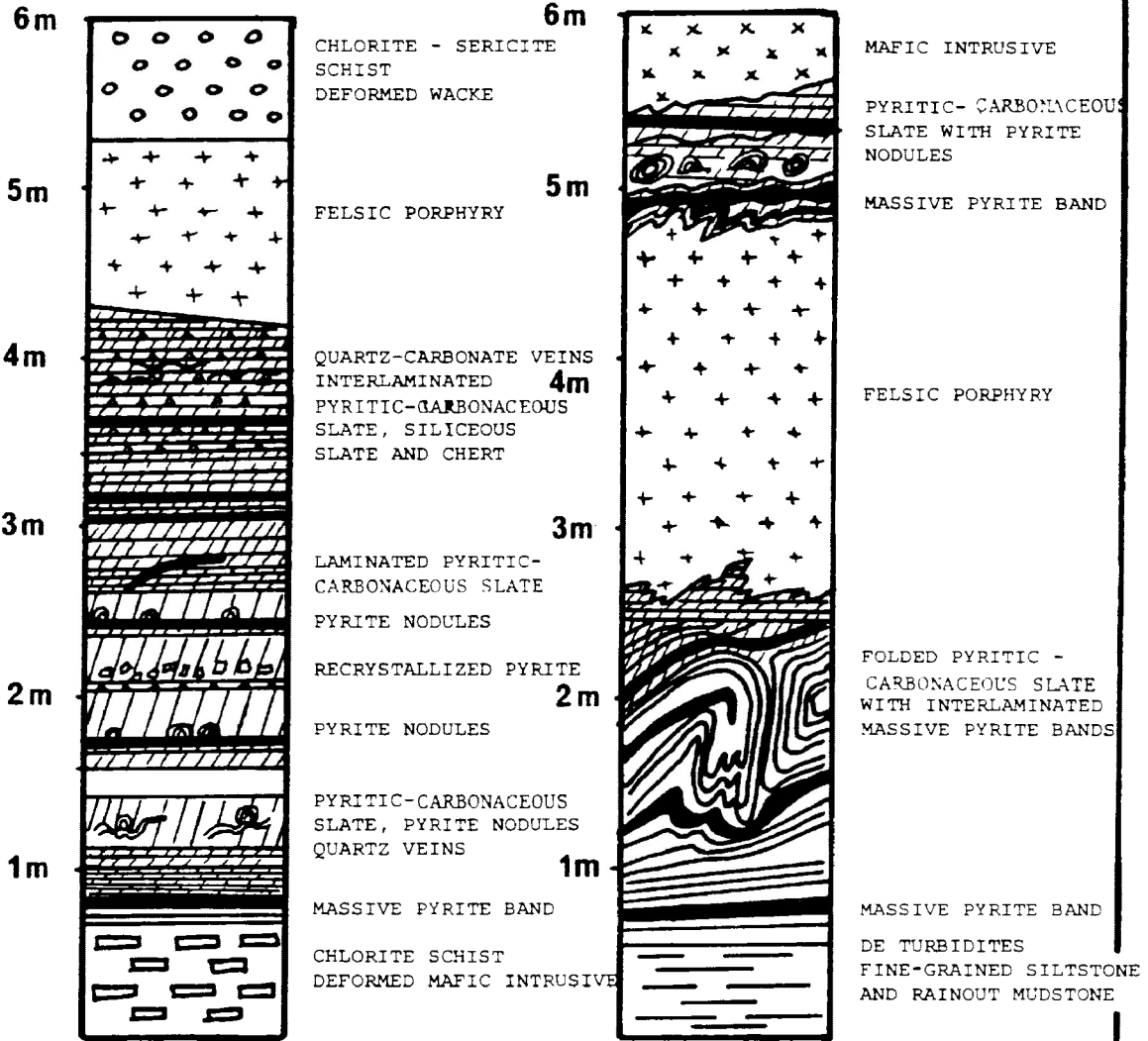
FIGURE 4:2

SIMARD - SWETZ  
A - B

(From Figure 3:9)

BLACK FOX LAKE  
A - B

(From Figure 3:8)



- |  |   |  |                               |
|--|---|--|-------------------------------|
|  | CHERT, MASSIVE, LAMINATED                                 |  | CHLORITE - SERICITE SCHIST    |
|  | PYRITIC-CARBONACEOUS SLATE, LAMINATED FINE-GRAINED PYRITE |  | FINE-GRAINED TURBIDITES (D-E) |
|  | MASSIVE PYRITE, RECRYSTALLIZED BEDDED                     |  | FELSIC PORPHYRY               |
|  | CHLORITE SCHIST   |  | MAFIC INTRUSIVE               |

produced schistose and brecciated textures in the iron-rich slates. At the Kingdom, the iron-rich slate displays elongated lenses of quartz, sericite and pyrite. Alternating sulphide-opaque (likely carbon)-sericite-rich and quartz-rich laminations represent relict bedding.

At the Black Fox, layering in DE turbidites and interturbidite bands is due to the alternation of chlorite-opaque-rich and sericite-quartz-rich bands (Photo 4:1). In several specimens a faint grain-size gradation was evident in the latter bands. The DE turbidites are folded and display excellent axial planar cleavage.

At the Simard-Swetz occurrence, pyritic-carbonaceous slate occurs as both unbedded and laminated varieties, in alternation with slaty and siliceous laminations. The laminations contain microcrystalline quartz with large detrital plagioclase fragments and volcanic shards. Sulphide-rich laminations are generally associated with slaty laminations. The siliceous laminations consist of alternating bands (up to 2 mm thick) of fine-grained quartz with carbonate, and coarser-grained quartz with abundant secondary carbonate. Secondary carbonates are probably related to the intrusion of metagabbroic and felsic porphyritic dikes.

Chemical analysis (Table 4:1) of the light and dark colored siliceous laminations indicated that the dark laminations (BRS-30) contained about 2 % less  $\text{SiO}_2$  than the lighter laminations (BRS-31). In addition, the total  $\text{Fe}_2\text{O}_3$  and S contents in the darker laminations were higher, probably indicating a greater sulphide content. The light laminations and layers also contain considerably more  $\text{CaCO}_3$  than the darker ones. Because of high  $\text{Al}_2\text{O}_3$  contents of the siliceous layers, they are termed

TABLE 4:1 - SAMPLE DESCRIPTIONS

SAMPLE NUMBER

BRS-5	Pyritic-carbonaceous slate, Kingdom Property. Sample collected near contact with large diabase dike. Disseminated to laminated pyrite. Thin section displays pressure shadow quartz, a well developed fabric and recrystallization of the pyrite. Analysis performed Lakehead University.
BRS-6	Pyritic-carbonaceous slate, pyrite lens near diabase dike, Kingdom Property. Pyrite is recrystallized. Trace elements and Fe analysed at Geoscience Laboratories, Toronto.
BRS-8	Pyritic-carbonaceous slate, Kingdom Property. Disseminated pyrite in finely laminated sediment. Thin section displays fine-grained pyrite grains and secondary recrystallized pyrite. Abundant opaques present. Analysis performed at Geoscience Laboratories, Toronto.
BRS-9	Pyritic-carbonaceous slate, Kingdom Property. Massive pyrite lenses are fine-grained and oriented along possible bedding. Rock displays a finely laminated texture. Thin section indicates intense deformation, alternating pyrite-carbonaceous-rich and clastic-rich layers. Brecciated secondary pyrite is abundant. Analysis performed at Lakehead University.
BRS-22	Pyritic-carbonaceous slate, Kingdom Property. Disseminated, fine-grained, pyrite-rich sample. Black in colour. Analysis performed at Lakehead University.
BRS-25	Pyritic-carbonaceous slate, Simard-Swetz occurrence. Siliceous slate, pyritic-rich. Disseminated and laminated pyrite. Analysis performed at Lakehead University.
BRS-27	Pyritic-carbonaceous slate, Simard-Swetz occurrence. Fine disseminated pyrite with radial nodules. Sample of slate component. Analysis performed at Lakehead University.
BRS-29	Pyritic-carbonaceous slate, Simard-Swetz occurrence. Slate-rich, generally pyrite-poor.
BRS-29 (A)	Pyritic-carbonaceous slate, Simard-Swetz occurrence. Sampled at 4 locations, generally pyrite-rich. Some secondary galena and sphalerite. Secondary carbonate.

TABLE 4:1 (con't)

BRS-30	Siliceous sediment, Simard-Swetz occurrence. Laminated dark coloured bands, secondary quartz and carbonate veins. Recrystallized pyrite. Minor galena and sphalerite. Analysis performed at Lakehead University.
BRS-31	Siliceous sediment, Simard-Swetz occurrence. Laminated light coloured bands. Secondary carbonate. Recrystallized pyrite and secondary galena and sphalerite. Analysis performed at Lakehead University.
BRS-40	Pyritic-carbonaceous slate, Black Fox Lake occurrence. Highly folded slate with axial planar cleavage and abundant pyrite nodules and disseminations and pressure shadow quartz. Analysis performed at Geoscience Laboratories, Toronto.
BRS-40 (A)	Pyritic-carbonaceous slate, Black Fox Lake occurrence. Pyrite consists of radial nodules.

TABLE 4:1  
COMPOSITION OF PYRITIC-CARBONACEOUS  
SLATE IN THE IRON-FORMATION

	<u>BRS-5</u>	<u>BRS-6</u>	<u>BRS-8</u>	<u>BRS-9</u>	<u>BRS-22</u>	<u>BRS-25</u>	<u>BRS-27</u>	<u>BRS-29</u>	<u>BRS-29(A)</u>	<u>BRS-30</u>	<u>BRS-31</u>	<u>BRS-40</u>	<u>BRS-40(A)</u>
SiO <sub>2</sub>	61.07	---	61.2	57.0	52.31	59.72	51.32	---	---	56.73	58.82	66.7	---
Al <sub>2</sub> O <sub>3</sub>	10.91	---	13.5	12.1	4.52	6.68	9.44	---	---	12.96	12.79	12.7	---
Fe <sub>2</sub> O <sub>3</sub> (T)	14.36	---	5.6	9.3	23.28	18.77	14.61	---	---	4.98	4.04	6.43	---
Fe <sub>2</sub> O <sub>3</sub>	---	---	---	---	23.13	17.74	14.46	---	---	---	---	---	---
FeO	---	---	---	---	0.06	0.70	0.26	---	---	---	---	---	---
Fe	N/A	27.0	3.66	5.50	N/A	N/A	N/A	---	---	---	---	3.96	---
MgO	1.66	---	0.4	0.4	0.01	0.14	0.38	---	---	1.16	2.52	0.62	---
CaO	2.77	---	0.3	0.7	0.01	0.29	8.66	---	---	2.01	6.24	1.90	---
Na <sub>2</sub> O	0.01	---	2.02	1.37	0.03	0.01	0.01	---	---	4.50	3.62	4.51	---
K <sub>2</sub> O	1.67	---	2.99	2.89	0.45	0.54	0.01	---	---	0.01	0.01	1.31	---
TiO <sub>2</sub>	0.14	---	0.15	0.10	0.22	0.23	0.31	---	---	0.42	0.48	0.32	---
P <sub>2</sub> O <sub>5</sub>	0.13	---	0.01	0.02	0.01	0.16	0.01	---	---	0.12	0.26	Nil	---
MnO	0.03	---	Nil	Nil	0.01	9.05	0.01	---	---	0.01	0.01	0.01	---
C	.85	---	4.97	5.0	.62	2.1	---	---	---	---	---	1.7	---
CO <sub>2</sub>	4.96	3.44	---	---	3.41	6.56	1.91	---	---	1.83	5.76	7.62	---
H <sub>2</sub> O	1.26	---	---	---	0.90	0.90	0.72	---	---	0.81	1.17	N/A	---
S	10.31	---	4.22	7.16	22.1	17.9	11.3	---	---	4.60	3.83	0.97	---
LOI	6.26	---	10.1	13.1	4.31	7.46	2.63	---	---	2.64	6.93	4.6	---
TOTAL	99.13	---	96.5	96.0	85.07	93.72	87.5	---	---	85.54	95.69	99.1	---
Zn (ppb)	600	110	---	---	---	12	110	69(4)	---	18(6)	7(5)	11	13(2)
Ag (ppm)	11	8	---	---	---	---	14	10(4)	---	---	---	<2	2(2)
Co (ppm)	33	84	36	520	---	47	---	26	---	181	109	21	---
Cr (ppm)	26	56	72	65	---	26	---	10	3(4)	25	26	96	---
Cu (ppm)	38	163	32	24	---	43	212	12	90(4)	28	29	40	289(2)
Mn (ppm)	280	192	12	14	---	---	---	70	---	---	---	---	---
Ni (ppm)	47	270	43	47	---	61	---	7	---	35	41	39	---
Pb (ppm)	20	620	32	59	---	86	1010	10	1010(4)	4150	3250	Nil	---
Zn (ppm)	230	1060	102	51	-	755	420	185	312(4)	4700	3320	325	1150(2)

(4) Represents average of 4 samples  
--- Not Analyzed

siliceous slates. X-Ray diffraction studies (Appendix A) of two pyritic-carbonaceous slates (BRS-9, 40) indicated the presence of quartz, muscovite, chlorite, albite, oligoclase, pyrite, carbon (graphite?), calcite and siderite.

The geochemistry of the pyritic-carbonaceous slates must be considered semi-quantitative due to analytical problems discussed in Appendix A. Slate-rich samples are listed in Table 4:1, and sulphide concentrates in Table 5:1. Although the former samples were selected on the basis of minimal sulphide content, they still contained variable amounts of finely disseminated sulphides. Nevertheless, the variation in composition of the pyritic-carbonaceous slates falls within the range reported by Pettijohn (1975) for black carbonaceous shales.

The pyritic-carbonaceous slates contain 51.3 to 66.7% SiO<sub>2</sub>, similar to values for this lithology given by Shegelski (1978). Al<sub>2</sub>O<sub>3</sub> varies from 4.5% in the more sulphide-rich layers to 13.5% in slate-rich layers. Maximum Al<sub>2</sub>O<sub>3</sub> values are not as high as in Shegelski's (1978) samples.

Total Fe<sub>2</sub>O<sub>3</sub> varies from 4.0 to 23.3%, the higher values reflecting finely disseminated and laminated sulphides which could not be removed. Total iron is closely related to sulphur content, indicating that much of the iron is present as iron sulphides. The Na<sub>2</sub>O content varies from zero to 4.5 % at the Black Fox and Little Steel occurrences. The higher Na<sub>2</sub>O % could reflect an increased tuffaceous component.

#### b) Tuffaceous Component

A tuffaceous component is present within iron-formations and other chemical sedimentary rocks at the Kingdom, Little Steel,

Black Fox, Simard Swetz and Little Bruin occurrences (Figure 1:2). This component occurs in fine-grained laminated chert, tuffaceous chert, iron-rich siliceous slate and siliceous schist. It generally consists of pyroclastic fragments of quartz and plagioclase. Sample BRS-51 (Table 4:2), a tuffaceous chert contains subrounded to subangular quartz and plagioclase fragments up to one millimeter in size (Photo 4:3).

At the Little Bruin occurrence, a possible tuffaceous rock (BRS-56, Table 4:3) contains pyrite laminations alternating with quartz-rich and chlorite-sericite laminations. The latter contain large scattered fragments of quartz and plagioclase feldspar of probable pyroclastic origin.

#### CHEMICAL OR BIOCHEMICAL COMPONENTS

A chemical sedimentary rock is defined as a sedimentary rock formed directly by precipitation from solution or colloidal suspension (as by evaporation) or by the deposition of insoluble precipitates (Glossary of Geology, AGI). A chemical sedimentary rock has less than 50 % detrital material.

##### a) Pyrite

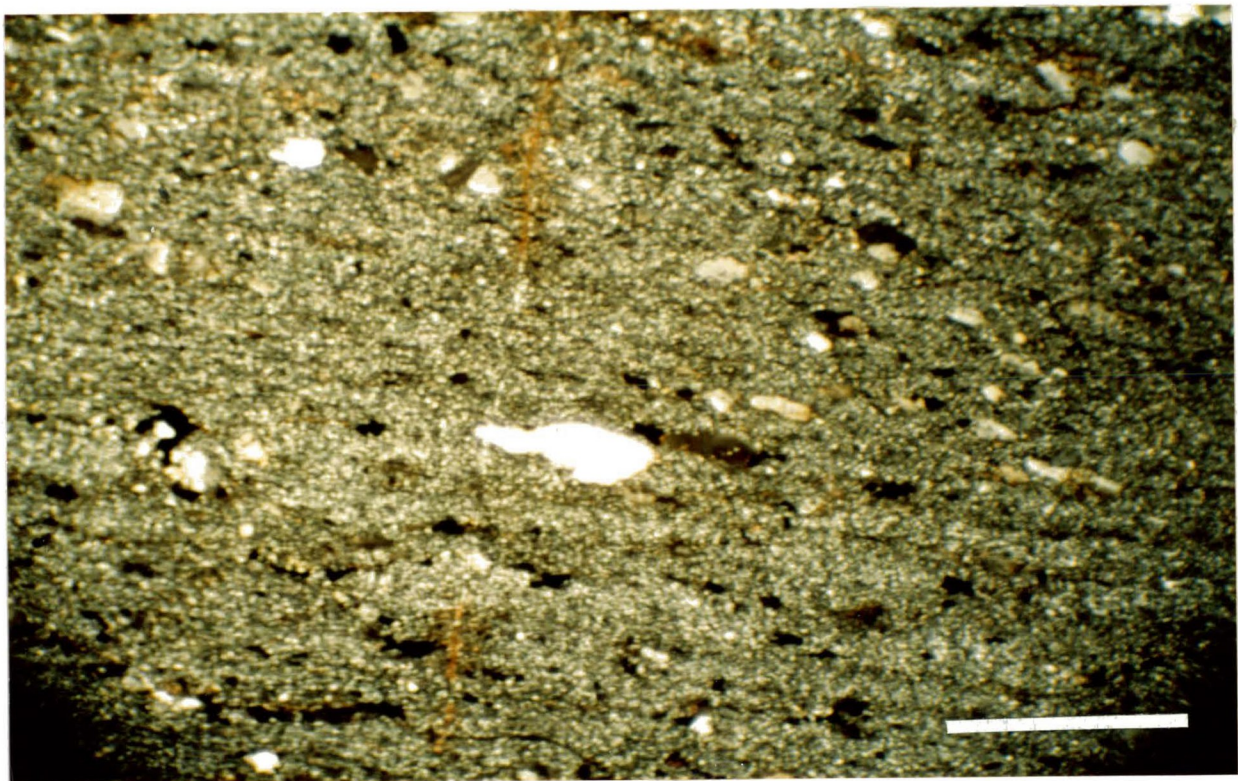
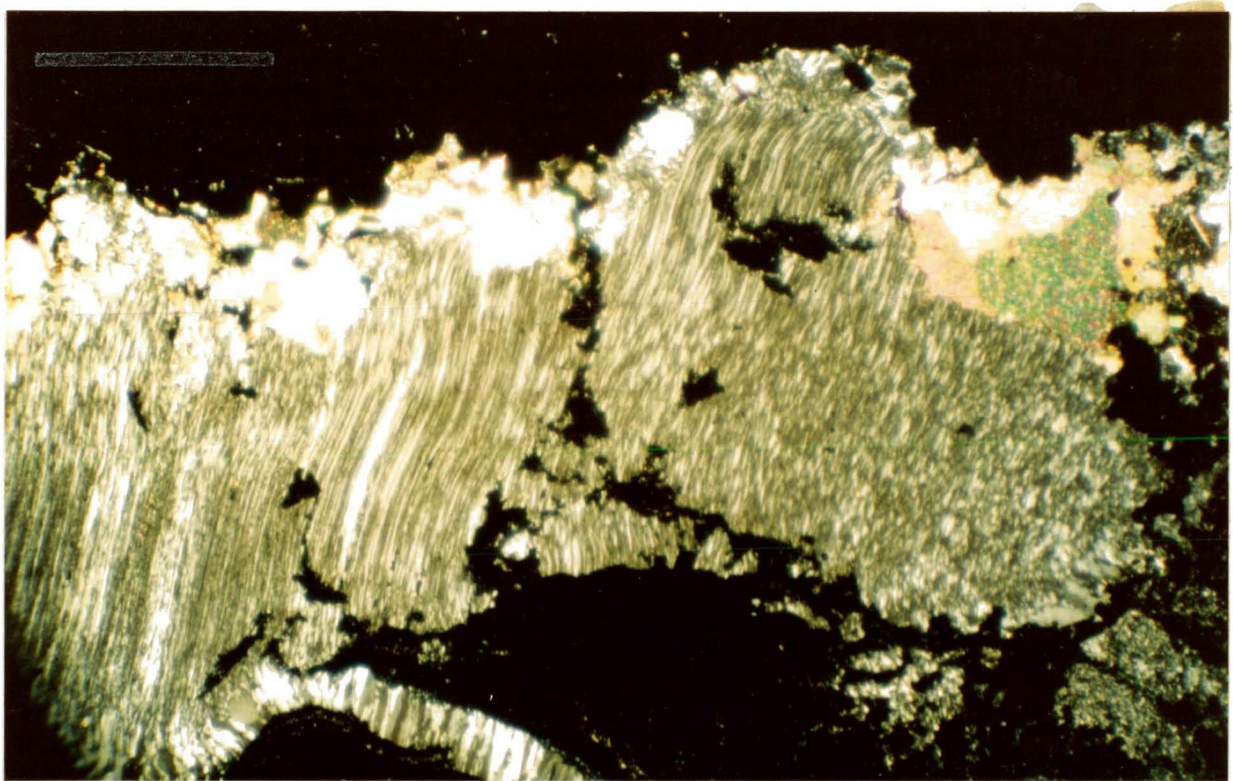
General Sulphide minerals, predominantly pyrite, make up most of the chemical component within the iron-formations in the Schreiber-Terrace Bay area. Minor amounts of pyrrhotite, sphalerite, chalcopyrite and galena are also present.

Pyrite occurs within the cherts and pyritic-carbonaceous slates and as disseminated grains or spheres, laminations, layers or bands, lenses, euhedral recrystallized grains and masses, and



**PHOTO 4:2** PRESSURE SHADOW QUARTZ (BOEHM LAMELLAE) FORMING WEDGE OR LENSE-SHAPED STRUCTURES, IN CONTACT WITH PYRITE NODULE, BLACK FOX OCCURRENCE. SCALE BAR REPRESENTS 1 mm.

**PHOTO 4:3** TUFFACEOUS COMPONENT, INCLUDING VOLCANIC SHARDS AND FRAGMENTS WITHIN SILICEOUS SEDIMENTARY ROCK, LITTLE STEEL RAILWAY OCCURRENCE. NOTE: QUARTZ AND PLAGIOCLASE FRAGMENTS IN A SILICEOUS MATRIX. SCALE BAR REPRESENTS 1 mm. SAMPLE BRS-51.



as breccias and nodules. In many cases, all these types of pyrite are intercalated with each other.

In the Savant-Sturgeon Lake area, pyrite occurs as layers, lenses and breccia within a quartz matrix, or as large nodules in carbonaceous shale (Shegelski, 1978). Euhedral pyrite crystals were interpreted by Shegelski (1978) as secondary or recrystallized, while granular aggregates were considered as primary features.

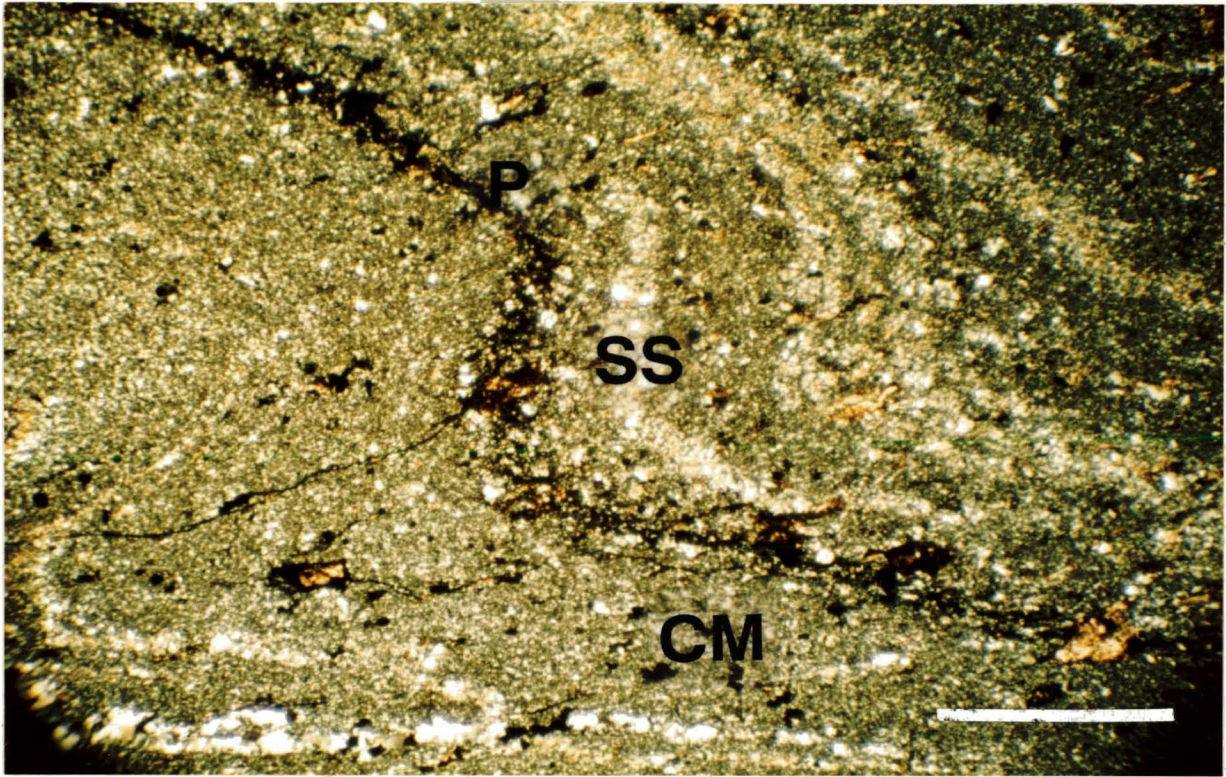
Easdon (1969) described four types of pyrite in northwestern Quebec: a) massive, frequently brecciated and fractured layers, 5mm to 7.5cm thick; b) isolated nodules ranging from 2mm to 5 cm in diameter; c) massive sheared and brecciated pyrite, with abundant pyrrhotite; and d) fine-grained disseminations. As in the Schreiber-Terrace Bay area, these types of pyrite can occur in any combination of each other.

#### i) Fine-Grained, Disseminated Pyrite

In many of the chert and iron-rich slate units, pyrite occurs as fine grains, spheres, and granular aggregates, with individual grains generally less than 0.01 mm in diameter. The pyrite is commonly found in trains or layers with other opaque minerals, apparently marking the bedding (Photo 4:4). Subhedral to euhedral crystals of pyrite up to 0.1 to 0.2 mm in diameter also occur. Such crystals probably develop during the regional metamorphism of shales (Vokes, 1969). Blastic and triple-junction mosaic textures were observed in several types of pyrite. These result from metamorphic recrystallization of thicker, more massive sulphide layers (Vokes, 1969).

**PHOTO 4:4**      PHOTOMICROGRAPH OF ALTERNATING  
LAMINATIONS OF PYRITE (P),  
SILICEOUS SEDIMENT (SS) AND  
CLASTIC MATERIAL (CM), SIMARD-  
SWETZ OCCURRENCE. NOTE:  
FOLDED BEDDING DISPLAYS AXIAL  
PLANAR CLEAVAGE. SCALE BAR  
REPRESENTS 1 mm. SAMPLE BRS-27.

**PHOTO 4:5**      MASSIVE AND LAMINATED PYRITE,  
KINGDOM PROPERTY. SAMPLE BRS-7.



In foliated samples, recrystallized pyrite crystals are generally orientated subparallel to the foliation. The blastic textured pyrite crystals are equant with interfacial angles near 120 degrees. This feature, combined with associated pressure shadow or lamellar quartz, suggests annealing effects during metamorphism (Craig and Vaughan, 1981). However, recrystallization during diagenesis may also lead to the growth of euhedral, almost porphyroblastic crystals of pyrite.

#### ii) Massive Pyrite

At the Kingdom occurrence, pyrite is also present in massive layers up to 20 cm thick which may be internally laminated (Photo 4:5). In addition, pyrite lenses of variable width are present which appear to represent tectonically deformed layers. Pyrite layers and lenses are commonly associated with the pyritic-carbonaceous slates and chert.

Fine-grained laminated pyrite from interpillow sedimentary rocks at the Kingdom occurrence displays laminations of pyrite-rich and clastic rich sediment ranging from 0.01 to 0.1 mm in thickness (Photos 4:6, 4:7). Finely laminated pyrite is also present at the Morley, Simard-Swetz, Black Fox and Harkness-Hays occurrences.

At the Morley, laminated pyrite occurs within a predominantly massive pyrite zone. Laminations range from 0.03 mm to 1mm in width, and are generally convex upwards (Photo 4:8). Sedimentary structures within the pyrite include possible slump and ball-and-pillow structures (Photo 4:8). Other structures include rounded load casts and mammillary growths (Photo 4:9). Internally laminated domal structures are orientated in a convex-upwards

**PHOTO 4:6** FINELY LAMINATED PYRITE, AS  
INTERPILLOW SEDIMENTARY ROCK,  
KINGDOM PROPERTY. SAMPLE BRS-21.

**PHOTO 4:7** PHOTOMICROGRAPH OF LAMINATED  
PYRITE (P), DISPLAYING CHEMICAL  
(PYRITE) AND CLASTIC (SILICATE-  
OXIDE) RICH LAMINATIONS, KINGDOM  
PROPERTY. SCALE BAR REPRESENTS  
0.5 mm. SAMPLE BRS-21.

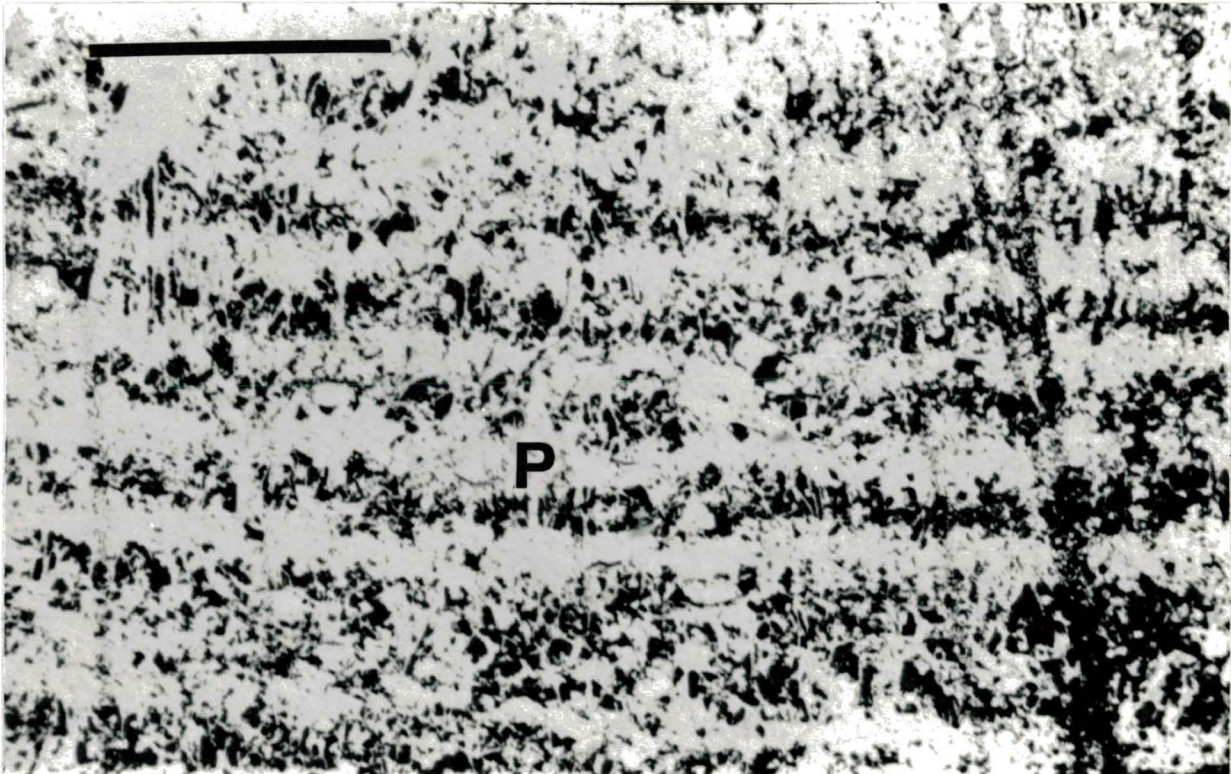
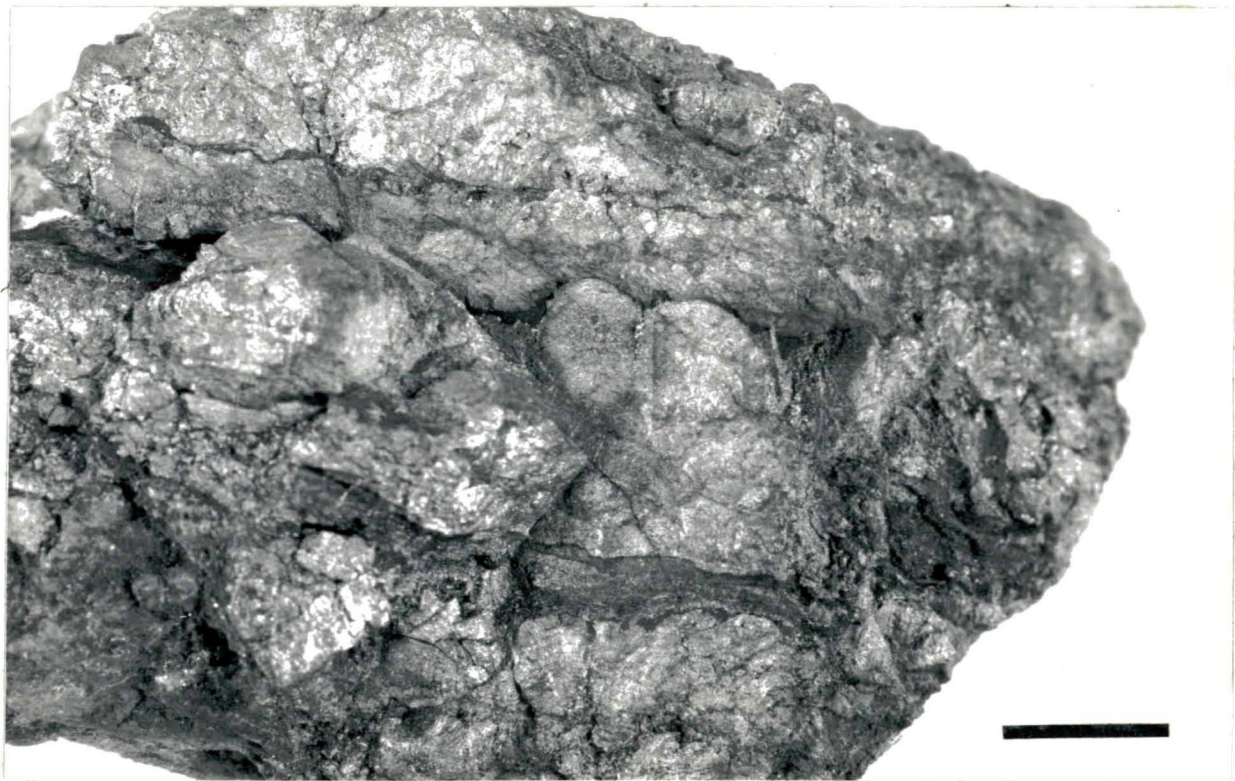
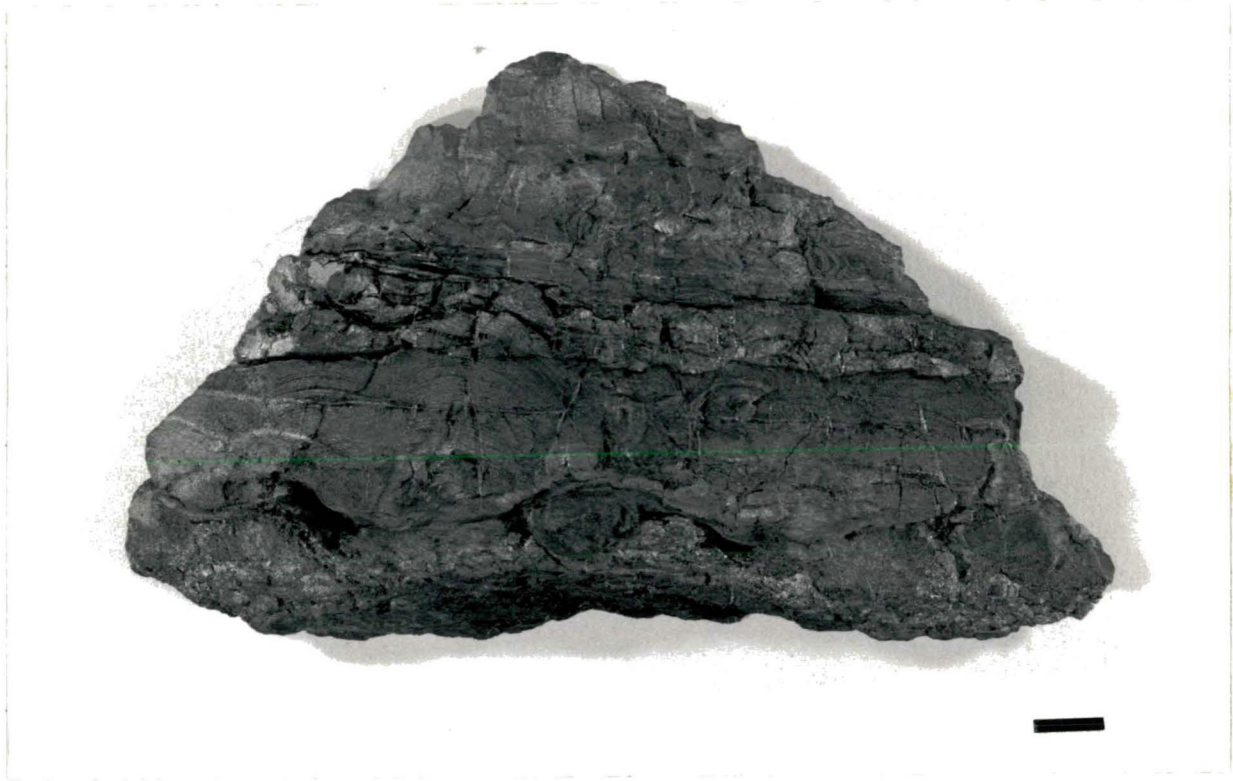




**PHOTO 4:8** FINELY LAMINATED PYRITE,  
DISPLAYING SLUMP STRUCTURES  
(ARROW), BRECCIATION, AND  
SHALE INTERCALATIONS, MORLEY  
PROPERTY. SCALE BAR REPRESENTS  
1 cm.

**PHOTO 4:9** LAMINATED TO MASSIVE PYRITE  
DISPLAYING LOAD CAST STRUCTURE  
(ARROW), MORLEY PROPERTY. NOTE:  
SLATE INTERCALATIONS. SCALE BAR  
REPRESENTS 1 cm.



direction. Where the younging direction of the domal structures is unknown, it is uncertain whether they are draped by the shale, growing into the shale, or loading down into the shale.

The finely laminated pyrite generally forms concentric structures. The laminations consists of recrystallized aggregates of crystals with interfacial angles close to 120 degrees. A "boxwork"-like texture (Craig and Vaughn, 1981), also known as a pseudographic or star texture (Neilsen, 1974), maybe present (Photo 4:10). The laminations generally define concentric banding.

XRD data indicate that the pyrite-rich laminations also contain carbon (graphite?) and minor quartz, while the oxide-silicate laminations contain quartz, hematite, goethite, pyrite, minor chlorite and muscovite, and possible glauconite. Several laminations were dominated by iron oxide minerals, while others were rich in quartz and chlorite.

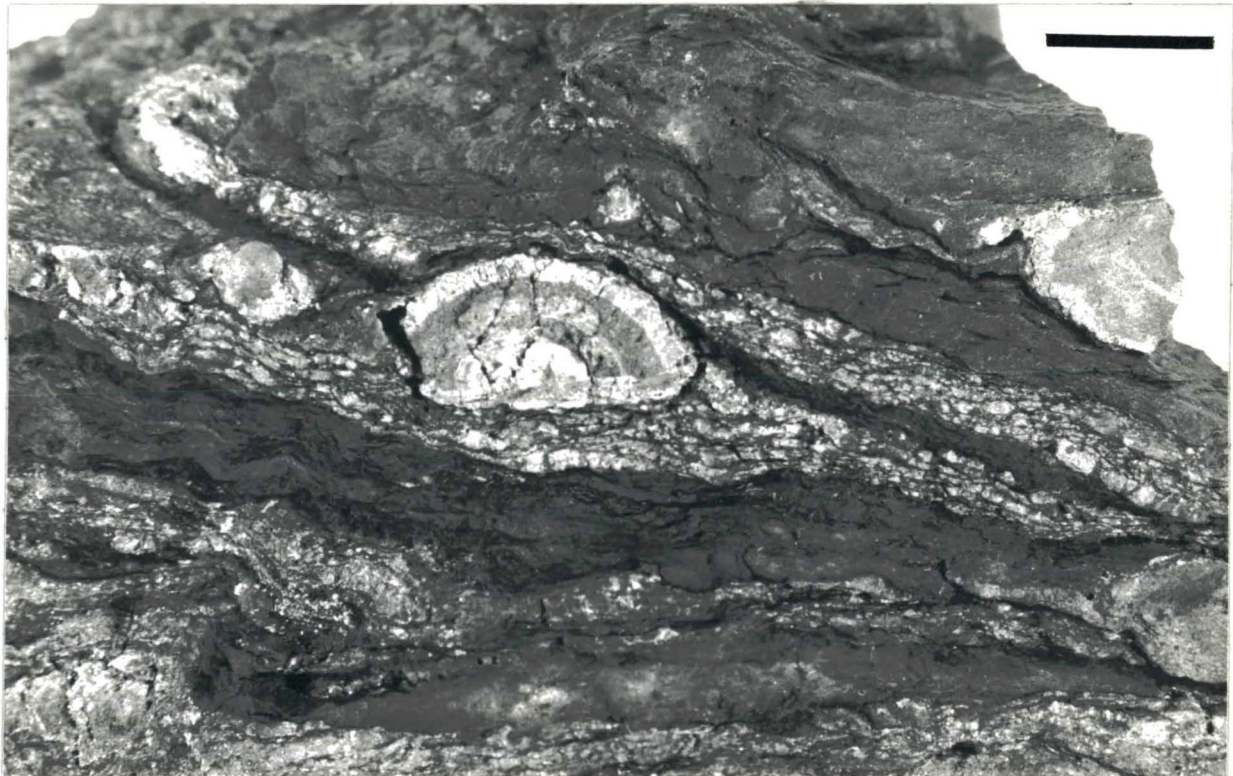
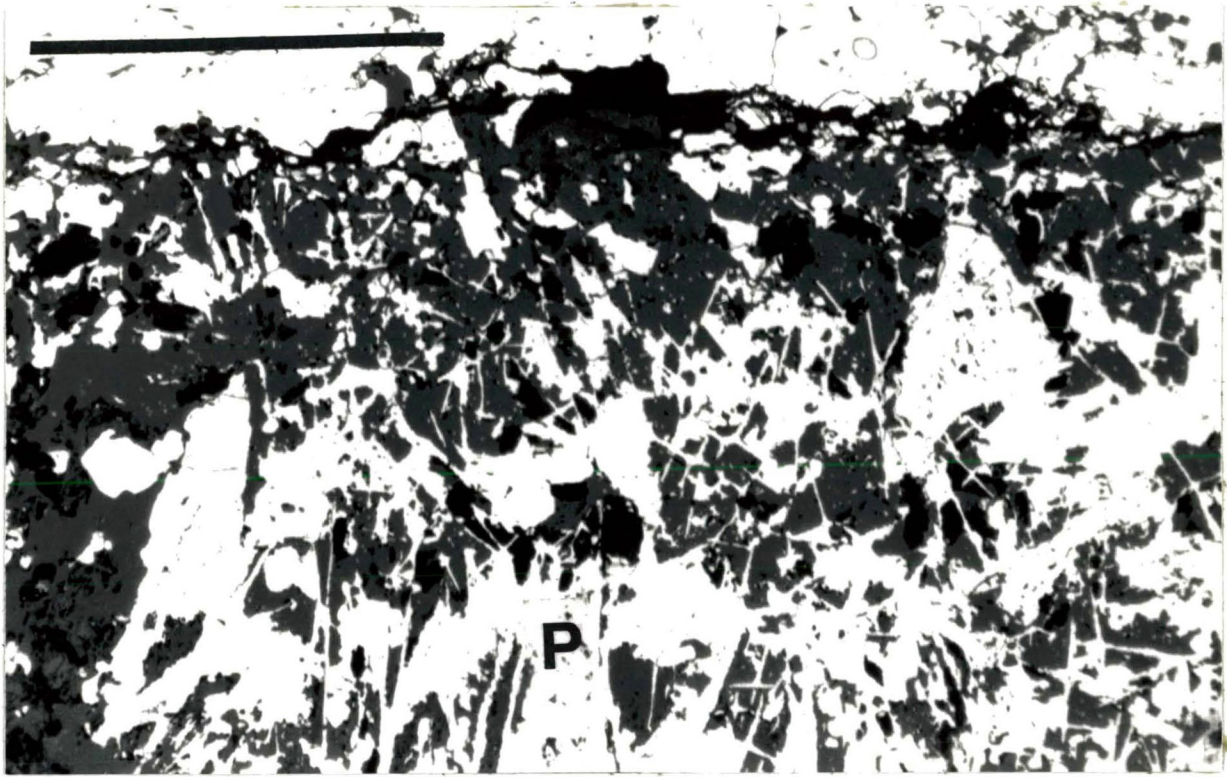
### iii) Nodular Pyrite

General Elliptical pyrite structures in sulphide-facies iron-formations have been termed ball-like bodies (Fenwick, 1976) concretions (Woolverton, 1960), nodules (Rose, 1965; Easdon, 1969; Fenwick, 1971; Shegelski, 1978), globules (Voytkevich et al.) and botryoidal pyrite (Wolf, 1980). Other workers have termed them diagenetic segregations, accretions, intercretions, geodes and septaria. The term nodule will be used in this study.

Nodules vary in size from as small as 4 mm at the Little Bruin occurrence, to as large as 3 cm at the Black Fox. Nodules are commonly associated with pyritic-carbonaceous slates and with sulphide-facies iron-formations, a feature which is not

**PHOTO 4:10** PHOTOMICROGRAPH OF "BOX WORK"-  
LIKE TEXTURE OF PYRITE LAMINATION (P)  
IN CONTACT WITH OXIDE-SILICATE-RICH  
LAMINATION, MORLEY PROPERTY. SCALE  
BAR REPRESENTS 0.25 mm.

**PHOTO 4:11(A)** COLLOFORM OR CONCENTRIC NODULE  
IN PYRITIC-CARBONACEOUS SLATE,  
FINLAYSON LAKE AREA. SCALE BAR  
REPRESENTS 1 cm.



restricted to the Schreiber-Terrace Bay area (Fenwick, 1971). The size and type of nodules can be related to the intensity of deformation, which ranges from minor at the Morley to intense at the Black Fox occurrence.

a) Colloform (Concentric) Nodules Elliptical nodules consisting of alternating, concentrically banded pyrite and clastic-rich sediment (photo 4:11A) occur at several locations in the Schreiber -Terrace Bay area, and also in the Finlayson Lake area (Fenwick, 1971). They are best developed at the Morley occurrence (Photo 4:11B). At this locality, nodules appear to have grown upwards, with convex surfaces, from a base of massive pyrite. Nodule surfaces are in sharp contact with drapings of pyritic-carbonaceous slate (Photo 4:9). The long axes of the nodules are orientated subparallel to bedding. Easdon (1969) described concentric pyrite nodules with alternating inclusion-free and inclusion-bearing pyrite.

The concentric banding is defined by pyrite-rich laminations containing minor quartz, sericite and carbon, in alternation with laminations rich in oxide and silicate minerals (Photo 4:11C). Nodule rims may consist of monomineralic, recrystallized pyrite with interfacial angles near 120 degrees (Photo 4:11A). Microtextures are similar to those in the finely laminated pyrite (e.g. "boxwork"-like structure), as is the mineralogy of the clastic laminations within the nodules.

b) Radial Nodules At the Morley and Black Fox occurrences, radial nodules up to 2 cm in diameter display a "wagon-wheel texture" (Figure 4:12A), occasionally with a rim of concentric rings. In the Finlayson Lake area, Fenwick (1976) reported a small nodule

**PHOTO 4:11(B)** COLLOFORM NODULE DISPLAYING  
ALTERNATING CONCENTRICALLY  
BANDED PYRITE AND CLASTIC-RICH  
LAMINATIONS, MORLEY PROPERTY.  
SCALE BAR REPRESENTS 0.5 cm.

**PHOTO 4:11(C)** PHOTOMICROGRAPH OF COLLOFORM  
NODULE DISPLAYING PYRITE-RICH  
AND CLASTIC-RICH LAMINATIONS,  
MORLEY PROPERTY. SCALE BAR  
REPRESENTS 0.1 mm.

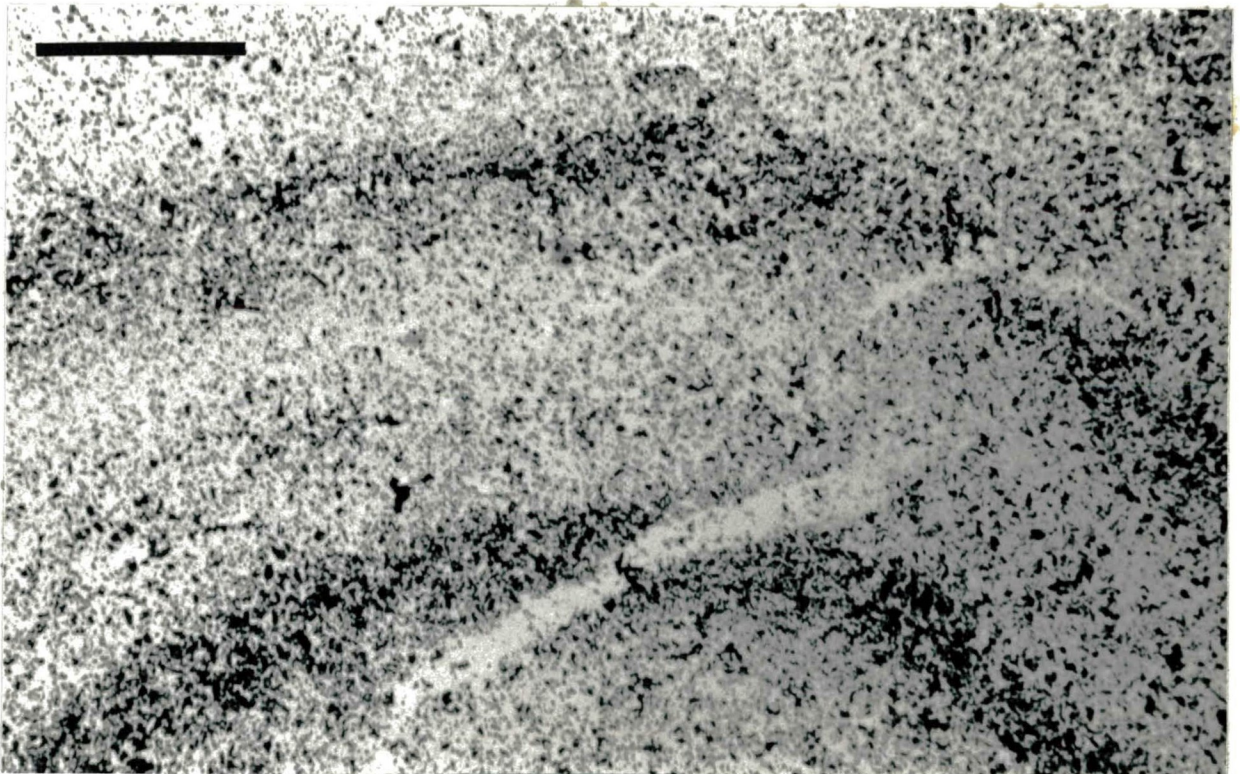
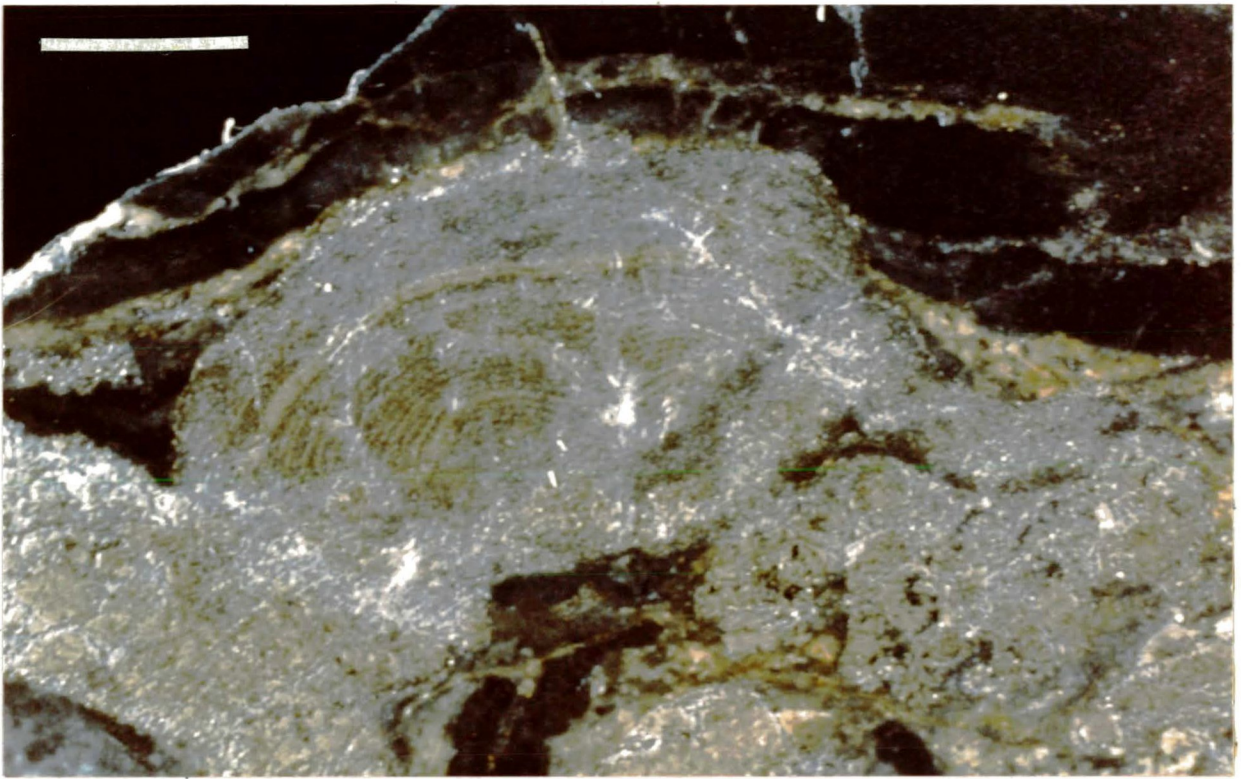
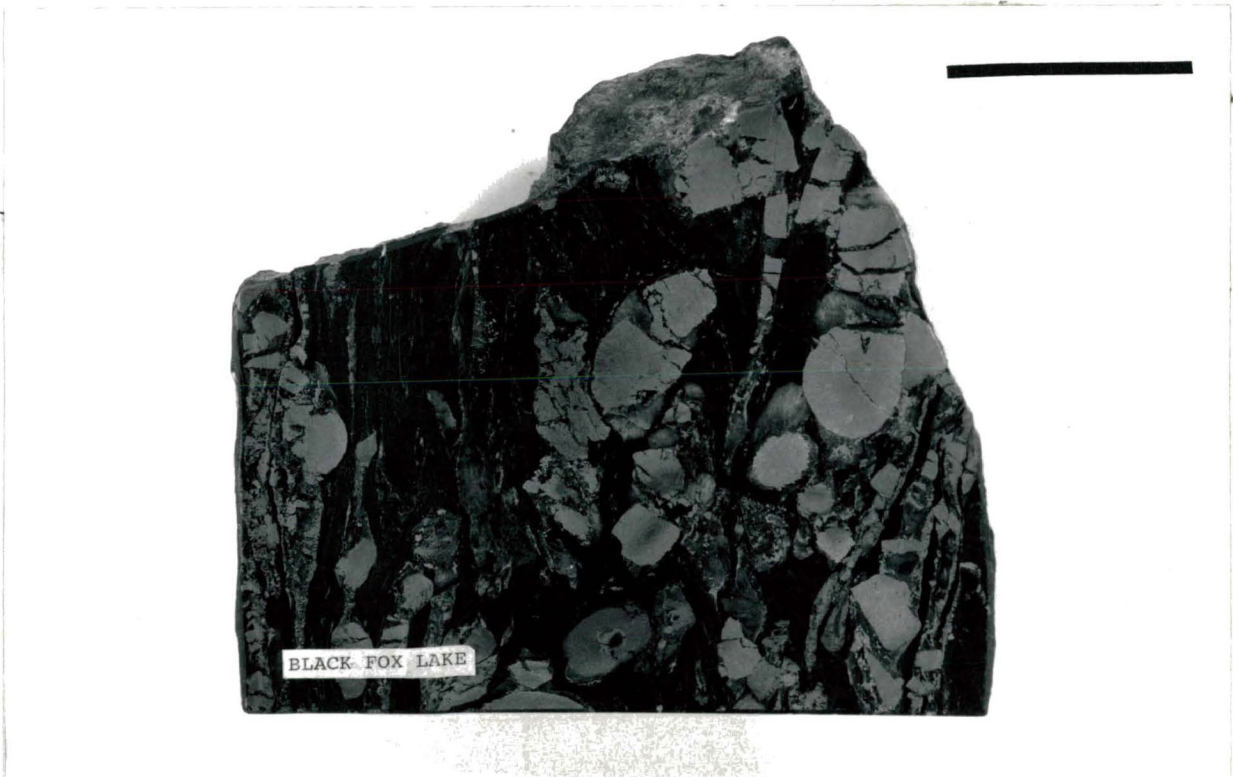
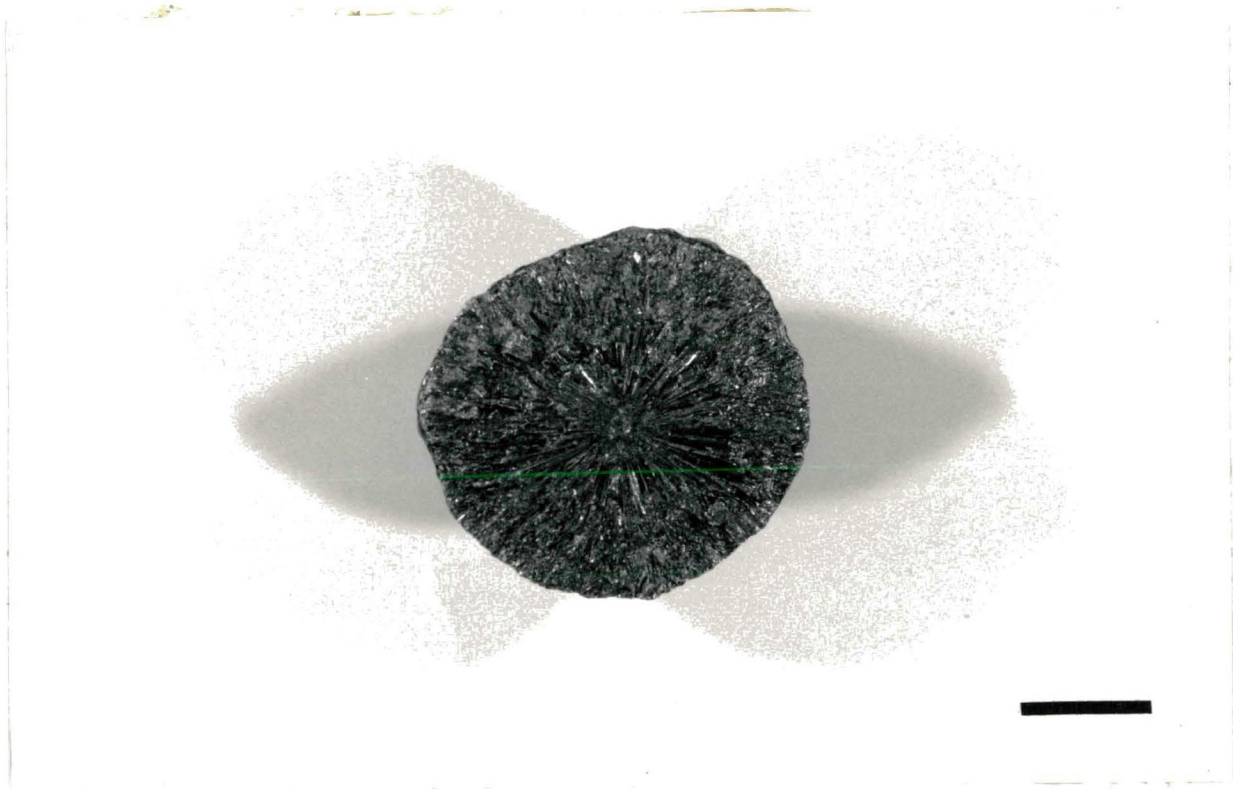




**PHOTO 4:12(A)** RADIAL NODULE, MORLEY PROPERTY.  
SCALE BAR REPRESENTS 1 cm.

**PHOTO 4:12(B)** DEFORMED NODULAR PYRITE LAYER,  
BLACK FOX LAKE OCCURRENCE. NOTE:  
RADIAL NODULES AND RADIAL-COLLOFORM  
NODULES IN PYRITIC-CARBONACEOUS  
SLATE. NODULES ARE ELONGATED ALONG  
FOLIATION DIRECTION. BRECCIATION  
IS EVIDENT. SCALE BAR REPRESENTS 5 cm.



type with radial structure, and a larger type containing concentric rings and cone-in-cone structures.

Most of the radial nodules at the Black Fox occurrence are highly deformed and brecciated (Photos 4:12B, 4:13), with long axes orientated subparallel to the schistosity (see also Photo 4:1A). The nodules usually have quartz pressure shadows which form wedge-shaped tails to the nodules. These tails contain lamellar, ribbon and pressure shadow quartz. One such nodule was cut into a series of slices which showed a transition from an elliptical nodule through a spherical nodule with quartz tails, to an irregular wedge of quartz with a pyrite core and finally a wedge of pure quartz. The two intermediary phases are shown in Photos 4:12 C, D. Remnant nodules have recrystallized pyrite rims; pyrrhotite and magnetite replace the pyrite, with magnetite occurring the core of the nodules (Photo 4:13). Deformed nodules at the Black Fox occurrence have been brecciated and stretched into wispy streaks.

c) Layered Nodule At the Simard-Swetz occurrence, layers of pyrite have been folded, brecciated, rotated and deformed into lenses which give the appearance of layers of nodules.

iv) Recrystallized Pyrite

Large subhedral to euhedral crystals of pyrite up to 5 mm in width are observed in the pyritic-carbonaceous slate, chert and massive pyrite units of the iron-formations. The pyrite crystals display interfacial angles near 120 degrees, and are commonly aligned subparallel to the foliation direction. These pyrite crystals are considered secondary.

**PHOTO 4:12(C)** NODULAR PYRITE (P) WITH QUARTZ (Q)  
PRESSURE SHADOWS, BLACK FOX LAKE  
OCCURRENCE. SCALE BAR REPRESENTS  
1 cm.

**PHOTO 4:12(D)** REVERSE SIDE OF **4:12(C)** DISPLAYING  
REDUCTION IN SIZE OF PYRITIC AREA (P)  
(CORRODED NODULE), AND AN INCREASE  
IN SIZE OF SILICEOUS AREA (Q), BLACK  
FOX OCCURRENCE. SLICE IS 3 mm THICK.  
SCALE BAR REPRESENTS 1 cm.

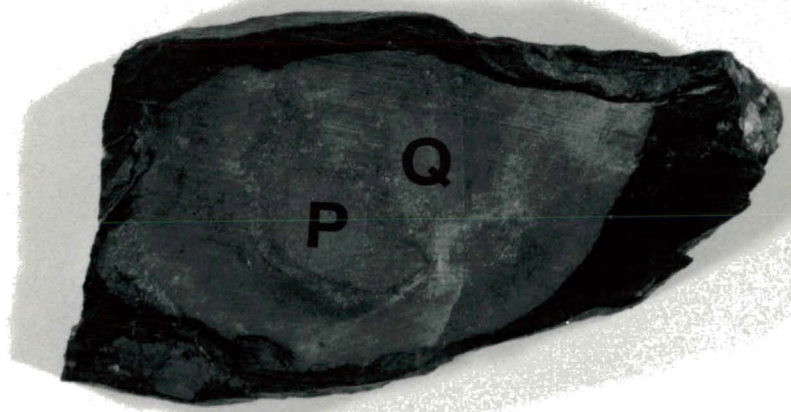
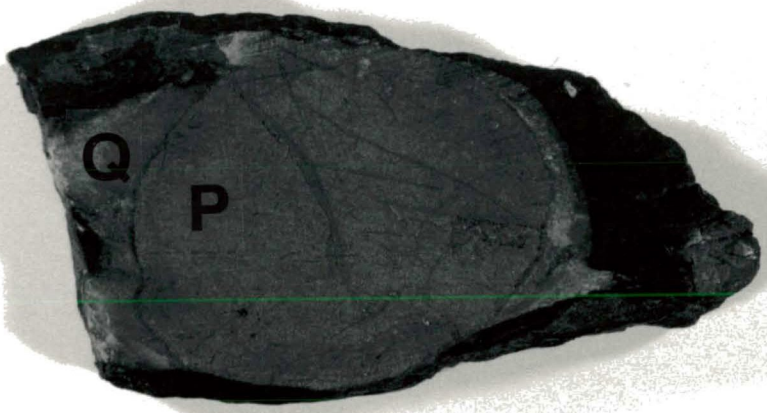
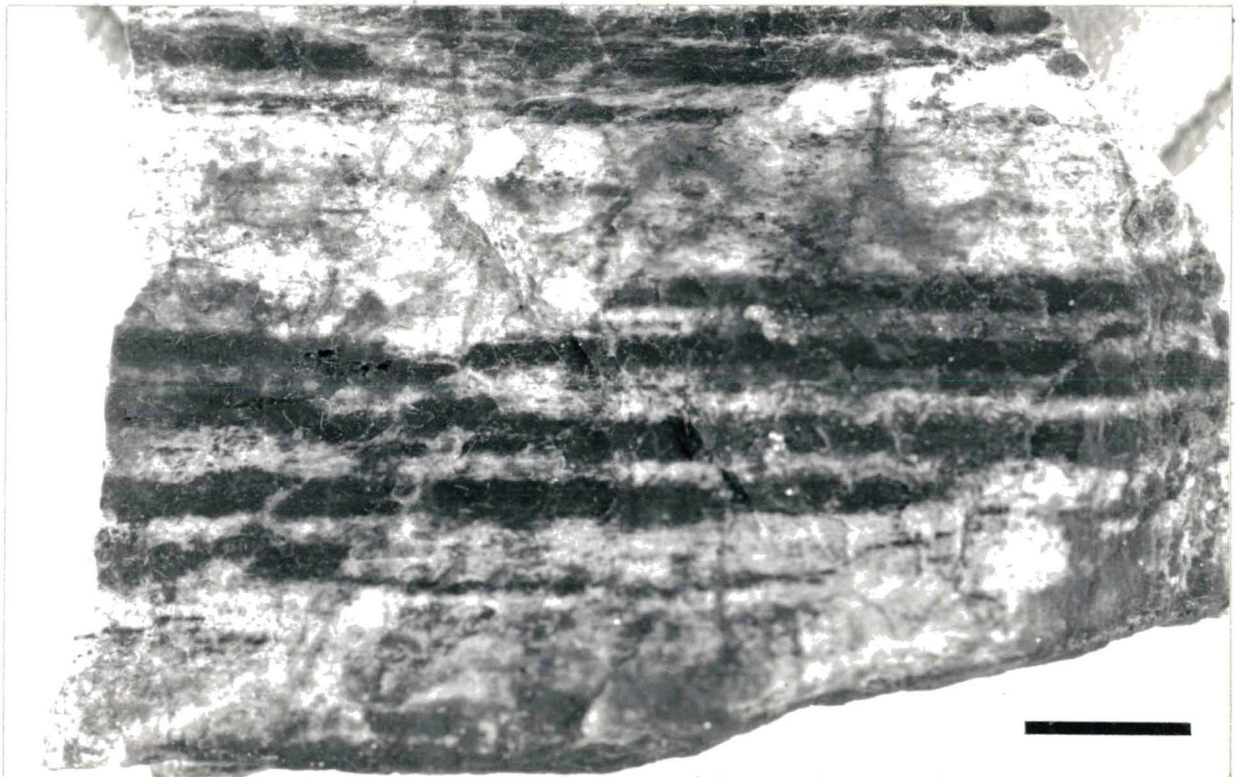
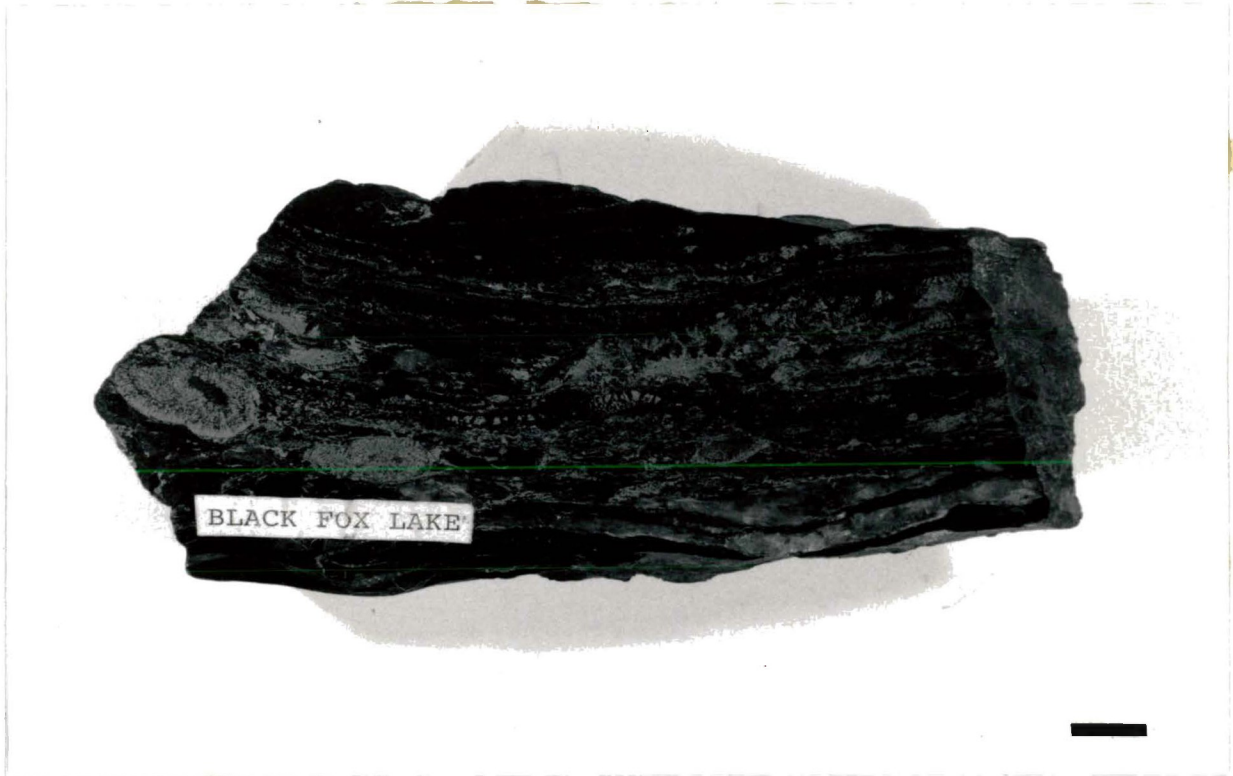


**PHOTO 4:13** INCREASED DEFORMATION OF NODULAR  
PYRITE LAYER, BLACK FOX OCCURRENCE.  
NOTE: RECRYSTALLIZED PYRITE RIMMING  
NODULES WITH MAGNETITE REPLACEMENT  
OF CORES. STREAKY LAMINATIONS  
PARALLEL TO FOLIATION. SCALE BAR  
REPRESENTS 1 cm.

**PHOTO 4:14(A)** ALTERNATING DARK AND LIGHT  
LAMINATIONS IN CHERT, MORLEY  
PROPERTY. SAMPLE BRS-52, 53.  
SCALE BAR REPRESENTS 1 cm.



## v) Brecciated Pyrite

All the above forms of pyrite are also found brecciated. At the Black Fox occurrence in particular, massive, laminated and nodular pyrite layers, up to 60 cm thick are commonly brecciated (Photo 4:12 B).

## vi) Other Sulphides

In addition to pyrite, which constitutes more than 90% of the sulphides, pyrrhotite, chalcopyrite, sphalerite and galena are also present in varying amounts. Pyrrhotite is the second most abundant sulphide and is found at the Little Steel (Highway and Railway) and Morley Road occurrences (Figure 1:3).

At the Little Steel Highway occurrence, pyrrhotite is hosted by chloritic schisted and brecciated chert, and is intruded by a metagabbroic dike. Since the dike contains brecciated fragments of the sulphide iron-formation, contact metamorphism has probably affected the primary sulphide assemblage, leading to an increase in the proportion of pyrrhotite (Stanton, 1972).

Sphalerite is present at the Little Steel Railway, Little Bruin and Simard-Swetz occurrences. At the first two locations the sphalerite is bedded and possibly primary. At the Little Steel, sphalerite is associated with laminated chert, whereas at the Little Bruin, it is included within pyrite layers which alternate with tuffaceous sedimentary rock.

Sphalerite and galena are present in the siliceous black slates of the Simard-Swetz occurrence. Sphalerite and galena are orientated along the foliation which crosscuts the bedding at a low angle, and are commonly associated with pressure shadow quartz, carbonate and recrystallized pyrite.



Polished thin section examination of many samples of iron-formation indicated minor amounts of chalcopyrite, sphalerite and galena. Chalcopyrite is located in fractures within the chert, mudstone, and brecciated pyrite. Sphalerite is common as small grains within the massive pyrite and pyritic-carbonaceous slate.

b) Chert

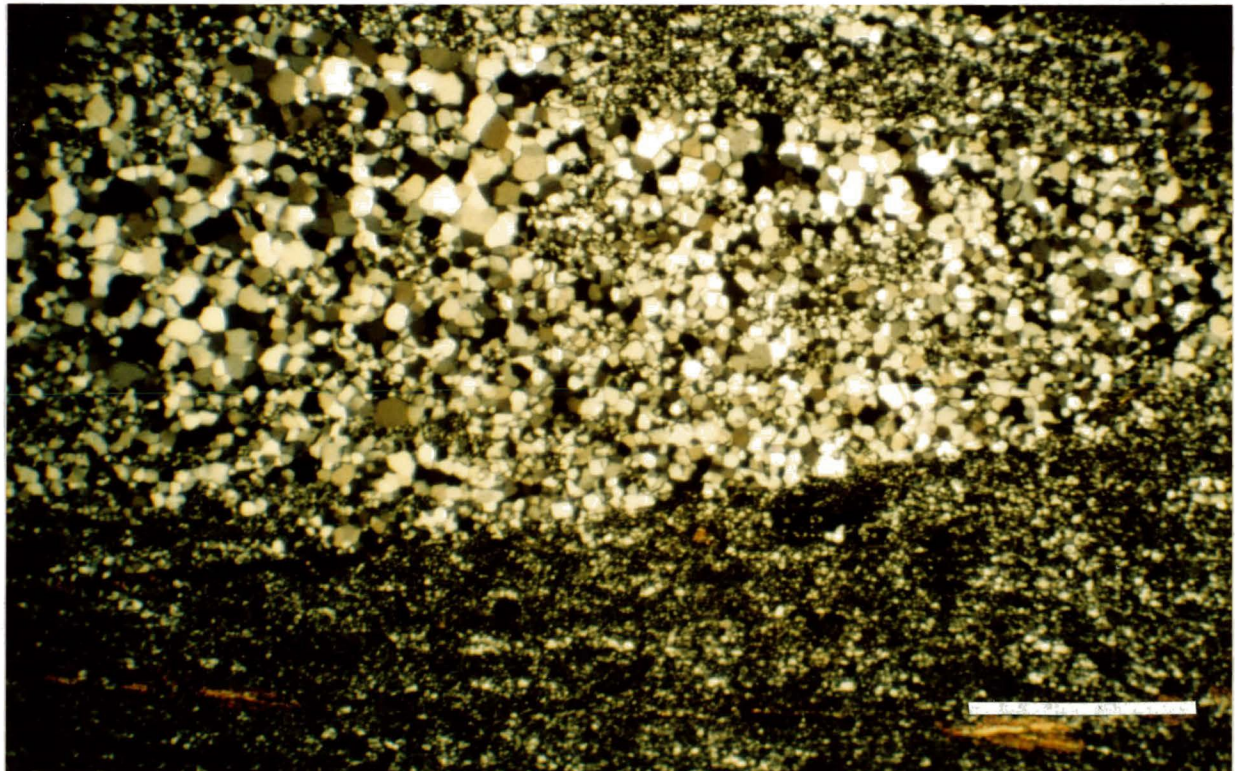
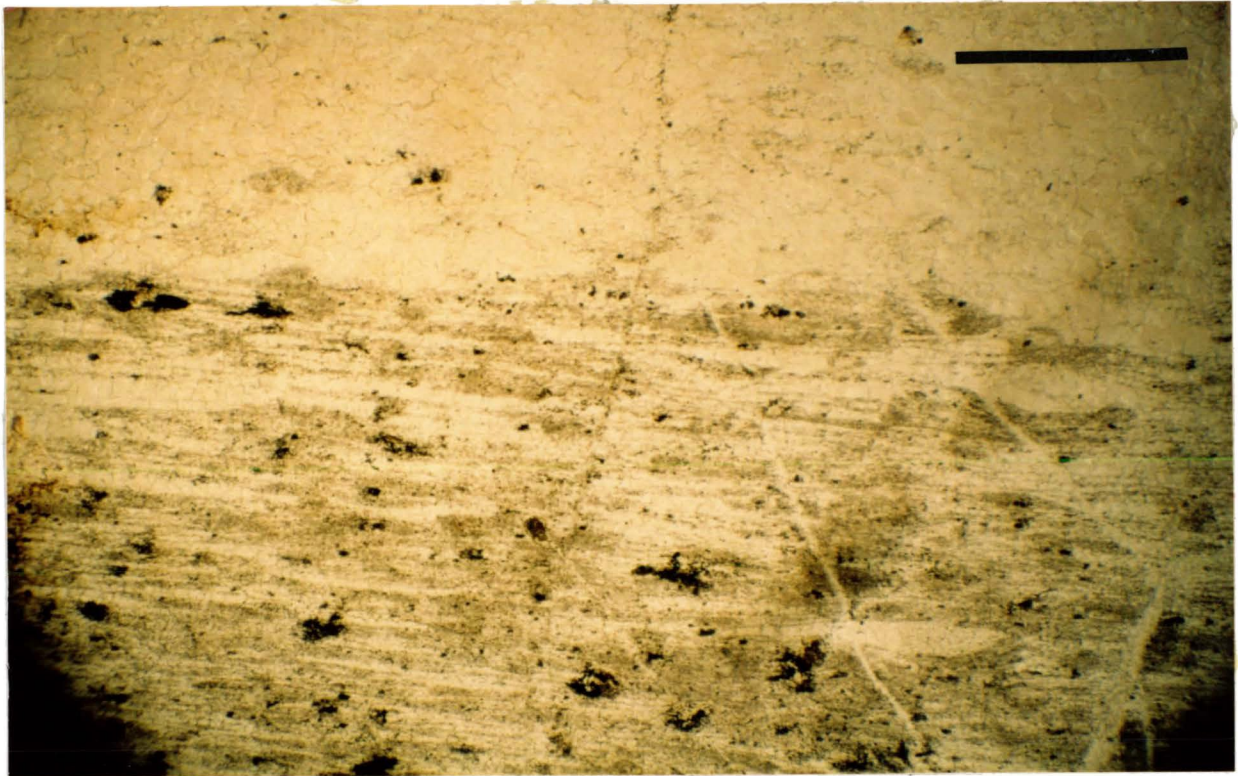
Chemical or biochemical chert layers are interlaminated with the sulphide and slate components of the sulphide-facies iron-formation at the Harkness Hays, Morley and Kingdom occurrences, and with magnetite and minor pyrrhotite of the oxide-facies iron-formations at the Schreiber Beach and Schreiber Rail occurrences.

Cherts range in appearance from fine-grained dense and blackish-blue, to saccharoidal, crumbly and white. Bed thicknesses range from less than 1 mm (Kingdom laminations) to greater than 6 m thick (Harkness-Hays layers). At the Morley, an excellent exposure of chert displays well developed banding (Photo 4:14 A). The layers and laminations of black fine-grained chert alternate with white sugary quartz. Pyrite mineralization is commonly intimately associated, including bedded and nodular forms.

Individual layers of chert consist of uniform-sized grains ranging from cryptocrystalline to medium-grained with a granular texture (Photos 4:14 B,C). The larger quartz grains are subrounded; the long axes are subparallel to the foliation. At the Morley Pyrite, Kingdom, Little Steel, Little Bruin and Simard-Swetz Properties, fine-grained chert contains carbon

**PHOTO 4:14(B)** PHOTOMICROGRAPH OF DARK AND LIGHT COLORED CHERT LAMINATIONS, MORLEY PROPERTY. (UNCROSSED NICHOLS, ppl). SCALE BAR REPRESENTS 1 mm.

**PHOTO 4:14(C)** PHOTOMICROGRAPH OF DARK AND LIGHT COLORED CHERT LAMINATIONS, MORLEY PROPERTY. (CROSSED NICOLS). SCALE BAR REPRESENTS 1 mm. NOTE: SAME VIEW AS **4:14(B)** ONLY TILTED.



(graphite?) as well as sulphides, chlorite and sericite, whereas coarser-grained chert layers consist almost entirely of quartz. Easdon (1969) also observed that an increase in the grain size of the quartz was generally associated with a decrease in the graphite content.

At the Morley Pyrite occurrence, samples of alternating light and dark chert were sampled and analysed mineralogically and chemically. Table 4:2 lists the characteristics of each type of layer. Both varieties contain minor chlorite, pyrite, calcite, carbonaceous material and chalcopyrite (Appendix A), but dark layers contain more chlorite, pyrite and carbonaceous material.

At the Little Steel and Simard-Swetz properties, beds of fine-grained quartz contain trains or laminations of sulphide and carbonaceous material (Photo 4:4). The sulphides make good marker horizons which provide evidence for folding and faulting on the microscopic level.

Care must be taken in the field to ensure that chert layers, rather than quartz veins or remobilized quartz, are sampled (Table 4:3). True cherts are present at the Kingdom occurrence (BRS-1, 18), Morley occurrence (BRS-52, 53, ), Granite Mountain property (BRS-64) and Schreiber Rail occurrence (BRS-73). Cherts are also present at the Harkness-Hays, Schreiber Beach, Simard-Swetz and Ottisse properties. True cherts generally contain about 90% SiO<sub>2</sub> (Table 4:2) unless the sample was high in iron and/or secondary carbonate (e.g. BRS-1). Total iron (as Fe<sub>2</sub>O<sub>3</sub>) ranged from 0.2 to 9.9%. Although most of the iron is in the form of pyrite, iron-formations at the Schreiber Beach, Victoria Lake and Wildrose Resources occurrences have a considerable iron oxide component. Cherts contained up to 1.3 %

TABLE 4:2

COMPARISON OF LIGHT AND DARK CHERT LAYERS: MORLEY PROPERTY

	<u>DARK CHERT (BRS-52)</u>	<u>LIGHT CHERT (BRS-53)</u>
Hand Sample	dense, crypto-crystalline bluish-black colour	white, sugary, fine grained
Thin Section	quartz grains in 10 micron range, numerous opaques including pyrite and sulphides in laminations	granular quartz grains up to 50 to 100 microns, minor sericite, little to no sulphides, minor grain-size gradation of quartz
X-Ray Diffraction	quartz with pyrite, carbon, and chlorite, minor chalcopyrite	quartz with minor pyrite
Chemical Composition	$< \text{SiO}_2$ $> \text{Fe}_2\text{O}_3$ $> \text{Al}_2\text{O}_3$	$> \text{SiO}_2$ $< \text{Fe}_2\text{O}_3$ $< \text{Al}_2\text{O}_3$

TABLE 4:3 - SAMPLE DESCRIPTIONS

<u>SAMPLE NUMBER</u>	
BRS-1	Chert, Kingdom occurrence. Hand sample is fine-grained blue-black and pyrite-rich. Secondary carbonate is common in thin section. Analysis performed at Lakehead University.
BRS-11	Interpillow chert, Kingdom occurrence. Disseminated pyrite mineralization. Trace element analysis performed at Geoscience Laboratories, Toronto.
BRS-18	Interpillow chert, Kingdom occurrence. Blue-black, fine, grained quartz with minor pyrite. Analysis performed at Lakehead University.
BRS-23 (A)	Carbonate dike (secondary), Kingdom occurrence. Analysis performed at Geoscience Laboratories, Toronto.
BRS-44	Siliceous tuffaceous sediment, Little Steel Railway occurrence. Hand sample displays fine banding and sulphides. Analysis performed at Lakehead University.
BRS-51	Siliceous tuff, Little Steel Railway occurrence. Sample taken from near BRS-44. Finely laminated, white to green, cherty sediment. Thin section displays primary quartz-rich and clastic-disseminated sulphide-rich laminations. Tuffaceous shards (plagioclase) are also present. Analysis performed at Geoscience Laboratories, Toronto.
BRS-52	Dark chert bands, Morely Property. Bands are black-blue and appear sulphide-rich. Thin section displays microcrystalline quartz (10 micron range) and possible clastic material such as chlorite, sericite, and opaques. Analysis performed at Lakehead University.
BRS-53	Light chert bands, Morley Property. Off-white bands have a saccharoidal texture. Thin section displays fine-grained quartz (50-100 microns) with little or no clastic component. Analysis performed at Lakehead University.
BRS- 55 (A)	Dark chert bands, Morley Property. Analysis performed at Lakehead University.
BRS-56	Cherty-siliceous bands, Little Bruin Property. Siliceous laminated bands alternating with pyrite. Thin section displays a tuffaceous (plagioclase) component. Analysis performed at Geoscience Laboratories, Toronto.
BRS-64	Chert, Granite Mountain. Bluish colour. Analysis performed at Lakehead University.
BRS-73	Chert, Schreiber Rail occurrence. Alternating cherty and pyrrhotite-oxide bands in iron-formation. Analysis performed at Lakehead University.
BRS-76	Chert-siliceous sediment, Gold Bar Lake. Analysis performed at Lakehead University.

TABLE 4: 3

COMPOSITION OF NON-SULPHIDE CHEMICAL-RICH  
SEDIMENTS ASSOCIATED WITH IRON-FORMATION

	BRS-1	BRS-11	BRS-18	BRS-23(A)	BRS-44	BRS-51	BRS-52	BRS-53	BRS-55(A)	BRS-56	BRS-64	BRS-73	BRS-76
SiO <sub>2</sub>	69.06	---	94.41	5.33	68.7	87.1	93.26	94.34	91.85	68.4	91.93	93.15	83.4
Al <sub>2</sub> O <sub>3</sub>	0.66	---	1.32	0.80	7.21	2.93	0.34	0.01	0.01	9.2	Nil	0.01	2.8
Fe <sub>2</sub> O <sub>3</sub> (T)	9.96	---	1.68	0.58	7.34	3.39	2.51	0.22	4.89	9.4	6.42	5.00	7.0
Fe <sub>2</sub> O <sub>3</sub>	8.56	---	---	---	---	---	---	---	---	Nil	6.03	---	---
Fe	1.24	---	---	---	---	2.18	---	---	---	2.98	0.14	---	1.98
Fe	N/A	---	---	---	---	---	---	---	---	---	---	---	---
HgO	0.01	---	Nil	0.02	0.53	0.36	0.01	0.01	0.01	1.2	Nil	0.01	0.5
CaO	9.46	---	0.76	48.9	7.53	1.79	0.20	0.08	0.54	0.9	0.28	0.01	Nil
Na <sub>2</sub> O	0.05	---	0.44	0.45	2.76	0.48	0.15	0.10	0.01	0.22	0.08	0.01	0.16
K <sub>2</sub> O	0.01	---	Nil	Nil	0.01	0.22	0.01	0.01	0.01	3.01	0.01	0.01	0.48
TiO <sub>2</sub>	0.07	---	0.08	0.02	0.21	0.11	0.09	0.08	0.05	0.28	0.05	0.11	0.05
P <sub>2</sub> O <sub>5</sub>	0.14	---	Nil	0.05	0.11	Nil	0.01	0.01	0.01	0.12	0.01	.01	0.03
MnO	0.24	---	0.01	0.09	0.05	0.06	0.01	0.01	0.01	0.01	0.01	0.10	0.01
C	.15	---	---	---	---	---	---	---	---	---	---	---	---
CO <sub>2</sub>	8.51	---	0.77	37.3	5.79	1.49	0.88	0.81	1.14	0.26	0.95	0.38	0.13
H <sub>2</sub> O	0.45	---	0.27	N/A	0.63	N/A	0.27	0.27	0.45	N/A	0.27	0.27	N/A
S	6.80	---	---	0.62	---	1.14	---	---	---	5.55	5.12	---	3.03
LOI	8.96	---	1.04	36.6	6.41	2.3	1.15	1.08	1.59	5.1	1.22	0.65	3.5
TOTAL	98.45	---	99.73	92.8	100.85	98.7	97.13	95.96	98.97	97.8	100.15	99.07	97.5
Au (ppb)	17	---	---	---	13(4)	13	---	---	585(5)	---	---	4	---
Ag (ppm)	< 2	---	---	---	2(4)	3	---	---	---	---	---	2	---
Co (ppm)	77	33	---	---	---	100	---	---	---	63	---	---	---
Cr (ppm)	Nil	Nil	---	---	---	14	---	---	---	28	---	---	---
Cu (ppm)	76	20	127	---	685(4)	24	---	---	---	35	---	79	---
Ni (ppm)	88	57	---	---	---	220	---	---	---	22	---	5	---
Pb (ppm)	138	Nil	---	---	---	Nil	---	---	---	33	---	---	---
Zn (ppm)	98	118	---	88	570(4)	695	---	---	---	780	---	141	---

--- Not Analysed

Al<sub>2</sub>O<sub>3</sub>, indicating the presence of up to several percent aluminosilicate minerals.

Rocks in Table 4:2 with low SiO<sub>2</sub> and high Al<sub>2</sub>O<sub>3</sub> contents, although identified in the field as cherts, are more appropriately termed siliceous siltstone/mudstone (BRS-30, 31, 55A) or tuffaceous chert (BRS-44, 51, 56).

#### c) Carbonates

Carbonate is a minor component of the iron-formation and chemical sediments in the Schreiber - Terrace Bay area. Most of this carbonate is secondary.

At the Kingdom occurrence, pervasive carbonate alteration is present in the metavolcanic rocks and within the iron-formation. A carbonate dike, (BRS-23A, Table 4:2) consisted almost entirely of calcite, with about 5% silica, and less than 1% alumina and sulphides.

At the Schreiber Rail occurrence, a bed of carbonate up to 1 m thick was discovered in association with sulphide-oxide-facies iron-formation. Beds and layers of calcite are display slump features. This is the only iron-formation containing an apparently primary carbonate component.

#### d) Oxides

Several of the iron-formations contain layers of iron oxides which appear to be primary, while others also contain secondary oxide components.

Magnetite, hematite, and goethite are present in minor amounts within the sulphide-facies iron-formations. Generally the oxides



occur as irregular grains within the sulphide grains, or as layers or rings rimming the pyrite nodules.

At Schreiber beach, a chert-magnetite iron-formation (1m thick) occurs at the contact between pillowed and massive volcanic flows. Magnetite and chert laminations are up to 5 mm thick. In the Victoria Lake, Otisse and Schreiber-Pyramid areas, chert-magnetite iron-formations up to 2 m thick are highly contorted and contain iron sulphides where fractured and faulted. At the Schreiber Rail occurrence a layered magnetite and pyrrhotite iron-formation up to one metre thick is present.

At the Clem Downey occurrence, fine-grained magnetite occurs as layers between recrystallized pyrite; replacement textures suggest that the pyrite is secondary. At the Black Fox occurrence, magnetite occurs in the cores of pyrite nodules, generally in areas of increased deformation.

#### e) Carbonaceous Component

Carbonaceous material is common in sulphide-facies iron-formations and pyritic slates. Hand specimens are near-black with a greasy lustre, and leave a black film on the hand. Carbon contents as determined with a CHN analyser ranged up to a maximum of 5% (Table 4:1).

The carbonaceous material is present both in the sulphide layers (associated with or as inclusions in sulphide grains), and the slate layers (where it may be a major component). It occurs in seams, streaks and lenses commonly separated by sulphide-quartz-sericite-rich laminations (Photo 4:14 B). The carbon is considered to represent relicts of bacterial or

microbial communities flourishing near hydrothermal vent sites (cf. Goodwin et al., 1985).

The carbonaceous material is generally amorphous with no crystalline texture. Only at the Black Fox occurrence were small laths of a carbonaceous mineral (graphite ?) present. XRD results for a pyritic-carbonaceous slate (BRS-8; Table 4:1) gave a pattern which closely corresponds to graphite, although an exact fit of peaks was not obtained. Easdon (1969) also found that true crystalline graphite was not present in the graphitic occurrences in Quebec. A similar conclusion was reached by Neilsen (1974) for pyritic-carbonaceous shales in the Savant-Sturgeon Lake area. By contrast, Shegelski (1978) found patterns characteristic of graphite for carbonaceous material associated with sulphide-facies iron-formation in the Savant-Sturgeon Lake area.

## 5) DEPOSITIONAL ENVIRONMENTS

### SEDIMENTOLOGY; CLASTIC UNITS

The majority of the iron-rich rocks in the Schreiber-Terrace Bay area is sulphide-facies iron-formation which is associated with mafic to intermediate volcanic flows and clastic sedimentary rocks. These units were deposited subaqueously, as indicated by the presence of pillows at several locations including the Kingdom, Little Steel and Harkness-Hays occurrences.

In the Steel River area in particular, excellent sedimentary structures are present which provide clues about the depositional environment. Sediments in Section 1 consist of turbidites up to 2 m in thickness which have medium- to coarse-grained sandstone bases. A vertical sequence graph (Figure 5:1) indicates 3 thinning-upward sequences in which AA and AE turbidites are predominant. Section 2 consists of graded sandstone beds up to 50 cm thick, with siltstone and slate tops up to 40 cm thick. Overall this section displays a gradually thickening- and coarsening-upward sequence. Thickening-upward cycles are commonly interpreted as reflecting progradation of lobe deposits in the outer fan region (Mutti and Ricci Lucchi, 1972) or deposition on suprafan lobes in the lower mid-fan area (Walker, 1976).

There are at present two major submarine fan models: i) an integrated facies model in which suprafan lobes develop when there is a regular sand supply to the fan apex (Walker, 1976); and ii) a model in which mud-dominated fans lack suprafan lobes due to entrapment of sand on the continental shelf (Mutti & Ricci Lucchi, 1972).

## VERTICAL SEQUENCE BED NUMBER VS THICKNESS

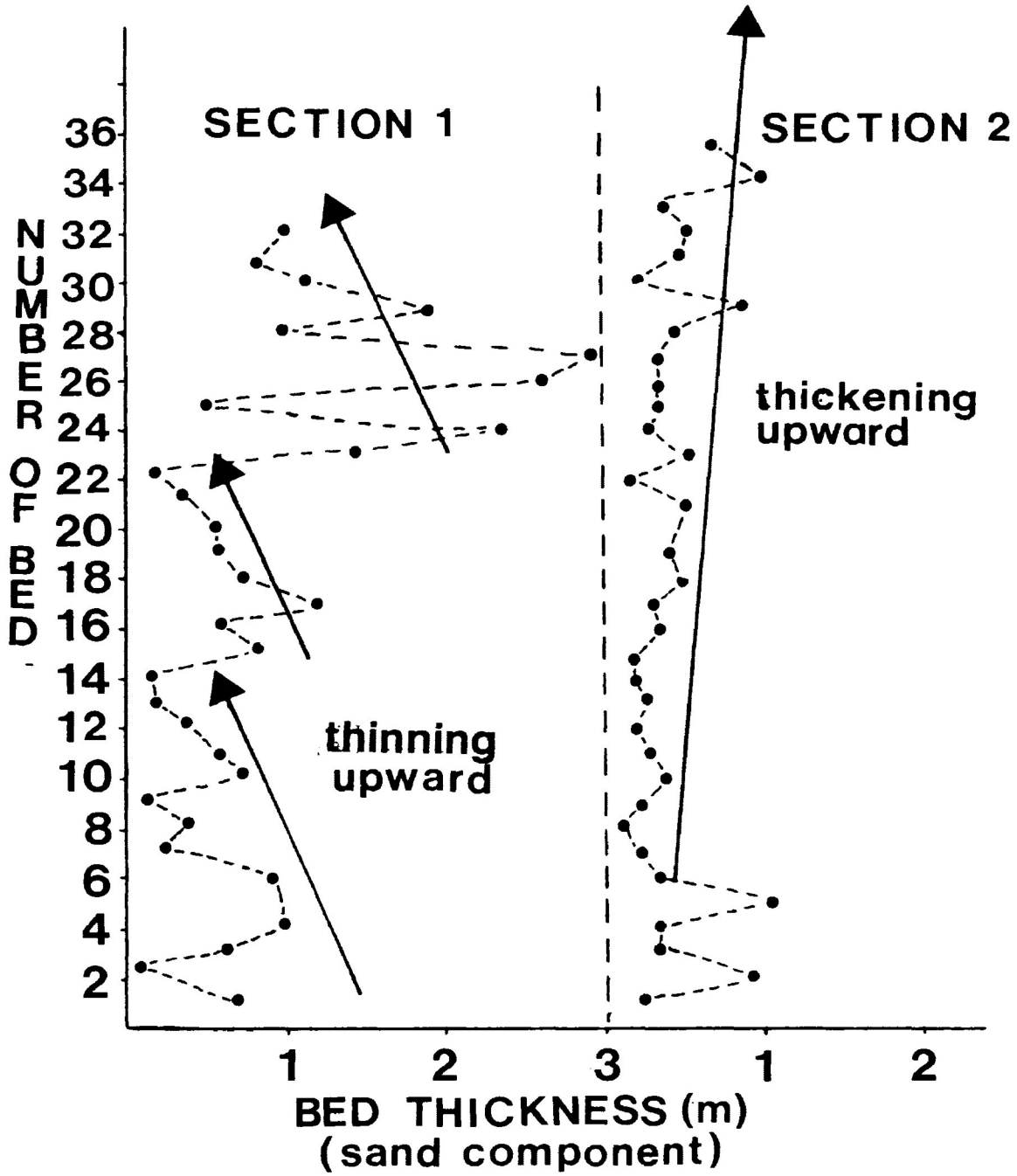


FIGURE 5:1

In terms of the Walker model (Figure 5:2) which is more applicable to the study area, the thinning-upward trends of massive sandstones, and "AA" and "AE" turbidites in Section 1 suggest that these sediments were deposited in a distributary channel of the upper mid-fan area. The thinner "AE" turbidites and near classical turbidites of Section 2, combined with the thickening-upward trend, suggest that these sediments were deposited on suprafan lobes in the lower mid-fan area.

The Steel River sections could also be interpreted in terms of trench sedimentation at an active margin. The thickening-upward trend of Section 2 could represent small outer fan lobes prograding along a trench. The thicker sandstones in Section 1 could represent either the infilling of isolated channel thalwegs, or sand-rich grain flows that ponded in the trench. A trench environment is suggested by the presence of cherts, greywacke-slates and volcanic rocks. These lithologies are typical of trench melanges, as for example the Gundahl Complex of Australia (Ferguson, 1984). Cross-stratification and loaded ripples at one locality suggest that the paleodirection of sediment transport was from west to east. However, since these rocks have been subjected to complex deformation, such a paleodirection is unreliable.

At the Kingdom, Simard-Swetz, Black Fox and Schreiber Road occurrences, DE and E(t) turbidites up to 10 cm thick are present in the pyritic-carbonaceous slate and sulphide-facies iron-formation. E(p) sediment representing pelitic rainout material also occurs. The lithological associations suggest either a channel-distal back-levee inner fan setting, or a channel-distal outer-fan environment. However, the lack of

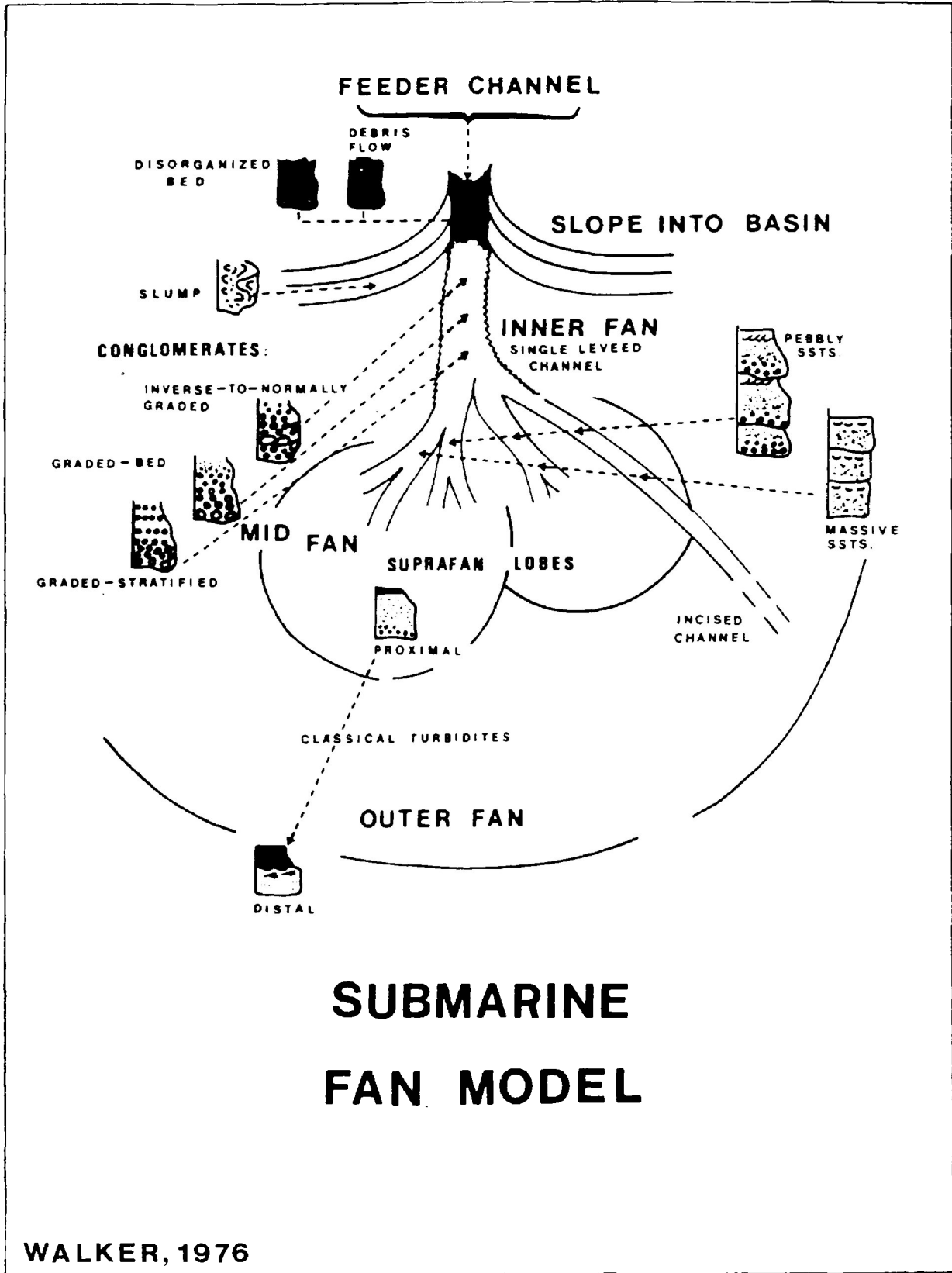


FIGURE 5:2

head-spill sandstones and channel conglomerates, together with the positioning of these lithologies at the base of the submarine fan succession, all favour a basin plain environment on the outer fan.

#### SEDIMENTOLOGY; IRON-FORMATION

As discussed above, the turbidites associated with iron-formations strongly suggest a lower mid-fan to outer fan depositional environment. The presence of laminated and nodular pyrite within sulphide-facies iron-formation requires a reducing bottom water environment. The laminated pyrite appears to reflect a combination of dominant chemical precipitation and minor clastic deposition. Vokes (1969) concluded that the banding of many, if not most sulphide deposits, is a primary texture or relict of the original sedimentary fabric, although metamorphism can exert a modifying influence. Fenwick (1971) also concluded that the laminated, banded and colloform nodular pyrite in the Finlayson Lake area was primary in origin. However, Shegelski (1971) noted that hydrated oxides could have been precipitated under oxidising conditions at the sediment-water interface; upon burial and development of reducing conditions, these may have been converted into metastable sulphides and eventually pyrite.

One possible genetic model for the production of colloform pyrite and nodules is: 1) leaching of iron from volcanic rocks by circulating seawater, and 2) precipitation of massive, colloform, nodular and finely laminated pyrite at and immediately around vent sites. At the East Pacific Rise, colloform pyrite is precipitated from low-temperature hydrothermal solutions at vent sites (Hekinian and Fouquet, 1985). Finely laminated pyrite in

the study area may be analagous to laminated sulphides in the Red Sea, where laminated metalliferous sediments occur in temperature- and salinity-stratified deeps (Degens and Ross, 1969). Zierenberg and Shanks (1983) accounted for the finely laminated nature of such sediments through quiet accumulation in subbasins removed from the active vent areas. The upward-growing, dome-shaped mounds of the colloform and interlaminated pyrite at the Morley occurrence resemble stromatolitic structures. The presence of carbon in these domal structures supports original organic activity (microbial mats). If hydrothermal input to local bottom waters occurred, organic activity may have been favored by seawater temperatures which were higher than normal (cf. Williams et al, 1982).

Radial nodules which coexist with colloform nodules generally display evidence of deformation, brecciation and recrystallization. It is suggested that these nodules form by the growth of small iron spherules during diagenesis. The radial texture and monomineralic rims of these nodules appear to develop during metamorphic recrystallization.

In the Schreiber-Terrace Bay area, predominantly sulphide-facies iron-formations are present at the contacts between volcanic and sedimentary rocks. This constitutes an overlap between Gross' (1965) Graded Greywacke-Siltstone Association and Mafic Volcanic Association (Table 1:2). However, most of the iron-formations can be accommodated in Shegelski's (1978) Algoman Mafic to Felsic Association (Mixed Facies) and Algoman Felsic Volcanic Association. Tectonic settings for sulphide-facies iron-formations include volcanic-arcs, back-arcs, basins, rifts and ocean ridges (Gross, 1983)



Parameters which can affect lithofacies characteristics of iron-formation include: 1) reducing versus oxidizing ambient water; 2) Eh-pH conditions and concentrations in discharging and bottom waters; 3) temperature differences; 4) tectonic activity; 5) variability in volcanic processes; and 6) clastic sedimentation rate.

A paleotopographical reconstruction of an Archean terrane (Figure 5:3) is modified after Shegelski (1978). The general depositional environment inferred for the iron-formations in the study area is shown within the box in Figure 5:3B. A detailed interpretation of the paleoenvironmental settings for all 16 iron-formations investigated is shown in Figure 5:4.

A geological cross-section of the Kingdom occurrence (Figure 5:5) displays sulphide-facies iron-formation occurring at a volcanic-sedimentary contact. The presence of thin laminations and absence of a major tuffaceous component suggests that the iron-formation formed distally to active volcanic centres. Layers, pods, and stringers of pyrite between individual pillows, pillowed flows and at the contacts between sedimentary and volcanic assemblages, suggest precipitation from hydrothermal solutions in the shallow subsurface and at the seafloor. Fine-grained DE and E(t) turbidites stratigraphically overlie pyritic-carbonaceous slate and suggest eventual submarine-fan progradation in the area.

Iron-formation at the Morley Occurrence represents episodic hydrothermal venting, probably within a restricted, small-scale basin (Figure 5:4). This is supported by the presence of finely laminated pyrite, alternating clastic (including tuffaceous) and chemical components and the dominance of volcanic rocks. By

# THEORETICAL PALEOTOPOGRAPHIC RECONSTRUCTION OF AN ARCHEAN TERRAIN

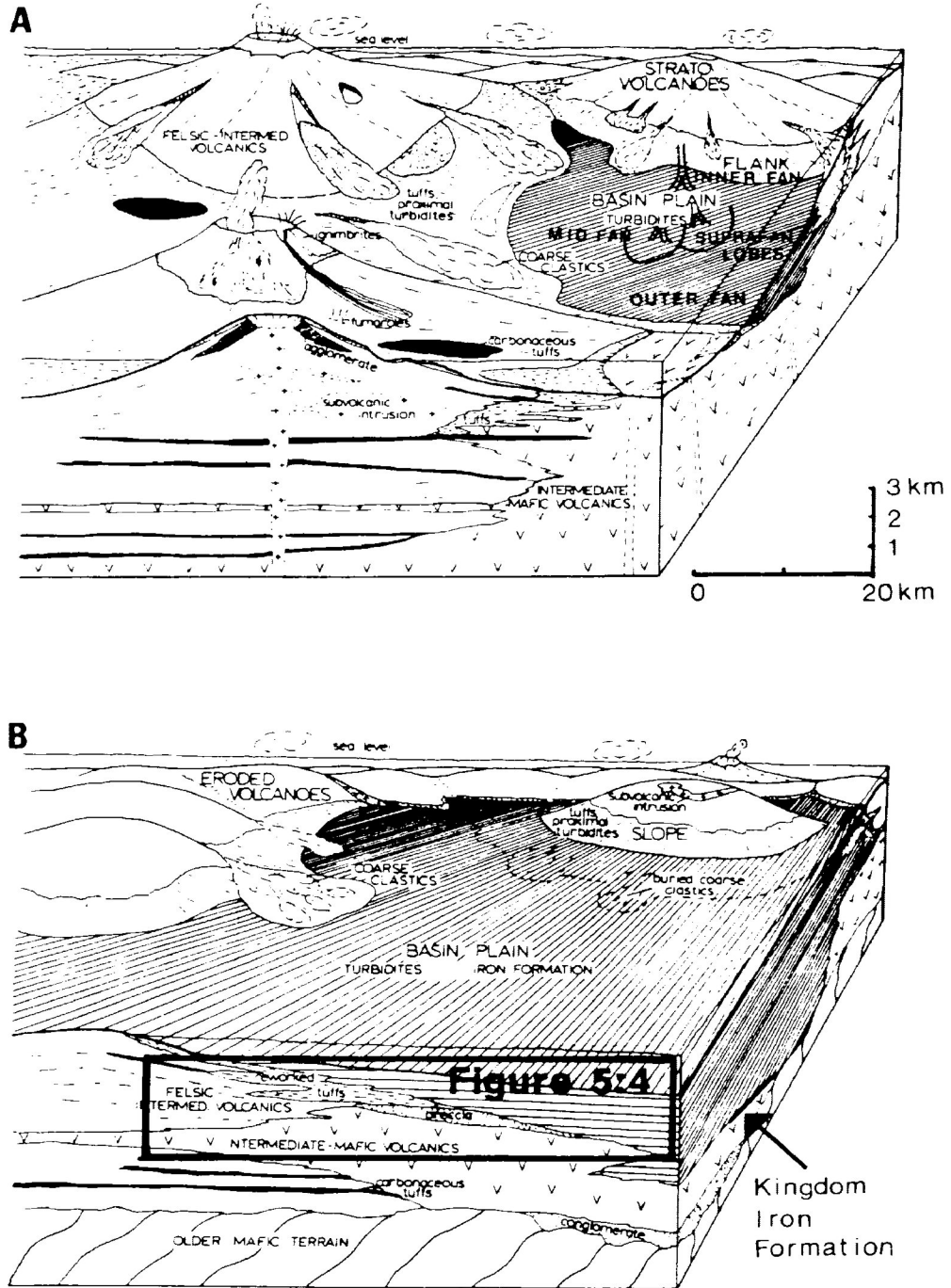
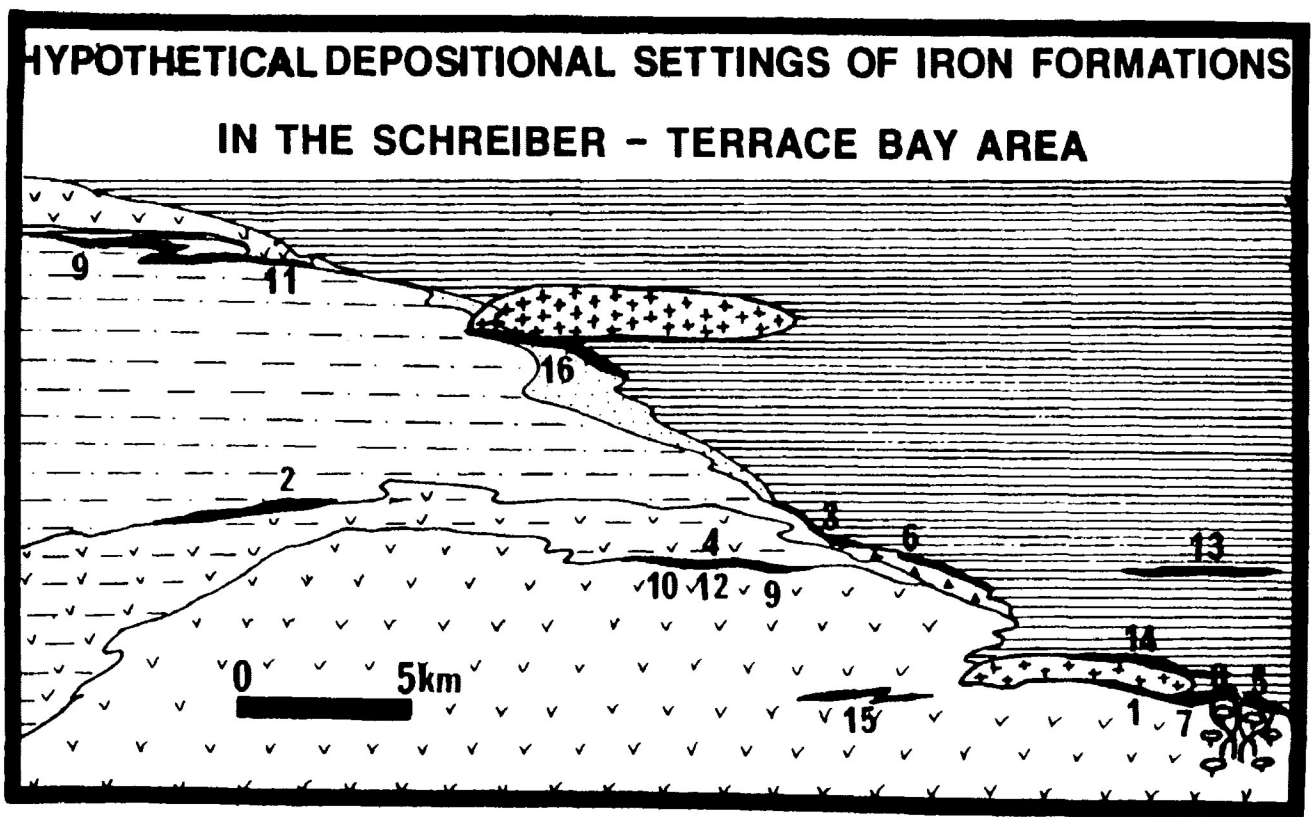


Figure 5:3

after Shegelski - 1976



OCCURRENCES

- 1 BLACK FOX LAKE
- 2 DOWNWY (EAST & WEST)
- 3 GOLDBAR LAKE
- 4 HARKNESS-HAYS
- 5 KINGDOM
- 6 LITTLE BRUIN
- 7 LITTLE STEEL (RAILWAY)
- 8 LITTLE STEEL (HIGHWAY)
- 9 MORLEY
- 10 SCHREIBER BEACH
- 11 SCHREIBER ROAD
- 12 SCHREIBER RAIL
- 13 SILVER SCEPTRE
- 14 SIMARD-SWETZ
- 15 WILDROSE
- 16 WINSTON LAKE

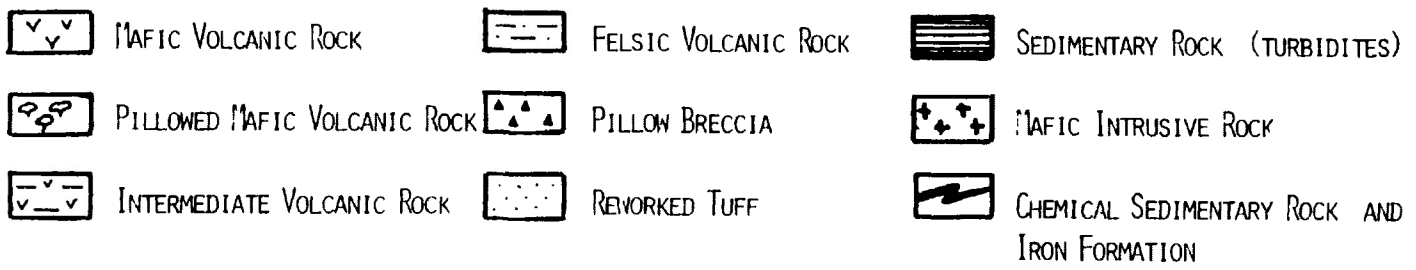
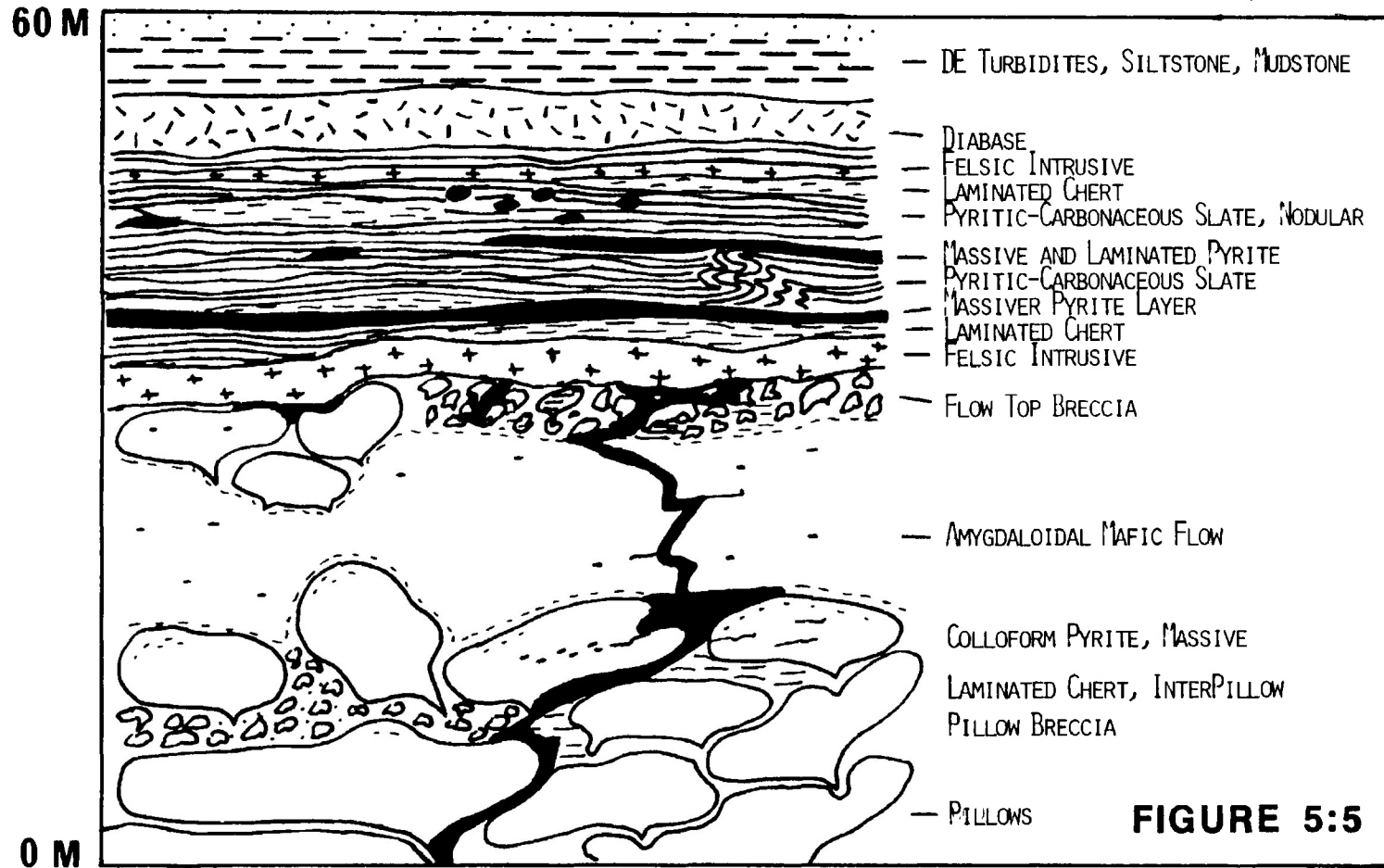


**FIGURE 5:4**

# GEOLOGICAL SECTION OF THE KINGDOM OCCURRENCE



UNITS NOT TO SCALE

contrast, iron-formation in the Little Steel Lake - Lower Steel River area was deposited in submarine fan environments ranging from upper to lower mid-fan.

## GEOCHEMICAL CONSTRAINTS

### a) Co/Ni Ratios

Numerous workers have used Co/Ni ratios in pyrite as a discriminator of depositional environment (Fleisher, 1955; Hawley and Nicol, 1961; Davidson, 1962; Roscoe, 1965; Wright, 1965; Loftus-Hills and Solomon, 1967; Fenwick, 1971; Neilson, 1974; Shegelski, 1978). Generally their findings indicated that Co/Ni ratios greater than 1 are supportive of a volcanogenic-hydrothermal origin for the pyrite. Hydrogenous pyrite (or iron oxide particulates that are later transformed into pyrite) precipitated from near-normal seawater distally removed from the vents has Co/Ni ratios of less than 1. For example, pyrite associated with graphitic slate displays a low Co/Ni ratio of about 0.38 (Loftus-Hill and Solomon, 1967). On the basis of more than 1,000 samples, Davidson (1962) concluded that there is no known (non-hydrothermal) sedimentary environment in which cobalt accumulates in excess of nickel.

When Co/Ni ratios of pyritic samples are combined with field and laboratory investigations of rocks they can become a useful tool in deciphering depositional environments. Samples of pyrite from the Schreiber-Terrace Bay area iron-formations were first subdivided into several groups as discussed below. Trace element data for the sulphide separates are given in Table 5:1, and Co/Ni ratios in Table 5:2. Several interesting geochemical characteristics emerge for these 5 categories, as summarized in Table 5:2.

1) Pyrite in Chert: Samples from two different properties contain 5 to 40% pyrite. Co/Ni ratios vary from 0.21 to 0.87, suggesting

TABLE 5:1 - SAMPLE DESCRIPTIONS

<u>SAMPLE NUMBER</u>	
BRS-2	Pyrite concentrate from laminated chert, Kingdom Property. Abundant disseminated pyrite and secondary recrystallized pyrite.
BRS-3	Pyrite concentrate from massive pyrite layer, Kingdom Property. Pyrite alyer is up to 6 cm thick.
BRS-7	Pyrite concentrate from massive pyrite layer, Kingdom Property. Laminated pyrite layer is 25 cm thick.
BRS-28	Pyrite concentrate from nodular pyrite, in pyritic-graphitic slate, Simard-Swetz occurrence. Nodules have recrystallized rims and radial textures.
BRS-39	Pyrite concentrate from nodular pyrite layer, Black Fox Lake Property. Nodules are brecciated, rotated, recrystallized; textures are colloform to radial.
BRS-49	Pyrrhotite concentrate from massive pyrrhotite bands, Little Steel Highway occurrence.
BRS-50	Secondary pyrite in chert, Little Steel Railway occurrence.
BRS-54 (A)	Pyrite concentrate from colloform pyrite nodules, Morely Property. Convex surfaces of colloform nodules are directed away from slate.
BRS-54 (B)	Pyrite concentrate from finely laminated pyrite bed, Morley Property. Same section as BRS-54 (A).
BRS-57	Pyrite concentrate from Little Bruin occurrence. Alternating chert/tuff and pyrite bands. Primary pyrite and sphalerite.
BRS-66	Pyrite concentrate from secondary recrystallized pyrite lens, with pyrrhotite and magnetite, Clem Downey (West) occurrence.
BRS-67	Pyrite and magnetite concentrate from magnetite-rich section, Clem Downey (West) occurrence.
BRS-74	Pyrite and pyrrhotite concentrate, Schreiber Rail occurrence.
BRS-78	Pyrite concentrate from radial nodules, Simard-Swetz occurrence.

NOTE: All trace element analyses performed by Geoscience Laboratories, Toronto.

**TABLE 5:1**  
**COMPOSITION OF SULPHIDE MINERALIZATION**  
**CONCENTRATES FROM THE IRON-FORMATION**

	<u>BRS-2</u>	<u>BRS-3</u>	<u>BRS-7</u>	<u>BRS-28</u>	<u>BRS-39</u>	<u>BRS-49</u>	<u>BRS-50</u>	<u>BRS-54</u> (A)	<u>BRS-54</u> (B)	<u>BRS-57</u>	<u>BRS-57</u> (D)	<u>BRS-66</u>	<u>BRS-67</u>	<u>BRS-74</u>	<u>BRS-78</u>
Fe (%)	35.9	31.0	37.8	39.2	32.9	51.8	---	37.9	---	23.0	---	---	48.8	---	---
C (%)	---	---	0.3	0.30	0.50	---	---	0.2	---	---	---	---	---	---	---
Au (ppb)	300	---	---	---	---	---	---	---	---	---	---	---	---	---	---
Ag (ppm)	7	---	---	---	---	---	---	---	---	---	---	---	---	---	---
Co (ppm)	195	600	730	47	187	157	90	59	855	114	---	30	21	60	50
Cr (ppm)	Nil	Nil	Nil	12	97	Nil	13	Nil	10	15	---	Nil	Nil	11	29
Cu (ppm)	265	230	143	118	1190	193	106	36	1280	108	121(5)	41	42	102	117
Ni (ppm)	855	485	30	70	315	380	425	48	340	52	---	50	31	90	82
Pb (ppm)	400	108	250	52	82	45	10	Nil	11	45	387(4)	Nil	Nil	Nil	53
Zn (ppm)	250	81	139	50	730	80	220	19	32	1480	856(6)	42	55	180	51

(D) Represent Duplicate Analysis

--- Not Analysed

(4) Represents average of 4 samples



COBALT/NICKEL RATIOS:

PYRITE CONCENTRATES

TABLE 5:2

<u>CATEGORY 1</u>		<u>CATEGORY 2</u>		<u>CATEGORY 3</u>		<u>CATEGORY 4</u>		<u>CATEGORY 5</u>	
Pyrite in Chert, (disseminated, laminated)		Massive Pyrite (layers, lenses, beds in chert, slate)		Pyrite Nodules (Radial Texture)		Pyrite Nodules (Colloform Texture)		Pyrite in Pyritic- Carbonaceous Slate (disseminated, laminated)	
BRS-1	.87 K	BRS-3	1.24 K	BRS-28	.67 SS	BRS-54 A	1.23 M	BRS-5	.70 K
BRS-11	.58 K	BRS-7	23.3 K	BRS-29	.59 BF			BRS-6	.70 K
BRS-50	.21 LS	BRS-9	11.06 K	BRS-78	.61 SS			BRS-25	.77 SS
BRS-51	.45 LS	BRS-56	2.86 LB						

NOTE:

K = Kingdom Occurrence  
SS = Simard-Swetz  
LS = Little Steel  
LB = Little Bruin  
M = Morley  
BF = Black Fox

that the sediment precipitated from normal seawater, however, the higher ratios (over 0.75) suggest a minor hydrothermal component.

2) Massive Pyrite: The Co/Ni ratios of 8 samples collected from four separate properties vary from 1.24 to 24.3, implying a hydrothermal origin with little mixing of the vent solutions with normal seawater prior to deposition.

3) Radial Nodules: Three radial nodules from two separate properties have Co/Ni ratios less than 1, again suggesting little or no hydrothermal influence during their precipitation. The Co/Ni ratios are consistent with field data which suggest a vent-distal setting.

4) Colloform Nodules: One colloform nodule from the Morley property has a Co/Ni ratio of 1.23, suggesting a minor hydrothermal influence. A massive colloform pyrite layer (BRS-54B) with which the nodule is associated has a Co/Ni ratio of 2.51, suggesting a greater hydrothermal component.

5) Pyritic-Carbonaceous Slate: Disseminated pyrite and pyrite laminations in 4 slaty samples from 2 properties have Co/Ni ratios ranging from 0.31 to 0.84. These ratios suggest precipitation mainly from normal seawater. However, the range is generally higher than that of black shales analysed by Loftus-Hills and Solomon (1967).

The Co/Ni ratios for all types of pyrites are plotted in Figure 5:6, together with the Co = Ni line. Generally the finely disseminated pyrite appears to represent mainly hydrogenous iron of a sedimentary-diagenetic origin deposited distally from a vent source, and with only a minor hydrothermal component. In

# PLOT OF Co vs. Ni

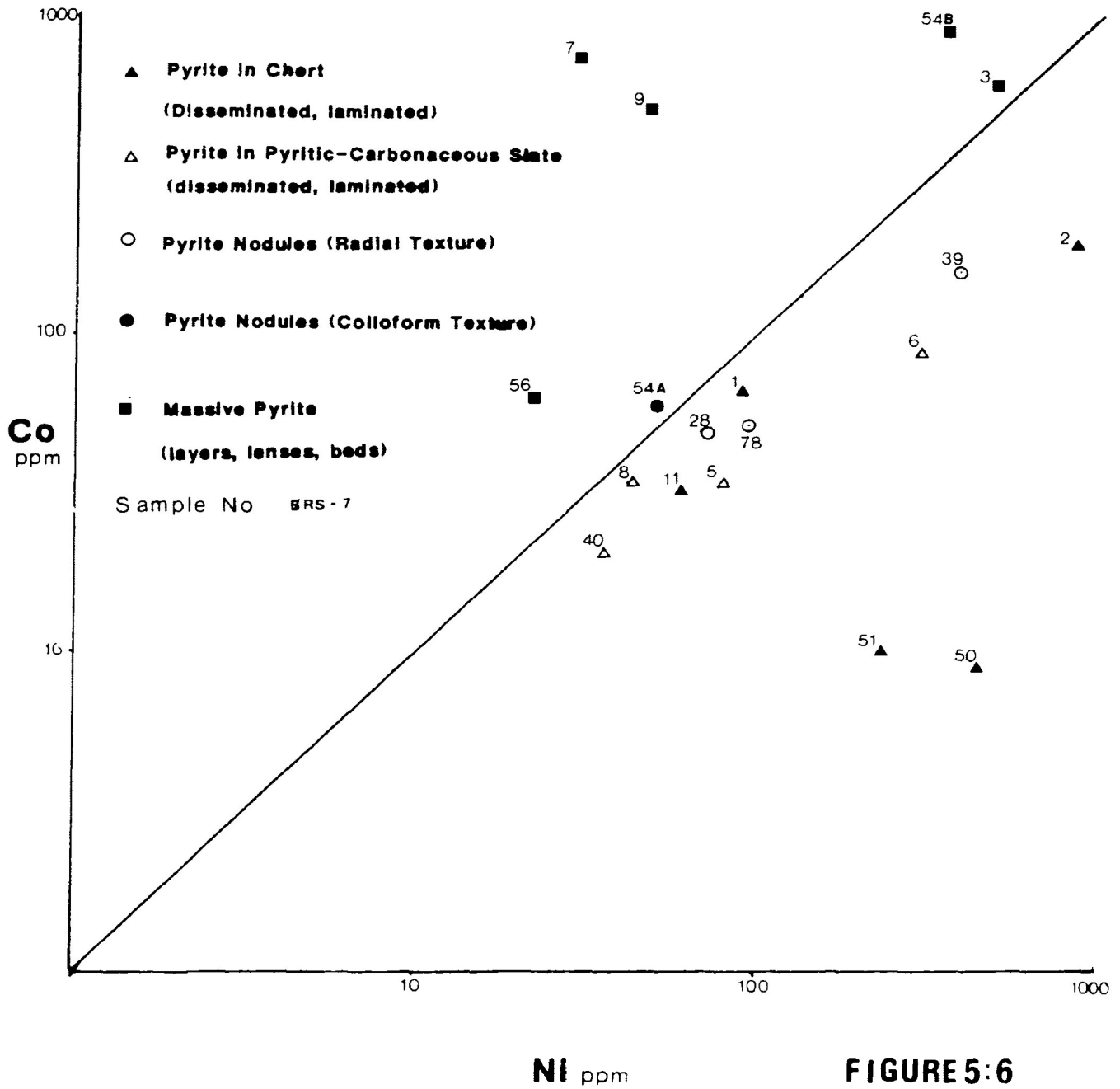


**FIGURE 5:6**

contrast, the massive laminated pyrite layers and lenses appear to represent more vent-proximal deposits precipitated from relatively unmodified hydrothermal solutions.

#### b) Hydrogenous versus Hydrothermal Input

The chemical classification scheme of Bonatti et al. (1972) and Bonatti (1975) also can be used to determine if metalliferous deposits are primarily hydrogenous or hydrothermal in origin (Figure 5:7). This scheme is based on the relative proportions of Fe, Mn, and (Ni+Co+Cu) in the sediment.

Samples of metalliferous sedimentary rocks (cherts and pyritic-carbonaceous slates (Tables 4:1 & 4:2) cluster near the hydrothermal Fe-rich end member in Figure 5:7. As shown above, Co/Ni ratios for these sedimentary rocks suggest only a weak hydrothermal component. This suggests that the Bonatti diagram is a more sensitive indicator of hydrothermal input than are Co/Ni ratios.

#### c) Clastic - Chemical Mixing

In order to estimate the component of clastic material present in the very fine-grained lithologies associated with the iron-formations, whole-rock chemical data were interpreted in terms of the mixing diagrams developed by Bostrom (1970, 1973). The position of the shale line (Figure 5:8, line c) close to the Ti/Al ratio for average continental crust (lines b) indicates that deep-sea shales more or less reflect the weathered products of average continental crust. When turbidite-associated slate and pyritic-carbonaceous slate from the study area (Tables 3:2, 4:1) are plotted, a near-linear trend (with two exceptions) is

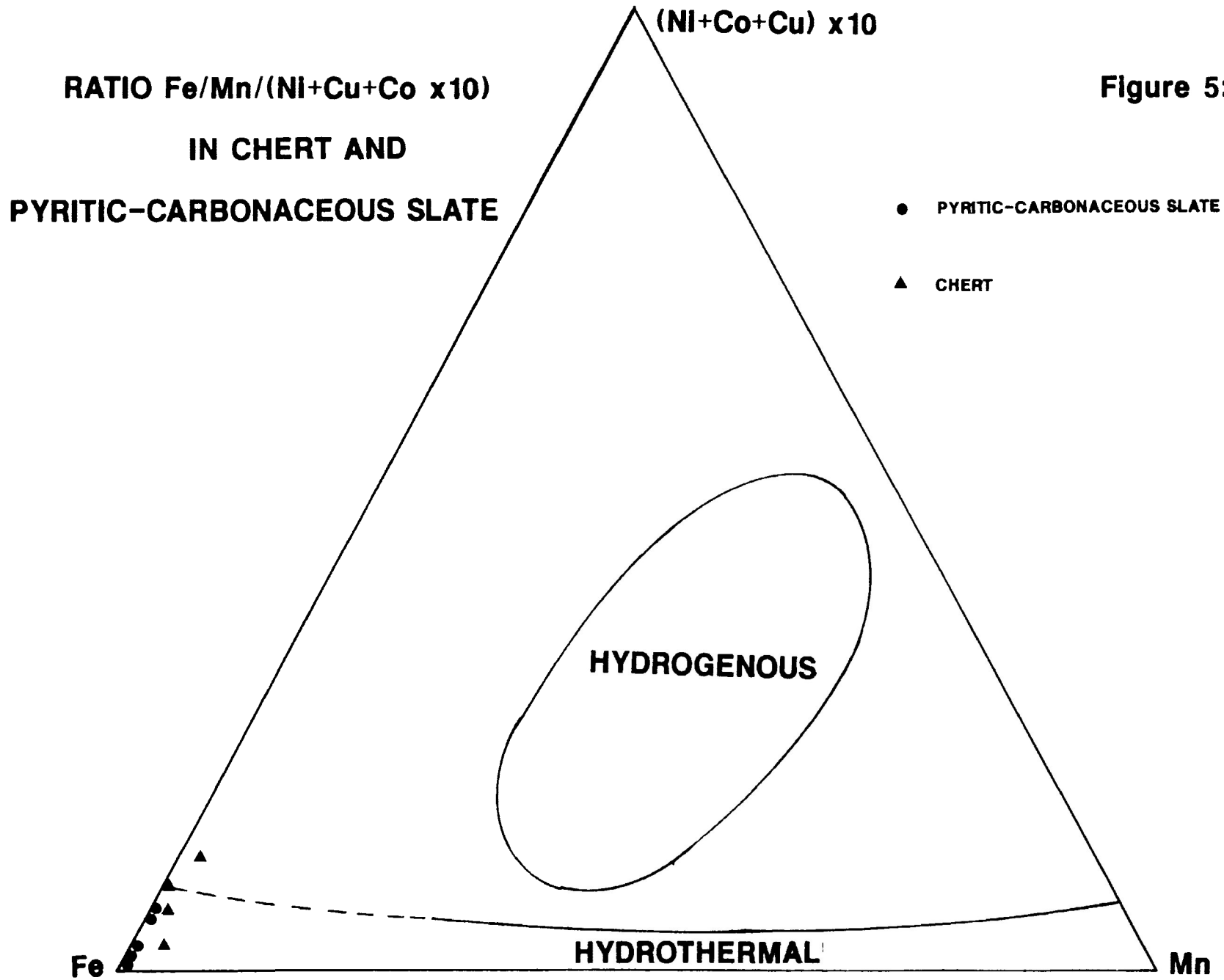


**Figure 5:7**

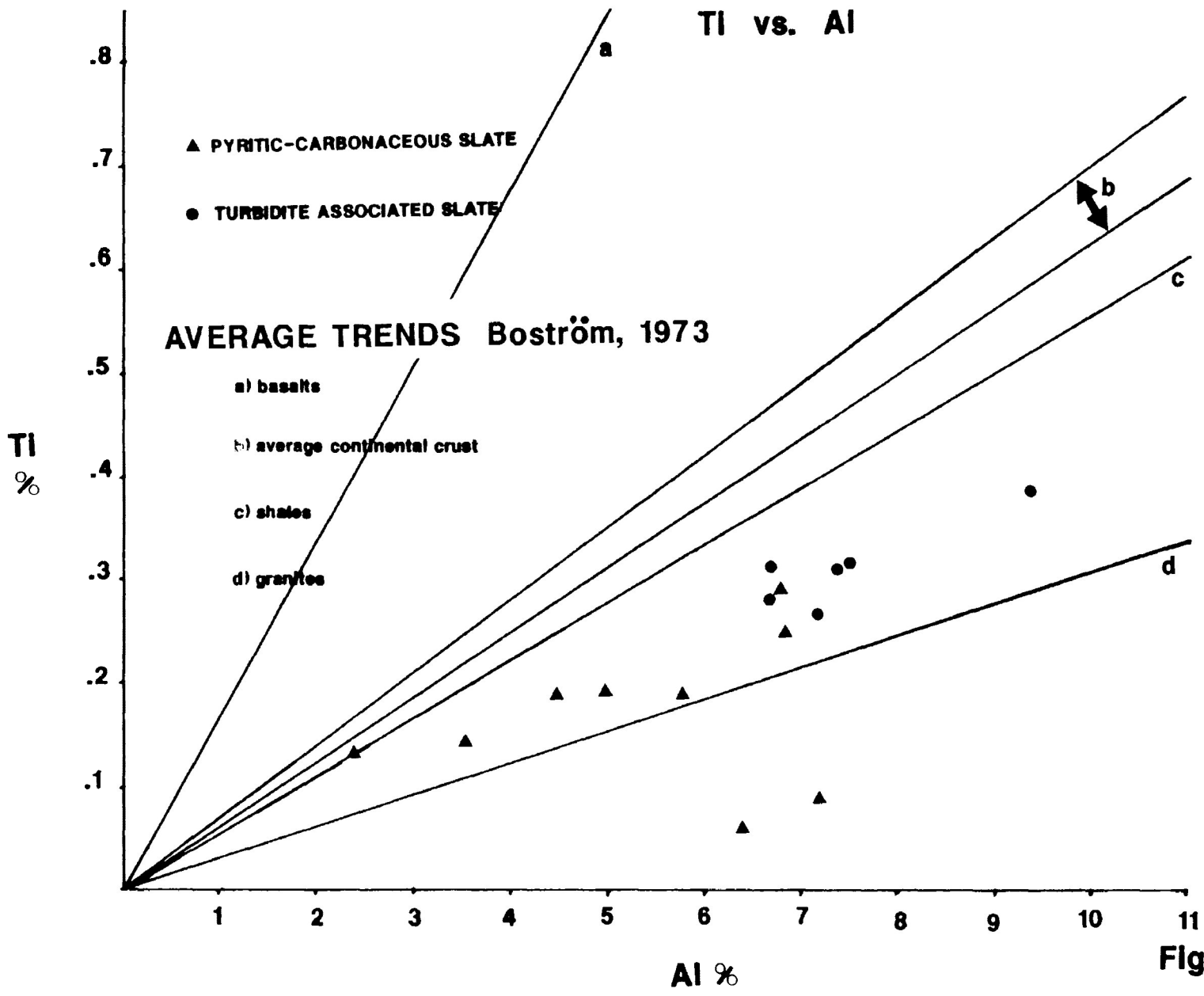
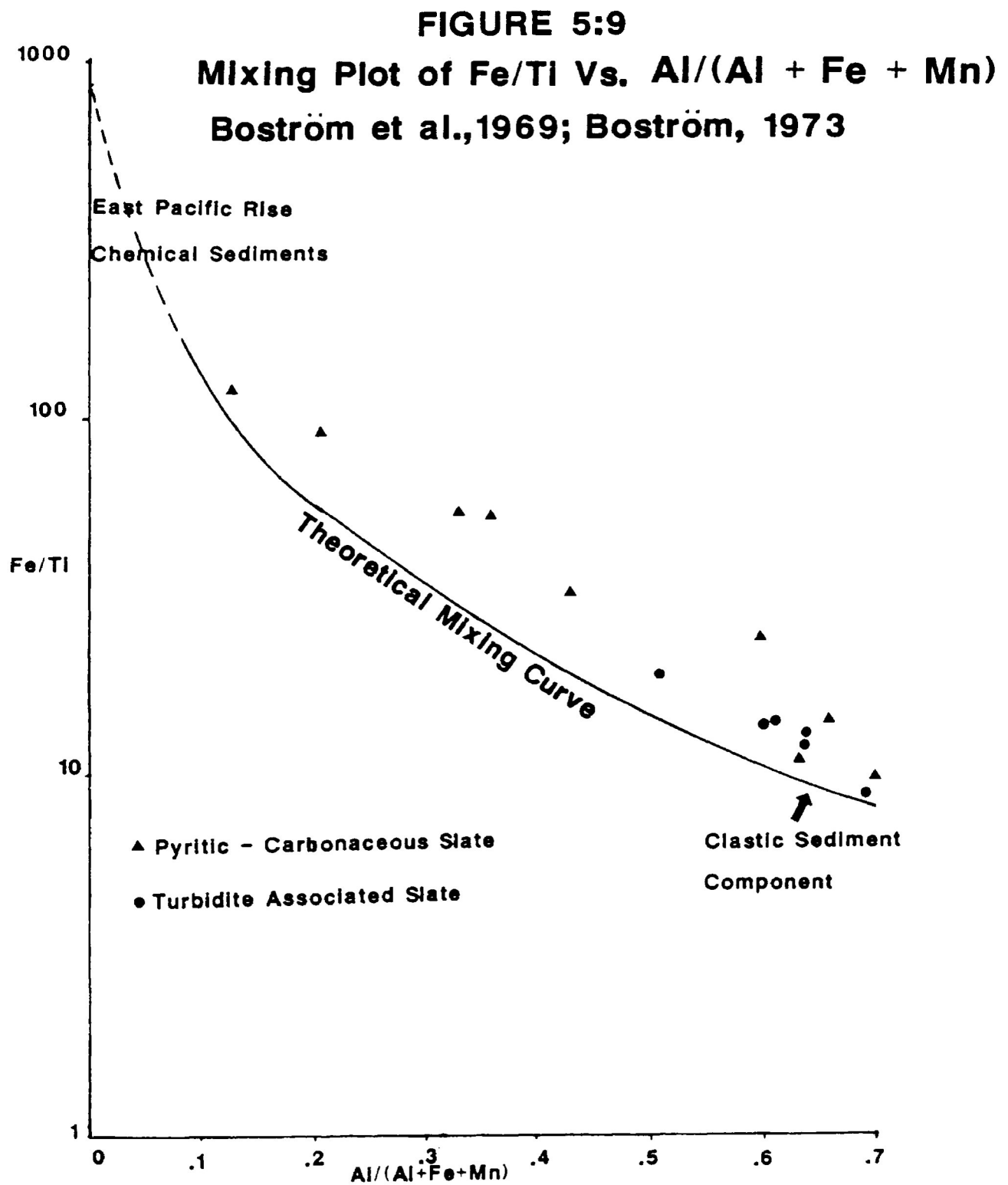


Figure 5:8

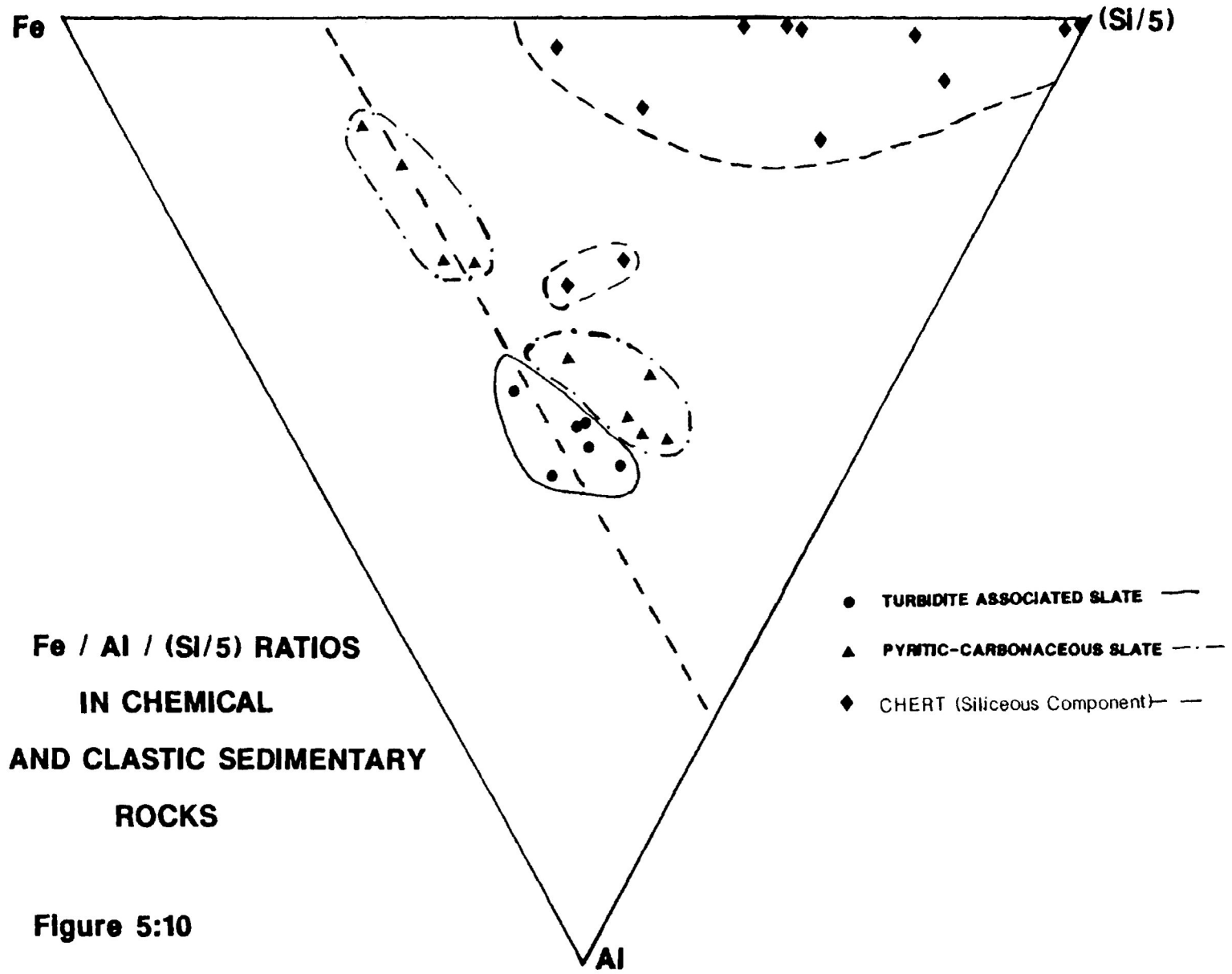
observed. The data indicate that: i) the pyritic-carbonaceous slates have lower absolute Ti and Al concentrations than the turbidite-associated slate, possibly due to mixing (dilution) with chemical precipitates and biogenic matter low in Ti and Al; and ii) the slope of the trend is lower than for modern deep-sea shales, suggesting that the Archean source terrane had a greater component of exposed granitic crust (line g) than modern average continental crust.

A plot of  $Fe/Ti$  versus  $Al/(Al+Fe+Mn)$  is shown in Figure 5:9. This diagram provides a useful method in assessing the relative contributions of clastic material and chemical precipitates to fine-grained sediments (Bostrom 1970; 1973). Turbiditic and pyritic-carbonaceous slate in the study area (Table 3:2, 4:1) plot close to, but somewhat above, a theoretical mixing line between deep-sea shale and metalliferous sediment from the crest of the East Pacific Rise. Pyritic-carbonaceous slate generally has a higher hydrothermal component than the turbidite-associated slate. A minor hydrothermal component in the latter could be due to incorporation of some chemical precipitates by bypassing turbidity currents, or to a distal hydrothermal influence on post-turbidite pelitic sedimentation. Samples from the present study plot above the theoretical mixing curve probably as a result of their somewhat lower Ti contents relative to modern shales (Figure 5:8).

Mixing of the clastic component with silica of possible hydrothermal derivation can be assessed using a ternary Fe-Al-Si plot (Figure 5:10). Turbiditic slates with a dominantly clastic component plot near the middle of the diagram. Relative to this field, the pyritic-carbonaceous slates display higher proportions







of silica for about half the samples; the other half have similar silica contents but much higher Fe and lower Al values. Assuming the cherts represent hydrothermal precipitates, as suggested by their close spatial association with volcanics and sulphide mineralization, then about half of the pyritic-carbonaceous slates contain a small component of hydrothermal silica. By contrast, the other half of these slate samples contain a significant component of hydrothermal iron, apparently in the form of sulphides. Figure 5:10 also shows the considerable range in iron content of the cherts. Since this range is essentially independent of Al content, variation in the content of iron sulphides (as opposed to iron silicates) is the likely cause.

## 6) POSSIBLE MODERN AND ANCIENT ANALOGS

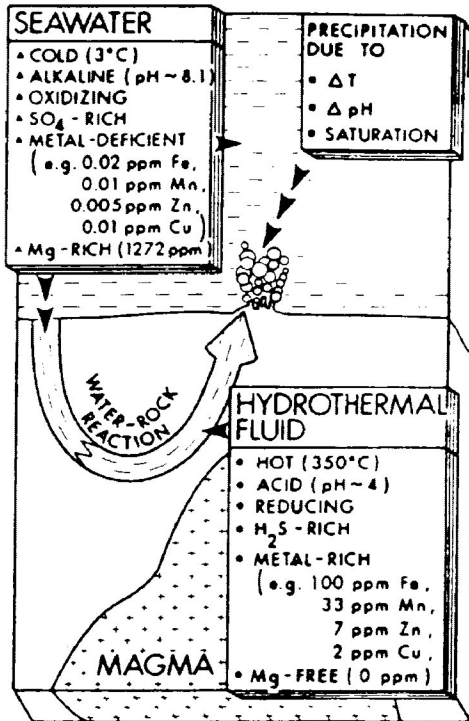
The genetic processes which produced sulphide-facies iron-formation and volcanogenic massive sulphide deposits during the Archean are considered to be similar to those producing metalliferous sediments and metal sulphide deposits on the seafloor today (Sangster and Scott, 1976). Volcanogenic massive sulphide deposits of the Archean were originally formed from submarine hot springs (Sangster and Scott, 1976) and are commonly compared to models advanced for deposits of the Cyprus, Kuroko or Besshi type.

Examples of metalliferous sediments of hydrothermal derivation include modern Fe-Mn-oxides (East Pacific Rise, Corliss et al., 1979) and Fe-silicates (Galapagos, Barrett et al., 1983), Mesozoic umbers and exhalites (Cyprus, Robertson and Hudson, 1973; Japan, Lambert and Sato, 1974) and Archean banded iron-formations (Knuckey et al., 1982). However, there are problems in making detailed analogies between modern and Archean metalliferous sediments, partly because of the lower levels of oxygen which existed in the Archean hydrosphere (Walker and Brimblecombe, 1984).

### a) Modern Polymetallic Deposits

Scott (1985) reviewed and summarized a hydrothermal convection model capable of generating massive sulphide deposits and metalliferous sediments (Figure 6:1A), including five essential requirements: 1) convection of seawater solutions through permeable ocean crust, during which metals such as Fe, Mn, Zn and Cu are leached, and seawater sulfate is reduced to hydrogen sulphide; 2) existence of a large, magmatic heat source to

# GENETIC MODELS FOR MODERN METALLIFEROUS SEDIMENTS AND POLYMETALLIC DEPOSITS

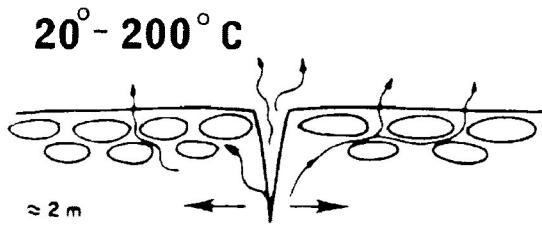


## HYDROTHERMAL CIRCULATION

MODEL DISPLAYS ON AXIS EXHALATION OF HYDROTHERMAL SOLUTIONS, TYPICAL FOR 21 DEGREES NORTH, EAST PACIFIC RISE. PRECIPITATION IS DUE TO MIXING OF THE COLD SEAWATER AND HYDROTHERMAL SOLUTIONS.

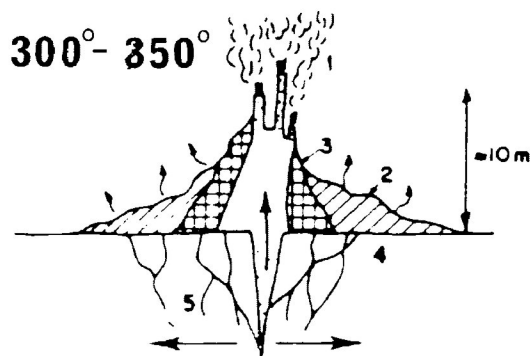
(SCOTT, 1985)

**FIGURE 6:1(A)**



## OFF-AXIS MODEL

LOW TEMPERATURE HYDROTHERMAL SOLUTIONS ARE DIFFUSED THROUGH LOBATE FLOWS. COLLOFORM PYRITE IS PRECIPITATED.



## ON-AXIS MODEL

HIGH TEMPERATURE DISCHARGE THROUGH CHIMNEYS (1), PRECIPITATES ZINC SULPHIDES (2), FE SULPHIDES (3), AND SULPHIDE VEINS (4) AND ALTERED THE SURROUNDING BASALT (5)

(HEKINIAN AND FOUQUET, 1985)

**FIGURE 6:1(B)**

produce circulation of the solutions; 3) a fracture or plumbing system that permits circulation through the oceanic crust, and focuses discharge on the seafloor; 4) a mechanism for precipitating sulphide minerals from the fluid; and 5) subsequent sedimentary or volcanic accumulations which bury and preserve the deposits.

Recent studies of the hydrothermal deposits at modern ridges in the Pacific Ocean indicate two contrasting environments of deposition and types of deposits formed (CYAMEX, 1979; RISE, 1980; Hekinian et al., 1980; Oudin, 1983; Curray et al., 1982; Scott, 1985). A third environment is proposed for the Atlantis II Deep, Red Sea (Zierenberg and Shanks III, 1983). Briefly, these environments are: 1) sediment-starved ridge crests such as the East Pacific Rise (21 and 13 degrees North, and the Galapagos Ridges); 2) heavily sedimented ridge crests such as Guaymas Basin, Gulf of California; and 3) spreading centers composed of subbasins in which metalliferous sediments are deposited in quiescent brine pools.

While the processes are similar in each environment, differences in the lithology of the host rocks, and in the composition of discharging and bottom waters, result in the formation of mineralogically and morphologically different types of deposits.

At the spreading axes of the East Pacific, sulphide-rich deposits are presently forming from high temperature "black smokers" (Corliss et al., 1979; Francheteau et al., 1979, RISE, 1980). The discharging hydrothermal fluids are hot (350 degrees C), acidic (pH approximately 4) and H<sub>2</sub>S-rich, with metal concentrations of about 100 ppm Fe, 33 ppm Mn, 7 ppm Zn and 2 ppm

Cu. The hydrothermal precipitates are primarily Cu, Zn and Fe sulphides, with lesser amounts of anhydrite and barite (Edmond and Van Damm, 1983). Pyrite or marcasite are the dominant Fe sulphides and PbS is virtually absent (Edmond et al., 1979; Scott, 1985). Massive sulphides precipitate at the discharge site, where the mixing of the hot hydrothermal solutions with cold, oxidised seawater produces a plume of black smoke (Converse et al., 1983). Lateral transport of plume material by ocean currents result in the formation of Fe-Mn-rich metalliferous sediments up to hundreds of kilometres from the vents. The iron in such sediments is in the form of oxide-hydroxide phases due to oxidation during transport (Dymond et al., 1973).

At the Guaymas basin, an echelon series of deep basins have developed. About 400 m of calcareous and pelitic sediments with a high organic carbon content (approximately 3 %) overlie the spreading axis. Magma intrudes the sediment pile in the form of thick sills and plugs. The spatial distribution of hydrothermal sulphide mounds in this area appears linked to the presence of sills at depth; heat from the sills drives hydrothermal convection within the sediment column. Reaction of solutions with the thick sequence of carbonate- and organic-rich sediments produces a highly reduced fluid. The hydrothermal precipitates formed when this fluid discharges into seawater are dominated by calcite, anhydrite and barite. Pyrrhotite is the dominant main phase, with lesser amounts of copper and zinc sulphides (Curry et al., 1982; Scott, 1985)

Metalliferous sediments forming along the spreading axes of the Red Sea range from oxide- to silicate- to sulphide-facies, and occur within temperature- and salinity-stratified brine deeps

occupying topographic subbasins (Degens and Ross, 1969; Zierenberg et al., 1984). These sediments are precipitates from warm bottom waters (44-56 degrees C). Temperatures of the hydrothermal solutions entering the subbasins probably exceed 200 degrees C (Zierenberg and Shanks, 1983). Well layered and laminated precipitates of different metalliferous facies are related to variable Eh-PH-T conditions which exist in the brine layers and overlying normal seawater (Bischoff, 1969).

Hekinian and Fouquet (1985) describe the formation of sulphide deposits at 13 degrees N on the East Pacific Rise. The first stage involves low temperature (<30 degrees C) hydrothermal discharge through fissured basement rocks. High temperature solutions (>300 degrees C) are vented in the following stages, leading to the production of polymetallic sulphide deposits in the axial graben.

In the off-axis regions, sulphide precipitates including colloform pyrite, are formed from lower temperature solutions (<100-200 degrees C, Hekinian and Fouquet, 1985; Figure 6:1B). The pyrite consists of colloform-layered and spherulitic pyrite, commonly coated with idiomorphic pyrite. Early formed pyrrhotite is altered to a mixture of native sulfur and iron sulfates, and in some cases transformed into pyrite or marcasite. Pyrrhotite is surrounded by spherulitic concretions of colloform pyrite. The upper pyrite of the colloform pyrite concretions may be partially altered into goethite. Goethite forms mammillary concretions covering massive sulphides and sometimes pillow lavas, as well as forming an interstitial product between them.

Koski et al. (1984) have also described precipitates of colloform Fe-sulphide, with minor sphalerite, which formed from

low temperature vents on the Juan de Fuca Ridge. Alt et al. (1987) report colloform pyritic structures from a chimney at 21 degrees N on the East Pacific Rise; however, the layering is vertical in this occurrence. Adshead et al. (1986) described thin metalliferous layers in sediments on the Juan de Fuca Ridge which are interpreted to represent episodic hydrothermal activity at a nearby vent.

Base metal-poor Archean iron-formations have been ascribed to relatively low-temperature hydrothermal solutions. Goodwin et al. (1985) suggested that the Helen iron-formation precipitated from solutions at temperatures of less than 200 degrees C.

#### b) Ancient Polymetallic Deposits

Cyprus Type: Cupriferous pyritic ores are associated with the Cyprus ophiolites. These Cretaceous deposits occur on basaltic pillow lavas representing the original surface of the ocean crust. Thus they have formed at sediment-starved oceanic spreading centers, possibly in a back-arc or interarc setting (Miyashiro, 1973). These massive sulphides most closely resemble the East Pacific Rise deposits.

Two types of metalliferous sediments, ochres and umbers, are associated with the Cyprus deposits. Robertson (1976) described ochres as ferruginous, sedimentary oxy-hydroxides, normally manganese-poor, apparently forming through the seafloor oxidation of the massive sulphide ore bodies. The umbers are also ferruginous sedimentary oxy-hydroxides; however, they are enriched in manganese and many trace elements, and are thought to have been precipitated from oxidised seawater.



Besshi Type: These Japanese deposits, of Permian to Mesozoic age, occur as extensive sheets of cupriferous pyrite mineralization. They are associated with tholeiitic basalts and thick, often highly metamorphosed, sedimentary rock sequences (Ikeda et al., 1971, 1972). Suggested tectonic settings for these deposits include a rifted cratonic margin or rifted fore-arc.

The Besshi sulphides have similarities to the Guaymas Basin deposits (Scott, 1985), including the extent of the mineralization, the association with pelitic sediments and basalt, the presence of nearby carbonate-rich rocks, and enrichments of manganese and carbon. Differences include a much higher ratio of sulphides to sulphate in Besshi deposits, and the occurrence of mineralization in sheets rather than as the mound-like structures characteristic of the Guaymas deposits.

Kuroko Type: The Kuroko deposits of Japan are Miocene in age, and are believed to have formed on the flanks of rhyolitic lava domes (Sato, 1974). These deposits contain abundant Pb-Cu-Zn sulphide mineralization. Their tectonic setting has been interpreted as a partially rifted, sialic craton (Sato, 1974; Scott, 1980; Cathles et al., 1983).

Horikoshi (1969) described Kuroko deposits as the result of hydrothermal activity during complex, polyphase eruptive cycles of the Kosaka Volcano. Sato (1977) suggested that the Kuroko sulphides could not have been produced solely by the circulation of sea water through host rocks, and inferred that magmatic water played an important role in the mineralization. No modern analogs for the Kuroko deposits of Japan have yet been identified.

Archean Volcanogenic Deposits: The Millenbach (Knuckey et al., 1982) and Corbet (Knuckey and Watkins, 1982) mines of the Noranda area are typical examples of Archean volcanogenic massive sulphide deposits formed from submarine hot springs. Hydrothermal activity has appreciably altered the surrounding host rocks. At the Millenbach, sulphides on the fringe of the main ore lens are relatively base metal-poor, and probably formed from lower temperature solutions than the main lens (Knuckey et al., 1982). Finely laminated base metal sulphides are observed at both Millenbach and Corbet. At the Agnico-Eagle gold deposit, Val d'Or, thick, laminated carbonate-sulphide-silicate-oxide-facies iron-formation is present (Barnett et al., 1982). These authors suggest the iron-formation is volcanogenic, with certain affinities to massive sulphide deposits.

#### c) Implications for the Study Area

The iron-formations of the Schreiber-Terrace Bay area generally occur as thin, lenticular to sheet-like deposits which are semi-continuous along strike. They are generally located at or near the contacts between sedimentary and volcanic rocks. In these respects, the iron-formations bear a resemblance to Besshi-type deposits. Although the iron-formations are thinner and less continuous laterally, this is conceivably the result of a much longer history of deformation.

At the Kingdom property, field evidence suggests that pillow lava extrusion was followed by sulphide deposition, which in turn was followed by mixed chemical and clastic sedimentation. The silicification and iron depletion in the volcanics (Chapter 3) could be produced by diffusion of low temperature solutions

through the pillowed flows, similar to the model of Hekinian and Fouquet (1985) (Figure 6:1B). Pyrite-rich, Mn-poor carbonaceous slates at the Kingdom occurrence may have been deposited in a locally more reducing environment than the Mn-bearing turbidite associated slates. Robertson (1976) noted that low Eh values in the discharge environment favoured precipitation of Mn-poor sediments.

The formation of colloform pyrite and the dominance of pyrite in the iron-formations is consistent with the relatively low-temperature, off-axis model of Hekinian and Fouquet (1985) (Figure 6:1B). Geochemical data on pyrites and associated slates in the iron-formation, together with the field relationships, suggest the following sequences of events: i) upward percolation of relatively low-temperature hydrothermal solutions through volcanic lava sequences; ii) precipitation of colloform and nodular pyrite at and near the fissure sites; and iii) precipitation of laminated pyritic sediments more distally to the fissures, but still in a reducing environment.

The existence of primary laminations in the sulphide-bearing sediments implies quiet and reduced bottom water conditions. The alternation of chemical and clastic laminations suggests episodic hydrothermal activity. Fault-bounded, topographic depressions with restricted circulation may provide the necessary environmental setting to account for both the undisturbed chemical laminations and the laterally discontinuous nature of sulphide-facies iron-formation as a lithologic unit. The finely laminated domal-structured pyrite at the Morley occurrence, and the general presence of carbon in the iron-formation and slate support the existence of organic (microbial) activity at

precipitation sites. A possibly analogous modern environment is represented by the Atlantis II deep in the Red Sea, where laminated sulphide-facies sediments are present, although organic influences are absent due to the very high salinity of the bottom waters.

## 7) CONCLUSIONS

1) Iron-formations in the Schreiber - Terrace Bay area are predominantly represented by the sulphide facies. They appear to share characteristics of both the Mafic to Felsic Volcanic Association and the Graded Greywacke - Siltstone Association (Gross, 1965; Shegelski, 1978). The depositional environments of the sulphide-facies iron-formations are highly variable, both within the study area and in general. For example, sulphide-facies iron-formation in the Lower Steel River - Little Steel Lake area was deposited in an outer fan basin plain depositional environment, whereas the Morley iron-formation appears to result from episodic hydrothermal venting possibly within a restricted small-scale basin.

2) Iron-formations in the study area occur at contacts between mafic volcanic and sedimentary rocks, within volcanic rocks, and occasionally within sedimentary units, suggesting that the iron-formations accumulated mainly during pauses in volcanism and at times during periods of limited clastic input. Hydrothermal solutions probably percolated up through the volcanic pile, causing alteration adjacent to solution pathways. At the Kingdom occurrence, where pillow lavas underlie the iron-formation, alteration effects are greater 10 m from the iron-formation than at a 30 m distance, and greater in pillow rims than in pillow cores.

3) Iron-formations consist of various interbedded combinations of chemical and dominantly clastic sediments, now recognizable as several common metasedimentary rocks, including: 1) pyritic - carbonaceous slate; 2) pyrite in massive, layered, lenticular, nodular and disseminated form; and 3) variably recrystallized chert. Alternation of these units occurs on millimetre to metre scales. The interbedded and interlaminated pyrite, chert and slate display a wide variety of primary structures.

4) Field evidence combined with thin section examination and trace element data allow interpretations for the source of iron and the depositional environment of the pyrite. The massive pyrite and colloform nodules were probably derived from a proximal volcanic-hydrothermal source. The iron in the radial pyrite nodules, and in the laminated and disseminated pyrite, was likely deposited from normal seawater with little hydrothermal influence. The present structures of the radial and layered nodules are interpreted as the result of diagenetic transformation and tectonic deformation.

5) The pyritic-carbonaceous slates contain a distinct hydrothermal component. About half of the samples are enriched in Fe and depleted in Al relative to the turbidite-associated slates; the other half display minor silica enrichment. Cherts are interpreted as

chemical precipitates with a variable iron sulphide component.

6) Carbon is present in the pyritic - carbonaceous slates, mainly in amorphous form. It was probably derived from organic bacterial activity associated with the discharging hydrothermal solutions.

7) Structural evidence suggests that competency differences between the fine-grained, carbon-rich chemical sedimentary rocks and the associated volcanic-sedimentary rocks focuses deformation and promotes dike emplacement in areas adjacent to and within iron-formations. The rocks of the Lower Steel River - Little Steel Lake area appear to have been subjected to a complex folding event related to one deformational period; refolded folds are present, but the absence of a folded cleavage suggests the first phase of folding was probably the result of syn-sedimentary slumping.

## REFERENCES

- Adshead, A.J.D., Bornhold, B.D. and Davis, E.E.  
1986: Indurated Deposits and Possible Plume Bands in a Hydrothermal Mound, northeast Pacific, in Current Research, Part A, Geol. Sur. Can., 86-1A, p. 737-748.
- Alt, J.G., Lonsdale, P., Haymon, R. & Muchlenbachs, K.  
1987: Hydrothermal Sulphide and Oxide Deposits on Seamounts near 21 Degrees N, East Pacific Rise., Geol. Soc. Am. Bull. 98, p. 157-168.
- Barnett, E.S., Hutchinson, R.W., Adamcik, A., and Barnett, R.  
1982: Geology of the Agnico-Eagle Gold Deposit, Quebec; in Precambrian Sulphide Deposits, H.S. Robinson Memorial Volume, ed. Hutchinson, R.W., Spence, C.D. and Franklin, J.M., Geol. Assoc. of Can. Sp. Pap. 25, p. 403-426.
- Barrett, T.J., and Fralick, P.W.  
1985: Sediment Redeposition in Archean Iron Formation from the Beardmore-Geraldton Greenstone Belt, Ontario; Jour. Sed. Petr., Vol. 55, No. 2, p. 205-212.
- Barrett, T.J., Friedrichsen, H., and Fleet, A.J.  
1983: Experimental and Stable Isotopic Composition of some Metalliferous and Pelagic Sediments from the Galapagos Mounds Area Leg 70; in: Honnorez, J., Von Herzen, et al., 1983. Initial Reports of the Deep Sea Drilling Project, Vol. 70, p. 315-323.
- Bartley, M.W.  
1939: The Northwestern Part of the Schreiber Area; Ontario Department of Mines, Annual Report for 1938, Volume 47, Part 9, p. 24-45. Accompanied by Map 47j; scale 1:31 680 or 1 inch to 1/2 mile.
- Beukes, N.J.  
1973: Precambrian Iron-Formations of Southern Africa; Econ. Geol., Vol. 68, p. 960-1004.
- Bischoff, J.L.  
1969: Red Sea Geothermal Brine Deposits: Their Mineralogy, Chemistry, and Genesis. in Hot Brines and Recent Heavy Metal Deposits in the Red Sea, (E.J. Degens & D.A. Ross, eds.) Springer-Verlag, N.Y., p. 368-401.
- Bonatti, E.  
1975: Metallogenesis at Ocean Spreading Centers; in Annual Revs. Ear. Plant. Sci., edited by F. Donath, F.G. Stehli and G.W. Wetherill, Vol. 3, p. 401-431.
- Bonatti, E., Kraemer T., and Rydell, H.  
1972: Classification and Genesis of Submarine Iron-Manganese Deposits; in Ferromanganese Deposits on the Ocean Floor, edited by D. Horn, Nat. Sci. Found. Washington, D. C., p. 149-165.



- Borradaile, G. J.  
1976: "Structural Facing" (Shackelton's rule) and the Paleozoic Rocks of the Malaguide Complex near Velez Rubio, SE Spain. Proc. K. Ned. Akad. Wet., Amsterdam, B79: 330-336.
- Borradaile, G.J.  
1980: Structural Mapping Techniques; (1979-1980) Edition Unpublished Laboratory Manual, 240pp.
- Borradaile, G.J., and Poulsen, K. H.  
1981: Tectonic Deformation of Pillow Lava; Tectonophysics, Vol. 79, p. 17-26.
- Bostrom, K.  
1970: Submarine Volcanism as a Source for Iron; Earth and Planet Sci. Letters, Vol. 9, p. 348-354.
- Bostrom, K.  
1973: The Origin and Fate of Ferromanganoan Active Ridge Sediments; Stockholm Contributions in Geology, Vol. 27, p. 148-243.
- Bouma, A.H.  
1962: Sedimentology of some Flysch Deposits; Elsevier Publ. Co., Amsterdam, p. 48-54, 168p.
- Cathles, L. M., Gruber, A. T., Lenagh, T. C., and Dudas, F. O.  
1983: Kuroko-Type Massive Sulphide Deposits of Japan: Products of an Aborted Island-Arc Rift? Econ. Geol Monogr. 5: p. 96-114.
- Carreras, J., Estrada, A., and White, S.  
1977: The Effects of Folding on the C-Axis Fabrics of a Quartz Mylonite, Tectonophysics, Vol. 39, p. 3-24
- Chauval, J.J., and Dimroth, E.  
1974: Facies Types and Depositional Environment of the Sokoman Iron Formation, Central Labrador Trough, Quebec, Canada; Jour. Sed. Petr., Vol. 44, p. 299-327.
- Cloud, P.E.  
1973: Paleocological Significance of the Banded Iron Formation; Econ. Geol., Vol. 68, p. 1135-1143.
- Cobbold, P.R. and Quinquis, H.  
1980: Development of Sheath Folds in Shear Regimes, Journal of Structural Geology, Vol. 2, p. 119-126.
- Corliss, J.B., Dymond, J., Gordon, L.I., Edmond, J.M., Von Herzen, R.P., Ballard, R.D., Green, K., Williams, D., Brainbridge, A., Crane, K. and Van Andel, T.H.  
1979: Submarine Thermal Springs on the Galapagos Rift. Science, Vol. 203, p. 1073-1083.
- Craig, J.R., and Vaughan, D.J.  
1981: Ore Microscopy and Ore Petrography, John Wiley and Sons, Inc., New York, New York, pp. 340.

Cummins, W.A., and Shackleton, R. M.

1955: The Ben Lui Recumbent Syncline (S.W. Highlands);  
Geol. Mag., Vol. 92, p. 353-363.

Curry, J.R., Moore, D.G., et al (sic).

1982: Initial Reports: DSDP 62., Washington, D.C.;  
U.S. Government Printing Office.

CYAMEX Scientific team.

1979: Massive Deep-Sea Sulphide Ore Deposits Discovered on  
East Pacific Rise, Nature, Vol. 277: p. 523-528.

Davidson, C. F.

1962: On the Cobalt:Nickel Ratio in Ore Deposits; The  
Mining Magazine, Vol. 106, p. 78-85.

Daziel, I.W.D., and Bailey, S.W.

1968: Deformed Garnets in a Mylonitic Rock  
from the Grenville Front and their Tectonic Significance;  
Am. Jour. Sci., Vol. 266, p. 542-562.

Degens, E.J. and Ross, D.A.

1969: Hot Brines and Recent Heavy Metal Deposits in the Red  
Sea. Springer-Verlag, N.Y., 601pp.

Dimroth, E.

1975: Paleo-Environment of Iron-Rich Sedimentary Rocks; Geol.  
Rundschau, Vol. 64, p. 751-767.

Dimroth, E.

1977a: Facies Models 5. Models of Physical Sedimentation of Iron  
Formations; Geoscience Canada, Vol. 4, p. 23-30.

Dimroth, E.

1977b: Facies Models 6. Diagenetic Facies of Iron Formations;  
Geoscience Canada, Vol. 4, p 83-88.

Dimroth, E., Boivin, P., and Larouche, M.

1973: Tectonic and Volcanological Studies in the Rouyn-Noranda  
Area; Quebec Dept. Nat. Res., Open File Manuscript, 60 pp.

Dimroth, E., and Kimberley, M.

1976: Precambrian Atmospheric Oxygen: Evidence in the  
Sedimentary Distributions of Carbon, Sulfur, Uranium and  
Iron; Can. Jour. Ear. Sci., Vol. 13, p. 1161-1185.

Drever, J.I.

1974: Geochemical Model for the Origin of Precambrian Banded  
Iron Formations; Geol. Soc. Am. Bull., Vol. 85, p. 1099-  
1106.

Dymond, J., Corliss, J.B., Heath, J.R., Field, C.W., Dasch,  
E.J. and Veeh, H.H.

1973: Origin of Metalliferous Sediments from the Pacific Ocean,  
Geol. Soc. Am. Bull., Vol. 84, p. 3355-3372.

- Easdon, M.M.  
1969: A Compilation of Graphitic Occurrences in the Archean of Part of Northwest Quebec; Unpubl. M.Sc. Thesis, McGill University, Montreal, 119 pp.
- Edmond, J.M., and Von Damm, K.  
1983: Hot Springs on the Ocean Floor; Sci. Am., Vol. 248, p. 78-93.
- Eichler, J.  
1976: Origin of the Precambrian Banded Iron-Formations; in Handbook of Strata-Bound and Stratiform Ore Deposits; edited by K.H. Wolf, Elsevier Sci. Publ. Co., New York, New York, Vol. 7, p. 157-201.
- Eugster, H.P., and Chou, I-Ming  
1973: The Depositional Environments of Precambrian Banded Iron Formations; Econ. Geol., Vol. 68, p. 1144-1168.
- Fenwick, K.G.  
1969: Finlayson Lake Area, District of Rainy River; Ont. Dept. Mines, Prelim. Maps P. 542 and P. 543, scale 1 inch to 1/4 mile. Geology completed 1968.
- Fenwick, K.G.  
1971: Origin of a Stratabound Pyrite Deposit in Predominantly Volcanic Derived Strata in the Finlayson Lake Area District of Rainy River, Ontario; Unpubl. M.Sc. Thesis, Michigan Technological University, Michigan, 90 pp.
- Fenwick, K.G.  
1976: Geology of the Finlayson Lake Area, District of Rainy River; Ontario Div. Mines, GR 145, 86p. Accompanied by Maps 2297 and 2298, scale 1 inch to 1/2 mile.
- Ferguson, G.L.  
1984: Trench Floor Sedimentary Sequences in a Paleozoic Subduct Subduction Complex, Eastern Australia; Sed. Geol., Vol. 42 p. 181-200.
- Fleischer, M.P.  
1955: Minor Elements in some Sulphide Minerals; Econ. Geol., 50th Anniv. Vol., p. 970-1024.
- Fralick, P.W.  
(in press): Depositional Environment of Archean Iron Formation : Inferences from Layering in Sediment and Volcanic Hosted End Members., 16 pp.
- Francheteau, J., Needham, H.D., Choukroune, P., Juteau, T., Seguret, M., Ballard, R.D., Fox, P.J., Normark, W., Carranza, A., Cordoba, D., Guerrero, J., Rangin, C., Boughault, H., Ceambon, P. and Hekinian, R.  
1979: Massive Deep-Sea Sulphide Ore Deposits Discovered on the East Pacific Rise., Nature, Vol. 277, p. 523-528.

Goodwin, A.M.

1962: Structure, Stratigraphy and Origin of Iron Formations, Michipicoten Area, Algoma District, Ontario, Canada; Geol. Soc. Am. Bull., Vol. 73, p. 561-586.

Goodwin, A.M.

1965: Geology at Pashkokogan Lake-Eastern Lake St. Joseph Area, Districts of Thunder Bay and Kenora; Ont. Dept. Mines, Geol. Rept. No. 42, 58 pp.

Goodwin, A.M., Monster, J., and Thode, H.G.

1976: Carbon and Sulfur Isotope Abundances in Archean Iron Formations and Early Precambrian Life; Econ. Geol., Vol. 71, p. 870-891.

Goodwin, A.M., Thode, H.G., Chou, C.L., and Karkansis, S.N.

1985: Chemostratigraphy and Origin of the Late Siderite-Pyrite Rich Helen Iron Formation, Michipicoten Belt, Canada; Can. Jour. Ear. Sci., Vol. 22, p. 72-84.

Gross, G.A.

1965: Origin of Precambrian Iron Formations; Econ. Geol., Vol. 60, p. 1065-1070.

Gross, G.A.

1973: The Depositional Environment of Principal Types of Precambrian Iron-Formations; p. 15 - 21 in Genesis of Precambrian Iron and Manganese Deposits. Proc. Kiev Symp., 1970, Ear. Sci., Vol. 9; p. 15-21.

Gross, G.A.

1983: Tectonic Systems and the Deposition of Iron Formation; Precambrian Research, Vol. 20, p. 171-187.

Harcourt, G.A.

1939: The Southwestern Part of the Schreiber Area, Thunder Bay District, Ontario; Ont. Dept. Mines Annual Report 1938, Vol. 47, part 9, p. 1-28. Accompanied by Map 47j, scale 1 inch to 1/2 mile.

Hawley, J.E., and Nichol, I.

1961: Trace Elements in Pyrite, Pyrrhotite and Chalcopyrite of Different Ores; Econ. Geol., Vol. 56, No. 3, p. 467-487.

Hekinian, R., Fevrier, M., Bischoff, J.L., Picot, P., and Shanks, W.C.

1980: Sulphide Deposits from the East Pacific Rise near 21 Degrees N, Science Vol. 207, p. 1433-1444.

Hekinian, R., and Fouquet, Y.

1985: Volcanism and Metallogenesis of Axial and Off-Axial Structures on the East Pacific Rise Near 13 Degrees North; Econ. Geol., Vol. 80, p. 221-249.

Henderson, J.R.

1981: Structural Analysis of Sheath Folds with Horizontal X-axes, Northeast Canada., Jour. of Struct. Geol., Vol. 3, No. 3, pp. 203-210.

Horikoshki, E.

1969: Volcanic Activity Related to the Formation of the Kuroko - type Deposits in the Kosaika District, Japan; Mineral Deposita, Vol. 4, p. 321-345.

Hutchinson, R.W.

1982: Syn-Depositional Hydrothermal Processes and Precambrian Sulphide Deposits; in Precambrian Sulphide Deposits, edited by R.W. Hutchinson, C.D. Spence and J.M. Franklin, Geol. Assoc. Can., Special Paper No. 25, p. 761-791.

Ikeda, S., Kubota, Y., and Nagamatsu.

1971: The Exploration of the Shimokawa Mine, Min. Geol., Vol. 21, p. 40-54 (in Japanese).

Ikeda, S., Kubota, Y., and Nagamatsu, T.

1972: Some New Facts Found at the Lower Levels of the Shimokawa Deposit, Hokkaido. Min. Geol., Vol. 22: p. 150-165 (in Japanese).

James, H.L.

1954: Sedimentary Facies of Iron-Formation; Econ. Geol., Vol. 49, p. 235 -293.

James, H.L.

1966: Chemistry of the Iron-rich Sedimentary Rocks; Data of Geochemistry, U.S. Geol. Surv. Prof Paper 440-J, 61 pp.

Kehlenbeck, M.M.

1984: Use of Stratigraphic and Structural-Facing Directions to Delineate the Geometry of Refolded Folds near Thunder Bay, Ontario, Geoscience Canada, Vol. 11, p. 23-32.

Kehlenbeck, M.M.

1986: Folds and Folding in the Beardmore-Geraldton Fold Belt, Canadian Journal of Earth Sciences, Volume 23, pp. 158-171.

Koski, R.A., Clague D.A., and Oudin, E.

1984: Mineralogy and Chemistry of Massive Sulphide Deposits from the Jaun de Fuca Ridge, Geol. Soc. Am. Bull., Vol. 95, p. 930-945.

Knuckey, M.J., and Watkins, J.J.

1982: The Geology of the Corbet Massive Sulphide Deposit, Noranda District, Quebec, Canada; in Precambrian Sulphide Deposits, H.S. Robinson Memorial Volume, R.W. Hutchinson, C.D. Spence and J.M. Franklin, eds., Geol. Assoc. Can. Sp. Pap. 25, p. 297-317.

- Knuckey, M.J., Comba, C.D.A., and Riverin, G.  
 1982: Structure, Metal Zoning and Alteration at the Millenbach Deposit, Noranda, Quebec;  
in Precambrian Sulphide Deposits, H.S. Robinson Memorial Volume, R.W. Hutchinson, C.D. Spence and J.M. Franklin, eds., Geol. Assoc. Can. Sp. Pap. 25, p. 255-295.
- Lacassin, R., and Mattauer, M.  
 1985: Kilometre-Scale Sheath Folds at Mattmark, and Implications For Transport Direction in the Alps., *Nature*, Vol. 315., p. 739-742.
- Lambert, I.B. and Sato, T.  
 1974: The Kuroko and Associated Ore Deposits of Japan : A Review of their Features and Metallogenesi,  
*Econ. Geol.*, Vol. 69, p. 1215-1236.
- Loftus-Hills, G., and Solomom, M.  
 1967: Cobalt, Nickel and Selenium in Sulphides as Indicators of Ore Genesis; *Min. Deposita*, Vol. 2, p. 228-242.
- Logan, B.W., Rezka, R., and Ginsburg, R.N.  
 1964: Classification and Environmental Significance of Algal Stromatolites., *Jour. of Geol.* 72., p. 68-83.
- Marmont, S.  
 1984: The Terrace Bay Batholith and Associated Mineralization; Ontario Geological Survey, Open File Report 5514, 95 pp., 10 photos, 7 figures, 4 tables, and 1 map in back pocket.
- Miyashiro, A.  
 1973: The Troodos Ophiolite Complex was Probably Formed in a Island Arc, *Earth Planet. Sci. Lett.*, Vol. 19, p. 218-224.
- Mitchell, R.H., Poulsen, H., and Jensen, E.  
 1980: Analysis of Silicate Rocks: Major Elements: Rb, Sr, Y, Zr, Nb and Ba by Wet Chemical and X-ray Fluorescence Methods; Dept. Geol., Geocem. Lab. Internal Report No. 1, Lakehead University, 51 pp.
- Mutti, E., and Ricci Lucchi, F.  
 1973: Turbidites of the Northern Apennines; translated by T.N. Nilsen, *Internat. Geol. Rev.*, Vol. 20, p. 125-166, (AGI Reprint Series 3).
- Nielson, P.E.  
 1974: The Geochemistry of the Lyon Lake-Claw Lake Sulphide Bearing Graphitic Shale, Sturgeon Lake Area, Ontario; Unpubl. B.Sc. Thesis, Lakehead University, 99 pp.
- Norrish, K., and Chappel, B.W.  
 1967: X-ray Fluorescence Spectrography: in, *Physical Methods in Determinative Mineralogy*; edited by J. Zussman, p. 161-214.

- Norrish, K, and Hutton  
1969: *Geochimica Cosmochimica Acta* 33, p. 431-453
- Oudin, E.  
1983: Hydrothermal Sulphide Deposits of the East Pacific Rise (21N). Part I: Descriptive Mineralogy. *Mar. Min.* Vol. 4, p. 39-72.
- Pandalai, H.S., Majumder, T., and Chandra, D.  
1983: Geochemistry of Pyrite and Black Shales of Amjhore, Rohtas District, Bihar, India; *Econ. Geol.*, Vol. 78, p. 1505 - 1513.
- Patterson, G.C., Mason, J.K., and Schnieders, B.R.  
1984: Report of Activities 1983, Thunder Bay Resident Geologist Area, North Central Region; in Report of Activities 1983, Regional and Resident Geologists, edited by C.R. Kustra, Ontario Geological Survey, Miscellaneous Paper 117, p. 47-106.
- Pettijohn, F.J.  
1975: *Sedimentary Rocks: Third Edition*; Harper and Row, Inc., New York, New York, 628 pp.
- Ramsay, J.G.  
1967: *Folding and Fracturing of Rocks*; McGraw-Hill, New York, New York, 568 pp.
- Rhodes, S., and Gayer, R. A.  
1977: Non-Cylindrical Folds, Linear Structures in the X Direction and Mylonite Developed During Translation of the Caledonian Kalak Narre Complex of Finmark; *Geol. Mag.*, Vol. 114, p. 329-341.
- RISE Project Group.  
1980: East Pacific Rise: Hot Springs and Geophysical Experiments. *Science*, Vol. 207: p. 1421-1433.
- Robertson, A.H.F.  
1976: Origins of Ochres and Umbers: Evidence from Skouriotissa, Troodos Massif, Cyprus; *Trans. Inst. Min. Met.*, (sect. B: Appl. Ear. Sci.), Vol. 85, p. 245-251.
- Robertson, A.H.F., and Hudson, J.D.  
1973: Cyprus Umbers: Chemical Precipitates on a Tethyan Ocean Ridge; *Earth Planet. Sci. Lett.*, Vol. 18, p. 93-101.
- Rona, P.A.  
1984: Hydrothermal Mineralization at Seafloor Spreading Centers; *Ear. Sci. Rev.*, Vol. 20, p. 1-104.
- Roscoe, S.M.  
1965: Geochemical and Isotopic Studies, Noranda and Mattagami Areas; *Can. Min. Metal. Bulletin*, Sept., p. 965-971.

Rose, E.R.

1965: Pyrite Nodules of the Timagami Copper-Nickel Deposit; Canadian Mineralogist, Vol. 8, p. 317-324.

Sangster, D.F., and Scott, S.D.

1976: Precambrian, Strata-Bound, Massive Cu-Zn-Pb Sulfide Ores of North America; in Handbook of Strata-Bound and Stratiform Ore Deposits, edited by K.H Wolf, Elsevier Sci. Publ. Co., Amsterdam, Vol. 6, p. 128-222.

Sato, T.

1977: Kuroko Deposits: Their Geology, Geochemistry and Origin, in Volcanic Processes in Ore Genesis, Spec. Publ. Geol. Soc. Lond., No. 7, p. 153-161.

Scott, S.D.

1980: Geology and Structural Control of Kuroko-Type Massive Sulphide Deposits. Geol Geol. Assoc. Can. Spec. Pap. 20, p. 706-721.

Scott, S.D.

1985: Seafloor Polymetallic Sulfide Deposits: Modern and Ancient; Marine Mining, Vol. 5, p. 191-212.

Shackleton, R.M.

1958: Downward Facing Structures of the Highland Border; Quar. Jour. Geol. Soc. London., Vol. 113, p.361-392.

Shegelski, R.J.

1971: General Stratigraphy and the Iron and Manganese Beds of Thunder Bay; Unpubl. B.Sc. Thesis, Lakehead University, 94 pp.

Shegelski, R.J.

1976: The Geology and Geochemistry of Archean Iron Formations and Their Relation to Reconstructed Terrains in the Sturgeon and Savant Lake Greenstone Belts; in Proceedings of the 1976 Geotraverse Conference, sponsored by the Precambrian Research Group, Univ. of Toronto, p. 109-127.

Shegelski, R.J.

1978: Stratigraphy and Geochemistry of Archean Iron Formations in the Sturgeon Lake-Savant Lake Greenstone Terrain, Northwestern Ontario; Unpubl. Ph.D Thesis, Univ. of Toronto, Canada, 251 pp.

Shegelski, R.J., and Bell, R.T.

1976: Coarse Clastic Facies of the Savant Lake and Sturgeon Lake Greenstone Belts; Midwest Superior Geotraverse Conference, p. 96-108.

Simonson, B.M.

1985: Sedimentological Constraints on the Origins of Precambrian Iron-Formations, Geol. Soc. Am. Bull., Vol. 96, p. 244-252.



Stanton, R. L.

1972: Ore Petrology; McGraw-Hill, New York,  
p. 129-140.

Vokes, F.M.

1969: A Review of the Metamorphism of Sulphide Deposits; Ear.  
Sci. Rev., Vol. 5, p. 99-143.

Voytkovich, G.V., Khayretdinov, I.A., Grineko, V.A., Prokhorov,  
V.G., and Chetmutova, V.I.

1969: Microorganisms and Oxidation of Pyrrhotite  
(Medvezh'ye Deposit); International Geology  
Review, Vol. 11, p. 867-874.

Walker, J.C.G., and Brimblecombe, P.

1984: Iron and Sulphur in the Pre-Biologic Ocean; Precambrian  
Research, Vol. 28, p. 205-222.

Walker, J.W.R.

1967: Geology of the Jackfish-Middleton Area, District of  
Thunder Bay; Ont. Dept. Mines, Geological  
Report 50, 41 pp. Accompanied by Maps 2107 and 2112, scale  
1:31,680 or 1 inch to 1/2 mile.

Walker, R.G.

1976: Facies Models 2. Turbidites and Associated Coarse Clastic  
Deposits; Geoscience Canada, Vol. 3, p. 25-36.

Walker, R.G., and Mutti, E.

1973: Turbidite Facies and Facies Associations: Turbidites and  
Deep Water Sedimentation; SEPM Short Course,  
p. 119-157.

Williams, N. Cohen, Y., Haack, U., Hallberg, R.O., Kaplan, I.R.,  
Nielsen, H., Sangster, D.F., Trudinger, P.A.,  
Truper, H.G., and von Gehlen, K.

1982: Stratified Sulphide Deposits: State of the Art Report;  
in Mineral Deposits and the Evolution of the Biosphere,  
edited by H.D. Holland and M. Schidlowski,  
Dahlem Konferenzen. Springer-Verlag, Berlin, p. 275-286.

Wolf, K.H.

1980: Handbook of Strata-bound and Stratiform Ore Deposits.,  
Ed., K.H. Wolf, Volumes. 6, 7.

Wright, C.M.

1965: Syngenetic Pyrite Associated with a Precambrian Iron Ore  
Deposit; Econ. Geol., Vol. 60, p. 998-1019.

Zierenberg, R.A., and Shanks W.C. III,

1983: Mineralogy and Geochemistry of Epigenetic Features in  
Metalliferous Sediments, Atlantis II Deep, Red Sea;  
Econ. Geol., Vol. 78, p. 57-72.

Zierenberg, R.A., Shanks W.C. III, and Bischoff, J.L.

1984: Massive Sulphide Deposits at 21 Degrees North, East  
Pacific Rise: Chemical Composition, Stable Isotopes,  
and Phase Equilibria; Geol. Soc. Am. Bull., Vol. 95,  
p. 922-929.

APPENDICIES

APPENDIX 'A'

Mineralogy of Lithologic Units  
from X-Ray Diffraction

	Pyrite-Carbonaceous Slate BRS-5, 8, 9, 22, 29, 40	DE Turbidite Slate BRS-23	Chert Dark Layers BRS-52	Chert Light Layers BRS-53	Chert (Tuffaceous) BRS-25, 44, 51	Interlaminated Colloform Pyrite Clastic Components BRS-7, 22, 54	Interlaminated Colloform Pyrite Chemical Components BRS-7, 22, 54	Massive Pyrrhotite BRS-49	Pillow Core BRS-14	Pillow Rim BRS-15
Quartz	A	A	A	A	A	A	R	C	A	A
Albite	A	C	C	R	A-C	C	R		C	C
Muscovite	C	R			C-R	R		R	C	C
Oligoclase	C	C			R	R			C	C
Chlorite	C	C	C	R	C	C		R-C	C	C
Calcite	A	A	C	C	A-C	R-C			C	C-A
Siderite	R									
Biotite	R	R								
Spinel	R	R								
Apatite	R									
Pyrite	A	R	C	C-R	A	R	A		R	C
Pyrrhotite	C-R	R			C		R	A		
Chalcopyrite			R							
Magnetite	R	R								
Goethite	R	C				A	R-C			
Hematite	R	R				C	R			
Glauconite	R	C				R-C				
Carbon	C	R	C	C-R	C		C	C		
	1	2	3	4	5	6	7	8	9	10

A Abundant  
C Common  
R Rare  
☐ Not Present  
☐ Not Detected

## APPENDIX B

## X-Ray Fluorescence Spectrography

Whole rock geochemistry for this thesis was performed at two locations, at Lakehead University, Thunder Bay (by the author), and at the Ontario Geoscience Laboratories in Toronto. Major element analysis was performed on 45 samples, 31 at Lakehead, and 14 in Toronto. Three duplicate samples were included to check analyses within the same laboratories and between laboratories. The results for all the analyses are given in Tables 3:1-3:4, 4:1, 4:3 and 5:1.

The samples analysed at Lakehead University were prepared and analysed using methods described by Mitchell et al. (1980). These methods utilise the procedures of Norrish and Hutton (1969) and Norrish and Chappel (1967). Glass discs and pressed pellets were analysed on a Phillips PW 1540 x-ray spectrometer. The samples were processed using a computer program for the calibration of standards and sample analyses (XRF PROCESS). The computer programs were written by H. Poulsen and R. Mitchell, and are listed in Mitchell et al. (1980).

Standard wet chemical methods were utilized for several other major elements as described in Mitchell et al. (1980). Na<sub>2</sub>O and MnO were determined by atomic absorption, P<sub>2</sub>O<sub>5</sub> by a "molybdenum blue" colorimetric method, and FeO by potassium dichromate titration.

Total water, and carbon dioxide and non-carbonate carbon were measured on a Perkin Elmer Carbon-Hydrogen-Nitrogen (CHN) analyser. One set of samples was analysed for the volatiles. The other set of splits were treated with hot nitric acid to

eliminate any carbonate present, then analysed for carbon content.

The Geoscience Laboratories (O.G.S.) in Toronto determined major elements by X-ray spectrophotographic methods using an ARL 72000 XRF Quantometer. The sample preparation was similar to that at Lakehead University. Sulphur was determined at the Toronto Laboratory using a Leco Induction Furnace and Titrator. Complete analytical methods are available in the Geosciences Laboratories Manual. Total iron (Fe) was determined for several samples by atomic absorption. Total carbon was measured using a Leco Induction Furnace and infra-red detection methods, and carbonate carbon by a rapid oil displacement method.

#### Trace Elements

In addition to major element analyses, 39 samples were analysed for trace elements at the Geoscience Laboratory, in Toronto. Cu, Zn, Pb, Ni, Co and Cr were determined by flame atomic absorption spectroscopy. Three duplicate samples were also included. Au and Ag were determined in a number of samples by both atomic absorption and fire assay methods. The results are presented together with the major element data.

#### Accuracy and Precision

Fused discs and solutions were prepared from USGS standard rocks BC1, GSP1, AGV1, DTS1, G2, PC1, W1, MRG-1 and SY-2. Recommended values for these international reference standards were used to establish calibration curves in all analytical methods.

Four samples (BRS-14, 15, 23, and 45) were analysed at both laboratories; results are observed in Tables 3:1 and 3:3. In addition the Geoscience Laboratories commonly run their own duplicates, for both major and trace element. The results are given in Appendix C (Samples 41 and 55B). Results indicate that the precision on duplicate samples and between laboratories is within 10 %.

### Discussion

Caution must be applied when interpreting analyses for a particular element are outside the range of the standards used. In the present study, some samples contained very high concentrations of silica, iron (as pyrite), and carbon. Shegelski (1978) noted that high contents of graphite and pyrite make complete fusions difficult, and therefore suggested that only semi-quantitative analyses of graphitic-pyritic shale could be obtained. The author had similar problems in attempting complete fusion of several pyritic-carbonaceous slates. Samples high in iron and carbon commonly remained black in color and produced cloudy or mottled glass discs. After fusion, the concentrations of iron oxides were above the values of most standards. For this reason, several samples were analysed for total iron by atomic absorption.

According to G. Platt (personal communication, 1986), fusion in platinum crucibles of samples with high iron or sulphide contents was not recommended due to iron-platinum interaction and likely loss of iron. Thus, totals for such samples may be slightly lower than ideal 100 percent. The totals for the major element analyses are therefore unadjusted. Graphite crucibles

have been suggested as alternatives to the platinum crucibles, but this is not suitable for the analysis of sulphide-facies iron-formation, which commonly contains carbon.

Major element analyses of the cherts initially posed some problems as the silica content of normal standards ranged between 45 and 65%, whereas many cherts contained 80 to 90% silica. For this reason, a 100% silica standard was also used in the calibrations. Potassium results from Lakehead and Toronto Laboratories are not in good agreement, particularly at lower concentrations. This may be because the standards used ranged from 1.5 to 5.5%, while many of the samples contained much lower K concentrations. In general, the major element analyses for iron-formation and associated rocks should be considered as semi-quantitative.

#### X-Ray Diffraction

Twenty-four samples were powdered and analysed by X-Ray diffraction using Cu-radiation. Appendix A lists the mineralogy of the various lithologic units investigated in the present study.

APPENDIX C : Representative Duplicate  
Analyses for Two Samples.  
(BRS-41 , BRS-55B)



SAMPLE BRS-41 : ANALYSIS 1

SAMPLE NUMBER(FIELD): BRS-41  
PROJECT NUMBER: 84-000RG

JOB NUMBER : 84-2270  
SAMPLE NUMBER(LAB):

GEOLOGIST: SCHNIEDERS B R

DATE SUBMITTED: 85-03-19  
DATE PROCESSED: 08/06/85

ROCK NAME : SHALE  
MATERIAL: META  
AGE : ARCH  
STRATIG.:  
AREA : TUURI TWP  
SAMPLE DESCRIPTION: SHALE, AWAY FROM SULPHIDES  
COMMENTS :

LOCATION:  
LATITUDE : 48.75826  
LONGITUDE: 86.79851

UTM:  
NORTHING: 5400383  
EASTING : 514809  
ZONE : 16  
NTS : 042D15SW

REFERENCE :

	ANALYSIS(WT%)	ANHYDROUS(WT%)	ADJUSTED(WT%)	CATION%	---	TRACES(PPM):	NEG VALUE =	DETECTION LIMIT---
SI02	61.40	64.16	62.78	57.69	CO	30		
TI02	0.78	0.82	0.80	0.55	CR	24		
AL2O3	17.00	17.76	17.38	18.83	CU	128		
FE2O3	5.80	6.06	5.93	4.10	MN	114		
FE0	0.0	0.0	0.0	0.0	NI	26		
MNO	0.02	0.02	0.02	0.02	PB	10		
MGO	1.91	2.00	1.95	2.67	ZN	119		
CA0	1.25	1.31	1.28	1.26				
NA2O	3.03	3.17	3.10	5.52				
K2O	3.94	4.12	4.03	4.72				
P2O5	0.07	0.07	0.07	0.06				
CO2	1.88	0.0	0.0	0.0				
S	2.60	0.0	2.66	4.58				
H2O+	0.0	0.0	0.0	0.0				
H2O-	0.0	0.0	0.0	0.0				
TOTAL	99.68							
LOI	4.30							
SP.GR.	0.0							

TOTAL FE (AS FEO) : 5.22 5.45 5.34 3.69  
TOTAL FE (AS FE2O3): 5.80 6.06 5.93 4.10  
COMMENTS: FE 3.39 % CARBONATE C AS CO2 0.66 % \*NON-CARBONATE C AS C 0.3 %  
MASS ABSORPTION COEFFICIENT = 53.194903

OPTIONS SELECTED: STANDARD RAT+IND MESONORM

CALCULATED ROCK NAMES

METHOD	ROCK NAME	
IRVINE & BARAGAR(COLR.IND VS NORM.PLAG):		DACITE
IRVINE & BARAGAR(AFM) DIAGRAM:	CALC-ALC	TERNARY PARAMETERS: A= 49.4 F= 37.0 M= 13.5
IRVINE & BARAGAR(AL2O3:PLAG):	CALC-ALC	
MIYASHIRO(SIO2 VS FE(TOTAL)/MGO):	CALC-ALC	ANDESITE
MIYASHIRO FE(TOTAL) VS FE(TOTAL)/MGO:	CALC-ALC	
JENSEN(AL-FE+TI-MG) DIAGRAM:	LIT-GREY CALC-ALC	DACITE TERNARY PARAMETERS: A= 72.0 F= 17.8 M= 10.2

SAMPLE BRS-41 : ANALYSIS 2

SAMPLE NUMBER(FIELD): BRS-41D  
PROJECT NUMBER: 84-000RG

JOB NUMBER : 84-2270  
SAMPLE NUMBER(LAB):

GEOLOGIST: SCHNIEDERS B R

DATE SUBMITTED: 85-03-19  
DATE PROCESSED: 08/06/85

ROCK NAME : SHALE  
MATERIAL: META  
AGE : ARCH  
STRATIG.:  
AREA : TUUR1 TWP  
SAMPLE DESCRIPTION:  
COMMENTS : SEE SAMPLE BRS-41

LOCATION:  
LATITUDE : 48.75826  
LONGITUDE: 86.79851

UTM:  
NORTHING: 5400383  
EASTING : 514809  
ZONE : 16  
NTS : 042D15SW

REFERENCE :

	ANALYSIS(WT%)	ANHYDROUS(WT%)	ADJUSTED(WT%)	CATION%	---	TRACES(PPM):NEG VALUE = DETECTION LIMIT---
SI02	61.30	64.32	62.61	57.53	CO	30
TI02	0.71	0.75	0.73	0.50	CR	24
AL2O3	17.40	18.26	17.77	19.25	CU	128
FE2O3	5.78	6.07	5.90	4.08	MN	114
FE0	0.0	0.0	0.0	0.0	NI	26
MNO	0.02	0.02	0.02	0.02	PB	10
MGO	1.79	1.88	1.83	2.50	ZN	118
CAO	1.25	1.31	1.28	1.26		
NA2O	2.99	3.14	3.05	5.44		
K2O	4.00	4.20	4.09	4.79		
P2O5	0.07	0.07	0.07	0.06		
CO2	1.92	0.0	0.0	0.0		
S	2.60	0.0	2.66	4.57		
H2O+	0.0	0.0	0.0	0.0		
H2O-	0.0	0.0	0.0	0.0		
TOTAL	99.83					
LOI	4.70					
SP.GR.	0.0					

TOTAL FE (AS FE0) : 5.20 5.46 5.31 3.67  
TOTAL FE (AS FE2O3): 5.78 6.07 5.90 4.08  
COMMENTS: FE 3.41 % CARBONATE C AS CO2 0.67 % \*NON-CARBONATE C AS C 0.3 %  
MASS ABSORPTION COEFFICIENT = 53.179474

OPTIONS SELECTED: STANDARD RAT+IND MESONORM

CALCULATED ROCK NAMES

METHOD	ROCK NAME	
IRVINE & BARAGAR(COLR.IND VS NORM.PLAG):	DACITE	
IRVINE & BARAGAR(AFM) DIAGRAM:	CALC-ALC	TERNARY PARAMETERS: A= 50.0 F= 37.2 M= 12.8
IRVINE & BARAGAR(AL2O3:PLAG):	CALC-ALC	
MIYASHIRO(SIO2 VS FE(TOTAL)/MGO):	THOLEITC	ANDESITE
MIYASHIRO FE(TOTAL) VS FE(TOTAL)/MGO:	CALC-ALC	
JENSEN(AL-FE+TI-MG) DIAGRAM:	LIT-GREY	CALC-ALC
	DACITE	TERNARY PARAMETERS: A= 73.1 F= 17.4 M= 9.5

SAMPLE BRS-55 : ANALYSIS 1

SAMPLE NUMBER(FIELD): BRS-55B  
PROJECT NUMBER: 84-000RG

JOB NUMBER : 84-2272  
SAMPLE NUMBER(LAB):

GEOLOGIST: SCHNIEDERS B R

DATE SUBMITTED: 85-03-19  
DATE PROCESSED: 08/30/85

ROCK NAME : INT. VOLC  
MATERIAL: VOLC  
AGE : ARCH  
STRATIG.:  
AREA : PRISKE  
SAMPLE DESCRIPTION:  
COMMENTS : SILICIFIED VOLCANIC

LOCATION:  
LATITUDE : 48.95000  
LONGITUDE: 87.18657

UTM:  
NORTHING: 5421694  
EASTING : 486339  
ZONE : 16  
NTS : 042D14NE

REFERENCE : MORLEY HIGH GRADE

	ANALYSIS(WT%)	ANHYDROUS(WT%)	ADJUSTED(WT%)	CATION%	---TRACES(PPM):NEG VALUE = DETECTION LIMIT---
SI02	58.30	61.05	61.31	57.18	
TI02	0.64	0.67	0.67	0.47	
AL2O3	15.70	16.44	16.51	18.15	
FE2O3	6.41	6.71	6.74	4.73	
FE0	0.0	0.0	0.0	0.0	
MNO	0.14	0.15	0.15	0.12	
MGO	3.44	3.60	3.62	5.03	
CAO	5.82	6.09	6.12	6.12	
NA2O	3.61	3.78	3.80	6.86	
K2O	0.81	0.85	0.85	1.01	
P2O5	0.07	0.07	0.07	0.06	
CO2	2.53	0.0	0.0	0.0	
S	0.15	0.0	0.16	0.28	
H2O+	0.0	0.0	0.0	0.0	
H2O-	0.0	0.0	0.0	0.0	
TOTAL	97.62				
LOI	4.50				
SP.GR.	0.0				
TOTAL FE (AS FE0) :	5.77	6.04	6.07	4.26	
TOTAL FE (AS FE2O3):	6.41	6.71	6.74	4.73	
MASS ABSORPTION COEFFICIENT =	53.488899				

OPTIONS SELECTED: STANDARD RAT+IND MESONORM

CALCULATED ROCK NAMES

METHOD	ROCK NAME	
IRVINE & BARAGAR(COLR.IND VS NORM.PLAG):	ANDESITE	
IRVINE & BARAGAR(AFM) DIAGRAM:	CALC-ALC	TERNARY PARAMETERS: A= 32.4 F= 42.3 M= 25.2
IRVINE & BARAGAR(AL2O3:PLAG):	CALC-ALC	
MIYASHIRO(SIO2 VS FE(TOTAL)/MGO):	CALC-ALC	ANDESITE
MIYASHIRO FE(TOTAL) VS FE(TOTAL)/MGO:	CALC-ALC	
JENSEN(AL-FE+TI-MG) DIAGRAM:	LIT-GREY	CALC-ALC ANDESITE TERNARY PARAMETERS: A= 64.0 F= 18.3 M= 17.7

SAMPLE BRS-55 : ANALYSIS 2

SAMPLE NUMBER(FIELD): BRS-558D  
PROJECT NUMBER: 84-0009G

JOB NUMBER : 84-2272  
SAMPLE NUMBER(LAB):

GEOLOGIST: SCHNIEDERS B R

DATE SUBMITTED: 85-03-19  
DATE PROCESSED: 08/30/85

ROCK NAME : INT.VOLC  
MATERIAL: VOLC  
AGE : ARCH  
STRATIG.:  
AREA : PRISKE  
SAMPLE DESCRIPTION:  
COMMENTS : SEE SAMPLE BRS-55B

LOCATION:  
LATITUDE : 48.95800  
LONGITUDE: 87.18657

UTM:  
NORTHING: 5421694  
EASTING : 486339  
ZONE : 16  
NTS : 042D14NE

REFERENCE :

	ANALYSIS(WT%)	ANHYDROUS(WT%)	ADJUSTED(WT%)	CATION%	---TRACES(PPM):NEG VALUE = DETECTION LIMIT---
SI02	58.50	61.26	61.24	57.15	
TI02	0.58	0.61	0.61	0.43	
AL2O3	15.80	16.54	16.54	18.19	
FE2O3	6.46	6.76	6.76	4.75	
FE0	0.0	0.0	0.0	0.0	
MNO	0.14	0.15	0.15	0.12	
MGO	3.48	3.64	3.64	5.07	
CA0	6.01	6.29	6.29	6.29	
NA2O	3.51	3.68	3.67	6.65	
K2O	0.82	0.86	0.86	1.02	
P2O5	0.08	0.08	0.08	0.07	
CO2	2.56	0.0	0.0	0.0	
S	0.15	0.0	0.16	0.27	
H2O+	0.0	0.0	0.0	0.0	
H2O-	0.0	0.0	0.0	0.0	
TOTAL	98.09				
LOI	4.50				
SP.GR.	0.0				
TOTAL FE (AS FE0) :	5.81	6.09	6.08	4.27	
TOTAL FE (AS FE2O3):	6.46	6.76	6.76	4.75	
MASS ABSORPTION COEFFICIENT = 53.870914					

OPTIONS SELECTED: STANDARD RAT+IND MESONORM

CALCULATED ROCK NAMES

METHOD	ROCK NAME	
IRVINE & BARAGAR(COLR.IND VS NORM.PLAG):	ANDESITE	
IRVINE & BARAGAR(AFM) DIAGRAM:	CALC-ALC	TERNARY PARAMETERS: A= 31.8 F= 42.7 M= 25.5
IRVINE & BARAGAR(AL2O3:PLAG):	CALC-ALC	
MIYASHIRO(SIO2 VS FE(TOTAL)/MGO):	CALC-ALC	ANDESITE
MIYASHIRO FE(TOTAL) VS FE(TOTAL)/MGO:	CALC-ALC	
JENSEN(AL-FE+TI-MG) DIAGRAM:	LIT-GRY CALC-ALC	ANDESITE TERNARY PARAMETERS: A= 64.0 F= 18.2 M= 17.8

## APPENDIX D

EXPLORATION HISTORY  
LOWER STEEL RIVER - LITTLE STEEL LAKE AREA

1896: Claim 362X known as the Fire Mountain area, situated 1.5 miles from northeast of Steel Lake siding was described as a gold quarry. Mr W. H. Arnold discovered the occurrence, described as ore of a slate formation, highly mineralized and carrying galena, copper, and iron pyrites in good quantities. Assays indicated values of \$1.50 to \$40.00 per ton gold. The quarry was said to be one half mile long at the base of an unnamed mountain.

1951: Claim TB 42700 was staked by H.E. Solly on the Kingdom occurrence, while G. Simard staked the immediate area of the Simard-Swetz. The Simard-Swetz occurrence was probably discovered during the construction of Highway 17. K.C. Rose prepared a preliminary geological report of 42 Simard-Swetz claims. Claim TB 42605 covered the Simard-Swetz occurrence. The 42 claims covered the Little Steel occurrences.

1952: One half interest was transferred to both G. Simard and P. Swetz. Trenching was carried out on the Simard-Swetz, Kingdom and Little Steel occurrences.

1953: The claims lapsed on the Blackfox Lake occurrence. J.W.R. Walker and assistants conducted reconnaissance mapping in the Lower Steel River - Little Steel Lake area for the Ontario Department of Mines. The mapping took place in the field seasons of 1953 and 1954.

1954: The claims lapsed on the Simard-Swetz, Little Steel and Kingdom Occurrences.

1955: The area was intermittently staked by various individuals, with little to no work recorded. A.L. Reading staked TB 76656 on the Kingdom occurrence. Claim was transferred to Thorncrest Explorations Ltd. in 1957: Claims lapsed, Kingdom area restaked by J. Walsh as TB87444.

1958: Claims lapsed.

1974: Kingdom area staked by J.G. Simard.

1975: No work was recorded, and claim lapsed.

1976: R.J. Pichette staked a 7 claim group covering the Simard-Swetz and Little Steel occurrences. All interest was transferred to HBOG Mining Limited.

1977: A geophysical (EM) survey was conducted on the claim group, and one diamond drill hole (165 ft) was drilled in the Simard-Swetz area, north of the highway. Sulphide-facies iron-formation was intersected, intercalated with both metagreywacke and meta-andesite. Assays indicated low copper

(0.05%) and zinc (0.37%) values with no gold and silver over 7.5 feet.

1978: Claims lapsed.

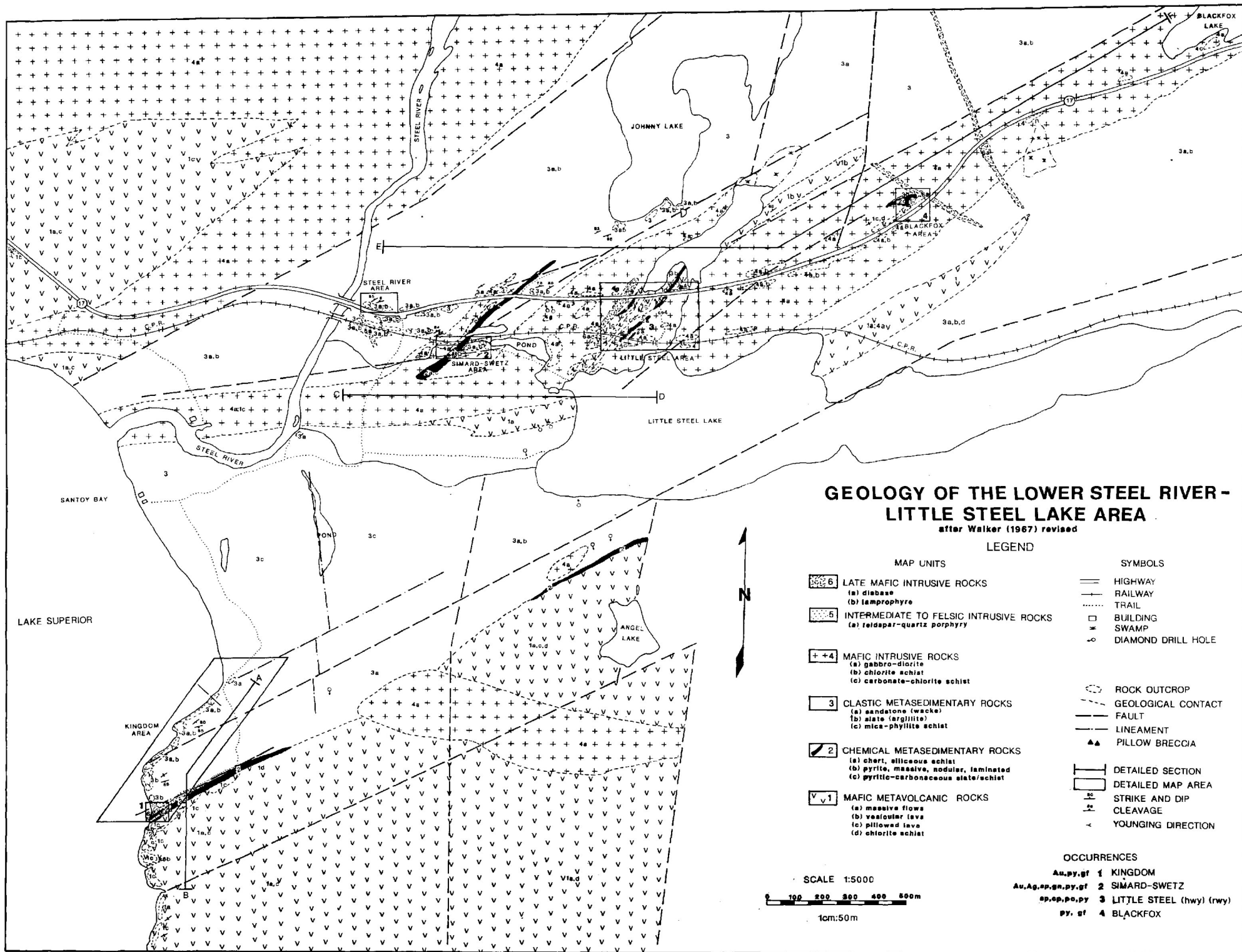
1982: L. Salo and D. McKinnon staked 29 claims covering the Little Steel and Simard-Swetz occurrences. M. Lefort staked the Kingdom occurrence. D. Lacroix staked the Blackfox Lake occurrence.

1983: Geophysical surveys (EM and magnetometer) were conducted on the Simard-Swetz and Little Steel occurrences. The claims were optioned to Silver Sceptre Mines Ltd. L. Salo's claims were transferred to D. McKinnon. M. Lefort's interest on the Kingdom occurrence was transferred to R.A. Schiralli (in trust). Airborne geophysical surveys (EM and magnetometer) were conducted by Aerodat Limited. D. Lacroix transferred all interest to D. McKinnon, who later optioned the 14 claim block on the Blackfox occurrence to Eastern Mines Limited. Geophysical surveys (VLF-EM, magnetometer) were conducted.

1984: 11 diamond drill holes, totalling 4041 feet (1231.7m) were drilled on the Simard-Swetz and Little Steel occurrences. Drilling indicated low, uneconomic gold and base metal values. Trenching, sampling and test pitting were undertaken. R.A. Schiralli transferred all interest in the Kingdom occurrence to Kingdom Resources Limited, thus the name. Prospecting, sampling and geophysical surveys (EM, magnetometer) were conducted. P. Hahn carried out sampling and prospecting on Lawson Island. Decker Resources conducted geological mapping in the adjacent ground to the west of the Silver Sceptre and Kingdom claim blocks.

1985: Kingdom Resources Limited conducted a geochemical sampling survey.

1986: Kingdom Resources Limited conducted diamond drilling.



MAP 1: Geology of the Lower Steel River -  
Little Steel Lake Area.